VASCULARIZATION FOR REGENERATIVE MEDICINE

EDITED BY: Andrea Banfi, Wolfgang Holnthoner, Mikaël M. Martino and Seppo Ylä-Herttuala

PUBLISHED IN: Frontiers in Bioengineering and Biotechnology and Frontiers in Cardiovascular Medicine

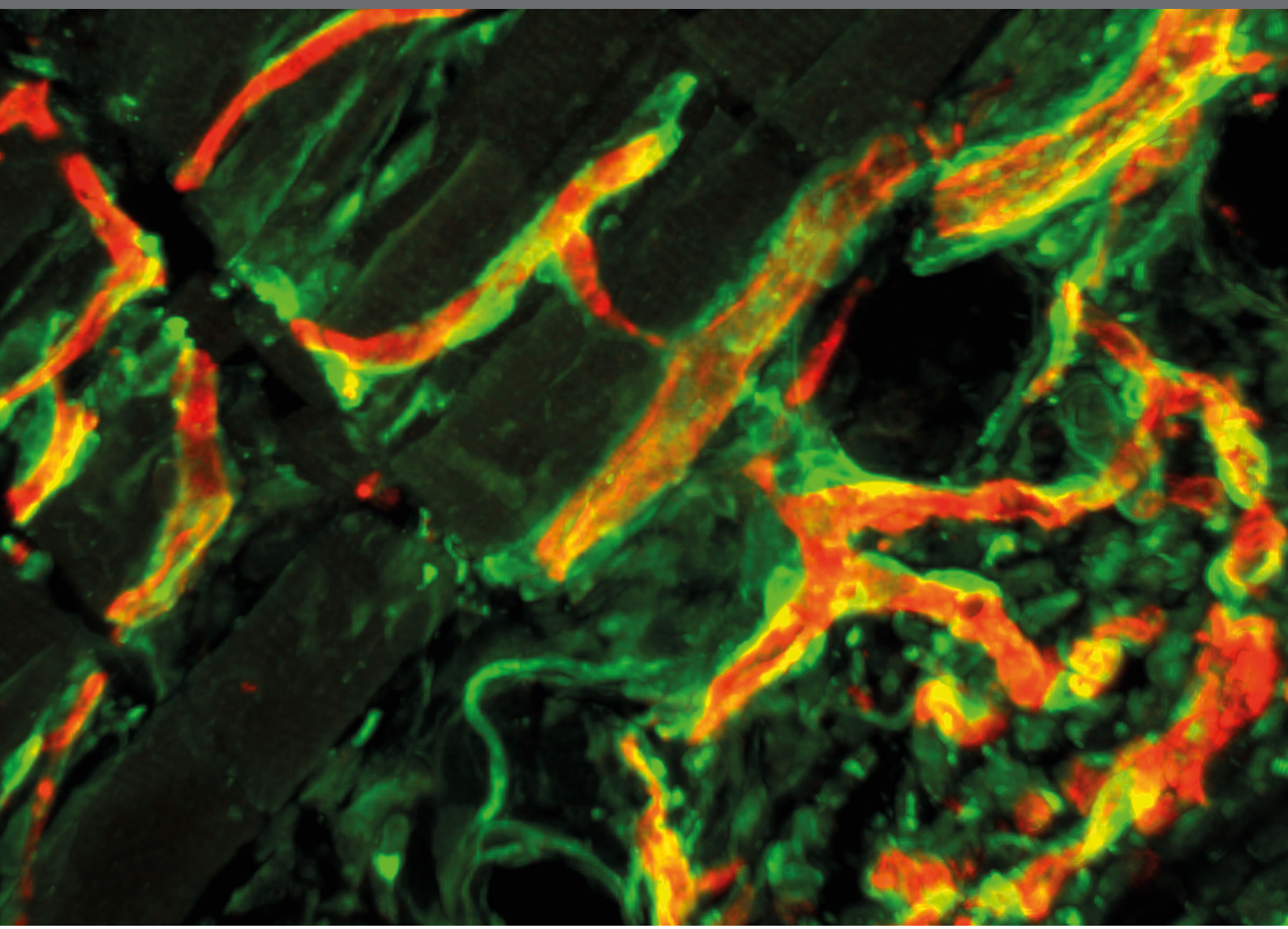

frontiers Research Topics

frontiers

ISSN 1664-8714
ISBN 978-2-88945-746-5
DOI 10.3389/978-2-88945-746-5

About Frontiers

Frontiers is more than just an open-access publisher of scholarly articles: it is a pioneering approach to the world of academia, radically improving the way scholarly research is managed. The grand vision of Frontiers is a world where all people have an equal opportunity to seek, share and generate knowledge. Frontiers provides immediate and permanent online open access to all its publications, but this alone is not enough to realize our grand goals.

Frontiers Journal Series

The Frontiers Journal Series is a multi-tier and interdisciplinary set of open-access, online journals, promising a paradigm shift from the current review, selection and dissemination processes in academic publishing. All Frontiers journals are driven by researchers for researchers; therefore, they constitute a service to the scholarly community. At the same time, the Frontiers Journal Series operates on a revolutionary invention, the tiered publishing system, initially addressing specific communities of scholars, and gradually climbing up to broader public understanding, thus serving the interests of the lay society, too.

Dedication to Quality

Each Frontiers article is a landmark of the highest quality, thanks to genuinely collaborative interactions between authors and review editors, who include some of the world's best academicians. Research must be certified by peers before entering a stream of knowledge that may eventually reach the public - and shape society; therefore, Frontiers only applies the most rigorous and unbiased reviews.
Frontiers revolutionizes research publishing by freely delivering the most outstanding research, evaluated with no bias from both the academic and social point of view. By applying the most advanced information technologies, Frontiers is catapulting scholarly publishing into a new generation.

What are Frontiers Research Topics?

Frontiers Research Topics are very popular trademarks of the Frontiers Journals Series: they are collections of at least ten articles, all centered on a particular subject. With their unique mix of varied contributions from Original Research to Review Articles, Frontiers Research Topics unify the most influential researchers, the latest key findings and historical advances in a hot research area! Find out more on how to host your own Frontiers Research Topic or contribute to one as an author by contacting the Frontiers Editorial Office: researchtopics@frontiersin.org

VASCULARIZATION FOR REGENERATIVE MEDICINE

Topic Editors:
Andrea Banfi, Basel University Hospital, Switzerland
Wolfgang Holnthoner, Ludwig Boltzmann Institute for Experimental and Clinical Traumatology, Austria
Mikaël M. Martino, Monash University, Australia
Seppo Ylä-Herttuala, University of Eastern Finland, Finland

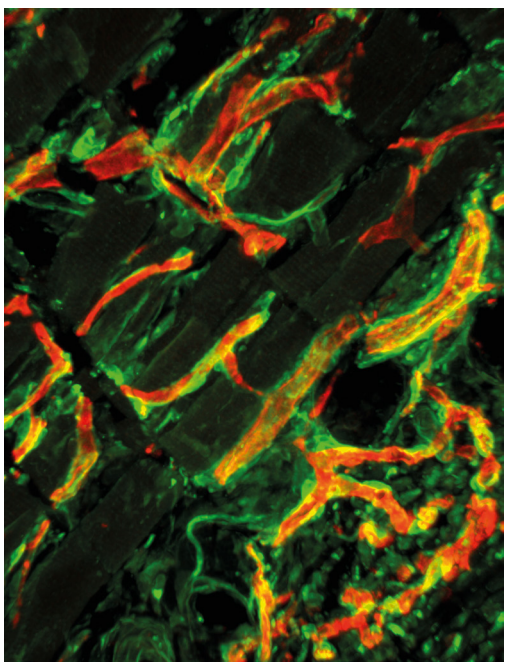

Microvascular network in the panniculus carnosus muscle layer of mouse skin, induced by angiogenic growth factor delivery. Endothelium is stained in red (podocalyxin) and pericytes in green (NG2).
Image courtesy of Dr. Roberto Gianni-Barrera (Department of Biomedicine, Basel University Hospital).

Citation: Banfi, A., Holnthoner, W., Martino, M. M., Ylä-Herttuala, S., eds. (2019). Vascularization for Regenerative Medicine. Lausanne: Frontiers Media. doi: 10.3389/978-2-88945-746-5

Table of Contents

PART C

PRE-VASCULARIZATION STRATEGIES AND TISSUE ENGINEERING

frontiers in Bioengineering and Biotechnology

EDITORIAL
published: 21 November 2018
doi: 10.3389/fbioe.2018.00175

Editorial: Vascularization for Regenerative Medicine

Andrea Banfi[1]*, *Wolfgang Holnthoner*[2], *Mikaël M. Martino*[3] and *Seppo Ylä-Herttuala*[4]

[1] Department of Biomedicine, University Hospital, University of Basel, Basel, Switzerland, [2] AUVA Research Centre, Ludwig Boltzmann Institute for Experimental and Clinical Traumatology, Vienna, Austria, [3] European Molecular Biology Laboratory Australia, Australian Regenerative Medicine Institute, Monash University, Melbourne, VIC, Australia, [4] A.I. Virtanen Institute for Molecular Sciences, Univeristy of Eastern Finland, Kuopio, Finland

Keywords: angiogenesis, lymphangiogeneis, vascularization, tissue engineeering, regenerative medicine

Editorial on the Research Topic

Vascularization for Regenerative Medicine

The generation of functional vascular networks is crucial for regenerative medicine, especially for the survival of engineered tissue grafts on one hand and blood flow restoration to ischemic tissues on the other.

Tissue engineering aims at developing biological substitutes to replace traumatic, neoplastic, or degenerative tissue loss, by the *in vitro* culture of appropriate progenitors with suitable material scaffolds. However, upon implantation *in vivo*, a major challenge for clinically relevant large-size grafts is the maintenance of cell viability in the core of the scaffold, which critically depends on the rapid invasion of the construct by the host blood vessels. In fact, diffusion from the surrounding blood vascular bed only reaches the outer shell of the graft, resulting in cell death in the central core of the implants and limiting tissue ingrowth to the outer 1–2 mm (Grosso et al., 2017). Furthermore, the presence of a functional vasculature also allows the recruitment of highly specialized cells, like circulating tissue progenitors or reparative myeloid cells, which can contribute to tissue regeneration and remodeling (Lo Sicco et al., 2015). The regulation of vascular growth and tissue regeneration by immune cells is also an emerging area of significant interest (Lo Sicco and Tasso, 2017). Finally, removal of interstitial fluid, comprising extravasated cells, proteins and lipids, through uptake by lymphatic capillaries and return to the blood stream by larger lymphatic vessels represents one of the challenges in vascular regeneration (Schaupper et al., 2016). Therefore, rapid vascularization within days of *in vivo* implantation is of vital importance for survival and function of tissue-engineered grafts of clinically relevant size and one of the major limiting factors toward their implementation for patient treatment.

On the other hand, ischemic conditions, due for example to atherosclerotic artery occlusion, still cause significant morbidity and mortality, which are not solved by current medical and surgical treatments (Benjamin et al., 2018). Hence there is an urgent need for new treatment strategies: therapeutic angiogenesis aims at stimulating the growth of new microvascular networks by local delivery of angiogenic factors and the subsequent functional remodeling of new collateral arteries, i.e. arteriogenesis (Annex, 2013).

Angiogenesis and lymphangiogenesis are complex and highly regulated processes (Potente et al., 2011). The design of rational therapeutic approaches stands to greatly benefit from a thorough understanding of the cellular and molecular mechanisms underlying the physiological growth and remodeling of vascular structures under therapeutic conditions.

This Frontiers Research Topic brings together contributions investigating different facets of promoting vascularization in tissue reconstruction and repair, spanning from basic mechanisms of blood and lymphatic vessel biology, to the study and quantification of vascularization dynamics *in vivo* under therapeutic conditions, to the translational aspects and challenges of achieving efficient vascularization of tissue-engineered grafts or even whole organs.

OPEN ACCESS

Edited by:
Ranieri Cancedda, Biorigen Srl., Italy

Reviewed by:
Giuseppe Orlando, Wake Forest School of Medicine, United States

***Correspondence:**
Andrea Banfi
Andrea.Banfi@usb.ch

Specialty section:
This article was submitted to Tissue Engineering and Regenerative Medicine, a section of the journal Frontiers in Bioengineering and Biotechnology

Received: *20 September 2018*
Accepted: *05 November 2018*
Published: *21 November 2018*

Citation:
Banfi A, Holnthoner W, Martino MM and Ylä-Herttuala S (2018) Editorial: Vascularization for Regenerative Medicine. Front. Bioeng. Biotechnol. 6:175. doi: 10.3389/fbioe.2018.00175

The importance of angiogenesis and lymphangiogenesis in regenerative medicine is highlighted by four articles, which describe several transcription factors, growth factors, and microRNAs important for stem cell and progenitor cell differentiation to mature endothelial cells, capillary sprouting and formation of large arteries and lymphatic vessels. Sturtzel et al. describe the importance of forkhead box transcription factor (FOXF1) in endothelial colony-forming cells, where it was found to stimulate vascular sprouting by inducing Notch2 receptors and augmenting expression of VEGF Receptor-2 and EphrinB2. Results were verified with knockdown experiments and in a zebrafish model. Along the same lines Belt et al. describe dynamics of gene expression during endothelial cell differentiation from human iPS cells. They provide the first systematic characterization and comparative analysis of seven different small molecule-mediated differentiation protocols to induce optimal endothelial cell phenotype. Key points appear to be early inhibition of Rho-associated kinase, activation of cyclic AMP signaling and inhibition of TGF-β signaling.

Improved tissue perfusion is not possible without generation of large arteries since capillaries alone cannot provide enough perfusion for large tissue masses. Heuslein et al. show that anti-miRNA-146a improved ischemic peripheral muscle perfusion and collateral artery diameters even though it did not have any significant effects on angiogenesis. Thus, different mechanisms appear to regulate large blood vessel formation and angiogenesis. This should be taken into account in therapeutic approaches. It has recently been recognized that equally important to stimulation of blood vessel growth is the adequate function of lymphatic vessels in ischemic tissues. Rauniyar et al. review the important role of VEGF-C in regulating the growth of lymphatic vessels. They show that VEGF-C biosynthesis has several steps and protolytic processing significantly affects VEGF-C biodistribution, receptor activation and growth of lymphatic vessels. Recognizing these properties will be essential for the utilization of VEGF-C for regenerative purposes *in vivo*.

Co-cultures of endothelial cells and supporting cells are widely used to generate microvasculature and pre-vascularized engineered grafts. Knezevic et al. show that blood vascular endothelial cells form stable and sustainable networks by using a co-culture model with adipose-derived stromal cells in fibrin matrix. Not only blood vessel networks, but also lymphatic networks are required for tissue constructs and the team shows that it can be achieved via VEGF-C. Landau et al. show migration of endothelial cells in the depths of the scaffold, resulting in microvasculature surrounded by supporting cells with different location-dependent phenotypes. The assessment of angiogenesis *in vivo* can still be challenging. Slezak et al. present a novel low-cost rat model to study angiogenesis, enabling spatial assessment of vascularization by a simple implantation procedure. Mesenchymal stem cells provide beneficial paracrine factors that improve cardiac function and regeneration, but their therapeutic potential depends on the method of delivery. Zlabinger et al. demonstrate that intracoronary delivery leads to diminished blood flow and impaired cell homing compared to intramyocardial injection through elevated MMP-2 and decreased expression of the homing factor CXCR4.

Finally, Pellegata et al. review the numerous approaches aiming at regenerating the full vascular tree of decellularized tissues for whole-organ engineering, while Carrabba and Madeddu review scaffold-based and cell-based approaches that have been developed to create tissue-engineered vascular grafts in the last decades. Notably, the review highlights the attempts made to translate the strategies from bench to bedside.

AUTHOR CONTRIBUTIONS

All authors listed wrote the manuscript and approved it for publication.

REFERENCES

Annex, B. H. (2013). Therapeutic angiogenesis for critical limb ischaemia. *Nat. Rev. Cardiol.* 10, 387–396. doi: 10.1038/nrcardio.2013.70

Benjamin, E. J., Virani, S. S., Callaway, C. W., Chamberlain, A. M., Chang, A. R., Cheng, S., et al. (2018). Heart disease and stroke statistics-2018 update: a report from the american heart association. *Circulation* 137, e67–e492. doi: 10.1161/CIR.0000000000000558

Grosso, A., Burger, M. G., Lunger, A., Schaefer, D. J., Banfi, A., and Di Maggio, N. (2017). It takes two to tango: coupling of angiogenesis and osteogenesis for bone regeneration. *Front. Bioeng. Biotechnol.* 5:68. doi: 10.3389/fbioe.2017.00068

Lo Sicco, C., and Tasso, R. (2017). Harnessing endogenous cellular mechanisms for bone repair. *Front. Bioeng. Biotechnol.* 5:52. doi:10.3389/fbioe.2017.00052

Lo Sicco, C., Tasso, R., Reverberi, D., Cilli, M., Pfeffer, U., and Cancedda, R. (2015). Identification of a new cell population constitutively circulating in healthy conditions and endowed with a homing ability toward injured sites. *Sci. Rep.* 5:16574. doi: 10.1038/srep16574

Potente, M., Gerhardt, H., and Carmeliet, P. (2011). Basic and therapeutic aspects of angiogenesis. *Cell* 146, 873–887. doi: 10.1016/j.cell.2011.08.039

Schaupper, M., Jeltsch, M., Rohringer, S., Redl, H., and Holnthoner, W. (2016). Lymphatic vessels in regenerative medicine and tissue engineering. *Tissue Eng. Part B Rev.* 22, 395–407. doi: 10.1089/ten.teb.2016.0034

Conflict of Interest Statement: The authors declare that the research was conducted in the absence of any commercial or financial relationships that could be construed as a potential conflict of interest.

frontiers in Bioengineering and Biotechnology

REVIEW
published: 12 February 2018
doi: 10.3389/fbioe.2018.00007

Biology of Vascular Endothelial Growth Factor C in the Morphogenesis of Lymphatic Vessels

*Khushbu Rauniyar[1], Sawan Kumar Jha[1] and Michael Jeltsch[1,2]**

[1] *Translational Cancer Biology Research Program, University of Helsinki, Helsinki, Finland,* [2] *Wihuri Research Institute, Biomedicum Helsinki, Helsinki, Finland*

Because virtually all tissues contain blood vessels, the importance of hemevascularization has been long recognized in regenerative medicine and tissue engineering. However, the lymphatic vasculature has only recently become a subject of interest. Central to the task of growing a lymphatic network are lymphatic endothelial cells (LECs), which constitute the innermost layer of all lymphatic vessels. The central molecule that directs proliferation and migration of LECs during embryogenesis is vascular endothelial growth factor C (VEGF-C). VEGF-C is therefore an important ingredient for LEC culture and attempts to (re)generate lymphatic vessels and networks. During its biosynthesis VEGF-C undergoes a stepwise proteolytic processing, during which its properties and affinities for its interaction partners change. Many of these fundamental aspects of VEGF-C biosynthesis have only recently been uncovered. So far, most—if not all—applications of VEGF-C do not discriminate between different forms of VEGF-C. However, for lymphatic regeneration and engineering purposes, it appears mandatory to understand these differences, since they relate, e.g., to important aspects such as biodistribution and receptor activation potential. In this review, we discuss the molecular biology of VEGF-C as it relates to the growth of LECs and lymphatic vessels. However, the properties of VEGF-C are similarly relevant for the cardiovascular system, since both old and recent data show that VEGF-C can have a profound effect on the blood vasculature.

Keywords: vascular endothelial growth factor C, lymphatic vessels, lymphedema, tissue engineering, A disintegrin and metalloproteinase with thrombospondin motifs 3, collagen and calcium binding EGF domains 1, growth factors, VEGF receptors

OPEN ACCESS

Edited by:
Wolfgang Holnthoner, Ludwig Boltzmann Gesellschaft (LBG), Austria

Reviewed by:
Joaquim Miguel Oliveira, University of Minho, Portugal
Mikaël M. Martino, Monash University, Australia
Arnaud Scherberich, University Hospital Basel, Switzerland

****Correspondence:***
Michael Jeltsch
michael@jeltsch.org

Specialty section:
This article was submitted to Tissue Engineering and Regenerative Medicine, a section of the journal Frontiers in Bioengineering and Biotechnology

Received: *01 November 2017*
Accepted: *19 January 2018*
Published: *12 February 2018*

Citation:
Rauniyar K, Jha SK and Jeltsch M (2018) Biology of Vascular Endothelial Growth Factor C in the Morphogenesis of Lymphatic Vessels. Front. Bioeng. Biotechnol. 6:7. doi: 10.3389/fbioe.2018.00007

INTRODUCTION

Lymphatic endothelial cells (LECs) form the innermost layer of lymphatic vessels, and they play a central role during the growth of the lymphatic system (Bautch and Caron, 2015). Lymphatic insufficiency can be the result of an underdeveloped lymphatic network (Butler et al., 2009), and hence the idea of growing lymphatic structures has been proposed early on as a potential treatment strategy for lymphedema (Karkkainen et al., 2001a; Saaristo et al., 2002). Irrespective of whether these structures are regrown *in situ* (Karkkainen et al., 2001b; Dai et al., 2010; Moriondo et al., 2010; Güç et al., 2017) or *in vitro* (Helm et al., 2007; Gibot et al., 2017; Knezevic et al., 2017), the growth and assembly of LECs into vessels and networks are central to the task of lymphatic engineering (Kanapathy et al., 2014; Schaupper et al., 2016).

Therefore, it is appropriate—when setting out to (re)construct lymphatic vessels—to get familiar with LEC proliferation, migration, assembly, and maintenance. The central growth factor that

mediates these tasks is vascular endothelial growth factor C (VEGF-C). While being a member of the VEGF family of growth factors, VEGF-C is in many aspects very different from the vascular endothelial growth factor prototype VEGF-A.

VEGFs AND VEGF RECEPTORS (VEGFRs)

The primary receptors of all VEGF family members are tyrosine kinase receptors. With certain exceptions (Olsson et al., 2006), they are only expressed by endothelial cells. However, all three VEGFRs (VEGFR-1, -2 and -3) are not equally distributed on endothelial cells. In the adult organism, VEGFR-3 expression is largely restricted to LECs (Kaipainen et al., 1995), while VEGFR-1 expression is very low on LECs (Shibuya, 2001), and VEGFR-2 can be found both on LECs and blood vascular endothelial cells (BECs) (Holmes et al., 2007). VEGFRs are activated by dimerization, which is achieved by the dimeric nature of the VEGF ligands. The two receptor binding epitopes of each VEGF ligand are composite epitopes and are absent in monomeric VEGF species (Muller et al., 1997). Hence, monomeric VEGF species bind their respective receptors only with low affinity (Fuh et al., 1998) or not at all (Grunewald et al., 2010).

Apart from the VEGFRs, most VEGFs bind to co-receptors, which stabilize the VEGF/VEGFR interaction and increase the effective growth factor concentration on the cell surface, for example, neuropilins (Grunewald et al., 2010), integrins (Soldi et al., 1999), or syndecans (Johns et al., 2016). However, these interactions are typically of lower affinity than the VEGF/VEGFR interaction (Soker et al., 2002).

In humans, five different genes encode VEGF family members: *VEGFA*, *VEGFB*, *VEGFC*, *VEGFD*, and *PGF* (placenta growth factor), respectively. Each VEGF can be roughly categorized as being hemangiogenic (VEGF-A, PlGF, and VEGF-B) or lymphangiogenic (VEGF-C and VEGF-D). Unique to the hemangiogenic VEGFs is their interaction with VEGFR-1, while only members of the lymphangiogenic group do interact with VEGFR-3. VEGFR-2, which is the receptor that drives proliferation and migration of BECs, can be activated by some but not all members from both groups (see **Figure 1**).

All VEGF family members are characterized by the central VEGF homology domain (VHD, aka PDGF/VEGF domain)

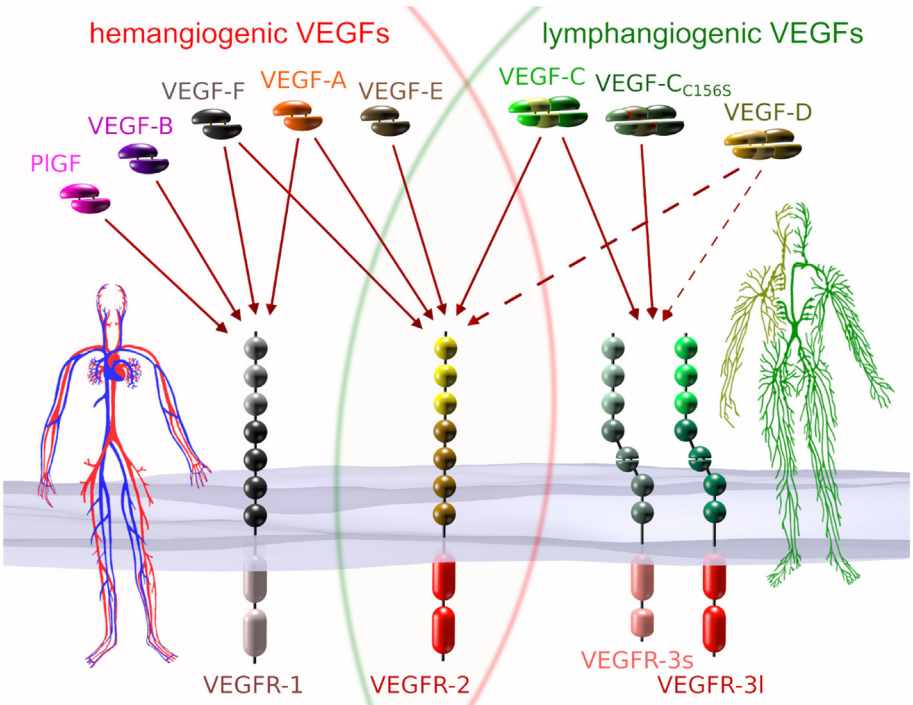

FIGURE 1 | VEGFs and VEGF receptors (VEGFRs). Each of the five mammalian VEGFs [PlGF, VEGF-A to -D], the viral VEGF-E, and the snake venom VEGF-F interacts specifically with a certain subset of the three VEGFRs. VEGF-C_{C156S} is an engineered vascular endothelial growth factor C (VEGF-C) variant that interacts predominantly with VEGF receptor 3 (VEGFR-3) (Joukov et al., 1998). VEGFs that interact with all three receptors do not naturally exist, but have been engineered (Jeltsch et al., 2006). VEGF receptor 1 (VEGFR-1) and VEGF receptor 2 (VEGFR-2) are expressed on blood vascular endothelial cells (BECs), while VEGFR-2 and VEGFR-3 are expressed on lymphatic endothelial cells. VEGFR-3 is the primary mitogenic receptor for lymphatic endothelium, while VEGFR-2 is the primary mitogenic receptor for blood vascular endothelium. Exclusive to higher primates is the appearance of a short splice isoform of VEGFR-3 (VEGFR-3s) (Pajusola et al., 1993; Borg et al., 1995; Hughes, 2001). Signaling pathways activated by VEGFR-3s are partially distinct from those activated by the long splice isoform (VEGFR-3l), since it lacks some of the phosphorylation sites required for mediator docking (e.g., for Shc-Grb2) (Fournier et al., 1995; Dixelius et al., 2003). The dotted arrows from VEGF-D indicate heterogeneous binding patterns. While mature human VEGF-D can activate VEGFR-2, this seems not to be the case for mouse VEGF-D (Baldwin et al., 2001), and consequently, VEGF-D function could have diverged since the evolutionary divide some 60–65 million years ago (O'Leary et al., 2013). Additionally, human VEGF-D can selectively lose its affinity for VEGFR-3 after proteolytic processing (Leppanen et al., 2011).

(EMBL-EBI, 2017). The VHD contains the receptor binding domain and features a pattern of characteristically spaced cysteine residues, which gives rise to a cystine knot (Holmes and Zachary, 2005). In addition to the VHD, most VEGFs feature accessory sequences that further delineate the specific properties of individual VEGFs: the affinity of, e.g., VEGF-A to the co-receptors neuropilin-1 and -2 (NP-1 and NP-2) (Neufeld et al., 2002), or of VEGF-C to the co-receptor NP-2 (Karpanen et al., 2006; Xu et al., 2010), heparan sulfate proteoglycans (HSPGs) (Johns et al., 2016), and to the extracellular matrix (Jha et al., 2017). In VEGF-C and VEGF-D, the N- and C-terminal accessory sequences are exceptionally long and function as propeptides, which fold into own domains (see **Figure 2**) and need to be removed for activation by two proteolytic cleavages.

While only five genes encode the mammalian VEGFs, the actual number of different VEGFs is much larger. Within the hemangiogenic VEGFs, functional diversity is generated mostly by alternative splicing, resulting in differences in the affinity for HSPGs ("heparin affinity") (Robinson and Stringer, 2001). For VEGF-C, no functions have been assigned yet to the described alternative splice variants (Lee et al., 1996; Ensembl, 2016).

THE LYMPHANGIOGENIC VEGFs

Vascular endothelial growth factor C was discovered more than 20 years ago as a binding partner of VEGFR-3 from the cell culture supernatant of the human prostate cancer cell line PC3 (Joukov et al., 1996). In the same year, also murine VEGF-C was described and initially named VRP (VEGF-related protein) (Lee et al., 1996). The specific lymphangiogenic properties of VEGF-C were demonstrated in various animal models (Jeltsch et al., 1997; Oh et al., 1997). VEGF-D is the second member of the lymphangiogenic VEGF subgroup. It was discovered independently by three research teams and named once FIGF (c-fos-induced growth factor) (Orlandini et al., 1996) and twice VEGF-D (Yamada et al., 1997; Achen et al., 1998). Both VEGF-C and VEGF-D use posttranslational modification by proteolytic cleavage to generate molecular species diversity (Joukov et al., 1997b; Stacker et al., 1999), but the proteases are different (Bui et al., 2016). While VEGF-D shares many similarities with VEGF-C, it cannot replace VEGF-C (see the VEGF-D paragraph).

DIFFERENT VEGF-C FORMS, THE VEGF-C_{C156S} MUTANT AND ANGIOGENIC "SIDE EFFECTS"

The most prominent differences between the different VEGF-C forms are the affinities for the receptors, co-receptors, and the extracellular matrix. With increasing processing (see **Figure 2**), VEGF-C's affinity for both VEGFR-2 and VEGFR-3 increases, and fully processed mature VEGF-C

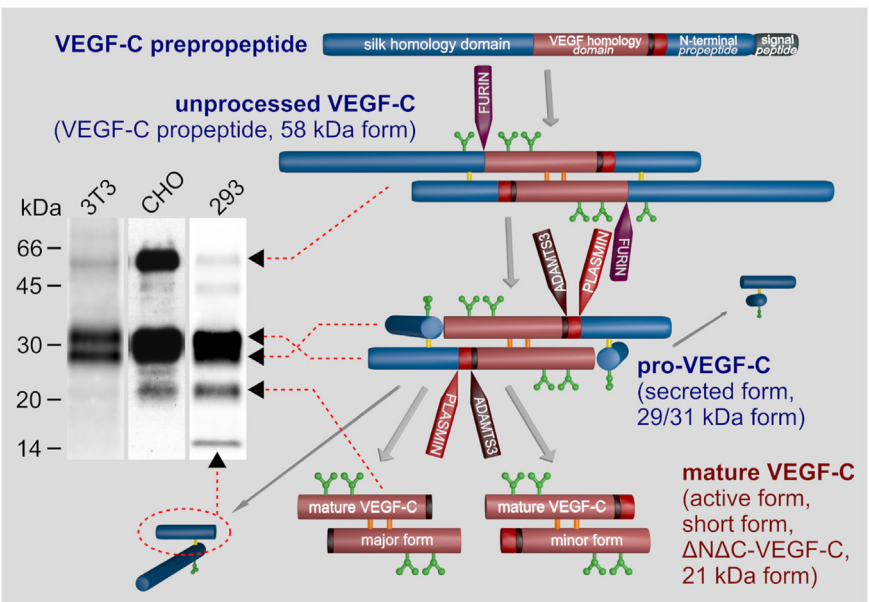

FIGURE 2 | Biosynthesis and activation of vascular endothelial growth factor C (VEGF-C). VEGF-C is produced as an inactive propeptide. Proprotein convertases such as furin, PC5, or PC7 cleave between the VEGF homology domain and the C-terminal silk homology domain resulting in pro-VEGF-C. The silk homology domain is not removed by this cleavage, but remains covalently connected *via* cysteine bridges to the rest of pro-VEGF-C (Joukov et al., 1997b). Pro-VEGF-C is able to bind VEGFR-3, but does not activate it (Jeltsch et al., 2014). The second proteolytic cleavage by A disintegrin and metalloproteinase with thrombospondin motifs 3 (ADAMTS3) removes both terminal domains resulting in mature, active VEGF-C. Cleavage by ADAMTS3 results in the major form of the mature VEGF-C, which is nine amino acids shorter compared to the minor form, which is likely a product of plasmin cleavage (Joukov et al., 1998; Baldwin et al., 2001; Jeltsch et al., 2014). Three N-glycosylation sites are found in VEGF-C (shown in green). Alternative names for different VEGF-C forms are given in brackets. The band pattern of VEGF-C produced from a full-length cDNA resolved by SDS-PAGE depends on the expressing cell line, expression levels and the antibody used for immunoprecipitation and/or Western blotting. 3T3 fibroblasts produce almost exclusively pro-VEGF-C. In high-level-expressing CHO cells, a significant fraction of the secreted protein can remain unprocessed. Among the most efficiently processing cells are 293 cells, but pro-VEGF-C still represents the majority of the VEGF-C protein.

is therefore not only lymphangiogenic but also angiogenic (Joukov et al., 1997a; Anisimov et al., 2009) and induces the permeability of blood vessels (Joukov et al., 1997b). To identify which functions of VEGF-C are mediated by which receptor (VEGFR-2 versus VEGFR-3), the VEGF-C_{C156S} mutant was developed (Joukov et al., 1998) (commercially available from R&D systems as 752-VC or its rat homolog from Reliatech as R20-016). This mutant largely lacks VEGFR-2 affinity and can therefore be used to exclude VEGF-C effects on the blood vasculature (Veikkola et al., 2001). However, despite its dual receptor binding, the effect of wild type VEGF-C on the blood vasculature is minimal in many models, and recent data suggest that the localization of pro-VEGF-C on LEC surfaces prior to activation could explain this specificity (Jha et al., 2017). Most reports that attribute a prominent angiogenic effect to VEGF-C have investigated prenatal development (Oh et al., 1997; Lohela et al., 2008) or used VEGF-C forms lacking the propeptides (Oh et al., 1997; Cao et al., 1998; Sweat et al., 2014). The propeptides keep VEGF-C inactive (Joukov et al., 1997b), are required for localizing VEGF-C (Jha et al., 2017), and are removed by sequential proteolysis by furin (Siegfried et al., 2003) and A disintegrin and metalloproteinase with thrombospondin motifs 3 (ADAMTS3) (Jeltsch et al., 2014) or plasmin (McColl et al., 2003).

The relationship between affinity and receptor activation is not straightforward: pro-VEGF-C is able to bind VEGFR-3 under cooperation of NP-2 without any detectable receptor activation. In fact, it is even a competitive inhibitor of mature VEGF-C for VEGFR-3 activation (Jeltsch et al., 2014).

VEGF-D

VEGF-D is the closest paralog of VEGF-C (Achen et al., 1998). The angiogenic potential of mature VEGF-D has been shown to be stronger compared to mature VEGF-C (Rissanen et al., 2003), which is explained by the fact that maximally processed VEGF-D exclusively binds to VEGFR-2, while VEGF-C retains in its maximally processed form the capacity to bind VEGFR-3 (Leppanen et al., 2011). It is differently activated than VEGF-C (Bui et al., 2016), and because the proteolytic environment is difficult to predict and control, the use of VEGF-D for LEC stimulation remains problematic. Moreover, *Vegfd* gene-deleted mice have no lymphatic phenotype arguing for no major role in the development of the murine lymphatic system (Baldwin et al., 2005).

REQUIREMENT FOR COLLAGEN AND CALCIUM BINDING EGF DOMAINS 1 (CCBE1) AND ADAMTS3

The two molecules that are required for the proteolytic activation of VEGF-C are the CCBE1 protein and the ADAMTS3 protease. ADAMTS3 catalyzes the final step in the proteolytic processing of VEGF-C, removing the N-terminal propeptide and releasing the fully active, mature VEGF-C (Jeltsch et al., 2014; see **Figure 2**). *In vitro*, large amounts of ADAMTS3 are able to activate pro-VEGF-C, but *in vivo*, ADAMTS3 requires the assistance of CCBE1 for the efficient activation of VEGF-C. CCBE1 enhances the VEGF-C activation by two different mechanisms: it increases the processivity of the ADAMTS3 enzyme (Roukens et al., 2015) and it colocalizes VEGF-C and ADAMTS3 on cell surfaces and ECM to form the trimeric activation complex (Bui et al., 2016; Jha et al., 2017). Similar to *Vegfc*, the genetic ablation of either *Ccbe1* or *Adamts3* in mice results in a general halt of lymphatic development (Bos et al., 2011; Hagerling et al., 2013; Janssen et al., 2015).

A disintegrin and metalloproteinase with thrombospondin motifs 3 cleavage results in the so-called "major" form of mature VEGF-C (Joukov et al., 1998; Jeltsch et al., 2014). The so-called "minor" form is nine amino acids longer at its N-terminus and is presumably generated by plasmin. Plasmin might activate VEGF-C during wound healing and inflammatory processes (McColl et al., 2003), where it could rapidly release large amounts of active VEGF-C from matrix-bound, "latent" pro-VEGF-C. However, it is still unclear, whether there is any difference between the lymphangiogenesis response to the "major" and "minor" forms of mature VEGF-C.

To bypass the complex proteolytic maturation of VEGF-C, the recombinant production of mature VEGF-C is almost exclusively done from a truncated cDNA. However, this is not without problems, since VEGF-C contains in its VHD—as opposed to VEGF-A—an extra cysteine residue (Cys 137), which interferes with intermolecular disulfide bond formation (Chiu et al., 2014) and protein stability (Anisimov et al., 2009; Leppanen et al., 2011) (see **Figure 3**). It has been proposed that when produced from a full-length cDNA, cysteine residues from the VEGF-C propeptides could protect Cys 137 and thus facilitate correct disulfide bond formation in the VHD.

THE ENIGMATIC "SILK HOMOLOGY" DOMAIN

Very intriguing is the repetitive arrangement of cysteine residues ($CX_{10}CXCXC$) in the C-terminal propeptide of VEGF-C. This signature is unique within vertebrate proteins, and its phylogenetic origin remains unknown. Except in VEGF-C, it occurs, e.g., in the balbiani ring protein 3 and salivary proteins of silk weaving mosquito larvae of the genus Chironomus (Dignam and Case, 1990). Therefore, the term "silk homology domain" was coined to describe the C-terminal propeptide (Joukov et al., 1996). In addition to regulating the activity of VEGF-C, this domain endows the molecule with most of its heparin affinity (Johns et al., 2016), and it is the determining factor for the ECM sequestration of VEGF-C (Jha et al., 2017). Interestingly, sequestration and proteolysis-mediated release of active VEGF-C have also been reverse engineered by concatenating a fibrin-binding (FB) and a MMP-degradable polypeptide sequence N-terminally to the mature VEGF-C sequence (Güç et al., 2017). This protein (FB-VEGF-C) compared favorably to mature VEGF-C in the local induction of lymphangiogenesis, but native sequestration of wild-type VEGF-C expressed from a full-length cDNA was not included in this comparison.

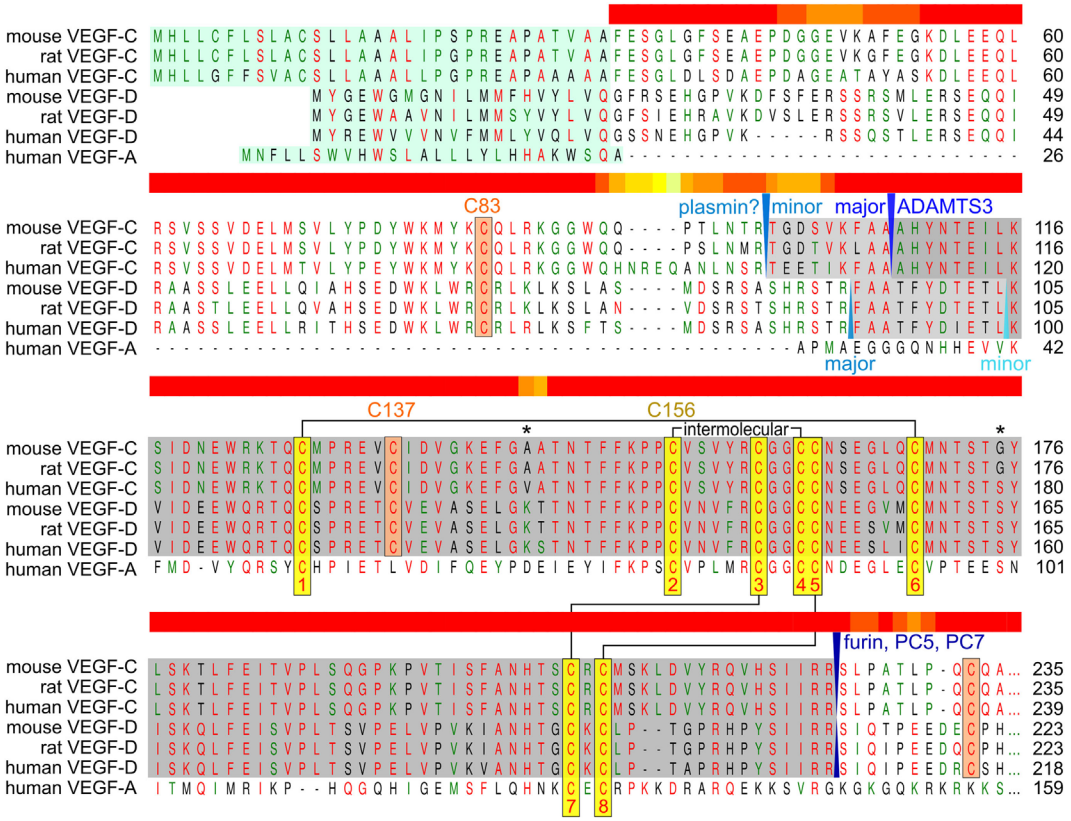

FIGURE 3 | Alignment of human, mouse, and rat vascular endothelial growth factor C (VEGF-C)/D with human VEGF-A. The sequences of the active, mature VEGF-C/D are boxed gray. Proteolytic cleavage sites and enzymes (if known) are indicated in blue colors. The signal peptide is boxed green. The eight conserved cysteines of the PDGF/VEGF signature (Muller et al., 1997) are boxed yellow and intra- and intermolecular disulfide bridges are indicated by black connecting lines. VEGF-C/D-specific conserved cysteine residues are boxed in orange. The two asterisks denote the only two amino acid residues that are different between fully processed mouse and human VEGF-C. Cysteine 156, which is mutated to serine in the VEGFR-3-monospecific variant VEGF-C_{C156S}, participates in the intermolecular cystine bridge (Joukov et al., 1998). When mature VEGF-C is produced from a truncated cDNA, the single cysteine 137 remains unpaired decreasing protein stability (Anisimov et al., 2009; Leppanen et al., 2011). When pairing with cysteine 156, cysteine 137 interferes with intermolecular disulfide bond formation and protein folding, explaining the observation of significant amounts of single-linked dimers, non-covalent VEGF-C dimers and VEGF-C monomers (Joukov et al., 1996; Jeltsch et al., 2006; Chiu et al., 2014). Above the alignment, a heat map indicates the areas of highest divergence, deduced from a more comprehensive alignment of VEGF-A, -C, and -D. The C-terminal domains of VEGF-C/D are not shown.

REGULATION OF VEGF-C SIGNALING

Compared to VEGF-A, not much is known about the regulation of VEGF-C expression *in vivo*. The fact that VEGF-C is produced as an inactive precursor (pro-VEGF-C) indicates that much of its regulation happens after its constitutive secretion at the level of proteolytic activation. However, while the activation mechanism itself has been studied extensively (Jeltsch et al., 2014; Roukens et al., 2015; Bui et al., 2016; Jha et al., 2017), virtually nothing is known about the regulation of the obligatory protease ADAMTS3 and its cofactor CCBE1.

In the adult organism, inflammation potently upregulates VEGF-C expression, most notably by macrophages (Ristimäki et al., 1998; Baluk et al., 2005; Krebs et al., 2012), resulting in a negative feedback loop (Zhou et al., 2011; Christiansen et al., 2016) promoting resolution in some models, while aggravating the situation in others (Kim et al., 2014).

The interstitial pressure that builds up during development in blood-vascularized but lymphatic-free tissues leads *via* β1-integrin-mediated mechanoinduction to enhanced VEGFR-3 phosphorylation (Planas-Paz et al., 2012). However, it remains unclear, whether meaningful VEGFR-3 phosphorylation can happen *in vivo* entirely without ligand, although the kinase activity of VEGFR-3 is dispensable *in vitro* (Galvagni et al., 2010). In any case, the interplay of mechanical forces with growth factor signaling for the establishment of functional lymphatic networks has been shown in many systems (Sabine et al., 2016). Binding of mature VEGF-C to VEGFR-3 results in the activation of both the MAPK/ERK and AKT intracellular signaling pathways (Mäkinen et al., 2001; Deng et al., 2015), which promote survival, growth, and migration in LECs (Mäkinen et al., 2001).

VEGF-C SIGNALING IN EMBRYONIC DEVELOPMENT

VEGF receptor 3 was discovered before VEGF-C and VEGF-D, and therefore, VEGFR-3 was between 1992 and 1996 an "orphan

receptor", i.e., a receptor without known ligand. However, soon after the discovery of VEGFR-3, the specific expression pattern of VEGFR-3 suggested that its function was closely related to the lymphatic system. In the early stages of embryonic development, all endothelial cells express VEGFR-3, but its expression becomes progressively restricted to LECs (Kaipainen et al., 1995). Finally, VEGFR-3 expression becomes sufficiently specific for LECs that it has been used to identify LECs (Petrova et al., 2008), despite the existence of other VEGFR-3 expressing endothelial cells, e.g., angiogenic, sinusoidal, and fenestrated BECs.

The pivotal role of the VEGFR-3 ligand VEGF-C in the establishment of the lymphatic vasculature is witnessed by the fact that mice devoid of VEGF-C do not develop any lymphatic structures and form generalized edema from E12.5, resulting in embryonic death around E16.5 (Karkkainen et al., 2004).

Interestingly, mice devoid of the VEGF-C receptor VEGFR-3 die already around E9.5, before the first lymphatic structures develop, from failures in the organization and maturation of blood vessels (Dumont et al., 1998). However, embryonic lethality after deletion of both VEGFR-3 ligands, VEGF-C and VEGF-D, occurs only around E16.5, suggesting no role of these ligands for VEGFR-3 activation in early embryogenesis (Haiko et al., 2008). Since VEGFR-3 can form heterodimers with VEGFR-2, this might be a substitute mechanism for VEGFR-3 activation (Dixelius et al., 2003; Nilsson et al., 2010). Alternatively, ligand-less baseline signaling (Zhang et al., 2005; Galvagni et al., 2010), mechanoinduction (Planas-Paz et al., 2012), or unrecognized ligands might provide a sufficient stimulus. Interestingly, neither the development of the blood vascular system nor of the lymphatic vascular system is affected by the lack of the second lymphangiogenic growth factor VEGF-D (Baldwin et al., 2005).

GENETIC LESIONS IN THE VEGF-C/VEGFR-3 SIGNALING PATHWAY

So far, mutations in 27 genes have been found to cause human lymphedema conditions. Several of these mutations affect components of the VEGF-C/VEGFR-3 signaling pathway (**Table 1**). Interestingly, a major fraction of hereditary lymphedema patients present with mutations in *VEGFR-3*, while mutations in the other genes are relatively rare (Brouillard et al., 2014, 2017).

Although in hereditary lymphedema type 1A and 1D, all cells carry the mutant *VEGFR-3* or *VEGF-C* gene, not all lymphatic vessels and body parts are equally affected. Hypoplastic or aplastic lymph capillaries are mainly found in peripheral, superficial regions (Bollinger et al., 1983). However, in addition to the underdeveloped lymphatic structures, a functional deficit seems to play a variable, but significant role in the manifestation of the edema (Mellor et al., 2010). A higher hydrostatic pressure resulting in increased drainage needs in the extremities could possibly explain localized symptoms. However, leg edema is as well observed in mice and newborns, where hydrostatic pressure differences are negligible (Karkkainen et al., 2001a). Alternatively, LECs from different vascular beds could have a different sensitivity for VEGFR-3 signaling, perhaps due to a different developmental origin.

LEC CULTURE AND VEGF-C SIGNALING

During embryonic growth, signaling by VEGF-C is necessary for the establishment of the lymphatic vasculature (Karkkainen et al., 2004). In the adult organism, the dependency on VEGF-C is less pronounced, and ablation of VEGF-C in the adult organism appears well tolerated also over longer periods of time,

TABLE 1 | Hereditary human lymphedema conditions involving the vascular endothelial growth factor C (VEGF-C)/VEGF receptor 3 (VEGFR-3) signaling pathway.

GENE **(protein)**	**Human condition (OMIM, alternative name)**	**Lymphedema phenotype**	**Reference for the initial linkage**	**Molecular etiology**	**Viable animal models**
FLT4 (VEGFR-3)	Hereditary lymphedema type 1A (153100, Milroy disease)	Predominantly the lower extremities	Irrthum et al. (2000), Karkkainen et al. (2000)	Dominant negative inactivation of the intracellular kinase domain (Irrthum et al., 2000; Karkkainen et al., 2000)	Chy mice (inactivating *Flt4* mutation) (Karkkainen et al., 2001b); VEGFR-3 inhibition (Mäkinen et al., 2001)
VEGFC (VEGF-C)	Hereditary lymphedema type 1D (615907, Milroy-like disease)		Gordon et al. (2013), Balboa-Beltran et al. (2014)	Secretion defect (Gordon et al., 2013; Villefranc et al., 2013)	Chy-3 mice (hemizygous *Vegfc* deletion) (Dellinger et al., 2007); conditional *Vegfc* ko mice (Nurmi et al., 2015)
CCBE1 (Collagen and calcium-binding EGF domain-containing protein 1)	Hennekam syndrome type 1 (235510)	Generalized	Alders et al. (2009)	A disintegrin and metalloproteinase with thrombospondin motifs 3 activation defect (Jeltsch et al., 2014; Roukens et al., 2015), localization defect (Jha et al., 2017)	Conditional *Ccbe1* ko mice (Bui et al., 2016)
	Cholestasis–lymphedema syndrome (214900, Aagenaes syndrome)		Shah et al. (2013), Viveiros et al. (2017)		
FAT4 (Protocadherin Fat4)	Hennekam syndrome type 2 (616006)		Alders et al. (2014)	Unknown molecular etiology	Vascular abnormalities were not reported for the full *Fat4* ko mice (Saburi et al., 2008)
	Van Maldergem syndrome type 2 (615546)				
ADAMTS3 (A disintegrin and metalloproteinase with thrombospondin motifs 3)	Hennekam syndrome type 3		Brouillard et al. (2017)	Secretion defect (Brouillard et al., 2017), localization defect (Jha et al., 2017)	Conditional *Adamts3* ko mice (Bui et al., 2016)

except for the intestinal lymphatics (the lacteals) and meningeal lymphatics, which depend on a steady supply with VEGF-C (Nurmi et al., 2015; Antila et al., 2017). It is not known, whether this difference is due to the higher stress or increased turnover of intestinal LECs compared to, e.g., adult skin LECs, which are mostly in the resting phase (Alexander et al., 2010). Despite the apparent VEGF-C requirements for proliferating LECs *in vivo*, LEC vendors specifically endorse only the use of the hemangiogenic VEGF-A for LEC culture. However, some researchers have modified such media to contain VEGF-C (Mäkinen et al., 2001; Petrova et al., 2002; Podgrabinska et al., 2002; Veikkola et al., 2003). While serum does typically contain VEGF-C in the single digit ng/ml-range (R&D Systems, 2017), serum-supplemented LEC culture medium would still contain only small amounts of VEGF-C compared to VEGF-A, which stimulates VEGFR-2, but not VEGFR-3. While VEGF-A stimulates LEC proliferation and lymphatic vessel dilation *in vitro* (Dellinger and Brekken, 2011) and increases the density of lymphatic *in vitro* capillary networks (Marino et al., 2014) to a similar degree as VEGF-C, its importance for *in vivo* LEC proliferation is arguable as only very few *in vivo* models of VEGF-A application seem to directly affect lymphatic networks (Shin et al., 2008). While VEGFR-2 and VEGFR-3 activation both result in PKC-dependent Akt phosphorylation, the activation routes and kinetics differ (Mäkinen et al., 2001). Importantly, SOX18 and KLF4, which are implicated in LEC differentiation (Francois et al., 2008; Park et al., 2014), are specifically regulated by VEGFR-3 (Dieterich et al., 2017).

The specific form of VEGF-C that is used for LEC culture supplementation is the active, mature form, but pro-VEGF-C also might be an attractive option, since the LEC-expressed ADAMTS3 and CCBE1 (Jha et al., 2017) would concertedly convert it into the mature form, providing a differently localized and perhaps more sustained stimulus. Due to its potent synergistic effect with VEGF-C, hepatocyte growth factor (HGF) also needs consideration as a LEC culture additive (Kajiya et al., 2005; Gibot et al., 2016).

WHEN VEGF-C IS NOT ENOUGH

While in some models, the angiogenic component of VEGF-C can be exposed (e.g., in the heart) (Losordo et al., 2002; Chen et al., 2014), VEGF-C predominantly affects the lymphatic system. Not surprisingly, most therapeutic applications of VEGF-C are targeting the lymphatics (Tammela et al., 2007; Honkonen et al., 2013; Klotz et al., 2015), and VEGF-C should therefore be considered the primary growth factor of choice in lymphatic engineering tasks that involve LECs. While necessary, VEGF-C alone is not sufficient for the successful establishment of a functional lymphatic network in some situations (Goldman et al., 2005), and blocking signals that inhibit lymphangiogenesis such as TGF-β1 (Avraham et al., 2010) might be necessary. An elegant way bypassing the need for VEGF-C supplementation is the coculture of LECs with other cell types. In addition to secreted factors, cell–cell contacts appear important for the establishment of lymphatic networks. In one model, lymphangiogenesis was sustained by fibroblast-derived VEGF-C and HGF. While VEGF-C appeared to be constitutively expressed by fibroblasts, HGF expression was induced only in the cocultures (Gibot et al., 2016). Whether the fibroblasts were also able to stimulate the release of Reelin from the LECs was not analyzed in this model. Reelin release from LECs is normally induced by smooth muscle cell contacts and is required for the establishment of collecting vessels (Lutter et al., 2012). In another coculture model, LECs, BECs, and adipose-derived stromal cells (ASCs) in a 3D fibrin matrix depended on the addition of exogenous VEGF-C for substantial LEC network formation in addition to cell–cell contacts between LECs and ASCs (Knezevic et al., 2017). In the same model, BEC network formation was not affected by the absence of exogenous VEGF-C.

DIRECTING REGENERATIVE LYMPHATIC GROWTH *IN VIVO*

The mechanisms of the directional growth are similar for blood vessels and nerve cell axons (Carmeliet, 2003): a specialized cell on the tip of the vascular sprout (tip cell) determines the direction of growth of subsequent cells (stalk cells) by extending filopodia with growth factor receptors (Gerhardt et al., 2003). However, *in vivo* evidence for the importance of VEGF gradients for the directed growth of vascular networks is sparse (Ruhrberg et al., 2002), and also *in vitro*, convincing evidence is largely absent (Bautch, 2012). Likewise, filopodia seems to be dispensable for vascular patterning (Wacker et al., 2014). In the expansion of lymphatic networks, similar directed sprouting can be observed, but e.g. in the mouse tail lymphedema model, the mere application of VEGF-C was not enough to induce sprouting lymphangiogenesis (Goldman et al., 2005). Moreover, and contrary to expectations, VEGF-C levels correlated even in some models with lymphedema formation, apparently *via* inducing vascular leakage and immune cell infiltration (Gousopoulos et al., 2017). Surgical grafting of engineered small lymphatic structures is difficult unless they are grafted as part of a larger tissue (e.g., a vascularized skin graft). Hence, the idea of generating lymphatics *in situ* is attractive and indeed has been successfully achieved in some animal models using different delivery strategies for VEGF-C (Karkkainen et al., 2001b; Szuba et al., 2002; Yoon et al., 2003). The question whether VEGF-C alone is enough (Breier, 2005; Goldman et al., 2005) has recently at least received a partial answer by the discovery of obligatory cofactors such as CCBE1 and ADAMTS3 for correct VEGF-C localization and efficient activation (Jeltsch et al., 2014; Jha et al., 2017), and the presence or absence of these factors might explain differences in the lymphatic response. After encouraging preclinical studies (Tammela et al., 2007), the therapeutic value of VEGF-C for an improved integration of transplanted lymph nodes into the regional lymph system is currently under investigation (Tervala et al., 2015). It is less obvious how large collecting lymphatics could be generated *in situ*, but flow-stimulated remodeling of smaller lymphatics might happen akin to the hemodynamic remodeling of blood vessels (Culver and Dickinson, 2010).

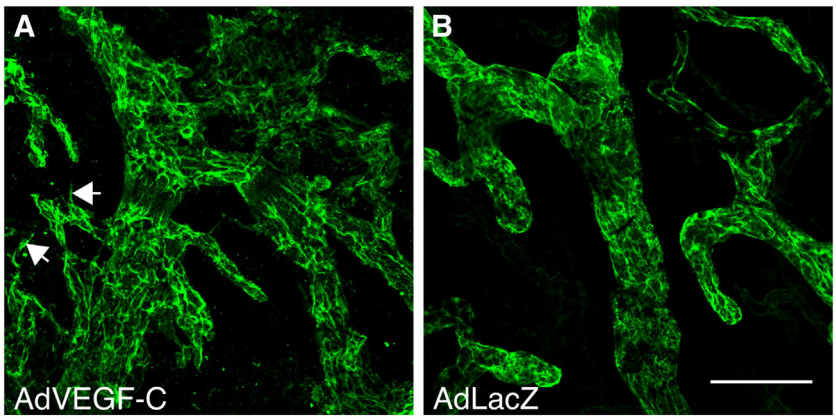

FIGURE 4 | Vascular endothelial growth factor C (VEGF-C) induces specifically the growth of the lymphatic vasculature. Whole-mount LYVE-1 staining of mouse ears 2 weeks after adenoviral transduction with VEGF-C **(A)** and LacZ **(B)**. AdVEGF-C induces hyperplasia of and neo-sprouting from the lymphatic vasculature. Arrows indicate lymphatic sprouting. Bar, 100 μm.

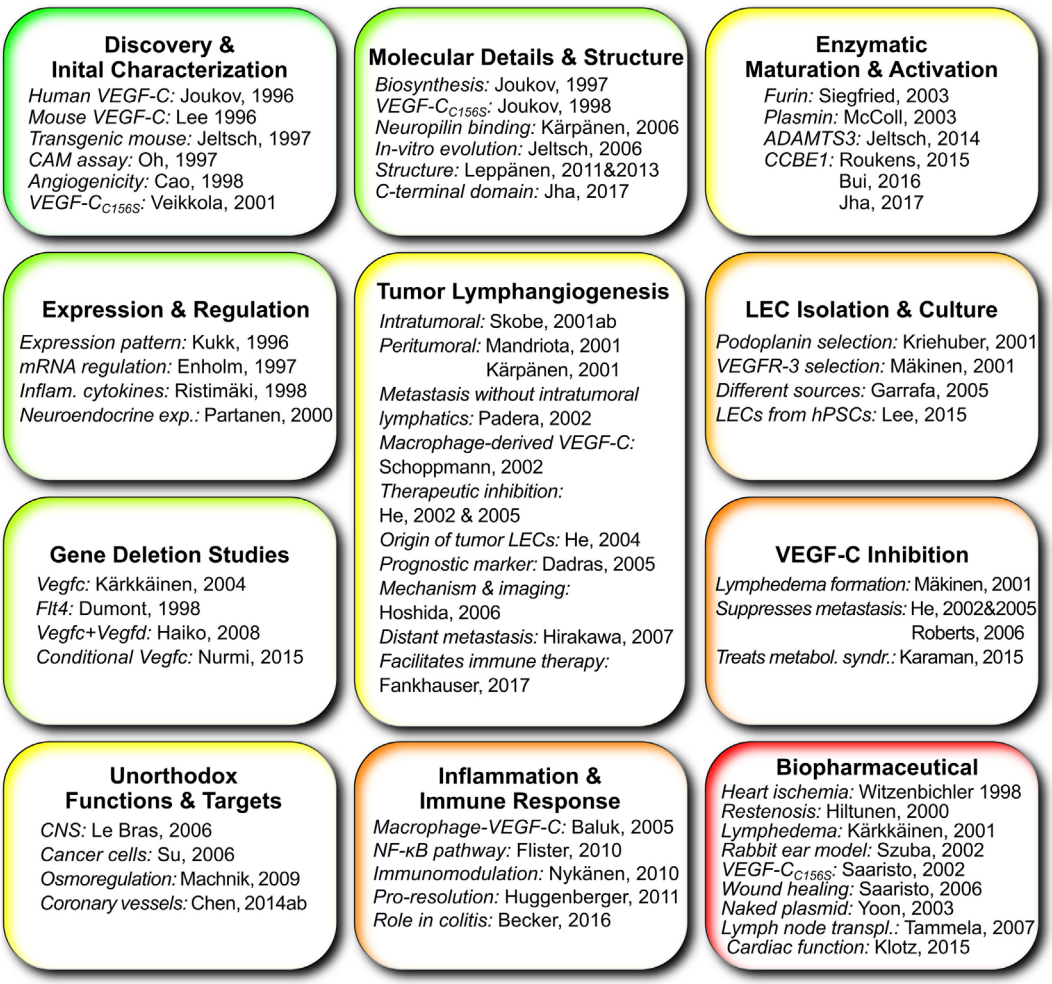

FIGURE 5 | Works that give important insights into vascular endothelial growth factor C (VEGF-C) and its function grouped according to topic. Publications about the use of VEGF-C specifically in lymphatic tissue engineering are not included since this list tries to highlight the elemental scientific insights on which tissue engineering can build.

Although preclinical experience with *in situ* reconstitution of lymphatic networks using VEGF-C exists for more than 15 years, there is only one ongoing phase I clinical trial using VEGF-C therapy, namely the application of a VEGF-C-expressing adenovirus (AdVEGF-C, see **Figure 4**), in combination with lymph node transplantation for the treatment of secondary lymphedema after breast cancer surgery. The slow adoption might partly result from animal studies that identify VEGF-C as a key inducer for the growth and dissemination of certain tumors (for references, see **Figure 5**). While it is prudent to take the complete picture of VEGF-C biology as shown in **Figure 5** into consideration when reconstructing lymphatics, the localized and limited availability of VEGF-C in this specific ongoing phase I study should exclude tumor-promoting side effects, paving the way for phase II studies.

AUTHOR CONTRIBUTIONS

All authors listed have made a substantial, direct, and intellectual contribution to the work, and approved it for publication.

ACKNOWLEDGMENTS

We thank Sinem Karaman for critical reading of the manuscript.

FUNDING

This work was supported by the Academy of Finland (award numbers 304042, 303778, 273612, and 265982), the K. Albin Johansson, and the Magnus Ehrnrooth Foundation. The ILS doctoral program, University of Helsinki supported the salary of SKJ.

REFERENCES

Achen, M. G., Jeltsch, M., Kukk, E., Mäkinen, T., Vitali, A., Wilks, A. F., et al. (1998). Vascular endothelial growth factor D (VEGF-D) is a ligand for the tyrosine kinases VEGF receptor 2 (Flk1) and VEGF receptor 3 (Flt4). *Proc. Natl. Acad. Sci. U.S.A.* 95, 548–553. doi:10.1073/pnas.95.2.548

Alders, M., Al-Gazali, L., Cordeiro, I., Dallapiccola, B., Garavelli, L., Tuysuz, B., et al. (2014). Hennekam syndrome can be caused by FAT4 mutations and be allelic to Van Maldergem syndrome. *Hum. Genet.* 133, 1161–1167. doi:10.1007/s00439-014-1456-y

Alders, M., Hogan, B. M., Gjini, E., Salehi, F., Al-Gazali, L., Hennekam, E. A., et al. (2009). Mutations in CCBE1 cause generalized lymph vessel dysplasia in humans. *Nat. Genet.* 41, 1272–1274. doi:10.1038/ng.484

Alexander, J. S., Ganta, V. C., Jordan, P. A., and Witte, M. H. (2010). Gastrointestinal lymphatics in health and disease. *Pathophysiology* 17, 315–335. doi:10.1016/j.pathophys.2009.09.003

Anisimov, A., Alitalo, A., Korpisalo, P., Soronen, J., Kaijalainen, S., Leppänen, V.-M., et al. (2009). Activated forms of VEGF-C and VEGF-D provide improved vascular function in skeletal muscle. *Circ. Res.* 104, 1302–1312. doi:10.1161/CIRCRESAHA.109.197830

Antila, S., Karaman, S., Nurmi, H., Airavaara, M., Voutilainen, M. H., Mathivet, T., et al. (2017). Development and plasticity of meningeal lymphatic vessels. *J. Exp. Med.* 214, 3645–3667. doi:10.1084/jem.20170391

Avraham, T., Daluvoy, S., Zampell, J., Yan, A., Haviv, Y. S., Rockson, S. G., et al. (2010). Blockade of transforming growth factor-β1 accelerates lymphatic regeneration during wound repair. *Am. J. Pathol.* 177, 3202–3214. doi:10.2353/ajpath.2010.100594

Balboa-Beltran, E., Fernández-Seara, M. J., Pérez-Muñuzuri, A., Lago, R., García-Magán, C., Couce, M. L., et al. (2014). A novel stop mutation in the vascular endothelial growth factor-C gene (VEGFC) results in Milroy-like disease. *J. Med. Genet.* 51, 475–478. doi:10.1136/jmedgenet-2013-102020

Baldwin, M. E., Catimel, B., Nice, E. C., Roufail, S., Hall, N. E., Stenvers, K. L., et al. (2001). The specificity of receptor binding by vascular endothelial growth factor-D is different in mouse and man. *J. Biol. Chem.* 276, 19166–19171. doi:10.1074/jbc.M100097200

Baldwin, M. E., Halford, M. M., Roufail, S., Williams, R. A., Hibbs, M. L., Grail, D., et al. (2005). vascular endothelial growth factor D is dispensable for development of the lymphatic system. *Mol. Cell. Biol.* 25, 2441–2449. doi:10.1128/MCB.25.6.2441-2449.2005

Baluk, P., Tammela, T., Ator, E., Lyubynska, N., Achen, M. G., Hicklin, D. J., et al. (2005). Pathogenesis of persistent lymphatic vessel hyperplasia in chronic airway inflammation. *J. Clin. Invest.* 115, 247–257. doi:10.1172/JCI200522037

Bautch, V. L. (2012). VEGF-directed blood vessel patterning: from cells to organism. *Cold Spring Harb. Perspect. Med.* 2, a006452. doi:10.1101/cshperspect.a006452

Bautch, V. L., and Caron, K. M. (2015). Blood and lymphatic vessel formation. *Cold Spring Harb. Perspect. Biol.* 7, a008268. doi:10.1101/cshperspect.a008268

Bollinger, A., Isenring, G., Franzeck, U. K., and Brunner, U. (1983). Aplasia of superficial lymphatic capillaries in hereditary and connatal lymphedema (Milroy's disease). *Lymphology* 16, 27–30.

Borg, J. P., deLapeyrière, O., Noguchi, T., Rottapel, R., Dubreuil, P., and Birnbaum, D. (1995). Biochemical characterization of two isoforms of FLT4, a VEGF receptor-related tyrosine kinase. *Oncogene* 10, 973–984.

Bos, F. L., Caunt, M., Peterson-Maduro, J., Planas-Paz, L., Kowalski, J., Karpanen, T., et al. (2011). CCBE1 is essential for mammalian lymphatic vascular development and enhances the lymphangiogenic effect of vascular endothelial growth factor-C in vivo. *Circ. Res.* 109, 486–491. doi:10.1161/CIRCRESAHA.111.250738

Breier, G. (2005). Lymphangiogenesis in regenerating tissue: is VEGF-C sufficient? *Circ. Res.* 96, 1132–1134. doi:10.1161/01.RES.0000170976.63688.ca

Brouillard, P., Boon, L., and Vikkula, M. (2014). Genetics of lymphatic anomalies. *J. Clin. Invest.* 124, 898–904. doi:10.1172/JCI71614

Brouillard, P., Dupont, L., Helaers, R., Coulie, R., Tiller, G. E., Peeden, J., et al. (2017). Loss of ADAMTS3 activity causes Hennekam lymphangiectasia–lymphedema syndrome 3. *Hum. Mol. Genet.* 26, 4095–4104. doi:10.1093/hmg/ddx297

Bui, H. M., Enis, D., Robciuc, M. R., Nurmi, H. J., Cohen, J., Chen, M., et al. (2016). Proteolytic activation defines distinct lymphangiogenic mechanisms for VEGFC and VEGFD. *J. Clin. Invest.* 126, 2167–2180. doi:10.1172/JCI83967

Butler, M. G., Isogai, S., and Weinstein, B. M. (2009). Lymphatic development. *Birth Defects Res. C Embryo Today* 87, 222–231. doi:10.1002/bdrc.20155

Cao, Y., Linden, P., Farnebo, J., Cao, R., Eriksson, A., Kumar, V., et al. (1998). Vascular endothelial growth factor C induces angiogenesis in vivo. *Proc. Natl. Acad. Sci. U.S.A.* 95, 14389–14394. doi:10.1073/pnas.95.24.14389

Carmeliet, P. (2003). Blood vessels and nerves: common signals, pathways and diseases. *Nat. Rev. Genet.* 4, nrg1158. doi:10.1038/nrg1158

Chen, H. I., Sharma, B., Akerberg, B. N., Numi, H. J., Kivelä, R., Saharinen, P., et al. (2014). The sinus venosus contributes to coronary vasculature through VEGFC-stimulated angiogenesis. *Development* 141, 4500–4512. doi:10.1242/dev.113639

Chiu, J., Wong, J. W. H., Gerometta, M., and Hogg, P. J. (2014). Mechanism of dimerization of a recombinant mature vascular endothelial growth factor C. *Biochemistry* 53, 7–9. doi:10.1021/bi401518b

Christiansen, A. J., Dieterich, L. C., Ohs, I., Bachmann, S. B., Bianchi, R., Proulx, S. T., et al. (2016). Lymphatic endothelial cells attenuate inflammation via suppression of dendritic cell maturation. *Oncotarget* 7, 39421–39435. doi:10.18632/oncotarget.9820

Culver, J. C., and Dickinson, M. E. (2010). The effects of hemodynamic force on embryonic development. *Microcirculation* 1994, 164–178. doi:10.1111/j.1549-8719.2010.00025.x

Dai, T.t, Jiang, Z.h, Li, S. I., Zhou, Gd, Kretlow, J. D., Cao, Wg, et al. (2010). Reconstruction of lymph vessel by lymphatic endothelial cells combined with polyglycolic acid scaffolds: a pilot study. *J. Biotechnol.* 150, 182–189. doi:10.1016/j.jbiotec.2010.07.028

Dellinger, M. T., and Brekken, R. A. (2011). Phosphorylation of Akt and ERK1/2 is required for VEGF-A/VEGFR2-induced proliferation and migration of lymphatic endothelium. *PLoS ONE* 6:e28947. doi:10.1371/journal.pone.0028947

Dellinger, M. T., Hunter, R. J., Bernas, M. J., Witte, M. H., and Erickson, R. P. (2007). Chy-3 mice are Vegfc haploinsufficient and exhibit defective dermal superficial to deep lymphatic transition and dermal lymphatic hypoplasia. *Dev. Dyn.* 236, 2346–2355. doi:10.1002/dvdy.21208

Deng, Y., Zhang, X., and Simons, M. (2015). Molecular controls of lymphatic VEGFR3 signaling. *Arterioscler. Thromb. Vasc. Biol.* 35, 421–429. doi:10.1161/ATVBAHA.114.304881

Dieterich, L. C., Ducoli, L., Shin, J. W., and Detmar, M. (2017). Distinct transcriptional responses of lymphatic endothelial cells to VEGFR-3 and VEGFR-2 stimulation. *Sci. Data* 4, 170106. doi:10.1038/sdata.2017.106

Dignam, S. S., and Case, S. T. (1990). Balbiani ring 3 in *Chironomus tentans* encodes a 185-kDa secretory protein which is synthesized throughout the fourth larval instar. *Gene* 88, 133–140. doi:10.1016/0378-1119(90)90024-L

Dixelius, J., Mäkinen, T., Wirzenius, M., Karkkainen, M. J., Wernstedt, C., Alitalo, K., et al. (2003). Ligand-induced vascular endothelial growth factor receptor-3 (VEGFR-3) heterodimerization with VEGFR-2 in primary lymphatic endothelial cells regulates tyrosine phosphorylation sites. *J. Biol. Chem.* 278, 40973–40979. doi:10.1074/jbc.M304499200

Dumont, D. J., Jussila, L., Taipale, J., Lymboussaki, A., Mustonen, T., Pajusola, K., et al. (1998). Cardiovascular failure in mouse embryos deficient in VEGF Receptor-3. *Science* 282, 946–949. doi:10.1126/science.282.5390.946

EMBL-EBI. (2017). *PDGF/VEGF Domain (IPR000072) < InterPro < EMBL-EBI*. Available at: https://www.ebi.ac.uk/interpro/entry/IPR000072

Ensembl. (2016). *Transcript: Vegfc-203 (ENSMUST00000210831.1) – Protein Sequence – Mus musculus – Ensembl Genome Browser 90*. Available at: https://www.ensembl.org/Mus_musculus/Transcript/Sequence_Protein?db=core;g=ENSMUSG00000031520;r=8:54077606-54187096;t=ENSMUST00000210831

Fournier, E., Dubreuil, P., Birnbaum, D., and Borg, J. P. (1995). Mutation at tyrosine residue 1337 abrogates ligand-dependent transforming capacity of the FLT4 receptor. *Oncogene* 11, 921–931.

Francois, M., Caprini, A., Hosking, B., Orsenigo, F., Wilhelm, D., Browne, C., et al. (2008). Sox18 induces development of the lymphatic vasculature in mice. *Nature* 456, 643–647. doi:10.1038/nature07391

Fuh, G., Li, B., Crowley, C., Cunningham, B., and Wells, J. A. (1998). Requirements for binding and signaling of the kinase domain receptor for vascular endothelial growth factor. *J. Biol. Chem.* 273, 11197–11204. doi:10.1074/jbc.273.18.11197

Galvagni, F., Pennacchini, S., Salameh, A., Rocchigiani, M., Neri, F., Orlandini, M., et al. (2010). Endothelial cell adhesion to the extracellular matrix induces c-Src–dependent VEGFR-3 phosphorylation without the activation of the receptor intrinsic kinase activity. *Circ. Res.* 106, 1839–1848. doi:10.1161/CIRCRESAHA.109.206326

Gerhardt, H., Golding, M., Fruttiger, M., Ruhrberg, C., Lundkvist, A., Abramsson, A., et al. (2003). VEGF guides angiogenic sprouting utilizing endothelial tip cell filopodia. *J. Cell Biol.* 161, 1163–1177. doi:10.1083/jcb.200302047

Gibot, L., Galbraith, T., Bourland, J., Rogic, A., Skobe, M., and Auger, F. A. (2017). Tissue-engineered 3D human lymphatic microvascular network for *in vitro* studies of lymphangiogenesis. *Nat. Protoc.* 12, 1077. doi:10.1038/nprot.2017.025

Gibot, L., Galbraith, T., Kloos, B., Das, S., Lacroix, D. A., Auger, F. A., et al. (2016). Cell-based approach for 3D reconstruction of lymphatic capillaries in vitro reveals distinct functions of HGF and VEGF-C in lymphangiogenesis. *Biomaterials* 78, 129–139. doi:10.1016/j.biomaterials.2015.11.027

Goldman, J., Le, T. X., Skobe, M., and Swartz, M. A. (2005). Overexpression of VEGF-C causes transient lymphatic hyperplasia but not increased lymphangiogenesis in regenerating skin. *Circ. Res.* 96, 1193–1199. doi:10.1161/01.RES.0000168918.27576.78

Gordon, K., Schulte, D., Brice, G., Simpson, M. A., Roukens, M. G., van Impel, A., et al. (2013). Mutation in vascular endothelial growth factor-C, a ligand for vascular endothelial growth factor receptor-3, is associated with autosomal dominant Milroy-like primary lymphedema. *Circ. Res.* 112, 956–960. doi:10.1161/CIRCRESAHA.113.300350

Gousopoulos, E., Proulx, S. T., Bachmann, S. B., Dieterich, L. C., Scholl, J., Karaman, S., et al. (2017). An important role of VEGF-C in promoting lymphedema development. *J. Invest. Dermatol.* 137, 1995–2004. doi:10.1016/j.jid.2017.04.033

Grunewald, F. S., Prota, A. E., Giese, A., and Ballmer-Hofer, K. (2010). Structure–function analysis of VEGF receptor activation and the role of coreceptors in angiogenic signaling. *Biochim. Biophys. Acta.* 1804, 567–580. doi:10.1016/j.bbapap.2009.09.002

Güç, E., Briquez, P. S., Foretay, D., Fankhauser, M. A., Hubbell, J. A., Kilarski, W. W., et al. (2017). Local induction of lymphangiogenesis with engineered fibrin-binding VEGF-C promotes wound healing by increasing immune cell trafficking and matrix remodeling. *Biomaterials* 131, 160–175. doi:10.1016/j.biomaterials.2017.03.033

Hagerling, R., Pollmann, C., Andreas, M., Schmidt, C., Nurmi, H., Adams, R. H., et al. (2013). A novel multistep mechanism for initial lymphangiogenesis in mouse embryos based on ultramicroscopy. *EMBO J.* 32, 629–644. doi:10.1038/emboj.2012.340

Haiko, P., Makinen, T., Keskitalo, S., Taipale, J., Karkkainen, M. J., Baldwin, M. E., et al. (2008). Deletion of vascular endothelial growth factor C (VEGF-C) and VEGF-D is not equivalent to vegf receptor 3 deletion in mouse embryos. *Mol. Cell. Biol.* 28, 4843–4850. doi:10.1128/MCB.02214-07

Helm, C.-L. E., Zisch, A., and Swartz, M. A. (2007). Engineered blood and lymphatic capillaries in 3-D VEGF-fibrin-collagen matrices with interstitial flow. *Biotechnol. Bioeng.* 96, 167–176. doi:10.1002/bit.21185

Holmes, D. I., and Zachary, I. (2005). The vascular endothelial growth factor (VEGF) family: angiogenic factors in health and disease. *Genome Biol.* 6, 209. doi:10.1186/gb-2005-6-2-209

Holmes, K., Roberts, O. L., Thomas, A. M., and Cross, M. J. (2007). Vascular endothelial growth factor receptor-2: structure, function, intracellular signalling and therapeutic inhibition. *Cell. Signal.* 19, 2003–2012. doi:10.1016/j.cellsig.2007.05.013

Honkonen, K. M., Visuri, M. T., Tervala, T. V., Halonen, P. J., Koivisto, M., Lahteenvuo, M. T., et al. (2013). Lymph node transfer and perinodal lymphatic growth factor treatment for lymphedema. *Ann. Surg.* 257, 961–967. doi:10.1097/SLA.0b013e31826ed043

Hughes, D. C. (2001). Alternative splicing of the human VEGFGR-3/FLT4 gene as a consequence of an integrated human endogenous retrovirus. *J. Mol. Evol.* 53, 77–79. doi:10.1007/s002390010195

Irrthum, A., Karkkainen, M. J., Devriendt, K., Alitalo, K., and Vikkula, M. (2000). Congenital hereditary lymphedema caused by a mutation that inactivates VEGFR3 tyrosine kinase. *Am. J. Hum. Genet.* 67, 295–301. doi:10.1086/303019

Janssen, L., Dupont, L., Bekhouche, M., Noel, A., Leduc, C., Voz, M., et al. (2015). ADAMTS3 activity is mandatory for embryonic lymphangiogenesis and regulates placental angiogenesis. *Angiogenesis* 19, 53–65. doi:10.1007/s10456-015-9488-z

Jeltsch, M., Jha, S. K., Tvorogov, D., Anisimov, A., Leppänen, V.-M., Holopainen, T., et al. (2014). CCBE1 enhances lymphangiogenesis via a disintegrin and metalloprotease with thrombospondin motifs-3–mediated vascular endothelial growth factor-C activation. *Circulation* 129, 1962–1971. doi:10.1161/CIRCULATIONAHA.113.002779

Jeltsch, M., Kaipainen, A., Joukov, V., Meng, X., Lakso, M., Rauvala, H., et al. (1997). Hyperplasia of lymphatic vessels in VEGF-C transgenic mice. *Science* 276, 1423–1425. doi:10.1126/science.276.5317.1423

Jeltsch, M., Karpanen, T., Strandin, T., Aho, K., Lankinen, H., and Alitalo, K. (2006). Vascular endothelial growth factor (VEGF)/VEGF-C mosaic molecules reveal specificity determinants and feature novel receptor binding patterns. *J. Biol. Chem.* 281, 12187–12195. doi:10.1074/jbc.M511593200

Jha, S. K., Rauniyar, K., Karpanen, T., Leppänen, V.-M., Brouillard, P., Vikkula, M., et al. (2017). Efficient activation of the lymphangiogenic growth factor VEGF-C requires the C-terminal domain of VEGF-C and the N-terminal domain of CCBE1. *Sci. Rep.* 7, 4916. doi:10.1038/s41598-017-04982-1

Johns, S. C., Yin, X., Jeltsch, M., Bishop, J. R., Schuksz, M., El Ghazal, R., et al. (2016). Functional importance of a proteoglycan coreceptor in pathologic lymphangiogenesis. *Circ. Res.* 119, 210–221. doi:10.1161/CIRCRESAHA.116.308504

Joukov, V., Kaipainen, A., Jeltsch, M., Pajusola, K., Olofsson, B., Kumar, V., et al. (1997a). Vascular endothelial growth factors VEGF-B and VEGF-C. *J. Cell. Physiol.* 173, 211–215. doi:10.1002/(SICI)1097-4652(199711)173:2<211:AID-JCP23>3.0.CO;2-H

Joukov, V., Sorsa, T., Kumar, V., Jeltsch, M., Claesson-Welsh, L., Cao, Y., et al. (1997b). Proteolytic processing regulates receptor specificity and activity of VEGF-C. *EMBO J.* 16, 3898–3911. doi:10.1093/emboj/16.13.3898

Joukov, V., Kumar, V., Sorsa, T., Arighi, E., Weich, H., Saksela, O., et al. (1998). A recombinant mutant vascular endothelial growth factor-C that has lost vascular endothelial growth factor receptor-2 binding, activation, and vascular permeability activities. *J. Biol. Chem.* 273, 6599–6602. doi:10.1074/jbc.273.12.6599

Joukov, V., Pajusola, K., Kaipainen, A., Chilov, D., Lahtinen, I., Kukk, E., et al. (1996). A novel vascular endothelial growth factor, VEGF-C, is a ligand for the Flt4 (VEGFR-3) and KDR (VEGFR-2) receptor tyrosine kinases. *EMBO J.* 15, 290–298.

Kaipainen, A., Korhonen, J., Mustonen, T., van Hinsbergh, V. W., Fang, G. H., Dumont, D., et al. (1995). Expression of the fms-like tyrosine kinase 4 gene

becomes restricted to lymphatic endothelium during development. *Proc. Natl. Acad. Sci. U.S.A.* 92, 3566–3570. doi:10.1073/pnas.92.8.3566

Kajiya, K., Hirakawa, S., Ma, B., Drinnenberg, I., and Detmar, M. (2005). Hepatocyte growth factor promotes lymphatic vessel formation and function. *EMBO J.* 24, 2885–2895. doi:10.1038/sj.emboj.7600763

Kanapathy, M., Patel, N. M., Kalaskar, D. M., Mosahebi, A., Mehrara, B. J., and Seifalian, A. M. (2014). Tissue-engineered lymphatic graft for the treatment of lymphedema. *J. Surg. Res.* 192, 544–554. doi:10.1016/j.jss.2014.07.059

Karkkainen, M. J., Ferrell, R. E., Lawrence, E. C., Kimak, M. A., Levinson, K. L., McTigue, M. A., et al. (2000). Missense mutations interfere with VEGFR-3 signalling in primary lymphoedema. *Nat. Genet.* 25, 153–159. doi:10.1038/75997

Karkkainen, M. J., Haiko, P., Sainio, K., Partanen, J., Taipale, J., Petrova, T. V., et al. (2004). Vascular endothelial growth factor C is required for sprouting of the first lymphatic vessels from embryonic veins. *Nat. Immunol.* 5, 74–80. doi:10.1038/ni1013

Karkkainen, M. J., Jussila, L., Alitalo, K., Ferrell, R. E., and Finegold, D. N. (2001a). Molecular regulation of lymphangiogenesis and targets for tissue oedema. *Trends Mol. Med.* 7, 18–22. doi:10.1016/S1471-4914(00)01864-5

Karkkainen, M. J., Saaristo, A., Jussila, L., Karila, K. A., Lawrence, E. C., Pajusola, K., et al. (2001b). A model for gene therapy of human hereditary lymphedema. *Proc. Natl. Acad. Sci. U.S.A.* 98, 12677–12682. doi:10.1073/pnas.221449198

Karpanen, T., Wirzenius, M., Mäkinen, T., Veikkola, T., Haisma, H. J., Achen, M. G., et al. (2006). Lymphangiogenic growth factor responsiveness is modulated by postnatal lymphatic vessel maturation. *Am. J. Pathol.* 169, 708–718. doi:10.2353/ajpath.2006.051200

Kim, J.-D., Kang, Y., Kim, J., Papangeli, I., Kang, H., Wu, J., et al. (2014). Essential role of apelin signaling during lymphatic development in zebrafish. *Arterioscler. Thromb. Vasc. Biol.* 34, 338–345. doi:10.1161/ATVBAHA.113.302785

Klotz, L., Norman, S., Vieira, J. M., Masters, M., Rohling, M., Dubé, K. N., et al. (2015). Cardiac lymphatics are heterogeneous in origin and respond to injury. *Nature* 522, 62–67. doi:10.1038/nature14483

Knezevic, L., Schaupper, M., Mühleder, S., Schimek, K., Hasenberg, T., Marx, U., et al. (2017). Engineering blood and lymphatic microvascular networks in fibrin matrices. *Front. Bioeng. Biotechnol.* 5, 25. doi:10.3389/fbioe.2017.00025

Krebs, R., Tikkanen, J. M., Ropponen, J. O., Jeltsch, M., Jokinen, J. J., Yla-Herttuala, S., et al. (2012). Critical role of VEGF-C/VEGFR-3 signaling in innate and adaptive immune responses in experimental obliterative bronchiolitis. *Am. J. Pathol.* 181, 1607–1620. doi:10.1016/j.ajpath.2012.07.021

Lee, J., Gray, A., Yuan, J., Luoh, S. M., Avraham, H., and Wood, W. I. (1996). Vascular endothelial growth factor-related protein: a ligand and specific activator of the tyrosine kinase receptor Flt4. *Proc. Natl. Acad. Sci. U.S.A.* 93, 1988–1992. doi:10.1073/pnas.93.5.1988

Leppanen, V.-M., Jeltsch, M., Anisimov, A., Tvorogov, D., Aho, K., Kalkkinen, N., et al. (2011). Structural determinants of vascular endothelial growth factor-D receptor binding and specificity. *Blood* 117, 1507–1515. doi:10.1182/blood-2010-08-301549

Lohela, M., Heloterä, H., Haiko, P., Dumont, D. J., and Alitalo, K. (2008). Transgenic induction of vascular endothelial growth factor-C is strongly angiogenic in mouse embryos but leads to persistent lymphatic hyperplasia in adult tissues. *Am. J. Pathol.* 173, 1891–1901. doi:10.2353/ajpath.2008.080378

Losordo, D. W., Vale, P. R., Hendel, R. C., Milliken, C. E., Fortuin, F. D., Cummings, N., et al. (2002). Phase 1/2 placebo-controlled, double-blind, dose-escalating trial of myocardial vascular endothelial growth factor 2 gene transfer by catheter delivery in patients with chronic myocardial ischemia. *Circulation* 105, 2012–2018. doi:10.1161/01.CIR.0000015982.70785.B7

Lutter, S., Xie, S., Tatin, F., and Makinen, T. (2012). Smooth muscle–endothelial cell communication activates Reelin signaling and regulates lymphatic vessel formation. *J. Cell Biol.* 197, 837–849. doi:10.1083/jcb.201110132

Mäkinen, T., Veikkola, T., Mustjoki, S., Karpanen, T., Catimel, B., Nice, E. C., et al. (2001). Isolated lymphatic endothelial cells transduce growth, survival and migratory signals via the VEGF-C/D receptor VEGFR-3. *EMBO J.* 20, 4762–4773. doi:10.1093/emboj/20.17.4762

Marino, D., Luginbühl, J., Scola, S., Meuli, M., and Reichmann, E. (2014). Bioengineering dermo-epidermal skin grafts with blood and lymphatic capillaries. *Sci. Transl. Med.* 6, ra14–ra221. doi:10.1126/scitranslmed.3006894

McColl, B. K., Baldwin, M. E., Roufail, S., Freeman, C., Moritz, R. L., Simpson, R. J., et al. (2003). Plasmin activates the lymphangiogenic growth factors VEGF-C and VEGF-D. *J. Exp. Med.* 198, 863–868. doi:10.1084/jem.20030361

Mellor, R. H., Hubert, C. E., Stanton, A. W. B., Tate, N., Akhras, V., Smith, A., et al. (2010). Lymphatic dysfunction, not aplasia, underlies Milroy disease. *Microcirculation* 17, 281–296. doi:10.1111/j.1549-8719.2010.00030.x

Moriondo, A., Boschetti, F., Bianchin, F., Lattanzio, S., Marcozzi, C., and Negrini, D. (2010). Tissue contribution to the mechanical features of diaphragmatic initial lymphatics. *J. Physiol.* 588, 3957–3969. doi:10.1113/jphysiol.2010.196204

Muller, Y. A., Li, B., Christinger, H. W., Wells, J. A., Cunningham, B. C., and de Vos, A. M. (1997). Vascular endothelial growth factor: crystal structure and functional mapping of the kinase domain receptor binding site. *Proc. Natl. Acad. Sci. U.S.A.* 94, 7192–7197. doi:10.1073/pnas.94.14.7192

Neufeld, G., Kessler, O., and Herzog, Y. (2002). The interaction of neuropilin-1 and neuropilin-2 with tyrosine-kinase receptors for VEGF. *Adv. Exp. Med. Biol.* 515, 81–90. doi:10.1007/978-1-4615-0119-0_7

Nilsson, I., Bahram, F., Li, X., Gualandi, L., Koch, S., Jarvius, M., et al. (2010). VEGF receptor 2/-3 heterodimers detected in situ by proximity ligation on angiogenic sprouts. *EMBO J.* 29, 1377–1388. doi:10.1038/emboj.2010.30

Nurmi, H., Saharinen, P., Zarkada, G., Zheng, W., Robciuc, M. R., and Alitalo, K. (2015). VEGF-C is required for intestinal lymphatic vessel maintenance and lipid absorption. *EMBO Mol. Med.* 7, 1418–1425. doi:10.15252/emmm.201505731

Oh, S.-J., Jeltsch, M. M., Birkenhäger, R., McCarthy, J. E. G., Weich, H. A., Christ, B., et al. (1997). VEGF and VEGF-C: specific induction of angiogenesis and lymphangiogenesis in the differentiated avian chorioallantoic membrane. *Dev. Biol.* 188, 96–109. doi:10.1006/dbio.1997.8639

O'Leary, M. A., Bloch, J. I., Flynn, J. J., Gaudin, T. J., Giallombardo, A., Giannini, N. P., et al. (2013). The placental mammal ancestor and the post–K-Pg radiation of placentals. *Science* 339, 662–667. doi:10.1126/science.1229237

Olsson, A.-K., Dimberg, A., Kreuger, J., and Claesson-Welsh, L. (2006). VEGF receptor signalling in control of vascular function. *Nat. Rev. Mol. Cell Biol.* 7, 359–371. doi:10.1038/nrm1911

Orlandini, M., Marconcini, L., Ferruzzi, R., and Oliviero, S. (1996). Identification of a c-fos-induced gene that is related to the platelet-derived growth factor/vascular endothelial growth factor family. *Proc. Natl. Acad. Sci. U.S.A.* 93, 11675–11680. doi:10.1073/pnas.93.21.11675

Pajusola, K., Aprelikova, O., Armstrong, E., Morris, S., and Alitalo, K. (1993). Two human FLT4 receptor tyrosine kinase isoforms with distinct carboxy terminal tails are produced by alternative processing of primary transcripts. *Oncogene* 8, 2931–2937.

Park, D.-Y., Lee, J., Park, I., Choi, D., Lee, S., Song, S., et al. (2014). Lymphatic regulator PROX1 determines Schlemm's canal integrity and identity. *J. Clin. Invest.* 124, 3960–3974. doi:10.1172/JCI75392

Petrova, T. V., Bono, P., Holnthoner, W., Chesnes, J., Pytowski, B., Sihto, H., et al. (2008). VEGFR-3 expression is restricted to blood and lymphatic vessels in solid tumors. *Cancer Cell* 13, 554–556. doi:10.1016/j.ccr.2008.04.022

Petrova, T. V., Mäkinen, T., Mäkelä, T. P., Saarela, J., Virtanen, I., Ferrell, R. E., et al. (2002). Lymphatic endothelial reprogramming of vascular endothelial cells by the Prox-1 homeobox transcription factor. *EMBO J.* 21, 4593–4599. doi:10.1093/emboj/cdf470

Planas-Paz, L., Strilić, B., Goedecke, A., Breier, G., Fässler, R., and Lammert, E. (2012). Mechanoinduction of lymph vessel expansion. *EMBO J.* 31, 788–804. doi:10.1038/emboj.2011.456

Podgrabinska, S., Braun, P., Velasco, P., Kloos, B., Pepper, M. S., Jackson, D. G., et al. (2002). Molecular characterization of lymphatic endothelial cells. *Proc. Natl. Acad. Sci. U.S.A.* 99, 16069–16074. doi:10.1073/pnas.242401399

R&D Systems. (2017). *Human VEGF-C Quantikine ELISA Kit DVEC00: R&D Systems*. Available at: https://www.rndsystems.com/products/human-vegf-c-quantikine-elisa-kit_dvec00

Rissanen, T. T., Markkanen, J. E., Gruchala, M., Heikura, T., Puranen, A., Kettunen, M. I., et al. (2003). VEGF-D is the strongest angiogenic and lymphangiogenic effector among VEGFs delivered into skeletal muscle via adenoviruses. *Circ. Res.* 92, 1098–1106. doi:10.1161/01.RES.0000073584.46059.E3

Ristimäki, A., Narko, K., Enholm, B., Joukov, V., and Alitalo, K. (1998). Proinflammatory cytokines regulate expression of the lymphatic endothelial mitogen vascular endothelial growth factor-C. *J. Biol. Chem.* 273, 8413–8418. doi:10.1074/jbc.273.14.8413

Robinson, C. J., and Stringer, S. E. (2001). The splice variants of vascular endothelial growth factor (VEGF) and their receptors. *J. Cell Sci.* 114, 853–865.

Roukens, M. G., Peterson-Maduro, J., Padberg, Y., Jeltsch, M., Leppänen, V.-M., Bos, F. L., et al. (2015). Functional dissection of the CCBE1 protein: a

crucial requirement for the collagen repeat domain. *Circ. Res.* 116, 1660–1669. doi:10.1161/CIRCRESAHA.116.304949

Ruhrberg, C., Gerhardt, H., Golding, M., Watson, R., Ioannidou, S., Fujisawa, H., et al. (2002). Spatially restricted patterning cues provided by heparin-binding VEGF-A control blood vessel branching morphogenesis. *Genes Dev.* 16, 2684–2698. doi:10.1101/gad.242002

Saaristo, A., Veikkola, T., Tammela, T., Enholm, B., Karkkainen, M. J., Pajusola, K., et al. (2002). Lymphangiogenic gene therapy with minimal blood vascular side effects. *J. Exp. Med.* 196, 719–730. doi:10.1084/jem.20020587

Sabine, A., Saygili Demir, C., and Petrova, T. V. (2016). Endothelial cell responses to biomechanical forces in lymphatic vessels. *Antioxid. Redox Signal.* 25, 451–465. doi:10.1089/ars.2016.6685

Saburi, S., Hester, I., Fischer, E., Pontoglio, M., Eremina, V., Gessler, M., et al. (2008). Loss of Fat4 disrupts PCP signaling and oriented cell division and leads to cystic kidney disease. *Nat. Genet.* 40, 1010. doi:10.1038/ng.179

Schaupper, M., Jeltsch, M., Rohringer, S., Redl, H., and Holnthoner, W. (2016). Lymphatic vessels in regenerative medicine and tissue engineering. *Tissue Eng. Part B Rev.* 22, 395–407. doi:10.1089/ten.TEB.2016.0034

Shah, S., Conlin, L. K., Gomez, L., Aagenaes, Ø, Eiklid, K., Knisely, A. S., et al. (2013). CCBE1 mutation in two siblings, one manifesting lymphedema-cholestasis syndrome, and the other, fetal hydrops. *PLoS ONE* 8, e75770. doi:10.1371/journal.pone.0075770

Shibuya, M. (2001). Structure and function of VEGF/VEGF-receptor system involved in angiogenesis. *Cell Struct. Funct.* 26, 25–35. doi:10.1247/csf.26.25

Shin, J. W., Huggenberger, R., and Detmar, M. (2008). Transcriptional profiling of VEGF-A and VEGF-C target genes in lymphatic endothelium reveals endothelial-specific molecule-1 as a novel mediator of lymphangiogenesis. *Blood* 112, 2318–2326. doi:10.1182/blood-2008-05-156331

Siegfried, G., Basak, A., Cromlish, J. A., Benjannet, S., Marcinkiewicz, J., Chrétien, M., et al. (2003). The secretory proprotein convertases furin, PC5, and PC7 activate VEGF-C to induce tumorigenesis. *J. Clin. Invest.* 111, 1723–1732. doi:10.1172/JCI17220

Soker, S., Miao, H.-Q., Nomi, M., Takashima, S., and Klagsbrun, M. (2002). VEGF165 mediates formation of complexes containing VEGFR-2 and neuropilin-1 that enhance VEGF165-receptor binding. *J. Cell. Biochem.* 85, 357–368. doi:10.1002/jcb.10140

Soldi, R., Mitola, S., Strasly, M., Defilippi, P., Tarone, G., and Bussolino, F. (1999). Role of alphavbeta3 integrin in the activation of vascular endothelial growth factor receptor-2. *EMBO J.* 18, 882–892. doi:10.1093/emboj/18.4.882

Stacker, S. A., Stenvers, K., Caesar, C., Vitali, A., Domagala, T., Nice, E., et al. (1999). Biosynthesis of vascular endothelial growth factor-D involves proteolytic processing which generates non-covalent homodimers. *J. Biol. Chem.* 274, 32127–32136. doi:10.1074/jbc.274.45.32127

Sweat, R. S., Sloas, D. C., and Murfee, W. L. (2014). VEGF-C induces lymphangiogenesis and angiogenesis in the rat mesentery culture model. *Microcirculation* 21, 532–540. doi:10.1111/micc.12132

Szuba, A., Skobe, M., Karkkainen, M. J., Shin, W. S., Beynet, D. P., Rockson, N. B., et al. (2002). Therapeutic lymphangiogenesis with human recombinant VEGF-C. *FASEB J.* 16, 1985–1987. doi:10.1096/fj.02-0401fje

Tammela, T., Saaristo, A., Holopainen, T., Lyytikkä, J., Kotronen, A., Pitkonen, M., et al. (2007). Therapeutic differentiation and maturation of lymphatic vessels after lymph node dissection and transplantation. *Nat. Med.* 13, 1458–1466. doi:10.1038/nm1689

Tervala, T. V., Hartiala, P., Tammela, T., Visuri, M. T., Ylä-Herttuala, S., Alitalo, K., et al. (2015). Growth factor therapy and lymph node graft for lymphedema. *J. Surg. Res.* 196, 200–207. doi:10.1016/j.jss.2015.02.031

Veikkola, T., Jussila, L., Makinen, T., Karpanen, T., Jeltsch, M., Petrova, T. V., et al. (2001). Signalling via vascular endothelial growth factor receptor-3 is sufficient for lymphangiogenesis in transgenic mice. *EMBO J.* 20, 1223–1231. doi:10.1093/emboj/20.6.1223

Veikkola, T., Lohela, M., Ikenberg, K., Makinen, T., Korff, T., Saaristo, A., et al. (2003). Intrinsic versus micro environmental regulation of lymphatic endothelial cell phenotype and function. *FASEB J.* 17, 2006–2013. doi:10.1096/fj.03-0179com

Villefranc, J. A., Nicoli, S., Bentley, K., Jeltsch, M., Zarkada, G., Moore, J. C., et al. (2013). A truncation allele in vascular endothelial growth factor c reveals distinct modes of signaling during lymphatic and vascular development. *Development* 140, 1497–1506. doi:10.1242/dev.084152

Viveiros, A., Reiterer, M., Schaefer, B., Finkenstedt, A., Schneeberger, S., Schwaighofer, H., et al. (2017). CCBE1 mutation causing sclerosing cholangitis: expanding the spectrum of lymphedema-cholestasis syndrome. *Hepatology* 66, 286–288. doi:10.1002/hep.29037

Wacker, A., Gerhardt, H., and Phng, L.-K. (2014). Tissue guidance without filopodia. *Commun. Integr. Biol.* 7, e28820. doi:10.4161/cib.28820

Xu, Y., Yuan, L., Mak, J., Pardanaud, L., Caunt, M., Kasman, I., et al. (2010). Neuropilin-2 mediates VEGF-C–induced lymphatic sprouting together with VEGFR3. *J. Cell Biol.* 188, 115–130. doi:10.1083/jcb.200903137

Yamada, Y., Nezu, J., Shimane, M., and Hirata, Y. (1997). Molecular cloning of a novel vascular endothelial growth factor, VEGF-D. *Genomics* 42, 483–488. doi:10.1006/geno.1997.4774

Yoon, Y., Murayama, T., Gravereaux, E., Tkebuchava, T., Silver, M., Curry, C., et al. (2003). VEGF-C gene therapy augments postnatal lymphangiogenesis and ameliorates secondary lymphedema. *J. Clin. Invest.* 111, 717–725. doi:10.1172/JCI15830

Zhang, X., Groopman, J. E., and Wang, J. F. (2005). Extracellular matrix regulates endothelial functions through interaction of VEGFR-3 and integrin alpha-5beta1. *J. Cell. Physiol.* 202, 205–214. doi:10.1002/jcp.20106

Zhou, Q., Guo, R., Wood, R., Boyce, B. F., Liang, Q., Wang, Y.-J., et al. (2011). VEGF-C attenuates joint damage in chronic inflammatory arthritis by accelerating local lymphatic drainage. *Arthritis Rheum.* 63, 2318–2328. doi:10.1002/art.30421

Conflict of Interest Statement: The authors declare that the research was conducted in the absence of any commercial or financial relationships that could be construed as a potential conflict of interest.

frontiers in Bioengineering and Biotechnology

ORIGINAL RESEARCH
published: 14 June 2018
doi: 10.3389/fbioe.2018.00076

FOXF1 Mediates Endothelial Progenitor Functions and Regulates Vascular Sprouting

Caterina Sturtzel[1†‡], Karoline Lipnik[1†], Renate Hofer-Warbinek[1], Julia Testori[1‡], Bettina Ebner[1], Jaqueline Seigner[1], Ping Qiu[1‡], Martin Bilban[2], Anita Jandrositz[3], Karl-Heinz Preisegger[3,4], Gerold Untergasser[5], Eberhard Gunsilius[5], Rainer de Martin[1], Jens Kroll[6] and Erhard Hofer[1]*

[1] Department of Vascular Biology and Thrombosis Research, Center for Physiology and Pharmacology, Medical University of Vienna, Vienna, Austria, [2] Department of Laboratory Medicine & Core Facility Genomics, Core Facilities, Medical University of Vienna, Vienna, Austria, [3] VivoCell Biosolutions GmbH, Graz, Austria, [4] Institut für morphologische Analytik und Humangenetik, Graz, Austria, [5] Laboratory for Tumor Biology & Angiogenesis, Medical University of Innsbruck, Innsbruck, Austria, [6] Department of Vascular Biology and Tumor Angiogenesis, European for Center for Angioscience, Medical Faculty Mannheim of Heidelberg University, Mannheim, Germany

Endothelial colony forming cells (ECFC) or late blood outgrowth endothelial cells (BOEC) have been proposed to contribute to neovascularization in humans. Exploring genes characteristic for the progenitor status of ECFC we have identified the forkhead box transcription factor FOXF1 to be selectively expressed in ECFC compared to mature endothelial cells isolated from the vessel wall. Analyzing the role of FOXF1 by gain- and loss-of-function studies we detected a strong impact of FOXF1 expression on the particularly high sprouting capabilities of endothelial progenitors. This apparently relates to the regulation of expression of several surface receptors. First, FOXF1 overexpression specifically induces the expression of Notch2 receptors and induces sprouting. Vice versa, knock-down of FOXF1 and Notch2 reduces sprouting. In addition, FOXF1 augments the expression of VEGF receptor-2 and of the arterial marker ephrin B2, whereas it downmodulates the venous marker EphB4. In line with these findings on human endothelial progenitors, we further show that knockdown of FOXF1 in the zebrafish model alters, during embryonic development, the regular formation of vasculature by sprouting. Hence, these findings support a crucial role of FOXF1 for endothelial progenitors and connected vascular sprouting as it may be relevant for tissue neovascularization. It further implicates Notch2, VEGF receptor-2, and ephrin B2 as downstream mediators of FOXF1 functions.

Keywords: endothelial progenitors, ECFC, vascular sprouting, FOXF1, Notch2, ephrinB2, intersegmental capillaries

OPEN ACCESS

Edited by:
Wolfgang Holnthoner, Ludwig Boltzmann Gesellschaft (LBG), Austria

Reviewed by:
Paola Rizzo, University of Ferrara, Italy
Michela Pozzobon, Università degli Studi di Padova, Italy

***Correspondence:**
Erhard Hofer
erhard.hofer@gmx.at

[†] These authors have contributed equally to this work.

[‡] Present Address:
Caterina Sturtzel, Innovative Cancer Models, St. Anna Kinderkrebsforschung e.V. Children's Cancer Research Institute, Vienna, Austria
Julia Testori, AGES—Österreichische Agentur für Gesundheit und Ernährungssicherheit, Vienna, Austria
Ping Qiu, QJRX Healthcare LLC, Reston, VA, United States

Specialty section:
This article was submitted to Tissue Engineering and Regenerative Medicine, a section of the journal Frontiers in Bioengineering and Biotechnology

Received: *30 January 2018*
Accepted: *24 May 2018*
Published: *14 June 2018*

Citation:
Sturtzel C, Lipnik K, Hofer-Warbinek R, Testori J, Ebner B, Seigner J, Qiu P, Bilban M, Jandrositz A, Preisegger K-H, Untergasser G, Gunsilius E, de Martin R, Kroll J and Hofer E (2018) FOXF1 Mediates Endothelial Progenitor Functions and Regulates Vascular Sprouting. Front. Bioeng. Biotechnol. 6:76. doi: 10.3389/fbioe.2018.00076

INTRODUCTION

Endothelial colony forming cells (ECFC), also termed blood outgrowth endothelial cells (BOEC), can be easily outgrown from human cord blood or adult peripheral blood using standard endothelial cell growth conditions (Yoder et al., 2007; Martin-Ramirez et al., 2012; Hofer-Warbinek et al., 2014; Medina et al., 2017). Due to their high proliferative potential they can be obtained in

large quantities suitable for regenerative medicine. Progenitor cells comparable to ECFC can also be generated from induced pluripotent stem cells (Prasain et al., 2014). In distinction from other so-called circulating endothelial progenitor cells (EPC), that can be obtained from blood by different isolation and culture conditions and are of hematopoietic origin, ECFC have characteristics of true endothelial progenitors. They form vascular networks and integrate into newly formed vessels *in vivo* (Dubois et al., 2010; Banno and Yoder, 2017). It has been proposed that ECFC originate from the endothelial lining of blood vessels and lung capillaries could be a major source for their shedding into the bloodstream (Alphonse et al., 2014, 2015). ECFC could therefore constitute a vascular organ-specific progenitor cell type involved in regeneration of endothelium and neovascularization. Although ECFC are difficult to obtain from murine blood, an endothelial progenitor/stem-like cell population has been also located at the inner surface of murine blood vessels (Naito et al., 2012).

Irrespective of their still debated origin and normal physiological role, ECFC are promising candidates for cell therapies. When transplanted into sites of ischemic injury, ECFC incorporate into damaged blood vessels improving blood perfusion and supporting repair processes and organ function (Schwarz et al., 2012; Alphonse et al., 2014; Palii et al., 2014; Banno and Yoder, 2017). Based on their simple isolation (Martin-Ramirez et al., 2012; Alphonse et al., 2015) and properties they are also primary candidates for the *ex vivo* generation of vascularized tissue batches or organs for regenerative therapies (Ruvinov and Cohen, 2014).

Given their therapeutic importance, a precise characterization of the cells in comparison to mature endothelial cells of the vessel wall is needed. In regard of relevant surface markers ECFC were reported to be indistinguishable from mature endothelial cells, but ECFC are distinct by their clonal growth properties and high proliferative capacity (Banno and Yoder, 2017). To further characterize ECFC we have undertaken transcriptional profiling and have identified FOXF1 to be the most preferentially expressed transcription factor in ECFC when compared to mature endothelial cells.

The FOX (forkhead box) family of transcription factors is generally involved in the determination of cell lineage and organ specificities. For example, FOXA is a pioneer transcription factor regulating accessible nucleosome configurations at enhancers for liver-specific genes (Iwafuchi-Doi et al., 2016), FOXP1 promotes neural stem cell differentiation (Braccioli et al., 2017) and FOXN1 has been used in the reprograming of fibroblasts for the formation of an ectopic thymus (Bredenkamp et al., 2014). In the vascular system it has been shown that FOXC factors are required for vascular development (Seo et al., 2006; De Val et al., 2008) and more recently that FOXF1 is involved in formation of embryonic vasculature by regulating VEGF receptor genes (Ren et al., 2014).

Whereas initial vessel formation in the embryo occurs via vasculogenesis, the assembly of angioblasts, most vessel formation during growth and in the adult is initiated by vascular sprouting, i.e., angiogenesis (Risau, 1997). In this process an endothelial tip cell, starting from an existing vessel, invades into the surrounding tissue. Tip cells follow an increasing gradient of VEGF-A generated by ischemic tissues that they sense via VEGF receptor-2 and in part also VEGF receptor-3 (Adams and Alitalo, 2007; Blanco and Gerhardt, 2013). The growing vascular sprout is further formed by so-called endothelial stalk cells that follow the tip cell and have the capacity to proliferate leading to sprout extension. Sprout growth and interplay between tip and stalk cells is regulated by an intricate balance of signals involving, aside the attracting VEGF-A/VEGFR2 and − 3 interactions, also repelling guidance cues (Adams and Eichmann, 2010) and Notch receptors and their ligands (Ehling et al., 2013). For example, the Notch ligand Dll4 expressed on tip cells interacts with Notch1 receptors on stalk cells to prevent additional tip cell formation.

Specification and separation into arterial or venous capillaries and vessels further involves signaling mediated via Ephrin receptors and their ligands (Sawamiphak et al., 2010; Salvucci and Tosato, 2012). Whereas ephrin B2 characterizes arterial endothelial cells, EphB4 receptors are preferentially expressed on venous endothelial cells.

An excellent model to investigate vessel formation and its modulation is the zebrafish (Hogan and Schulte-Merker, 2017). In the still transparent larvae at 23 to 48 h post fertilization the intersegmental arterial vessels are formed by sprouting from the dorsal artery. Processes involving arterial sprouting can therefore be easily analyzed by live imaging during this time period. In addition, formation of the venous and lymphatic systems can be analyzed (Isogai et al., 2001).

Here we report that FOXF1 is selectively expressed in ECFC and that FOXF1 expression is linked to the high sprouting and tip cell formation capacities of ECFC. Furthermore, we determine that FOXF1 expression can modulate Notch2 receptors and that reducing Notch2 expression inhibits sprouting comparable to downmodulation of FOXF1. In addition, FOXF1 augments VEGFR-2 expression and seems to preferentially support arterial vessel sprouting as it upregulates ephrinB2 and downregulates EphB4. A role of FOXF1 for arterial vessel formation is also corroborated by the finding that downmodulation of FOXF1 in zebrafish deteriorates arterial vessel formation by sprouting. Taken together the data support that FOXF1 is an important determiner of the progenitor status of ECFC and regulates sprouting capabilities.

MATERIALS AND METHODS

Cell Culture

Endothelial colony forming cells (ECFCs) were isolated from human cord blood samples obtained from the Department of Obstetrics and Gynecology, Medical University of Vienna, or supplied by VivoCell AG (Graz, Austria). Procedures of cord blood collection including a written informed consent have been approved for this study by the ethical committee of the Medical University of Vienna (protocol number 122/2010). Blood samples were collected in cord blood collection bags (MacoPharma, Mouvaux, France) and stored at room temperature. Then mononuclear cells (MNC) were isolated within 24 h over Lymphocyte Separation Medium LSM 1077 (PAA, now GE Healthcare) as recommended by the manufacturer. ECFC were obtained from the MNCs according to published procedures

(Yoder et al., 2007; Lucas et al., 2009). In short, MNC were resuspended in microvascular endothelial cell growth medium-2 (EGM-2 MV medium, Bio Whittacker, Lonza) and seeded onto 0.01% kangaroo or 0.1% rat collagen (Sigma-Aldrich) coated culture dishes. Twenty four hours after seeding the floating cells were removed and fresh medium was added to the adherent cells. Clonal outgrowth was observed after 2–6 weeks. ECFCs were expanded on 1% gelatin coated cell culture dishes in EGM-2 MV medium and used for further analysis.

Human umbilical vein endothelial cells (HUVECs) were isolated as described previously (Testori et al., 2011) and cultured on 1% gelatin coated cell culture dishes in EGM-2 MV medium. HUVECs of passage 2–3 were used for experiments.

Human embryonic kidney 293 cells (HEK 293 cells, ATCC No. CRL-1573) were cultured in Minimum Essential Medium α (MEM-α, Invitrogen LT, Carlsbad, CA) supplemented with 10% neonatal calf serum (NCS, Invitrogen LT), 2 mM glutamine, 100 U/ml penicillin and 1 mg/ml streptomycin (all PAA/now part of GE).

HEK 293T/17 cells (ATCC No. CRL-11268) were cultured in Dulbecco's Modified Eagle's Medium (DMEM, Invitrogen LT) with 10% fetal calf serum (FCS, Sigma-Aldrich), 2 mM glutamine, 100 U/ml penicillin and 1 mg/ml streptomycin.

All cells were maintained at 37°C applying 5% CO_2 and 95% humidity.

Immunocytochemistry

For immunostaining cells were seeded in chamber slides (Lab-Tek Brand Products; Nalge Nunc International). The day after seeding cells were fixed with 4% paraformaldehyde (PFA) at room temperature for 10 min. The murine anti-human CD31-FITC (R&D Systems), polyclonal anti-VE-cadherin-FITC (Bender MedSystems GmbH) as well as the sheep anti-human vWF-FITC (AbD Serotec) were diluted 1:100 in 1% BSA-PBS and incubated at 4°C overnight. For nuclear staining, cells were incubated with 1 ng/ml Hoechst stain (Sigma) for 5 min. Thereafter immunofluorescence was analyzed with a fluorescence microscope (Nikon eclipse 80i). Images were taken with an integrated CCD camera (Nikon) at indicated magnifications.

Flow Cytometry

For flow cytometry cells were harvested by treatment with accutase (PAA, Pasching, Austria). Cells were stained for VEGFR-2 in PBS containing 0.5% BSA and 2 mM EDTA with murine anti-human KDR-APC (R&D Systems) antibodies as recommended by the manufacturer. As isotype controls, IgG1-APC antibodies (Miltenyi) were used. Antibody binding was assessed on a FACSCalibur and evaluated using CellQuest software (BD Biosciences. San Jose, CA).

RNA Preparation, RT-PCR and Real-Time RT-PCR Analysis

For the extraction of RNA, cells were incubated with RNAlater (Ambion) for 1 min, washed with water and lysed in QIAzol (Qiagen). RNA was extracted according to manufacturer's instructions. 1 μg of total RNA was used to synthesize cDNA with Superscript II Reverse Transcriptase (Invitrogen LT) and oligo(dT) primers (Invitrogen LT) according to the recommended protocol.

Semi-quantitative RT-PCR was performed with GoTaq™ DNA polymerase (Promega) according to the instructions of the producer. For quantitative real-time RT-PCR a Rotor-Gene®Q LightCycler (Qiagen) detecting Rotor Gene SYBR Green (Qiagen) was used. All values were normalized to β-actin mRNA as internal standard. Oligonucleotide primers and annealing temperatures used for gene amplification are listed in Supplementary Table S2.

Affymetrix Microarray Hybridization

Extracted RNA was further purified using RNeasy kit (Qiagen). Total RNA (200 ng) was analyzed on genome-wide human Gene Level 1.0 ST GeneChips (Affymetrix, Santa Clara, CA, USA) as described in detail in Tauber et al. (2010). Scanning of the arrays was carried out according to manufacturer's protocols https://www.affymetrix.com. RMA signal extraction, normalization, and filtering was performed as described (http://www.bioconductor.org/). A variation filter was applied for selecting informative (i.e., significantly varying) genes. The filtering criteria for the exemplary data sets required an interquartile range > 0.5 and at least one sample with expression intensity > 50. The full obtained data sets are now available at Gene Expression Omnibus under the accession number GSE22695 (http://www.ncbi.nlm.nih.gov/geo/query/acc.cgi?acc=GSE22695).

Generation of Replication-Defective Adenoviruses Encoding FOXF1

A full-length open reading frame cDNA clone (BC089442) encoding for the human FOXF1 gene was ordered from ImaGenes (Berlin, Germany). The complete coding region was amplified from the cDNA clone described above using PCR primers containing additionally designed SalI (5′-primer) or XhoI (3′-primer) restriction sites and inserted into the respective restriction enzyme cleavage sites of the multiple cloning site of the pShuttle-IRES-hrGFP-1 vector plasmid, which is part of the AdEasyTM Adenoviral Vector System kit from Stratagene (Agilent Genomics, La Jolla, CA). pShuttle.FOXF1 and the pAdEasy-1 were co-transformed into supplied BJ5183 $RecA^+$ E. coli for recombination. The successfully recombined vector was sequenced for accuracy, linearized with PacI (New England Biolabs) and transfected into HEK293 cells using a mammalian transfection kit (Stratagene) to generate primary adenoviruses. These were subcloned, amplified and purified by ultracentrifugation over a $CsCl_2$ gradient (Sigma-Aldrich) as previously described (Testori et al., 2011). An empty control adenovirus was prepared in parallel. Viral titer was determined using the Adeno-X rapid titer kit (Clontech, Mountain View, CA) according to the recommended protocol.

Generation of Replication Defective Lentiviruses

Lentiviral vector DNA encoding shRNA directed against FOXF1 (pLKO.1-shRNA-FOXF1-puro), shRNA directed against Notch2

(pLKO.1-shRNA-Notch-2-puro) or scrambled shRNA (pLKO.1-shRNA-neg-puro) were obtained from Sigma-Aldrich. The packaging plasmids psPAX2 and pMD2.G were from Addgene (Cambridge, MA, USA). For the generation of lentiviral vehicles the lentivirus vector plasmids were co-transfected with the packaging plasmids into HEK 293T/17 cells using an optimized calcium phosphate method (Stratagene, LaJolla, CA) according to the recommendations of the manufacturer. Eight hours after transfection medium was changed and then viral supernatant was harvested 24 and 48 h later. For infection the 0.4 μm filtered virus supernatants were added to subconfluent ECFCs together with fresh medium (EGM2-MV) in a ratio of 1:1.

SDS-Page and Western Blot Analysis

Equal amounts of protein extracts from cells were separated by 10% SDS-polyacrylamide gel electrophoresis (PAGE) and transferred onto an Immobilon-P membrane (Millipore, Bedford, MA, USA) by semidry blotting. Membranes were blocked for 1 h in 5% organic skimmed milk (Sigma-Aldrich) in PBS containing 0.1% Tween-20 (Bio-Rad). For protein detection membranes were incubated in PBS/0.1% Tween-20/5% milk powder containing a 1:1000 diluted goat polyclonal anti-hFOXF1 antibody (R&D Systems) for endogenous FOXF1 expression or a 1:5000 dilution of the antibody for the visualization of the adenovirus mediated FOXF1 expression. The rat monoclonal anti-hNotch2 intracellular domain antibody (R&D systems) was used at a dilution of 1:500. Bound antibodies were detected by applying species-specific HRP-conjugated secondary antibody (GE Healthcare, city, state; diluted 1:5000) followed by enhanced chemiluminescence (GE Healthcare). As an internal control glyceraldehyde-3-phosphate dehydrogenase (GAPDH) was detected using a monoclonal mouse anti-GAPDH antibody (Millipore-Chemicon International, Vienna, Austria; diluted 1:5000).

Spheroid-Based *in Vitro* Sprouting Assay

ECFCs transduced with adeno- or lentiviruses were tested for their ability of sprout formation into an extracellular matrix similar setting upon stimulation based on the protocol of Korff and Augustin (1998) as described in Testori et al. (2011). Briefly, ECFC were suspended in culture medium containing 20% (wt/vol) methylcellulose (Sigma-Aldrich) to generate spheroids of defined cell number (400 cells/spheroid) in hanging drops overnight. In PBS/10% FCS harvested spheroids were embedded into rat collagen gels with the final concentration of 40% Methocel/10% FCS/ 40% collagen/10% 10xM199 (Sigma-Aldrich) and transferred into 24-well plates for suspension cells. After 30 min of gel formation at 37°C, EBM-2 MV without or containing VEGF and/or bFGF (50 ng/ml each) was layered onto the top of the gel. Following incubation at 37°C overnight, *in vitro* angiogenesis was stopped by fixation using 10 % PFA for 1 h. Pictures were taken on a Nikon eclipse 80i microscope equipped with a CCD camera (Nikon). Accumulated sprout length of at least 20 spheroids per condition were measured with ImageJ software. All experiments were performed at least three times with ECFCs of different donors.

Knock-Down of FOXF1 in Zebrafish

Embryos of the Tg(fli1:EGFP)y1 line were raised and staged as recently described (She et al., 2018). Embryos were kept in E3 medium (5 mM NaCl, 0.17 mM KCl, 0.33 mM CaCl2, 5–10% methylene blue) at 28.5°C with or without 0.003% 1-phenyl-2-thiourea (Sigma) to suppress pigmentation and staged according to somite number or hours post-fertilization (hpf). All experimental procedures on animals were approved by the local government authority, Regierungspräsidium Karlsruhe (license no.: 35-9185.64) and carried out in accordance with the approved guidelines.

Morpholinos (Gene Tools) were diluted in 0.1 M KCl, used by the indicated concentrations and injected through the chorion of one-cell or two-cell stage embryos. Splice blocking morpholino FoxF1 SB-FoxF1-MO (5′-CTTAAAAACTTTACCTTGGAGGTCG−3′) or a standard control morpholino (5′-CCTCTTACCTCAGTTACAATTTATA-3′) together with a p53 morpholino (Epting et al., 2010) were used and dose escalation studies were performed to determine submaximal morpholino concentrations. Knockdown efficiency was confirmed by RT-PCR with the primers 5′-GCCCCCGACATCTCTAAATA-3′ and 5′-TGTCACACATGCTGGGAGAT-3′ for FoxF1. PCR was conducted at 95°C for 5 min, (95°C for 30s, 56°C for 30s, 72°C for 45s) × 35 cycles and 72°C for 5 min and PCR products were loaded on a agarose gel. Tg(fli1:EGFP)y1 embryos were manually dechorionated and anesthetized with 0.05 % tricaine (Sigma). Morphological analysis of vessels was performed using a CTR 6000 microscope (Leica) or a TCS SP5 system (Leica). For quantitative morphological analysis the number of embryos with non-defective, partially defective and defective intersegmental vessels (ISVs), dorsal longitudinal anastomotic vessel (DLAV) connections between the investigated ISVs in the trunk vasculature, parachordal lymphangioblast (PLs), and thoracic duct (TD) was determined at 48 or 120 hpf, respectively. Results are given in percentage.

Statistics

Statistical analysis was performed with Prism 6 software (GraphPad, San Diego, CA, USA) using paired Student's *t*-test. A *p*-value of 0.05 was considered as statistically significant.

RESULTS

FOXF1 Is Preferentially Expressed in Blood ECFC When Compared to Vessel Wall Endothelial Cells

To decipher genes specifically expressed in endothelial progenitors of the ECFC type we have comparatively analyzed gene expression profiles of ECFC isolated from blood and of terminally differentiated endothelial cells of the vessel wall. For this purpose, we isolated ECFC from human cord blood or adult peripheral blood and mature endothelial cells from human umbilical cords or adult veins. Usually about 5 to 10 ECFC colonies were obtained from mononuclear cells of 50 ml of cord blood or adult peripheral blood. For comparative reasons,

to display a distinct gene expression profile to hematopoietic progenitor cells, we also isolated CD34 positive cells from cord blood.

The transcriptomic profiles of low passage ECFC from cord blood were evaluated in comparison to HUVEC and of ECFC from adult peripheral blood in comparison to adult saphenous vein endothelial cells (HSVEC). When focusing our analysis on transcriptional regulators, we found two transcription factors more than 5-fold overrepresented in the ECFC of both sources, the winged helix transcription factor FOXF1 and the Krueppel-related zinc finger protein 117 (Supplemental Table S1). FOXF1 was the most preferentially expressed transcription factor in both ECFC (10–20-fold). In contrast, its expression was below background levels in $CD34^+$ cells from cord blood supporting an endothelial progenitor and non-hematopoietic progenitor function. In addition, the data obtained provide evidence that otherwise the ECFC used in this study are highly similar to mature endothelial cells in the expression of endothelial markers such as VEGFR-2, Tie-2, VE-cadherin, and von Willebrand factor (Supplementary Table S2). Since ECFC from cord blood were more easily obtained and seemed to have advantageous proliferation potential we focused further work on the role of FOXF1 in cord blood-derived ECFC.

First we reassessed the transcriptomic profiling data by investigating the mRNA levels of FOXF1 by realtime RT-PCR as well as by Western Blot analysis using multiple isolates of ECFC ($n = 12$) and HUVEC ($n = 11$) derived from different donors at passage 2–3. In parallel, the expanded cells were analyzed for markers of endothelial and hematopoietic cells by immunocytochemistry.

Consistent with the microarray analysis FOXF1 mRNA was on average 10-fold higher in ECFC when compared to HUVEC and FOXF1 protein was strongly stained in Western blots of ECFC lysates, whereas it was undetectable in HUVEC lysates (**Figure 1A**). ECFC regularly displayed strong staining for surface markers of the endothelial cell lineage such as CD31, VE-cadherin, and vWF (Supplementary Figure S1). Other markers of hematopoietic cells tested such as CD45 and CD14 could never be detected verifying that the isolated ECFC were not significantly contaminated with other cell types of hematopoietic origin (data not shown). This is also supported by the absence of signals for CD45, CD14, and CD133 in the microarray data of ECFC, whereas strong expression of these genes is readily detected in blood $CD34^+$ cells (Supplementary Figure S2).

FOXF1 Controls a Program That Provides Increased Sprouting Capacity to ECFC

Despite displaying surface markers very similar to mature endothelial cells, ECFC are diverse by their potential to proliferate over extended time periods (Yoder et al., 2007) and to integrate into newly forming blood vessel *in vivo* (Dubois et al., 2010). We have regularly found that the capacity of ECFC to form tubular sprouts *in vitro* is significantly higher than for HUVEC (Schneller and Hofer, unpublished observation).

To show a potential involvement of FOXF1 in this property we performed gain- and loss-of-function studies. For this purpose, we produced on the one hand a replication defective adenoviral vector encoding FOXF1, which mediates strong FOXF1 overexpression as confirmed by realtime RT-PCR and Western blot analysis (Supplementary Figure S2A). On the other hand, we used lentiviruses expressing short hairpin RNAs (shRNAs) to downregulate endogenous FOXF1 expression levels. Up to 90% decrease in FOXF1 mRNA expression was achieved 48 h after infection leading to a strong reduction of FOXF1 protein (Supplementary Figure S2B).

Indeed, when we analyzed the cumulative lengths of sprouts formed by ECFC without and in the presence of adenoviral overexpression of FOXF1 a strong induction of basal sprouting activity without addition of proangiogenic factors was revealed (**Figure 1B**). When VEGF-A-induced sprouting was analyzed, no statistically significant increase for FOXF1 overexpressing cells was observed, although the data seemed to display a tendency for increased sprouting also in this case. Much more prominent, however, was the FOXF1-elicited sprouting in the absence of exogenous angiogenic factors which resulted in nearly 50% of the cumulative sprout length triggered by VEGF-A.

Vice versa, when we knocked down endogenous FOXF1 by shRNA-expressing lentiviruses a strongly reduced sprouting activity was observed in control as well as VEGF-A-induced assays (**Figure 2A**). These data are in line with an important role of FOXF1 for basal as well as VEGF-A-induced sprouting of ECFC.

Remarkably, it appeared from these analyses that especially the number of initiated sprouts per spheroid was strongly altered by FOXF1 and we therefore explored if FOXF1 influences the potential of ECFC to form tip cells. These are responsible for initiation of sprout formation, thereby controlling the number of sprouts. For this purpose, the influence of knocked-down FOXF1 expression on the probability of the cells to reach the tip cell position was evaluated in a mosaic expression experiment. ECFC infected with lentiviruses expressing shRNA-FOXF1 or control shRNA were mixed with 5% of ECFC infected with a lentivirus encoding GFP and then the spheroid sprouting assay was performed. Green tip cells with normal FOXF1 expression were scored in relation to non-GFP containing tip cells originating from cells transduced with either shRNA-FOXF1 or control shRNA. As expected from the mixing ratio, the combination of control shRNA transduced cells with 5% GFP expressing cells gave rise to 5% of green tip cells. However, when we co-cultured shRNA-FOXF1 expressing cells with 5% of GFP expressing cells it became apparent that downregulation of FOXF1 reduced the probability of these cells to reach tip cell position and nearly doubled the proportion of green tip cells with normal FOXF1 expression from 5 to about 10% (**Figure 2B**). This finding implies that FOXF1 controls sprouting via modulating the capacity of the cells to form tip cells and to initiate sprouting.

FOXF1 Specifically Upregulates Notch2 Receptor Expression, Which Is Involved in Controlling Sprouting Activity

Given the impact of FOXF1 on sprouting, we analyzed the influence of the factor on the expression of surface proteins

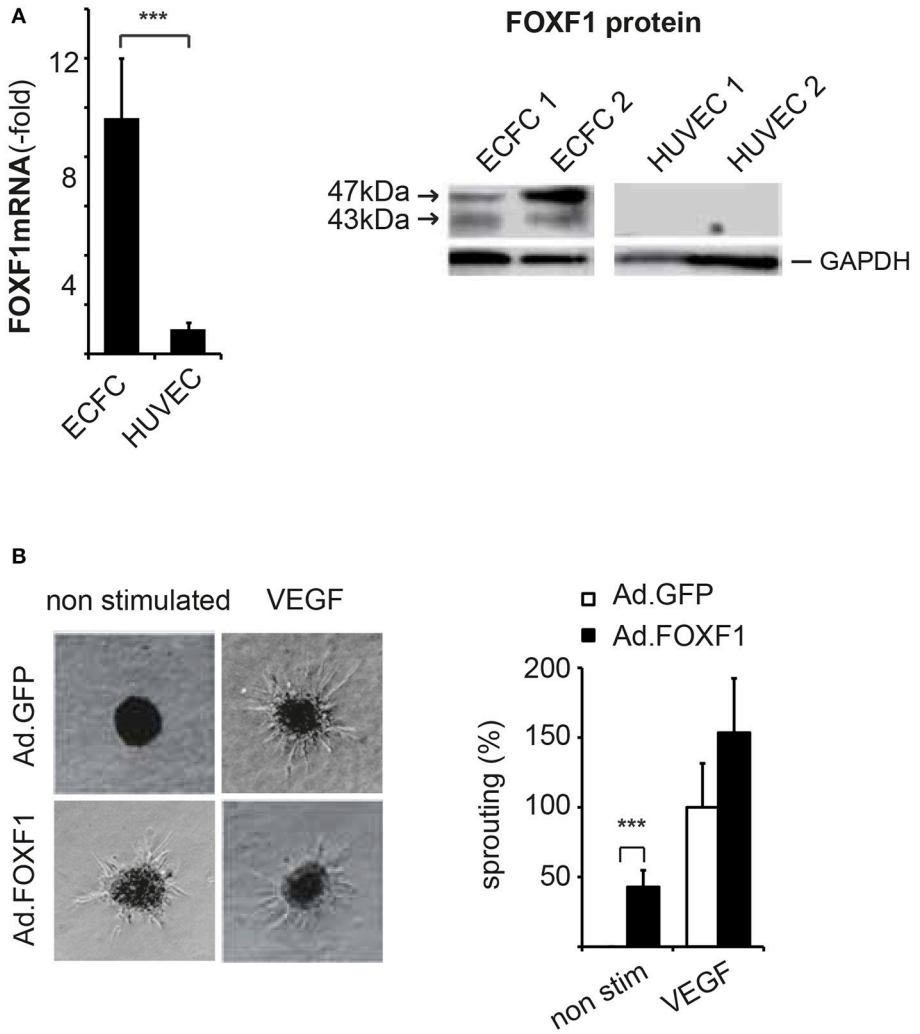

FIGURE 1 | FOXF1 is preferentially expressed in ECFC and induces sprouting. **(A)** Real-time RT-PCR and Western blot analysis of FOXF1 mRNA and protein in ECFC and HUVEC: ECFC and HUVEC were isolated from cord blood and umbilical cords, respectively, and cultured to density in 6-well plates as described in the Methods section. First to second passage cells were used for mRNA isolation, cDNA syntheses, and real-time RT-PCR or were lysed in sample buffer, the proteins separated by polyacrylamide gel electrophoresis and Western blotted. The left part shows the overrepresentation of FOXF1 mRNA in samples from ECFC compared to those of HUVEC. Mean values ± SEM of at least 10 different donors are shown, asterisks indicate statistical significance of difference. The right part shows the selective expression of FOXF1 protein in Western blots of ECFC compared to HUVEC. Two different isolates of ECFC and HUVEC representative of 10 analyzed are shown. Membranes were probed for FOXF1 and GAPDH as internal standard using corresponding antibodies. **(B)** Overexpression of FOXF1 induces sprouting in the spheroid assay: ECFC were infected with Ad.FOXF1 or Ad.GFP with an MOI of 8. The following day spheroids were generated and embedded into collagen gels without or in the presence of VEGF (100 ng/mL) as described in the Methods section. After 24 hours spheroids were fixed and photographic images taken. Representative images of spheroids generated from Ad.FOXF1- or Ad.GFP-infected cells are displayed in the left panel. The quantification of the cumulative sprout length is depicted in the right panel. Results are displayed as mean values ± SEM. The cumulative sprout lengths observed for spheroids transduced with control adenoviruses (Ad.GFP) and induced with VEGF were arbitrarily set to 100%. One representative experiment of four performed is shown (***$p < 0.001$).

previously shown to determine the probability to form tip cells and to initiate sprouting. This included members of the Notch receptor family, since the Notch signaling pathway has been shown to be of crucial importance for tip cell generation (Phng and Gerhardt, 2009).

Indeed, when we quantified by realtime RT-PCR the expression of mRNAs for the major Notch receptors in response to FOXF1 overexpression we found Notch2 mRNA significantly upregulated. Western Blot analysis furthermore revealed an increase of an about 100 kD cleaved Notch2 fragment containing the intracellular domain of Notch2 that mediates Notch activity (**Figure 3A**). In line with a transcriptional upregulation of Notch2 by FOXF1, knocking down FOXF1 via short hairpin RNA caused a massive decrease of Notch2 mRNA (**Figure 3B**).

To investigate, if the effects of FOXF1 on sprouting were mediated via Notch2, we analyzed the potential influence of downmodulation of Notch2 on sprouting activity. A significant and selective shRNA-mediated downregulation of Notch2 was

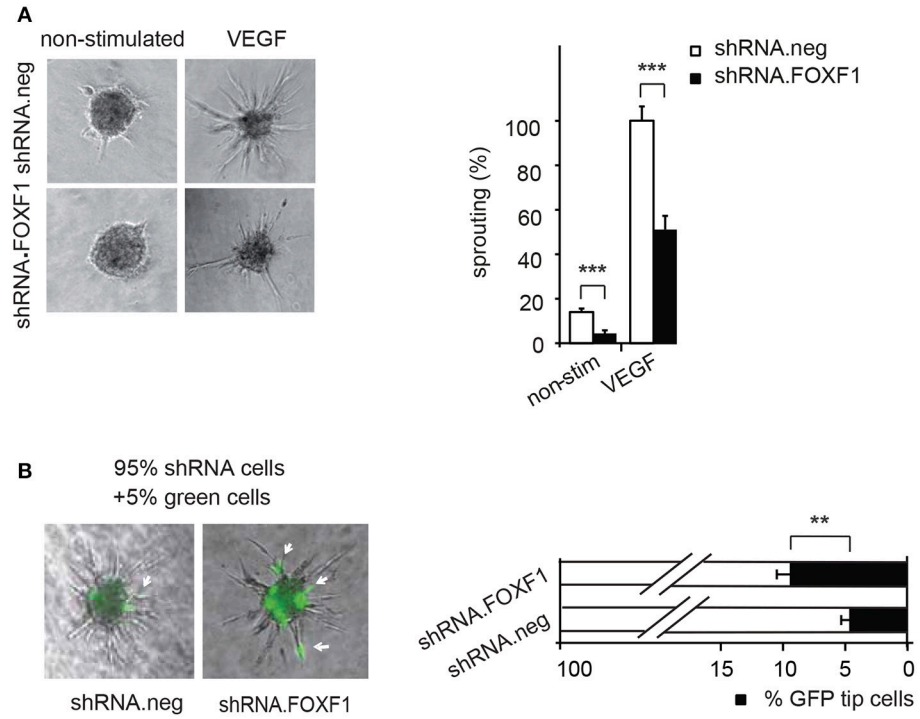

FIGURE 2 | Downmodulation of FOXF1 reduces sprouting and the number of cells in tip cell position. **(A)** Downmodulation of FOXF1 reduces sprouting: Cells were transduced with lentiviruses expressing shRNA.FOXF1 or control viruses (shRNA.neg) for 48 h. Then the spheroid assay was performed without stimulation or in the presence of VEGF-A. Representative images of spheroids are displayed in the left panel. A corresponding quantification is depicted in the right panel and displayed as mean values ± SEM. The cumulative sprout lengths observed for spheroids transduced with shRNA.neg viruses and induced with VEGF-A were arbitrarily set to 100%. One representative experiment of 3 performed is shown. **(B)** Downmodulation of FOXF1 reduces the capacity of ECFC to generate tip cells: Cells were separately transduced with lentiviruses expressing shRNA.FOXF1 or control (shRNA.neg) lentiviruses for 48 h. Then the cells were mixed with 5% of cells transduced with a lentivirus encoding GFP and the spheroid assay performed. The number of GFP-expressing tip cells was scored. The left panel depicts representative pictures of spheroids comprised of combinations of 95% of shRNA-neg (left) or 95% of shRNA-FOXF1 (right) transduced cells mixed with 5% of GFP-expressing cells. Arrows indicate GFP expressing green cells in tip cell position. The right panel shows the quantification of green cells found in tip cell position. Mean percentages of green tip cells ± SEM calculated from 40 spheroids per sample and three experiments with different isolates of ECFC are shown (**$p < 0.01$; ***$p < 0.001$).

achieved by lentiviral transduction (Supplementary Figure S3). Intriguingly, this downmodulation resulted in a reduction of sprouting capacity (**Figure 3C**), which was similar to the reduced sprouting observed after knocking down FOXF1 (**Figure 2A**). Furthermore, we tested whether shRNA-mediated downmodulation of Notch-2 in Ad.FOXF1 transduced cells would reduce the FOXF1-induced sprouting. Indeed, a strong reduction of sprouting was obtained (**Figure 3D**). Taken together, these results provide strong evidence that the Notch2 receptor contributes to the initialization of sprout formation by FOXF1 in ECFC.

FOXF1 Promotes Expression of Ephrinb2 as Well as VEGF Receptor-2, Whereas It Reduces EphB4 Expression

Ephrin B2 has been shown to characterize arterial endothelial cells and to be upregulated in endothelial tip cells during sprouting (Sawamiphak et al., 2010; Salvucci and Tosato, 2012). We therefore tested whether FOXF1 could alter the expression of ephrinB2 and its counteracting receptor EphB4. Indeed, we found that not only the mRNA for the arterial marker ephrinB2 was significantly upregulated upon FOXF1 overexpression, but that concomitantly also the mRNA for the venous marker EphB4 was significantly downregulated (**Figure 4A**).

Furthermore, we have been interested to determine whether another regulator of sprouting activity, the VEGF receptor-2, is regulated by FOXF1. Indeed we find that VEGF receptor-2 is upregulated by FOXF1 at the mRNA and protein level (**Figure 4B**). By flow cytometry we detect a significant increase in surface expression of VEGFR-2, suggesting its contribution to the high sprouting activity of ECFC.

FOXF1 Contributes to the Formation of Intersegmental Vessels as Well as the Lymphatic Trunk

The zebrafish is an excellent model to investigate vessel formation and sprouting during embryogenesis as vasculo- and angiogenesis are highly stereotypical and tightly regulated by defined genetic programs, several transgenic zebrafish lines expressing fluorescent markers in the vascular system are highly established and they can be easily genetically modified (Hogan and Schulte-Merker, 2017).

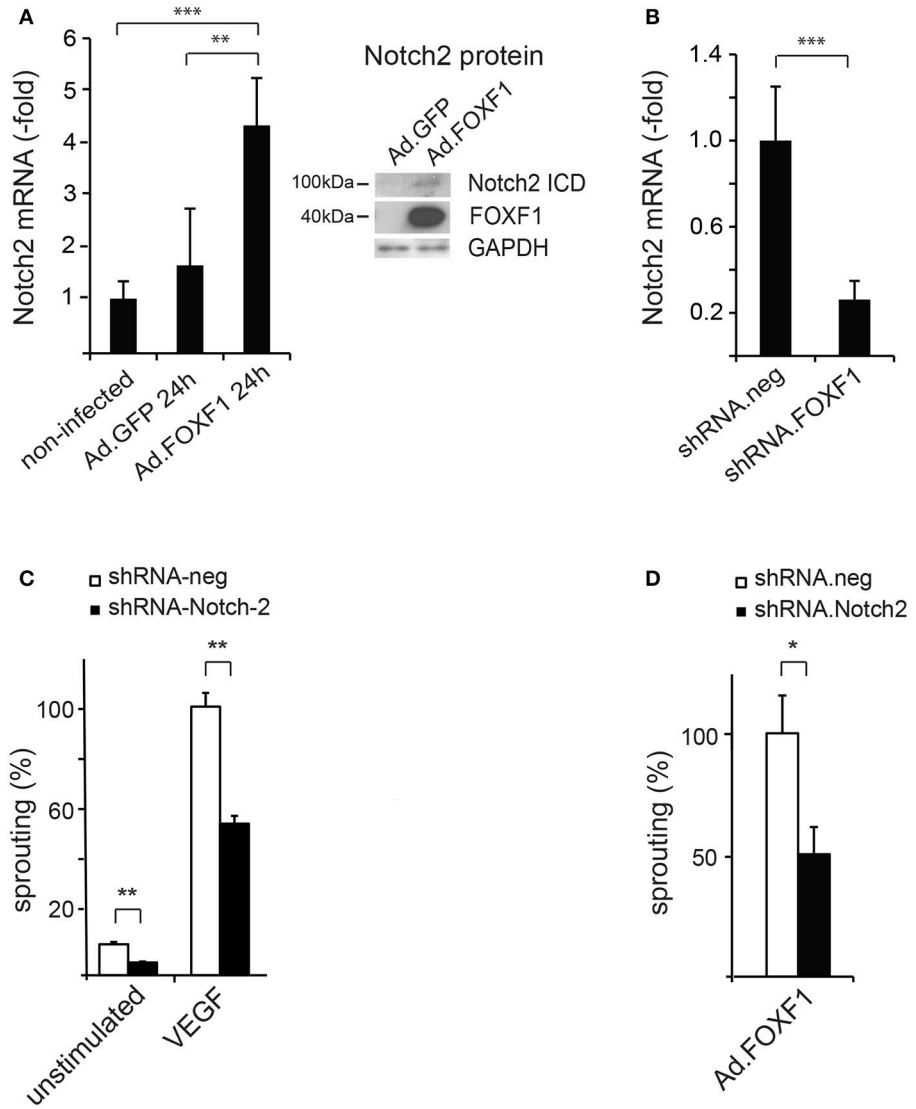

FIGURE 3 | FOXF1 regulates Notch2 expression, which mediates sprouting capability. **(A)** FOXF1 overexpression upregulates Notch2 mRNA and protein: ECFC were transduced with Ad.FOXF1 or Ad.GFP for 24 h. The left panel displays the realtime RT-PCR analyse giving mean values ± SEM of one experiment representative of 4 performed. The right panel shows Western blot images obtained after incubation of membranes with antibodies recognizing the Notch2 intracellular domain or FOXF1. Blots were further reprobed with antibodies for GAPDH as expression controls. **(B)** Downmodulation of FOXF1 reduces Notch2 mRNA: Cells were transduced with lentiviruses expressing shRNA.FOXF1 or control viruses (shRNA.neg) for 48 h. Then total RNA was isolated and realtime RT-PCR analysis performed. Mean values ± SEM were calculated using ß-actin as an internal standard. **(C)** Downmodulation of Notch2 strongly reduces sprouting: ECFC were transduced with shRNA.Notch2 or shRNA.neg viruses for 48 h. Then the spheroid sprouting assay was performed without stimulation or using induction with VEGF-A. Results are displayed as mean values of the cumulative sprout length ± SEM. Results obtained with control virus-infected and VEGF-stimulated spheroids were arbitrarily set to 100%. One representative experiment of 3 performed is shown. **(D)** Downmodulation of Notch2 inhibits FOXF1-induced sprouting: ECFC were first transduced with shRNA.Notch-2 or shRNA.neg lentiviruses and after 24 h in addition infected with Ad.FOXF1. After another 24 h the spheroid sprouting assay was performed. Results are mean values ± SEM calculated from three experiments (*$p < 0.05$; **$p < 0.01$; ***$p < 0.001$).

To investigate a potential role of FOXF1 *in vivo* during embryonic vessel formation we downregulated zFOXF1 in zebrafish using a splice blocking morpholino (SB-FOXF1-MO) (Supplementary Figure S4). We observed at 48 hpf dose-dependent distorting effects on the formation of intersegmental vessels, which originate by sprouting from the dorsal aorta or posterior cardinal vein and usually regularly pervade every somite and eventually connect to the dorsal longitudinal anastomic vessel (**Figures 5A–C**). Aberrant numbers of intersegmental vessels, inefficient sprout formation and anastomosis of the dorsal longitudinal anastomosing vessel, or undirected sprouting patterns were observed. This was presumably at least in part due to defective sprouting of arterial vessels.

A second effect was the nearly entire absence of a forming lymphatic network presenting with nearly completely lacking parachordal lymphangioblasts at 48 hpf and a missing thoracic duct at 120 hpf (**Figures 5D–F**). These data suggest that in

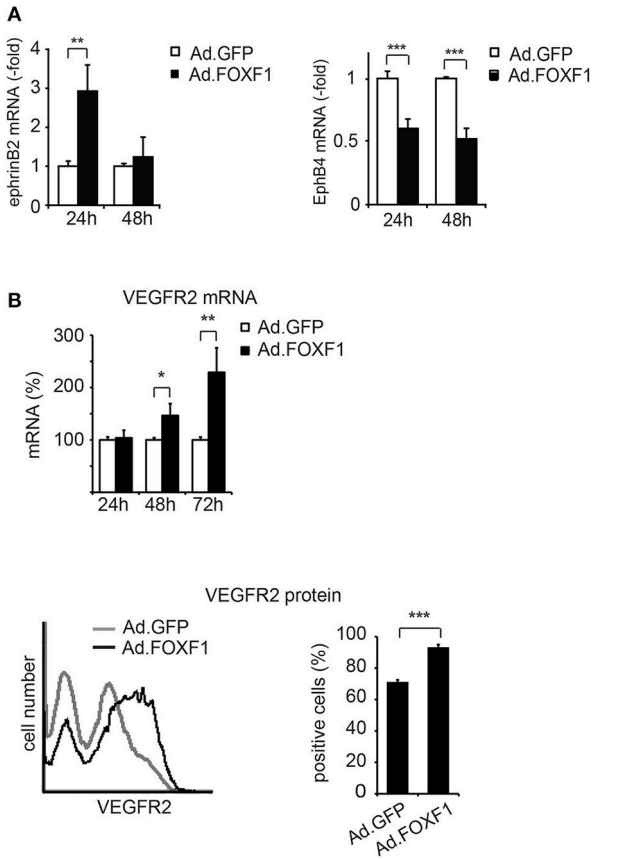

FIGURE 4 | FOXF1 induces ephrinB2 and VEGF receptor-2, but reduces EphB4 expression. **(A)** FOXF1 overexpression upregulates ephrin B2 mRNA and downmodulates EphB4 mRNA: ECFC were infected with Ad.FOXF1 or control Ad.GFP for 24 and 48 h. Then total RNA was isolated and ephrinB2 (left panel) and EphB4 (right panel) mRNAs quantified by real-time RT-PCR analysis. Values were normalized to ß-actin mRNA as internal standard. Mean values ± SEM calculated from results obtained from three experiments with different donors are illustrated (**$p < 0.01$, ***$p < 0.001$). **(B)** FOXF1 overexpression upregulates expression of VEGFR-2 at mRNA and protein level: ECFCs were transduced for 24, 48, and 72 h. Then total RNA was isolated and real-time RT-PCR performed or cells were stained with anti-KDR antibodies and analyzed by flow cytometry. The upper panel depicts the real-time RT-PCR analysis, mean values ± SEM calculated from at least three different donors are depicted. Values were normalized to β-actin mRNA as internal standard. Asterisks label values with significant differences (*$p < 0.01$, **$p < 0.001$). The lower left panel shows a representative flow cytometry histogram of cells 48 h after transduction of cells with Ad.FOXF1 (black line) compared to Ad.GFP infected cells (gray line). The lower right panel displays the quantification of the flow cytometry data, mean percentages ± SD of three independent experiments each performed in triplicates are depicted (***$p < 0.0001$).

zebrafish FOXF1 plays an instructive role for arterial sprouting *in vivo,* and is additionally involved in organizing lymphatic vessel formation.

DISCUSSION

New blood vessels can form by two distinct mechanisms: first by vasculogenesis, a process in which in the embryo a vascular system is assembled de novo starting from endothelial progenitor cells; second by angiogenesis which enlarges the vasculature during growth by sprouting from existing vessels, endothelial proliferation and remodeling (Risau, 1997; Adams and Alitalo, 2007). Sprouting angiogenesis appears to be also the dominant form of neovascularization during wound repair and tumor formation (Sturtzel, 2017). The description of endothelial progenitor-like cells in circulating blood led to the concept of post-natal vasculogenesis, i.e., that EPC may contribute to angiogenic vessel growth and repair in the adult (Bautch, 2011). Whereas part of the cell types described in this context may be rather monocyte lineage-derived cells that contribute to angiogenesis by secretion of paracrine factors, a certain kind of human progenitors termed ECFC are believed to constitute true endothelial progenitors, to be descendants of progenitor cells resident in the vessel wall and to be competent to stimulate angiogenesis as well as to contribute to newly formed vessel wall endothelial cells (Banno and Yoder, 2017).

In this study we have been interested to identify characteristics of these progenitor cells of the vasculature with regard to transcription factors and surface receptors and their potential functional role. To gain evidence for specific functions defining the progenitor status of ECFC, we have comparatively investigated ECFC by transcriptomic profiling to vessel wall endothelial cells. We detected FOXF1, a member of the FOX family, as the most consistently overrepresented transcription factor in ECFC from human cord and adult blood. This is intriguing, as several FOX transcription factors have been described as pioneer transcription factors important for cell type-specific transcription defining different tissues (Bredenkamp et al., 2014; Iwafuchi-Doi et al., 2016; Braccioli et al., 2017). Furthermore, knock-down of FOXC2 in combination with Etv2 has been shown to disrupt vascular development in the zebrafish (De Val et al., 2008) and mouse embryo compound mutants for FOXC1 and FOXC2 display arteriovenous malformations (Seo et al., 2006). It was therefore possible that FOXF1 might control specific endothelial progenitor-type transcription and functions.

A hypothetical mechanism, how ECFC could contribute to neovascularization, is by invasion into hypoxic vessel areas followed by stimulation of angiogenic sprouting. This could be triggered via cell-to-cell contact inducing sprouting of neighboring endothelial cells, or by forming tip cells and initiating sprouts by the incorporated ECFCs themselves. That this is a conceivable process is supported by our finding that the sprouting capacities of ECFC are consistently higher than of vessel wall endothelial cells (Schneller and Hofer, unpublished observation).

We were therefore interested to see whether the high sprouting capacity of ECFC may be related to the high expression levels of FOXF1. Indeed, the level of FOXF1 expression determined the sprouting capacity of the cells as overexpression increased and knock-down strongly decreased sprouting. We also obtained evidence that the level of FOXF1 expression determined the probability of cells to reach tip cell position. These findings suggested that FOXF1 might control a transcriptional program that leads to the upregulation of proteins important for tip cell functions.

Among the surface molecules important for tip cell functions are members of the Notch family, VEGF receptors and ephrins

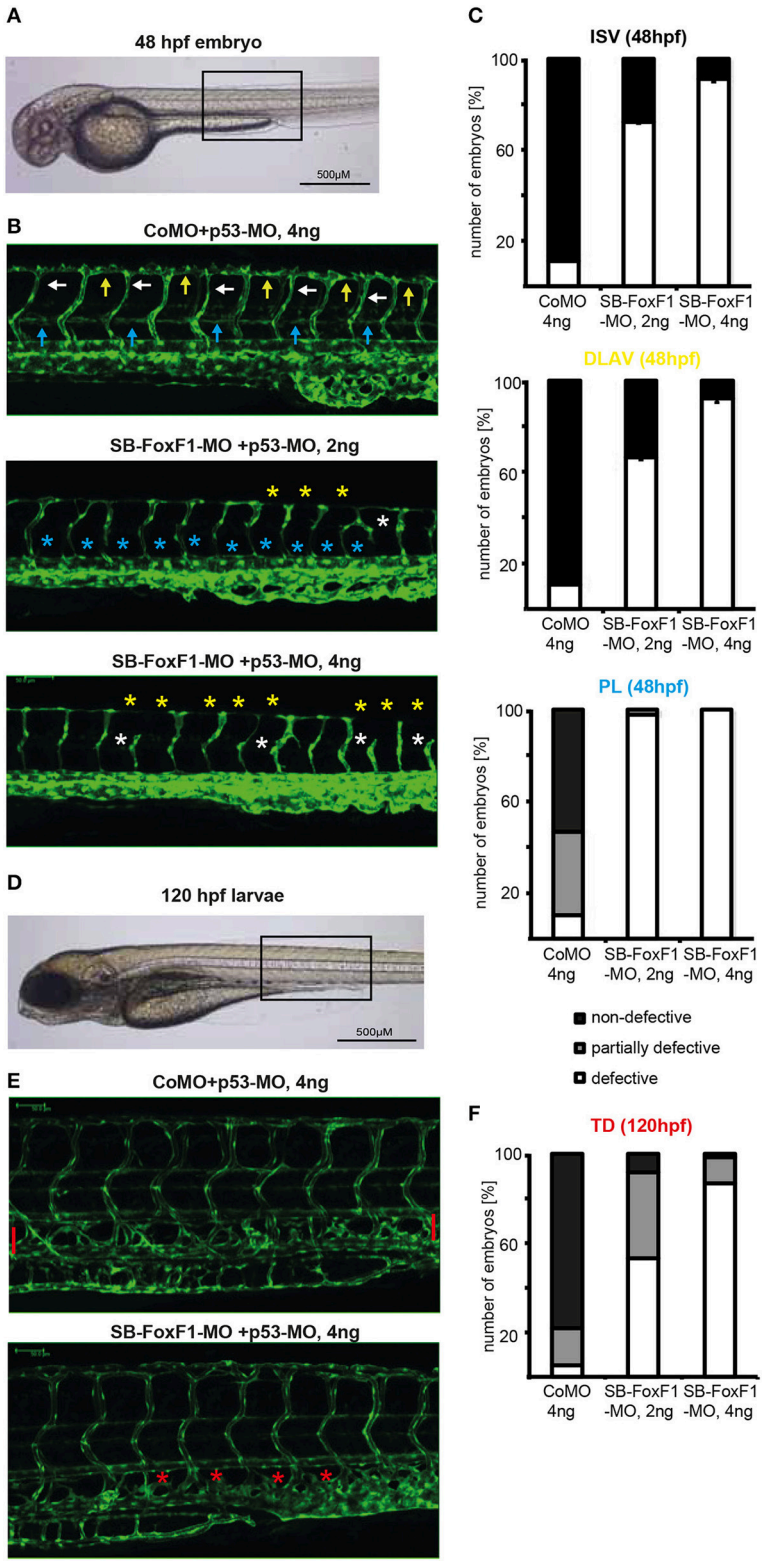

FIGURE 5 | Downregulation of FOXF1 in zebrafish impairs vascular development. **(A–C)** Light and confocal microscopic images and quantification (at least 100 embryos per group) of tg(fli1:EGFP) embryos at 48 h post-fertilization injected with control (CoMO) or FoxF1 morpholino (SB-FoxF1-MO). Injection of the FoxF1 morpholino resulted in an impaired formation of the ISVs (white marks), DLAVs (yellow marks), and PLs (blue marks). **(D–F)** Light and confocal microscopic images and quantification (at least 100 embryos per group) of tg(fli1:EGFP) embryos at 120 h post-fertilization injected with control (CoMO) or FoxF1 morpholino (SB-FoxF1-MO). Injection of the FoxF1 morpholino resulted in an impaired formation of the TD (red marks).

(Adams and Alitalo, 2007; Adams and Eichmann, 2010). We were therefore first interested to test Notch family members. We detected that Notch2 was strongly upregulated on mRNA and protein level, whereas we could not detect differences for other Notch members. That Notch2 is directly regulated by FOXF1 was confirmed by downmodulation of FOXF1 resulting in diminished Notch2 expression. Importantly, knock-down of Notch2 further reduced *in vitro* angiogenic sprouting similar to knock-down of FOXF1. It also prevented increased sprouting induced by FOXF1 overexpression. This demonstrated that Notch2 is an important mediator of FOXF1 functions.

In this context it may be important that several lines of evidence suggest that Notch1 and Notch2 have different and at times opposing biological functions. For example, in a non-small cell lung cancer model, Notch2 mediates differentiation and has tumor suppressor function, whereas Notch1 promotes tumor initiation and progression (Baumgart et al., 2015). Similarly, Notch1 and Notch2 have been reported to have opposite prognostic effects in patients with colorectal cancer (Chu et al., 2011). Furthermore, in a study on mouse osteoclastogenesis Notch1 was found to inhibit, whereas Notch2 promoted the differentiation (Sekine et al., 2012). Although the details of the potential differential signaling and functions of Notch1 and Notch2 have not yet been clarified, it is conceivable that comparable mechanisms could lead to the increased sprouting capacity of ECFC with increased Notch2 expression, whereas Notch1 in stalk cells inhibits sprouting upon binding to Dll4 expressed on tip cells (Blanco and Gerhardt, 2013). Furthermore, there seem to be differences in the processing of the active intracellular domains as Notch2 cleavage appeared not to be sensitive to inhibition by standard concentrations of the γ-secretase inhibitor DAPT, which efficiently block Notch 1 cleavage (Fortini et al., 2017). A concurrent theme is the differential function of Notch ligands on sprouting. Whereas Dll4 on tip cells inhibits stalk cell sprouting via Notch, Jagged1 can activate sprouting by interfering with Dll4/Notch signaling (Benedito et al., 2009). In our work we have not further analyzed expression and contribution of Notch1 and of Notch ligands to sprouting of ECFC, the question of the ligand(s) interacting with Notch2 and a potential role of ligands such as Dll1 and Dll4 remains to be determined.

Additionally, while this work was already in progress, a study on FOXF1 knock-out in mice was published (Ren et al., 2014). It described that FOXF1 is required for formation of the embryonic vasculature and that this is in part due to effects on VEGF signaling. Using a Tie2-Cre-mediated conditional knock-out of the FOXF1 gene in endothelial cells, the authors found that FOXF1 deletion led to embryonic lethality between days 13.5 and 16.5, the embryos displaying growth retardation and abnormalities in various organs including cardiovascular defects. Furthermore, a decreased vascular branching in the yolk sac and placenta and a diminished number of blood vessels in the lung was observed. These defects were, as shown by chip analysis, to be likely caused in part by the direct regulation of angiogenesis related receptor genes by FOXF1, including VEGF receptor-1,−2, and Tie-2. In acccordance with this finding we show that FOXF1 overexpression upregulates surface expression of VEGF receptor-2. It is therefore likely that increased VEGF signaling via upregulation of VEGFR-2 contributes to the increased sprouting capabilities of ECFC.

Another surface protein implicated in important functions of tip cells as well as in arterial endothelial specification is ephrinB2 (Sawamiphak et al., 2010; Salvucci and Tosato, 2012). It has been shown that ephrinB2 reverse signaling via PDZ domain proteins regulates the guidance of endothelial tip cells and is important for efficient filopodial extensions at the vascular front. This is likely due to promoting of VEGFR-2 internalization and signaling. In addition, several studies have portrayed the key function of ephrinB2 in the determination of the arterial fate of endothelial cells, whereas its receptor EphB4 characterizes venous endothelial cells (Herbert et al., 2009).

When we tested a potential effect of FOXF1 on the expression of ephrinB2 and EphB4 we indeed detected an upregulation of ephrinB2 and a concomitant downmodulation of EphB4. These data suggest that the opposite effects of FOXF1 on ephrinB2 and EphB4 may favor arterial sprouting.

To substantiate a role of FOXF1 for *in vivo* sprouting we chose to investigate FOXF1 downmodulation by morpholino oligonucleotides (Blum et al., 2015) during zebrafish development as this model is an emerging disease model and allows to monitor consecutive cellular dynamics (Kirchberger et al., 2017). The first effect we observed was inefficient intersegmental vessel sprouting that starts from the dorsal artery about 1 day post fertilization. This led to flawed formation of the DLAV. This is in line with a preferential role of FOXF1 during arterial sprouting *in vivo*. Unexpectedly, a second phenotypic effect became apparent. Normally, during secondary venous angiogenesis and lymphangiogenesis, endothelial cells from secondary sprouts constitute a transient pool of lymphatic endothelial progenitors, called parachordal lymphangioblasts (PLs). These migrate individually and reassemble later to form the major trunk lymphatics, such as the thoracic duct (TD) (Hogan and Schulte-Merker, 2017). As shown in **Figure 5**, formation of the PLs at 48 hpf and TD at 120 hpf was strongly blocked. These data in zebrafish support a further role of FOXF1 during the generation, migration or reassembly of lymphatic progenitors. Whether this indicates a general role of FOXF1 for migrating endothelial progenitors that may contribute to post-natal vasculogenic processes will need further investigations.

In mammals, two lines of *in vivo* evidence further support a preferential role of FOXF1 in the development of lung capillaries. First, a conditional knock-out of FOXF1 in mice impairs the development of the pulmonary vascular plexus and leads to reduced numbers of capillaries in the lung (Ren et al., 2014). Second, in human patients alveolar capillary dysplasia (ACDMPV), a developmental disorder of the lung, has been shown to result from haploinsufficiency of FOXF1 (Stankiewicz et al., 2009; Sen et al., 2014). ACDMPV patients display drastically reduced numbers of capillaries and lobular underdevelopment. The importance of FOXF1 for correct lung vessel formation can be seen in line with the possibility that vasculogenic processes contribute to the development of lung vasculature (Peng et al., 2013; Gao et al., 2016) as well as with the hypothesis that lung

capillaries could be a major origin of ECFC with preferential expression of FOXF1.

Taken together our data support that the forkhead box transcription factor FOXF1, aside being essential for embryonic vascular development, determines important properties of endothelial progenitor cells. These functions of FOXF1 appear to be mediated through the upregulation of angiogenesis-related genes that provide sprouting capabilities. We show here for the first time that Notch2 is a major mediator of FOXF1 functions, which emphasizes the importance of Notch signaling in the context of endothelial progenitors and suggests that a potential opposing interaction of different Notch isoforms needs to be considered for vascular sprouting and should be investigated in more detail. A further upregulation of ephrinB2 and of VEGF receptor-2, as seen by others (Ren et al., 2014) and also by us, contribute to the FOXF1-mediated sprouting capabilities. It remains to be determined to which extent those are linked to Notch signaling. Finally, it is tempting to speculate that based on these properties ECFC may function to initiate sprouting following integration into ischemic vessels.

In any case it is conceivable that FOXF1 could be used as a marker to identify proposed endothelial progenitor cells in the vessel wall. In addition, it is a candidate to engineer endothelial progenitor cells with improved sprouting capabilities for cell therapies of ischemic diseases or for the ex vivo generation of vascularized tissues.

AUTHOR CONTRIBUTIONS

CS and KL did the majority of detailed planning, experimental work and analysis, as well as the first draft of the manuscript. JT, BE, JS, PQ, MB, AJ, and GU performed experiments, analyzed data, and generated individual figures. K-HP, EG, RdM, and RH-W contributed to the design of the study and to conclusions from the results. JK designed and interpreted the zebrafish experiments. EH perceived and designed the research project and corrected and finished the manuscript.

FUNDING

This research was funded by grants of the Austrian Science Fund (FWF-P21291-B11), the Austrian Forschungsförderungsgesellschaft (FFG-RSA2349689) and the European Commission (EC Health-F2-2009-222995) to EH and of the Austrian Science Fund (FWF-F-5406-B21) to RdM.

ACKNOWLEDGMENTS

We thank the midwives of the Department of Obstetrics and Gynecology of the University Hospital Vienna for continuous supply with cord blood and umbilical cords and Maria Witkowski and Katrin Bennewitz for expert technical assistance in the isolation of and culture of ECFC and HUVEC and the zebrafish experiments, respectively. Furthermore, we acknowledge the supply of additional cord blood samples by Vivocell Biosolutions AG, Graz, during the initial phase of the project. Our thanks go further to the members of the molecular vascular biology group of the Medical University of Vienna for technical help and discussions.

SUPPLEMENTARY MATERIAL

The Supplementary Material for this article can be found online at: https://www.frontiersin.org/articles/10.3389/fbioe.2018.00076/full#supplementary-material

REFERENCES

Adams, R. H., and Alitalo, K. (2007). Molecular regulation of angiogenesis and lymphangiogenesis. *Nat. Rev. Mol. Cell Biol.* 8, 464–478. doi: 10.1038/nrm2183

Adams, R. H., and Eichmann, A. (2010). Axon guidance molecules in vascular patterning. *Cold Spring Harb. Perspect. Biol.* 2:a001875. doi: 10.1101/cshperspect.a001875

Alphonse, R. S., Vadivel, A., Fung, M., Shelley, W. C., Critser, P. J., Ionescu, L., et al. (2014). Existence, functional impairment, and lung repair potential of endothelial colony-forming cells in oxygen-induced arrested alveolar growth. *Circulation* 129, 2144–2157. doi: 10.1161/CIRCULATIONAHA.114.009124

Alphonse, R. S., Vadivel, A., Zhong, S., McConaghy, S., Ohls, R., Yoder, M. C., et al. (2015). The isolation and culture of endothelial colony-forming cells from human and rat lungs. *Nat. Protoc.* 10, 1697–1708. doi: 10.1038/nprot.2015.107

Banno, K., and Yoder, M. C. (2017). Tissue regeneration using endothelial colony-forming cells: promising cells for vascular repair. *Pediatr. Res.* 83, 283–290. doi: 10.1038/pr.2017.231

Baumgart, A., Mazur, P. K., Anton, M., Rudelius, M., Schwamborn, K., Feuchtinger, A., et al. (2015). Opposing role of Notch1 and Notch2 in a Kras(G12D)-driven murine non-small cell lung cancer model. *Oncogene* 34, 578–588. doi: 10.1038/onc.2013.592

Bautch, V. L. (2011). Stem cells and the vasculature. *Nat. Med*, 17, 1437–1443. doi: 10.1038/nm.2539

Benedito, R., Roca, C., Sörensen, I., Adams, S., Gossler, A., Fruttiger, M., et al. (2009). The notch ligands Dll4 and Jagged1 have opposing effects on angiogenesis. *Cell* 137, 1124–1135. doi: 10.1016/j.cell.2009.03.025

Blanco, R., and Gerhardt, H. (2013). VEGF and Notch in tip and stalk cell selection. *Cold Spring Harb. Perspect. Med.* 3:a006569. doi: 10.1101/cshperspect.a006569

Blum, M., De Robertis, E. M., Wallingford, J. B., and Niehrs, C. (2015). Morpholinos: antisense and sensibility. *Dev. Cell* 35, 145–149. doi: 10.1016/j.devcel.2015.09.017

Braccioli, L., Vervoort, S. J., Adolfs, Y., Heijnen, C. J., Basak, O., Pasterkamp, R. J., et al. (2017). FOXP1 promotes embryonic neural stem cell differentiation by repressing jagged1 expression. *Stem Cell Rep.* 9, 1530–1545. doi: 10.1016/j.stemcr.2017.10.012

Bredenkamp, N., Ulyanchenko, S., O'Neill, K. E., Manley, N. R., Vaidya, H. J., and Blackburn, C. C. (2014). An organized and functional thymus generated from FOXN1-reprogrammed fibroblasts. *Nat. Cell Biol.* 16, 902–908. doi: 10.1038/ncb3023

Chu, D., Zhang, Z., Zhou, Y., Wang, W., Li, Y., Zhang, H., et al. (2011). Notch1 and Notch2 have opposite prognostic effects on patients with colorectal cancer. *Ann. Oncol.* 22, 2440–2447. doi: 10.1093/annonc/mdq776

De Val, S., Chi, N. C., Meadows, S. M., Minovitsky, S., Anderson, J. P., Harris, I. S., et al. (2008). Combinatorial regulation of endothelial gene expression by ets and forkhead transcription factors. *Cell* 135, 1053–1064. doi: 10.1016/j.cell.2008.10.049

Dubois, C., Liu, X., Claus, P., Marsboom, G., Pokreisz, P., Vandenwijngaert, S., et al. (2010). Differential effects of progenitor cell populations on left ventricular remodeling and myocardial neovascularization after myocardial infarction. *J. Am. Coll. Cardiol.* 55, 2232–2243. doi: 10.1016/j.jacc.2009.10.081

Ehling, M., Adams, S., Benedito, R., and Adams, R. H. (2013). Notch controls retinal blood vessel maturation and quiescence. *Development* 140, 3051–3061. doi: 10.1242/dev.093351

Epting, D., Wendik, B., Bennewitz, K., Dietz, C. T., Driever, W., and Kroll, J. (2010). The Rac1 regulator ELMO1 controls vascular morphogenesis in zebrafish. *Circ. Res.* 107, 45–55. doi: 10.1161/CIRCRESAHA.109.213983

Fortini, F., Vieceli Dalla Sega, F., Caliceti, C., Aquila, G., Pannella, M., Pannuti, A., et al. (2017). Estrogen receptor β-dependent Notch1 activation protects vascular endothelium against tumor necrosis factor α (TNFα)-induced apoptosis. *J. Biol. Chem.* 292, 18178–18191. doi: 10.1074/jbc.M117.790121

Gao, Y., Cornfield, D. N., Stenmark, K. R., Thébaud, B., Abman, S. H., and Raj, J. U. (2016). Unique aspects of the developing lung circulation: structural development and regulation of vasomotor tone. *Pulm. Circ.* 6, 407–425. doi: 10.1086/688890

Herbert, S. P., Huisken, J., Kim, T. N., Feldman, M. E., Houseman, B. T., Wang, R. A., et al. (2009). Arterial-venous segregation by selective cell sprouting: an alternative mode of blood vessel formation. *Science* 326, 294–298. doi: 10.1126/science.1178577

Hofer-Warbinek, R., Sturtzel, C., Preisegger, K.-H., and Hofer, E. (2014). "Endothelial progenitor cells derived from cord or peripheral blood and their potential for regenerative therapies," in *Adult and Pluripotent Stem Cells: Potential for Regenerative Medicine of the Cardiovascular System,* eds J. Hescheler and E. Hofer (Heidelberg; New York, NY; London: Springer), 37–51.

Hogan, B. M., and Schulte-Merker, S. (2017). How to plumb a pisces: understanding vascular development and disease using zebrafish embryos. *Dev. Cell* 42, 567–583. doi: 10.1016/j.devcel.2017.08.015

Isogai, S., Horiguchi, M., and Weinstein, B. M. (2001). The vascular anatomy of the developing zebrafish: an atlas of embryonic and early larval development. *Dev. Biol.* 230, 278–301. doi: 10.1006/dbio.2000.9995

Iwafuchi-Doi, M., Donahue, G., Kakumanu, A., Watts, J. A., Mahony, S., Pugh, B. F., et al. (2016). The pioneer transcription factor foxa maintains an accessible nucleosome configuration at enhancers for tissue-specific gene activation. *Mol. Cell* 62, 79–91. doi: 10.1016/j.molcel.2016.03.001

Kirchberger, S., Sturtzel, C., Pascoal, S., and Distel, M. (2017). Quo natas, Danio?-Recent Progress in Modeling Cancer in Zebrafish. *Front. Oncol.* 7:186. doi: 10.3389/fonc.2017.00186

Korff, T., and Augustin, H. G. (1998). Integration of endothelial cells in multicellular spheroids prevents apoptosis and induces differentiation. *J. Cell Biol.* 143, 1341–1352.

Lucas, T., Abraham, D., Untergasser, G., Zins, K., Hofer, E., Gunsilius, E., et al. (2009). Adenoviral-mediated endothelial precursor cell delivery of soluble CD115 suppresses human prostate cancer xenograft growth in mice. *Stem Cells* 27, 2342–2352. doi: 10.1002/stem.145

Martin-Ramirez, J., Hofman, M., van den Biggelaar, M., Hebbel, R. P., and Voorberg, J. (2012). Establishment of outgrowth endothelial cells from peripheral blood. *Nat. Protoc.* 7, 1709–1715. doi: 10.1038/nprot.2012.093.

Medina, R. J., Barber, C. L., Sabatier, F., Dignat-George, F., Melero-Martin, J. M., Khosrotehrani, K., et al. (2017). Endothelial progenitors: a consensus statement on nomenclature. *Stem Cells Transl. Med.* 6, 1316–1320. doi: 10.1002/sctm.16-0360

Naito, H., Kidoya, H., Sakimoto, S., Wakabayashi, T., and Takakura, N. (2012). Identification and characterization of a resident vascular stem/progenitor cell population in preexisting blood vessels. *EMBO J.* 31, 842–855. doi: 10.1038/emboj.2011.465

Palii, C. G., Vulesevic, B., Fraineau, S., Pranckeviciene, E., Griffith, A. J., Chu, A., et al. (2014). Trichostatin A enhances vascular repair by injected human endothelial progenitors through increasing the expression of TAL1-dependent genes. *Cell Stem Cell* 14, 644–657. doi: 10.1016/j.stem.2014.03.003

Peng, T., Tian, Y., Boogerd, C. J., Lu, M. M., Kadzik, R. S., Stewart, K. M., et al. (2013). Coordination of heart and lung co-development by a multipotent cardiopulmonary progenitor. *Nature* 500, 589–592. doi: 10.1038/nature12358

Phng, L. K., and Gerhardt, H. (2009). Angiogenesis: a team effort coordinated by notch. *Dev. Cell* 16, 196–208. doi: 10.1016/j.devcel.2009.01.015

Prasain, N., Lee, M. R., Vemula, S., Meador, J. L., Yoshimoto, M., Ferkowicz, M. J., et al. (2014). Differentiation of human pluripotent stem cells to cells similar to cord-blood endothelial colony-forming cells. *Nat. Biotechnol.* 32, 1151–1157. doi: 10.1038/nbt.3048

Ren, X., Ustiyan, V., Pradhan, A., Cai, Y., Havrilak, J. A., Bolte, C. S., et al. (2014). FOXF1 transcription factor is required for formation of embryonic vasculature by regulating VEGF signaling in endothelial cells. *Circ. Res.* 115, 709–720. doi: 10.1161/CIRCRESAHA.115.304382

Risau, W. (1997). Mechanisms of angiogenesis. *Nature* 386, 671–674 doi: 10.1038/386671a0

Ruvinov, E., and Cohen, S. (2014). "Biomaterials for cardiac tissue engineering and regeneration," in *Adult and Pluripotent Stem Cells: Potential For Regenerative Medicine of the Cardiovascular System,* eds J. Hescheler and E. Hofer (Heidelberg; New York, NY; London: Springer), 83–111.

Salvucci, O., and Tosato, G. (2012). Essential roles of EphB receptors and EphrinB ligands in endothelial cell function and angiogenesis. *Adv. Cancer Res.* 114, 21–57. doi: 10.1016/B978-0-12-386503-8.00002-8

Sawamiphak, S., Seidel, S., Essmann, C. L., Wilkinson, G. A., Pitulescu, M. E., Acker, T., et al. (2010). Ephrin-B2 regulates VEGFR2 function in developmental and tumour angiogenesis. *Nature* 465, 487–491. doi: 10.1038/nature08995

Schwarz, T. M., Leicht, S. F., Radic, T., Rodriguez-Arabaolaza, I., Hermann, P. C., Berger, F., et al. (2012). Vascular incorporation of endothelial colony-forming cells is essential for functional recovery of murine ischemic tissue following cell therapy. *Arterioscler. Thromb. Vasc. Biol.* 32, e13–e21. doi: 10.1161/ATVBAHA.111.239822

Sekine, C., Koyanagi, A., Koyama, N., Hozumi, K., Chiba, S., and Yagita, H. (2012). Differential regulation of osteoclastogenesis by Notch2/Delta-like 1 and Notch1/Jagged1 axes. *Arthritis Res. Ther.* 14:R45 doi: 10.1186/ar3758

Sen, P., Dharmadhikari, A. V., Majewski, T., Mohammad, M. A., Kalin, T. V., Zabielska, J., et al. (2014). Comparative analyses of lung transcriptomes in patients with alveolar capillary dysplasia with misalignment of pulmonary veins and in foxf1 heterozygous knockout mice. *PLoS ONE* 9:e94390. doi: 10.1371/journal.pone.0094390

Seo, S., Fujita, H., Nakano, A., Kang, M., Duarte, A., and Kume, T. (2006). The forkhead transcription factors, Foxc1 and Foxc2, are required for arterial specification and lymphatic sprouting during vascular development. *Dev. Biol.* 294, 458–470. doi: 10.1016/j.ydbio.2006.03.035

She, J., Yuan, Z., Wu, Y., Chen, J., and Kroll, J. (2018). Targeting erythropoietin protects against proteinuria in type 2 diabetic patients and in zebrafish. *Mol. Metab.* 8, 189–202. doi: 10.1016/j.molmet.2017.11.006

Stankiewicz, P., Sen, P., Bhatt, S. S., Storer, M., Xia, Z., Bejjani, B. A., et al. (2009). Genomic and genic deletions of the FOX gene cluster on 16q24.1 and inactivating mutations of FOXF1 cause alveolar capillary dysplasia and other malformations. *Am. J. Hum. Genet.* 84, 780–791. doi: 10.1016/j.ajhg.2009.05.005

Sturtzel, C. (2017). Endothelial cells. *Adv. Exp. Med. Biol.* 1003, 71–91. doi: 10.1007/978-3-319-57613-8_4

Tauber, S., Jais, A., Jeitler, M., Haider, S., Husa, J., Lindroos, J., et al. (2010). Transcriptome analysis of human cancer reveals a functional role of heme oxygenase-1 in tumor cell adhesion. *Mol. Cancer* 9:200. doi: 10.1186/1476-4598-9-200

Testori, J., Schweighofer, B., Helfrich, I., Sturtzel, C., Lipnik, K., Gesierich, S., et al. (2011). The VEGF-regulated transcription factor HLX controls the expression of guidance cues and negatively regulates sprouting of endothelial cells. *Blood* 117, 2735–2744. doi: 10.1182/blood-2010-07-293209

Yoder, M. C., Mead, L. E., Prater, D., Krier, T. R., Mroueh, K. N., Li, F., et al. (2007). Redefining endothelial progenitor cells via clonal analysis and hematopoietic stem/progenitor cell principals. *Blood* 109, 1801–1809. doi: 10.1182/blood-2006-08-043471

Conflict of Interest Statement: AJ and K-HP were employed by the company VivoCell Biosolutions GmbH, Graz, Austria.

The remaining authors declare that the research was conducted in the absence of any commercial or financial relationships that could be construed as a potential conflict of interest.

frontiers in Cardiovascular Medicine

ORIGINAL RESEARCH
published: 14 March 2018
doi: 10.3389/fcvm.2018.00016

Temporal Dynamics of Gene Expression During Endothelial Cell Differentiation From Human iPS Cells: A Comparison Study of Signalling Factors and Small Molecules

Heini Belt [1], Jonna K. Koponen [1], Tuija Kekarainen [2], Katja A. Puttonen [1,2], Petri I. Mäkinen [1], Henri Niskanen [1], Joni Oja [3], Galina Wirth [1], Jari Koistinaho [1], Minna U. Kaikkonen [1§] and Seppo Ylä-Herttuala [1,4§]*

[1] A. I. Virtanen Institute for Molecular Sciences, University of Eastern Finland, Kuopio, Finland, [2] Kuopio Center for Gene and Cell Therapy, Kuopio, Finland, [3] FinVector Vision Therapies Oy, Kuopio, Finland, [4] Heart Center and Gene Therapy Unit, Kuopio University Hospital, Kuopio, Finland

Endothelial cell (EC) therapy may promote vascular growth or reendothelization in a variety of disease conditions. However, the production of a cell therapy preparation containing differentiated, dividing cells presenting typical EC phenotype, functional properties and chemokine profile is challenging. We focused on comparative analysis of seven small molecule-mediated differentiation protocols of ECs from human induced pluripotent stem cells. Differentiated cells showed a typical surface antigen pattern of ECs as characterized with flow cytometry analysis, functional properties, such as tube formation and ability to uptake acetylated LDL. Gene expression analysis by RNA sequencing revealed an efficient silencing of pluripotency genes and upregulation of genes related to cellular adhesion during differentiation. In addition, distinct patterns of transcription factor expression were identified during cellular reprogramming providing targets for more effective differentiation protocols in the future. Altogether, our results suggest that the most optimal EC differentiation protocol includes early inhibition of Rho-associated coiled-coil kinase and activation of cyclic AMP signaling, and inhibition of transforming growth factor beta signaling after mesodermal stage. These findings provide the first systematic characterization of the most potent signalling factors and small molecules used to generate ECs from human induced pluripotent stem cells and, consequently, this work improves the existing EC differentiation protocols and opens up new avenues for controlling cell fate for regenerative EC therapy.

Keywords: endothelial differentiation, cell therapy, iPS cells, RNA sequencing, transcription factors, cardiovascular diseases

OPEN ACCESS

Edited by:
Carlo Gaetano,
Istituti Clinici Scientifici Maugeri Spa SB, Italy

Reviewed by:
Susumu Minamisawa,
Jikei University School of Medicine, Japan
Xuechong Hong,
Boston Children's Hospital, United States

***Correspondence:**
Seppo Ylä-Herttuala
seppo.ylaherttuala@uef.fi

[§]These authors share senior authorship

Specialty section:
This article was submitted to Cardiovascular Biologics and Regenerative Medicine, a section of the journal Frontiers in Cardiovascular Medicine

Received: *06 October 2017*
Accepted: *16 February 2018*
Published: *14 March 2018*

Citation:
Belt H, Koponen JK, Kekarainen T, Puttonen KA, Mäkinen PI, Niskanen H, Oja J, Wirth G, Koistinaho J, Kaikkonen MU and Ylä-Herttuala S (2018) Temporal Dynamics of Gene Expression During Endothelial Cell Differentiation From Human iPS Cells: A Comparison Study of Signalling Factors and Small Molecules. Front. Cardiovasc. Med. 5:16. doi: 10.3389/fcvm.2018.00016

INTRODUCTION

Atherosclerotic coronary artery disease (CAD) and peripheral arterial disease (PAD) are leading causes of morbidity and mortality worldwide (1). Adjuvant regenerative therapies to promote therapeutic angiogenesis are needed because current interventions are insufficient in patients with severe disease (2–4). It is also important to promote re-endothelialization and prevent late-stent thrombosis related to conventional therapies (4). In addition, ischemic stroke patients would benefit from efficient neovascularisation after ischemic cerebral injury (5). Therapeutic angiogenesis can be achieved with gene therapy (6) or cell therapy (4). Cell therapy could provide an effective means to enhance therapeutic angiogenesis to restore blood flow in ischemic areas (7, 8).

Endothelial cells (EC) are metabolically active and have a central role in the homeostatic control of angiogenesis, blood pressure, inflammatory cell recruitment, platelet activation, coagulation pathways and oxidative stress (9–12). Vascular growth, remodeling and maturation involve EC migration, proliferation, differentiation to arterial, venous, lymphatic or other special subtypes of ECs, extracellular matrix (ECM) modifications and recruitment of supportive cells (9, 13). In EC-based therapy, these cells could promote therapeutic angiogenesis by secreting protective, proangiogenic cytokines and growth factors that further modulate vascular function, angiogenesis, vascular regeneration and tissue homeostasis (7–9, 14).

EC therapy was first demonstrated by Asahara and colleagues when they isolated endothelial progenitor cells (EPC) from human peripheral blood (PB) (15). Since then, EC therapy research has expanded to many other cell types including bone barrow mononuclear cells (BMNC) (16), hematopoietic stem cells, mesenchymal stem cells and cardiac progenitor cells (4). In addition, ECs derived from embryonic stem cells (ESC) (17) or induced pluripotent stem cells (iPSC) (18, 19) have been extensively studied (20, 21). In theory, the amount of ECs differentiating from pluripotent stem cells (PSC) is limitless which makes them an attractive source of therapeutic cells for treating ischemic diseases.

Several cell culture protocols aiming to produce therapeutic ECs from PSCs have been published (22–33). Major efforts have been done to efficiently guide stem cells to functional, immune-compatible vascular cells. However, multistep manufacturing processes may be vulnerable and could reduce reproducibility of the cell preparations. The goal regarding future patient treatment is to have a cost-effective and consistent large scale cell culture process to obtain safe and therapeutically active ECs. In spite the numerous studies done in the field of EC therapy, an optimal *in vitro* cell culture method for producing therapeutic ECs still remain elusive (22, 26, 34).

In this work, we systematically tested and compared the effect of the most potent published signalling factors and small molecules used to generate ECs from human iPSC (hiPSC). Tested molecules included factors already known to drive EC differentiation, such as Rho-associated coiled-coil kinase (ROCK) inhibitor (25), transforming growth factor beta (TGFβ) inhibitor (24, 35), cyclic adenosine monophosphate (cAMP) analog 8-Br-cAMP (31) and bone morphogenic protein 4 (BMP-4) (30), which were used in seven different combinations. Successful differentiation to ECs was confirmed by cell morphology, phenotypic analyses and functional assays. RNA sequencing (RNA-Seq) was used to gain insight into the changing transcriptome during the differentiation from hiPSC to ECs. Our analysis demonstrated extensive changes in genes related to focal adhesion and regulation of pluripotency. As a proof of the success of the EC differentiation, major EC-specific transcription factors (TFs) were highly expressed in most differentiation groups. Comparison of mature EC gene expression profiles suggested that the most relevant factors in EC differentiation are the activation of cAMP signalling pathway already in the beginning of differentiation process, and the inhibition of TGFβ signalling after the mesodermal differentiation. The inhibition of ROCK signalling was also crucial as it has been proven to be essential to EC proliferation and differentiation from PSCs (25). In conclusion, this study provides the first comprehensive comparison of the effects of signalling factors and small molecules used in EC differentiation protocols on EC phenotype and transcriptome. The knowledge gained here could help to design more efficient EC production methods for regenerative therapy applications.

MATERIAL AND METHODS

HiPSC

Human induced pluripotent stem cell line UEFhfiPSC1.4 (36) was derived using lentiviral transduction of Yamanaka transcription factors Oct4, Klf4, Sox2 and c-Myc (18) into fibroblasts isolated from a skin sample taken during cecarean sectioning of a volunteer mother (36). Generation and testing of the UEFhfiPSC1.4 cell line has been described in detail elsewhere and the cells passed all pluripotency tests and differentiated well into any cell type (36, 37). These hiPSCs were cultured in a serum-free stem cell medium supplemented with 20% KnockOut™ Serum Replacement (GIBCO) and 8 ng/ml basic fibroblast growth factor (FGF-2) (R&D Systems) (38) on a feeder cell layer of mitotically inactivated foreskin fibroblasts (ATCC, CRL-2429) (36, 38), or in Essential 8 hESC cell culture media (Life Technologies) on Matrigel™ basement membrane matrix (Corning, growth factor reduced, phenol red free) supplemented with 50 IU/ml penicillin (Invitrogen) and 50 μg/ml streptomycin (Invitrogen). Medium was changed daily or every other day and cells were mechanically passaged once a week in the presence of 10 μg/ml ROCK inhibitor Y-27632 (Sigma-Aldrich) (39), or approximately 1–2 times a week with EDTA solution (Life Technologies, 0.5 M pH 8.0). To avoid feeder cell contamination before EC differentiation, UEFhfiPSC1.4 cell colonies were moved from a feeder cell layer to a feeder-free culture employing Matrigel® hESC-Qualified Matrix coating (BD Biosciences) and mTeSR™1 medium (STEMCELL Technologies) supplemented with 50 IU/ml penicillin (Invitrogen) and 50 μg/ml streptomycin (Invitrogen). Culturing of hiPSCs in these conditions was done according to a technical manual of STEMCELL Technologies or

Life Technologies (Culturing Pluripotent Stem Cells (PSCs) in Essential 8™ Medium).

HUVECs as Positive EC Controls

Human umbilical vein endothelial cells (HUVEC) were used as positive EC control in flow cytometric analyses and assays for functional EC characterization. Umbilical cords were collected from volunteer mothers according to a protocol approved by Ethics Committee of the Kuopio University Hospital (Kuopio, Finland, license number 341/2015).

HUVECs were isolated from umbilical cord samples as previously described (40). HUVECs were cultured in endothelial cell growth medium (Thermo Scientific) on fibronectin-gelatin coating (10 μg/ml, 0.05%; Sigma-Aldrich).

Differentiation of hiPSCs to ECs

HiPSC colonies were cut with a scalpel from Matrigel-coated dishes under a stereomicroscope and pieces of hiPSC colonies were washed with phosphate buffered saline (PBS). Cells were dissociated with Accutase (Sigma-Aldrich) and approximately 0.7×10^4 cells per cm^2 were plated on a fibronectin-gelatin (10 μg/ml, 0.05%; Sigma-Aldrich) coated dish. Cells were cultured in serum-free EBM™-2 Endothelial basal medium-2 (Lonza CC-3156) with EGM™-2 SingleQuots medium supplement with human epidermal growth factor (hEGF), recombinant human long R3 insulin like growth factor-*1 (*R3-IGF-1), ascorbic acid, hydrocortisone, human FGF-2, heparin and antibiotics GA-1000 (Lonza CC-4176). From this supplement, fetal bovine serum (FBS) and vascular endothelial growth factor (VEGF) were discarded to obtain serum free and VEGF-controlled cell culture conditions. Knockout serum replacement (GIBCO) was used at the final concentration of 20 μl/ml and recombinant human VEGF-A 165 (R&D Systems) was used at the final concentration of 200 ng/ml. Following small molecules and growth factors were used in different combinations and time courses: 10 μM TGFβ inhibitor SB431542 (Tocris Bioscience), 10 μM ROCK inhibitor Y-27632 (Sigma-Aldrich), 20 ng/ml recombinant human BMP-4 (R&D Systems) and 0.25 mM 8-Br-cAMP (SB 431542, Sigma-Aldrich). Cell culture medium was changhed every second day, and differentiating ECs were passaged every 4–6 days using Accutase (Sigma-Aldrich).

In our cell differentiation protocol, we hypothesize that differentiation stages advance from PSC stage through mesodermal commitment (differentiation day 5) towards mature EC stage (differentiation day 15) (22). Different cell culture conditions are described in **Table 1**. In all groups without the TGFβ inhibitor at day 1 during the differentiation, it was added at day 4 as TGFβ inhibition has been shown to enhance EC vascular identity after mesodermal fate (24). In those groups with BMP-4 at day 1, it was removed at day 4 since it promotes the mesodermal commitment from PSCs (30).

TABLE 1 | EC treatment groups.

Group name abbreviation	ROCK-inhibitor	TGFβ-inhibitor	8-Br-cAMP	BMP-4
R	+	–/added day 4	–	–
RT	+	+	–	–
RB	+	–/added day 4	–	+/removed day 4
RC	+	–/added day 4	+	–
RTB	+	+	–	+/removed day 4
RTC	+	+	+	–
RTCB	+	+	+	+/removed day 4

R = ROCK inhibitor, RT = ROCK inhibitor + TGFb inhibitor, RB = ROCK inhibitor + BMP-4, RC = ROCK inhibitor + 8 Br-cAMP, RTB = ROCK inhibitor + TGFb inhibitor + BMP-4, RTC = ROCK inhibitor + TGFb inhibitor + 8 Br-cAMP and RTCB = ROCK inhibitor + TGFb inhibitor + 8 Br-cAMP + BMP-4.

Flow Cytometry

For analyses, cells were detached with Accutase (Sigma-Aldrich) and incubated at +37°C for 5 min. Blocking was done using 2% FBS-PBS at +4°C for 20 min followed by fixing in 1% paraformaldehyde (PFA). Following antibodies (BD Biosciences) were used for staining according to manufacturer's instructions: mouse anti-human CD31-R-phycoerythrin (PE), mouse anti-human CD309-PE, mouse anti-human CD34-PE, mouse anti-human CD144-fluorescein isothiocyanate (FITC) and mouse anti-endothelial nitric oxide synthase (eNOS)-PE. For intracellular staining of eNOS and anti-Von Willebrand Factor (vWF)-FITC (Abcam), cell permeabilization was done using 0.5% Triton X-100 (Sigma-Aldrich) in 2% FBS-PBS at +4°C for 30 min. Data was captured with a BD FACSCalibur and analyzed with FCS Express 6 Flow Research Edition software (*De Novo* Software).

The statistical analysis of the data was done using GraphPad Prism software (version 5.04, GraphPad Software Inc., CA, USA). One-way ANOVA tests were done for analyzing the group differences for both expression of endothelial markers between the treatments and as a function of time. If differences were statistically significant with more than 95% confidence, paired differences between the groups were tested with Tukey's multiple comparison post-tests.

Functional Characterization of Differentiated ECs

Tube forming capacity of the differentiated ECs at day 14–15 was tested on 10 mg/ml Matrigel Basement Membrane Matrix (BD Biosciences) according to manufacturer's instructions. Briefly, 300 μl of Matrigel was plated per well of a 24-well culture plate kept on ice. Plates were incubated at +37°C for 50 min and 300 μl of cell suspension with 1.2×10^5 cells in the EC differentiation medium with appropriate supplements were seeded per well. 50 μM L-sulforaphane (Sigma-Aldrich) was used to inhibit specific EC tube formation (41). Pictures of forming tubes were taken by a continuous live cell imaging system, Cell-IQ Analyzer (Chip-Man Technologies) supplied with a 10× objective 12–15 h after cell seeding.

Uptake of acetylated LDL (Ac-LDL) by differentiated ECs at day 14–15 was confirmed by Alexa Fluor® 488 labeled Ac-LDL (L23380, Molecular Probes) at the final concentration of 1 μg/ml. Fibroblasts (ATCC, CRL-2429) cultured in endothelial cell growth medium (Thermo Scientific) on fibronectin-gelatin coating (10 μg/ml, 0.05%; Sigma-Aldrich) were used as negative controls.

Cells were incubated with Ac-LDL for 3 h prior to fixing in 1% PFA - 2% FBS in PBS. Flow cytometric analyses were performed using BD FACSCalibur and FCS Express 6 Flow Research Edition software.

RNA-Seq Libraries

RNA sequencing was performed to compare transcriptional profiles of different EC differentiation groups and hiPSCs. RNA was extracted from cells with RNeasy Mini Kit (Qiagen) and depleted from rRNAs using Ribo-Zero Gold Kit (Illumina). RNA was fragmented using TURBO DNase and RNA fragmentation reagents (Life Technologies) and purified using P-30 columns (Bio-Rad, Hercules, CA, USA). Fragmented RNA was dephosphorylated with polynucleotide kinase (New England Biolabs, Ipswich, MA, USA) followed by heat-inactivation and purification using RNA Clean & Concentrator™−5 kit (Zymo Research Corporation, Irvine, CA, USA). Poly(A)-tailing and reverse transcription were performed as previously described (42). Libraries were amplified using 11 cycles, size-selected (200–350 bp) in 10% TBE gels (Life Technologies) and sequenced using Illumina HiSeq 2000 for 50 cycles according to the manufacturer's instructions.

RNA-Seq Data Analysis

RNA-Seq results were trimmed to remove 3′ A-stretches originating from the library preparation and poor quality reads were filtered out (minimum 97% of bp over quality cut off 10). Reads were aligned to the hg19 genome using Tophat allowing up to two mismatches and reporting only one alignment for each read. Data analysis was performed using HOMER (43) (http://homer.ucsd.edu/homer/) and the differential gene expression using edgeR (44). Thresholds of FDR < 0.05, reads per kb per million reads >0.5 and fold change >4 were used. Clustering results were generated by Cluster 3.0 (45) by normalizing and centering the gene expression tags to range from −1 to 1. The output from clustering was viewed using Java Treeview (46). The gene ontology (GO) analysis was performed using DAVID Bioinformatics Resources 6.8 (47) and gene lists for selected top functions were exported to generate clustered heatmaps. QIAGEN's Ingenuity® Pathway Analysis (IPA®, QIAGEN Redwood City, www.qiagen.com/ingenuity) was used to perform Upstream Regulator Analysis with a focus on transcriptional regulators to identify which factors may be causing observed gene expression changes. Gene Expression Dynamics Inspector (GEDI) v2.1 (48) was used to generate self-organizing maps to visualize the expression profiles of different treatments and timepoints. Grid size 26 × 25, 1st phase training iteration 20 and 2nd phase training iteration 80, were used as settings to generate mosaic images. Principal component analysis (PCA) was performed using prcomp function in R environment and 3D plot was prepared using rgl R package.

Data Access

RNA-Seq data from this study has been submitted to NCBI Gene Expression Omnibus under accession number GSE103945.

RESULTS

Optimization of EC Differentiation Method and Characterization of Cells

In this study, we systematically tested and compared the effects of the most potent signalling factors and small molecules reported to generate ECs from hiPSCs. Tested molecules included ROCK inhibitor indispensable for EC differentiation (25), TGFβ inhibitor that maintains vascular identity after the EC specification and support endothelial cell expansion (24, 49), cAMP analog 8-Br-cAMP that promotes differentiation of ECs (23, 31), and BMP-4 that contributes to mesodermal commitment (30). These molecules were used in seven different combinations (**Table 1**) added to the serum-free endothelial basal medium. In addition, well-known and essential growth factors for EC differentiation and proliferation, VEGF-A and FGF-2, were always included in EC culture media (50–52).

The optimal time necessary for EC differentiation was determined by culturing hiPSCs in seven different conditions up to 36 days. At the end of the assay, endothelial markers were expressed only in low number of cells (**Figure S1**). This allowed us to conclude that differentiation of hiPSCs into mature ECs takes approximately 15 days, which is well in accordance with previous literature (53). As seen in **Figure 1**, a similar trend in cell surface marker expression was seen in all EC treatment groups where the number of cells expressing generally used EC markers, CD31 (PECAM1), CD34, CD309 (vascular endothelial growth factor receptor 2, VEGFR-2, KDR) and CD144 (VE-cadherin, CDH5), was increasing during the first two weeks. Treatments groups did not differ statistically at the end of differentiation (day 15–16) based on all four cell surface markers analyzed although there were statistical differences between single markers. Differentiating ECs also showed similar morphology across different cell culture groups at day 15 resembling the appearance of HUVECs (representative images in **Figure 2A–B**).

Lack of the ROCK inhibitor in the cell differentiation media resulted in a poor attachment of cells onto fibronectin-gelatin coating. Indeed, ROCK suppression has been shown to be indispensable to EC proliferation and differentiation from PSCs (25), and therefore it was included in all cell culture conditions. Consequently, the treatment group containing only the ROCK inhibitor (R) served as a reference group in the following studies. When the TGFβ inhibitor was included with the ROCK inhibitor from the beginning of the differentiation (RT), EC differentiation was promoted and more than 50% of the cells expressed CD31 and CD144 markers at day 15 (**Figure 1**). Addition of 8-Br-cAMP (RTC) did not have a major effect on the marker expression in comparison with the RT group. When comparing group RC to the reference group R, especially marker CD309 and CD144 expressions were higher. In contrast, adding BMP-4 at day 1 resulted in the EC marker suppression (RB, RTB and RTCB groups). HUVECs were used as positive controls and almost 100% of the cells were positive for CD31 and CD144. In comparison, the number of HUVECs positive for CD34 and CD309 were approximately 70%.

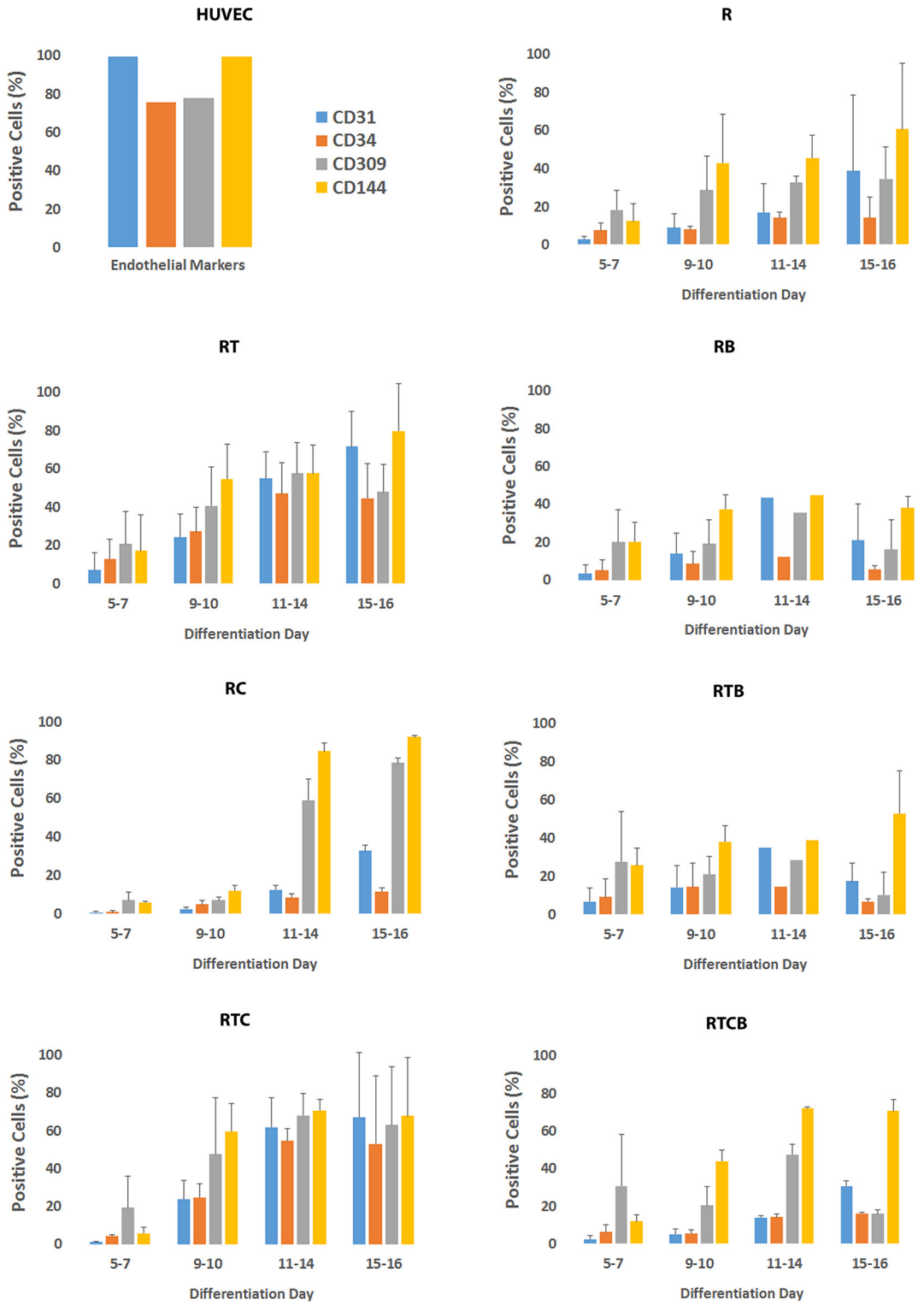

FIGURE 1 | Phenotypic marker analysis of differentiating ECs. Bar charts represent the percentage of positive cells and SD based on flow cytometric analyses of CD31, CD34, CD309 and CD144 markers. Staining protocol was performed approximately the same days during differentiation depending on the proliferation of cells. Number of experiments done differed between treatment groups (R, $n = 4$; RT, $n = 7$; RB, $n = 5$; RC, $n = 6$; RTB, $n = 5$; RTC, $n = 4$; RTCB, $n = 4$).

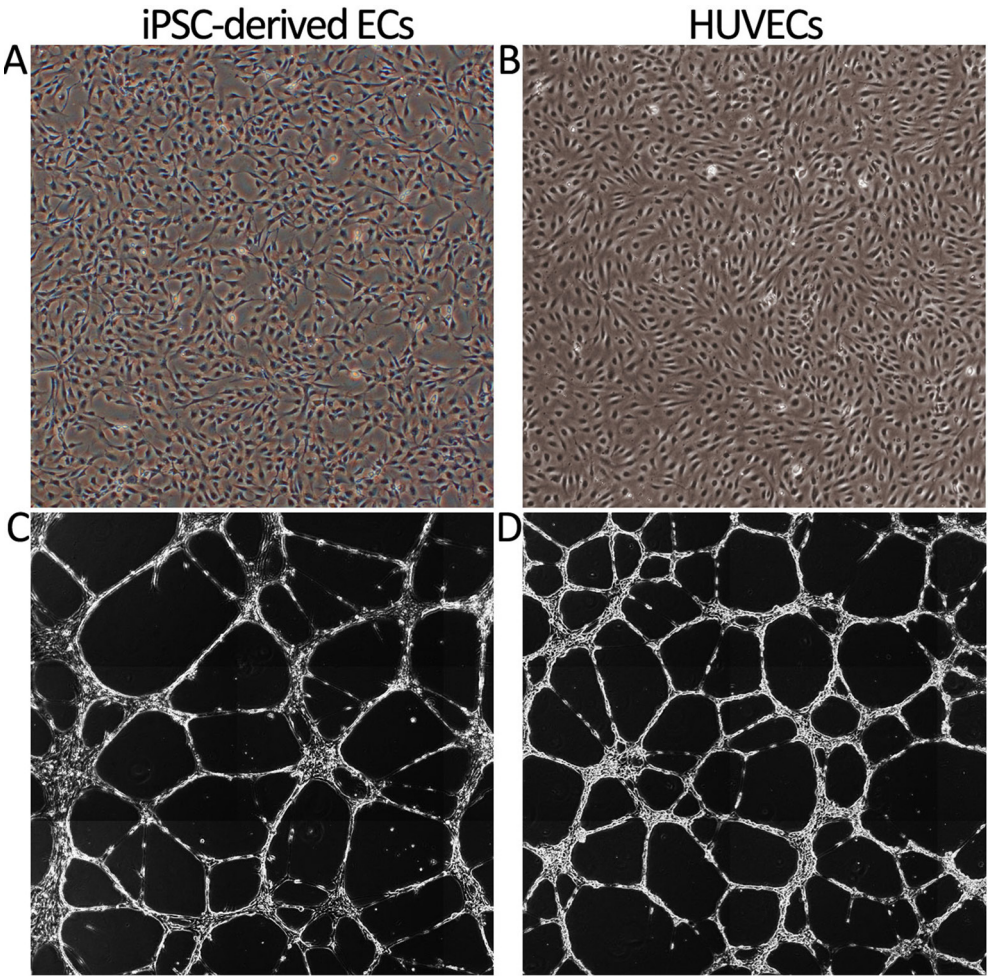

FIGURE 2 | Cell morphology and tube formation on Matrigel of iPSC-derived ECs and primary HUVECs. **(A)** The morphology of iPSC-derived ECs at day 16 (group RTC). Prolonged culturing resulted in a change of morphology towards spindle shape resembling fibroblasts (data not shown). **(B)** HUVEC cobble stone morphology. Images are taken with original magnification of 40×. **(C)** IPSC-derived ECs cultured on Matrigel form tube networks. The picture is a presentative example of tube forming for different EC differentiation groups (group RT). **(D)** Tube formation of HUVECs. Stitched images of tube formation are created by Cell-IQ Analyzer using 10× objective.

In addition, expression of intracellular EC markers vWF and eNOS was studied. As shown in **Figure 3A**, vWF was highly and uniformly expressed in RT, RC, RTB, RTC and RTCB groups and resembled the expression profile seen in HUVECs. eNOS was also expressed in all treatment groups but the number of positive cells was lower than in HUVECs (**Figure 3B**). The highest percentage of positive cells for eNOS (approximately 96%) was in RC group.

Functional Assays of Differentiated ECs

Next, we studied the functional characteristics of ECs originating from different treatment groups. First, tube formation assay was employed to demonstrate the angiogenic activity of ECs. Our analysis demonstrated that a similar tube formation potential on Matrigel was evident in all tested conditions compared to mature ECs (HUVECs) (**Figure 2C–D**). The tube formation was inhibited using 50 μM sulforaphane (data not shown). Secondly, we studied the capacity of the differentiated ECs to take up Ac-LDL. In all tested EC culture groups, cells were able to internalize Ac-LDL (**Figure 4**).

RNA Sequencing

The gene expression profiles of differentiating ECs were studied in more detail using RNA-Seq. For transcriptome analysis, cells were treated as described above and RNA was isolated at days 5 and 15 upon differentiation. Single replicates of day 5 were used to visualize the intermediate mesodermal stage, whereas two replicates were used for more throughout analysis of the end point of differentiation at day 15 and for the control hiPSC samples. The two timepoints were clearly separated by principal component analysis (PCA) (**Figure S2A**), with iPSC cells located next to day 5 samples and day 15 farther apart. Along the PC1 axis, which contributes most to the variance in the dataset (36% *vs* 17% for PC2), the day 15 samples situated closest to HAEC

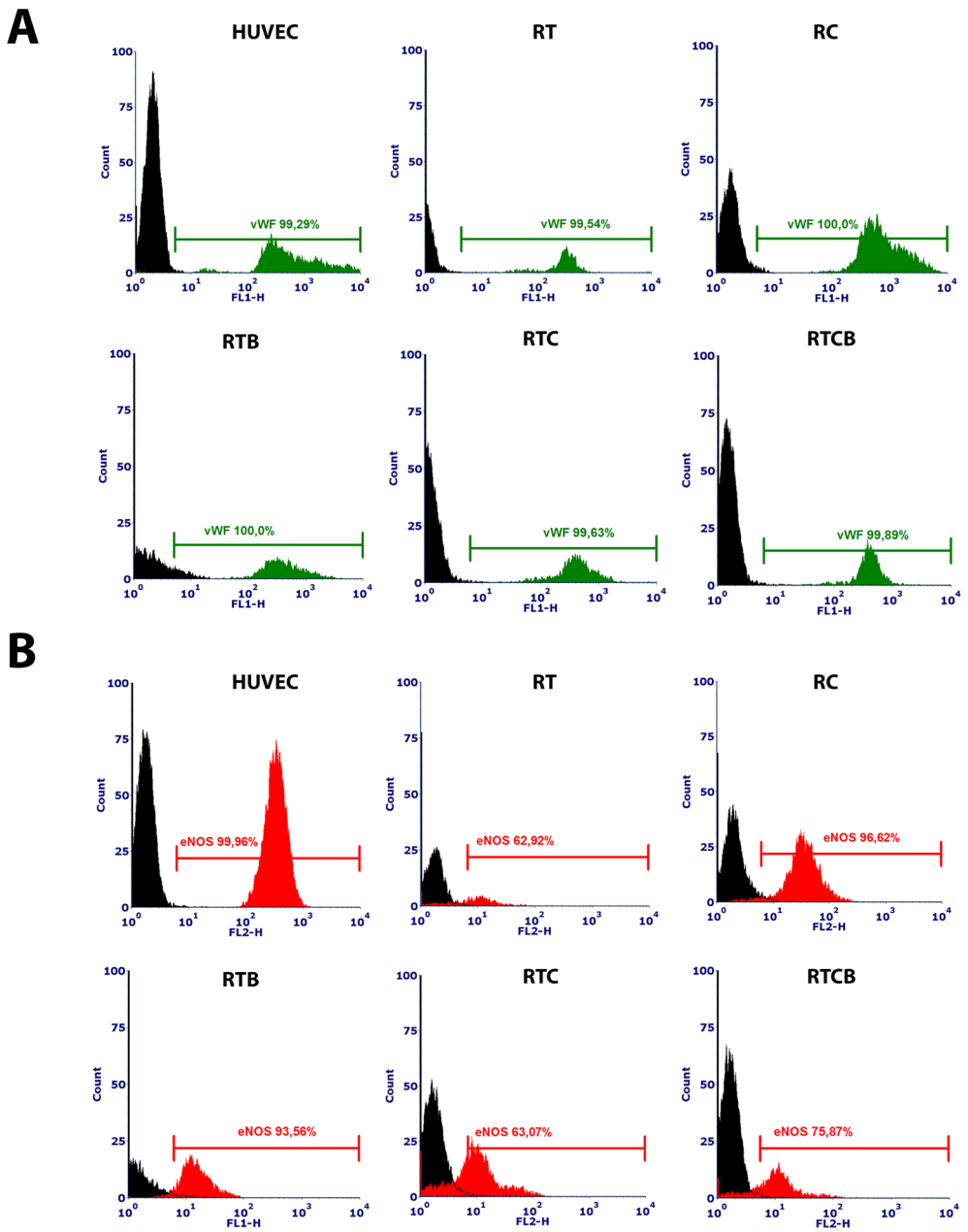

FIGURE 3 | Intracellular vWF **(3A)** and eNOS **(3B)** phenotype markers in different treatment groups at day 16. HUVECs were used as a positive control. Differentiated ECs showed a similar expression pattern of the markers in all tested cell culture groups, but the highest percentage of positively stained cells for eNOS was in RC group. The results of the stainings were similar between different experiments and they showed high reproducibility (data not shown). The numbers of experiments done: RT, *n* = 1; RC, *n* = 4; RTB, *n* = 3; RTC, *n* = 1; RTCB, *n* = 3.

and HUVEC controls supporting successful reprogramming. Also the two replicates exhibited high reproducibility by PCA (**Figure S2B**). The expression of EC markers studied by flow cytometry analyses was well in concordance with the sequencing results, suggesting that changes on the transcript levels were translated to a similar profile on the protein level (**Figure 5B** and **Table S1**). We also studied the expression of endothelial LDL scavenger receptor SCARF1 responsible for the uptake of Ac-LDL (53–56) and adhesion proteins and enzymes involved in ECM processing related to tube forming ability. At mesodermal phase at day 5, differentiating cells had lower expression of EC-related genes except vWF. Groups RB, RTB and RTCB clustered together at day 15 suggesting a significant connective role of BMP-4 for these groups (**Table S1**). In these groups, the expression of EC-related genes was the lowest which reflects the results seen visually in flow cytometric analyses even though no statistically significant differences between treatment groups was found (**Figure 1**). Among them, group RTCB had the lowest

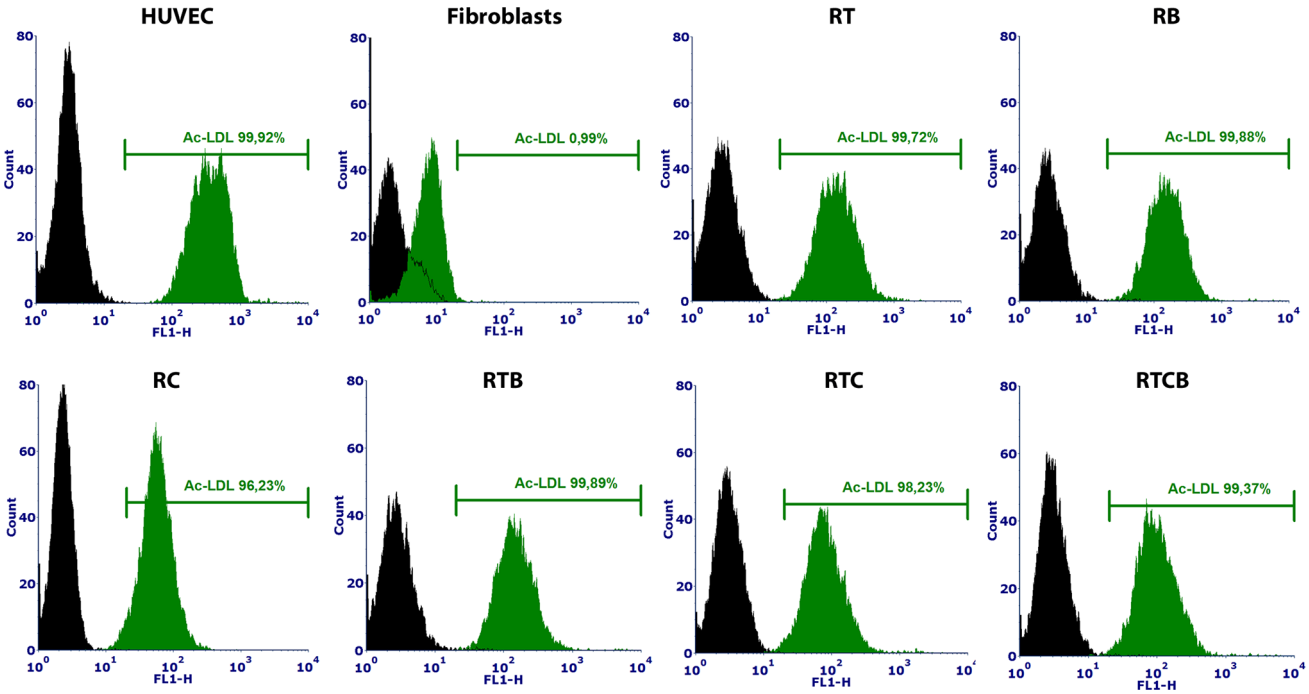

FIGURE 4 | Ac-LDL uptake assay analyzed by flow cytometry using Alexa Fluor® 488 labeled Ac-LDL. HUVECs and fibroblasts were used as positive and negative controls, respectively. HUVECs were 100% positive for Ac-LDL and among fibroblasts, only 1% were positive. Differentiated ECs (n = 1) showed similar percentages of internalized Ac-LDL (97–100%) to HUVECs at day 15.

expression of EC genes while the expression of *MMP1* and *PLAU* was high in this group. Interestingly, at a differentiation day 15, treatment group RC had more upregulated EC genes (*CD34*, *NOS3*, *KDR*) than the other treatment groups. RC group did not yet express EC surface markers on day 10 as evidenced by FACS (**Figure 1**) but the expression of EC markers took off by day 11. This suggests that the differentiation process is slower although still successful in this group.

First, we analyzed how the landscape of transcripts was changed in the differentiation groups compared to the hiPSC reference using the Gene Expression Dynamics Inspector (GEDI) analysis (48). Altogether 8535 RefSeq transcripts, corresponding to 4136 different genes, were found differentially regulated in at least one differentiation regimen at day 15 (FDR <0.05, FC > 4, RPKM > 0.5; **Table S1**). Majority (3690/4136) corresponded to protein-coding accessions (NM_), whereas the remaining 11% represented non-coding RNAs (NR_). GEDI genomic landscape maps demonstrated that the gene expression patterns of hiPSCs and differentiation groups at day 5 were more similar to each other than the day 15 groups (**Figure 5A**). Additionally, resulting GEDI representations also revealed that a distinctive EC-specific gene expression profile began to emerge in RB, RTB and RTCB groups already at day 5 (**Figure 5A**). However, by day 15 a more prominent shift in gene expression pattern was seen with shutting down of genes related to regulation of pluripotency and activation of genes related to focal adhesion in all groups (**Figure 5A**, star/hash, respectively). In line with this, the GO analysis revealed that pathways and signaling related to pluripotency and cellular adhesion, including focal adhesion, cell adhesion molecules, ECM-receptor interactions and tight junctions, were significantly enriched among the differentially regulated genes (**Figure 5C**). Notably, the pluripotency genes were more highly enriched at day 5 whereas at mature cell level the top GO term was associated with focal adhesion.

In **Figure 5D–E**, hierarchical clustering of genes related to focal adhesion and pluripotency demonstrated faster gene expression changes for RB, RTB and RTBC groups at day 5 and distinct upregulation of mesodermal genes *INHBA*, *BMP4*, *MEIS1*, *HAND1* and *TBX3*. In contrast, a higher similarity of all differentiation groups was seen especially in pluripotency related gene expression pattern at day 15. However, the RC group demonstrated the highest expression of VEGF-family members, including *FLT1*, *FLT4*, *KDR* and *VEGFC* in line with the role of cAMP signaling promoting the survival of VEGFR-2 positive cells (31) and TGFβ inhibition in maintaining vascular identity after mesodermal fate (24). In addition, a larger group of adhesion molecules, including integrins and collagens, were activated with the three conditions including BMP-4 treatment at day 15 (**Figure 5D**). Moreover, TFs, such as mesodermal related *MEIS1*, *HAND1* and *TBX3* (57, 58) (http://pathcards.genecards.org/card/mesodermal_commitment_pathway) together with *SMAD9*, *ISL1* and *ZFHX3*, were highly induced by the BMP-4 groups suggesting distinct differentiation signatures. This suggests that a distinct set of TFs could be induced by different cell culture conditions.

It has been suggested that there are master regulators that control lineage-specific gene expression and such TFs would be highly expressed in differentiated cell types (59–61). Therefore,

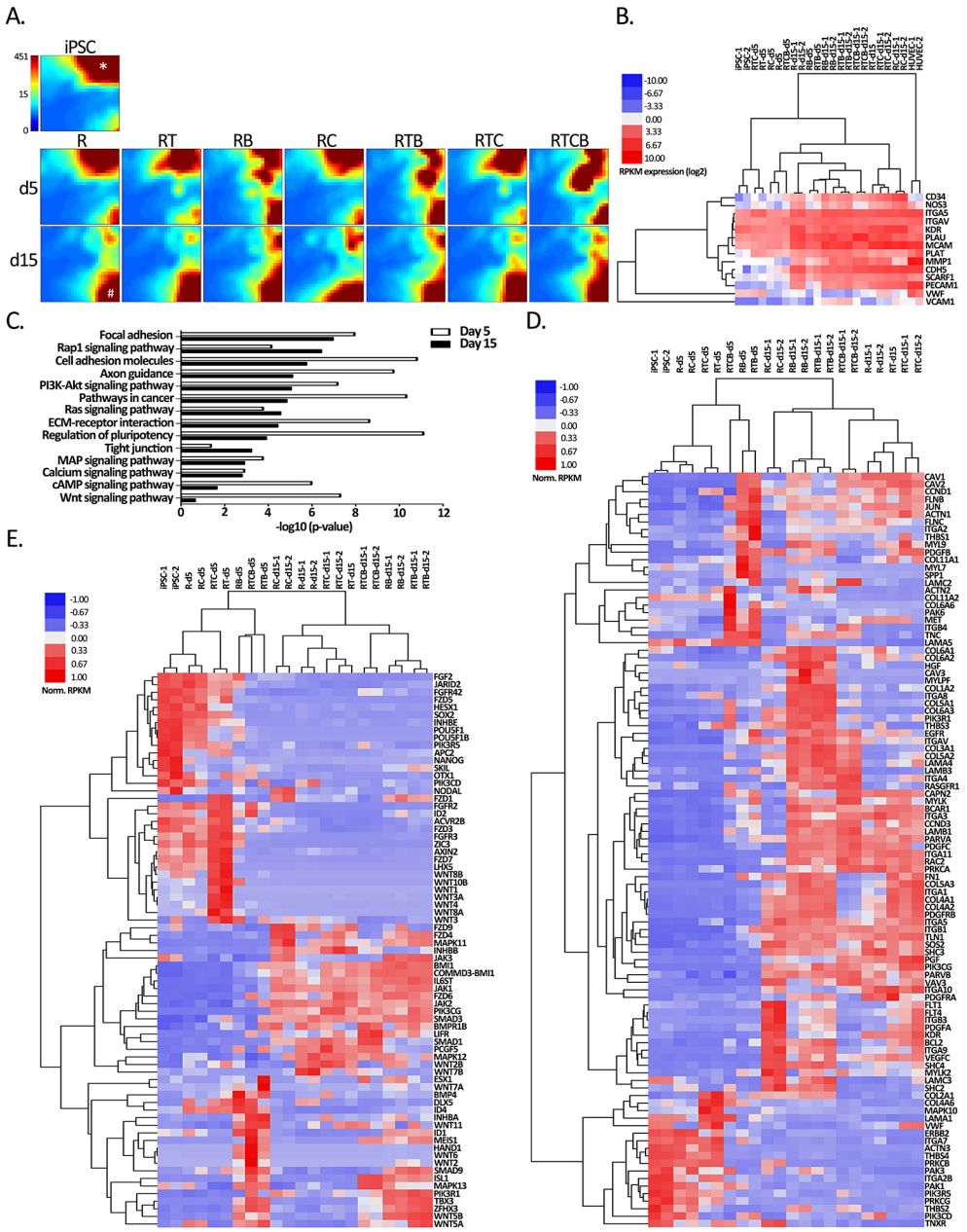

FIGURE 5 | Gene expression analyses of hiPSC compared to all EC treatment groups. **(A)** GEDI analysis of the genes differentially regulated (hiPSC vs treatment FC >4) at least in one differentiation regimen at day 15 (n = 8535 RefSeq genes). Each tile represents a cluster of genes with similar expression profiles across the samples. The color indicates the expression strength of a gene cluster (blue, low expression; red, high expression). Star shows a gene cluster highly expressed in iPSCs that correspond to pluripotency genes (data not shown) and hash mark shows a gene cluster induced during differentiation at day 15 related to focal adhesion (data not shown). **(B)** Heatmap of EC markers used in flow cytometric analyses (*CD34*, *NOS3*, *CDH5*, *KDR*, *PECAM1* and *VWF*) and genes related to EC functional assays. Spearman's rank correlation was used for sample clustering. **(C)** KEGG pathways (DAVID) of differentially expressed genes in at least one differentiation condition at day 5 (n = 6924) or day 15 (n = 8535). **(D–E)** Hierarchical clustering of genes associated with **(D)** focal adhesion and **(E)** regulation of pluripotency functions from B based on average correlation.

we studied the expression of differentially regulated TFs between the hiPSC and various EC differentiation conditions. Our analysis identified 186 TFs, which clearly clustered the samples based on the differentiation stage (**Figure 6A**). For example, pluripotency related TFs *POU5F1* (OCT-4), *SOX2*, *JARID2* and *GLI1* were highly repressed in all treatment groups except R and RC at day 5. The clustering of R/RC together with hiPSC samples at day 5 also suggests that 8-Br-cAMP does do not promote early cell differentiation. On the other hand, RT/RTC groups already exhibited repression of pluripotency genes, suggesting that early TGFβ inhibition promotes differentiation at day 5. Notably, the most striking difference was seen for the

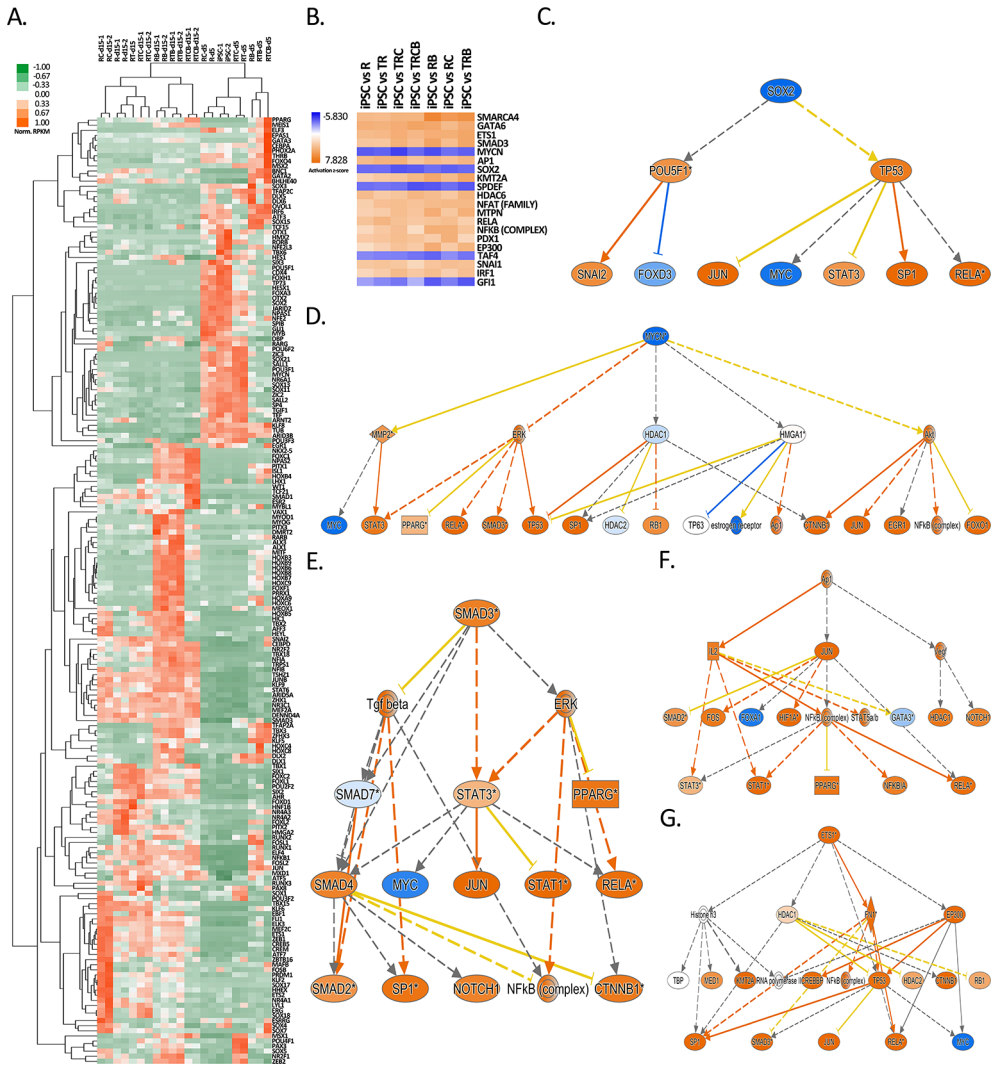

FIGURE 6 | Identification of top upstream regulators responsible for gene expression changes during EC differentiation. **(A)** Heatmap of normalized RPKM values (−1 to 1) of the top 186 transcription factors differentially regulated over 100-fold in response to differentiation treatments. Hierarchical clustering (average linkage) was performed for genes and samples. **(B)** IPA analysis of upstream transcription regulators for hiPSC *versus* EC treatment groups shown for the 20 top upstream regulators with the highest z-scores. **(C-G)** Mechanistic networks generated by IPA for selected transcription factors from B. Blue color stands for predicted inhibition and orange for predicted activation. The tones of color indicate confidence level (light = low confidence; dark = high confidence). Transcription factors **(C)** *SOX2* and **(D)** *MYCN* were predicted to be inhibited and **(E)** *SMAD3*, **(F)** *AP1* and **(G)** *ETS1* activated.

RB, RTB and RTBC groups that clustered away from the other treatment groups at day 5. This was most attributable to the early repression of *MYCN*, *SOX2*, *SOX21*, *SOX11*, *SOX13* and *POU3F1* genes, which was evident in the other treatment groups only at day 15. Additionally, these groups also exhibited a high expression level of mesodermal TFs *GATA2* and *GATA3* at day 5. This likely reflects the ability of exogenous BMP-4 to promote differentiation of pluripotent cells toward mesodermal cells (33).

As a demonstration of the success of differentiation, the major EC-specific TFs, such as *ETS1*, *ETS2*, *JUNB*, *ERG*, *SOX7*, *SOX17*, *SOX18*, *HHEX*, *ELK3*, *KLF6*, *MEF2C* and *FLI1* (62–68) were highly induced in the majority of differentiation groups at day 15 (**Figure 6A**). The highest expression of these crucial EC-related TFs was in RC group and the lowest in RTCB group. This suggests that RC, with the highest expression of EC markers (**Figure 5B**) and EC-specific TFs (**Figure 6A**) likely represents the most EC-like phenotype. This result was further confirmed by studying the expression of 50 most highly expressed TFs in HUVECs and HAECs, where RC group clustered closest to these mature EC types (**Figure S3**).

To study how changes in the TF expression could explain the global changes in gene expression patterns, we further searched for other upstream transcriptional regulators using Ingenuity Pathway Analysis (IPA). In line with TF expression, our analysis identified *MYCN* and *SOX2* as the top transcriptional regulators inhibited during differentiation, whereas *SMAD3*, *ETS1* and *AP1* signaling was activated (**Figure 6B–G**). Although not directly linked with the induction of the respective TF, also *SMARCA4*,

GATA6 and *KMT2A* were identified as possible activated upstream regulators (**Figure S4**). These TF networks could thus explain gene expression changes during EC differentiation. Interestingly, a similar pattern of activation was also highly associated with a chemical compound tretinoin (**Figure S5**).

DISCUSSION

In this study, we focused on systematically testing and comparing the efficacy of the most potent signalling factors and small molecules used to produce ECs from hiPSC. Stem cells are a renewable, limitless source of differentiating ECs. They are also less immunogenic due to the use of autologous patient-specific cells, making them an attractive therapeutic tool (21, 69). However, iPSCs have their own disadvantages related to the risk of teratomas because of the pluripotent nature of the cells (69). There are also concerns related to incorporation of the iPSC generating viral vectors with the host genome and continuing transcription of transgenes in iPSC-derived, differentiated cells (21). Concisely, it is essential to test all possible EC types in a clinical setting to evaluate which cells have the most potential for therapeutic applications. We present here the first systematic characterization of the existing EC differentiation protocols by testing the effect of relevant signaling factors and small molecules, and evaluating the subsequent efficacy of EC differentiation from hiPSC. We used a simple, 2D monolayer cell culture with serum-free, well-defined cell culture medium to rigorously control factors affecting EC differentiation. EC differentiation took approximately 15 days and was confirmed by EC marker expression with flow cytometry analysis. EC maturation was further confirmed by functional EC assays, such as tube formation and Ac-LDL uptake, which demonstrated similar functional characteristics of differentiated ECs compared to HUVECs.

RNA-Seq was used to provide a genome-wide view of the gene expression changes during the seven different treatment protocols. To our surprise, all treatment groups exhibited many similarities at day 15, exemplified by silencing of genes related to regulation of pluripotency and upregulation of genes related to focal adhesion. The high similarity of groups also indicates that one factor in common to all, the ROCK inhibitor, a major downstream effector protein RhoA, is indispensable for EC differentiation (25). RhoA controls diverse array of cellular processes such as cytoskeletal dynamics, cell polarity, membrane transport and gene expression (70). ROCK inhibitors controls the expression of adhesion molecules and accordingly, ROCKs have been shown to affect cell–cell adhesion of ECs, and to regulate the integrity of cellular junctions (71). The effects of ROCKs are also linked to cAMP signalling via exchange protein directly activated by cAMP (Epac) signalling (72). Epacs are guanine nucleotide exchange factors (GEFs) that bind to cAMP. This pathway enhances EC barrier function by influencing EC junctional protein and actin cytoskeleton organisation. It downregulates RhoA activation and stress fiber formation (73). Recently, ROCK inhibition has been associated with the inhibition of endothelial-to-mesenchymal transition (74). The interaction between ECs and extracellular matrix influences key signaling events involved in EC migration, invasion, proliferation, and survival that are indispensable for angiogenesis (13). Our results clearly demonstrate that the majority of the gene expression changes occuring during EC differentiation are related to the regulation of genes and pathways associated with cellular adhesion and ECM-receptor interaction supporting their central role in inducing and maintaining EC function.

As a further proof of differentiation, major EC-specific TFs, such as *ETS1*, *ETS2*, *JUNB*, *ERG*, *SOX7*, *SOX17*, *SOX18*, *HHEX*, *ELK3*, *KLF6*, *MEF2C* and *FLI1* (62–68) were highly expressed in the majority of differentiation groups at day 15. Ingenuity Pathway Analysis was used to reveal upstream transcriptional regulators that could explain changes in the gene expression patterns during our differentiation procedure from hiPSCs to mature ECs. We identified *MYCN* and *SOX2* as the top transcriptional regulators that were inhibited, while *SMAD3* (75), *ETS1* (62) and *AP1* (76) signalling was stimulated. This information could provide a future means for the generation of more efficient EC differentiation protocols through the modulation of TF expression or small molecule drugs targeting TF function (63, 66, 67, 77). Interestingly, a chemical compound tretinoin was shown to induce highly similar gene regulation networks suggesting that it could be used to further enhance EC differentiation. Supporting this finding, a natural retinoid all-trans retinoic acid has been shown to promote angiogenesis by stimulating EC proliferation and enhancing endogenous VEGF signaling (78–80).

Our analysis of TF expression also revealed that the treatment group RC had the highest expression of EC-specific TFs together with the strongest expression of EC marker genes and VEGF family members. This suggests that, in addition to the ROCK inhibition, the supplementation of a cAMP analog 8-Br-cAMP in the beginning of differentiation could promote the most efficient differentiation. CAMP-signalling has been shown to be associated with Notch and protein kinase A (PKA)/Epac pathways. Activating these signalling pathways promotes differentiation and proliferation of ECs and survival of VEGFR-2 positive cells (23, 31), enhances EC barrier function (73), and activates eNOS which is responsible for, for example, EC-mediated vasorelaxation (81). Interestingly, the expression of eNOS on protein and RNA level was highest in RC and RTB groups and lowest in RT, RTC and RTCB groups. These differences could be due to complex impacts of TGFβ and cAMP signalling on eNOS expression and activity (81, 82). It has been shown that TGFβ increases the expression of eNOS acting via Smad2 signalling (82) and inhibiting this TGFβ pathway might lower the eNOS expression shown in our results. On the other hand, cAMP signaling has been shown to enhance eNOS activity through PKA/Epac signalling that further activates PI3K/Akt pathway (81).

Our results for the RC group also demonstrate that the effects of cAMP signalling take at least two weeks to occur, since only little gene expression changes were seen at day 5 and expression of EC markers analyzed by flow cytometry were not yet evident at day 10. An explanation for the slow differentiation can be explained by the fact that the RC group received the TGFβ inhibitor at day 4,

in contrast to the RTC group which was cultivated in the presence of this inhibitor throughout the time course. TGFβ signalling has many roles including cell differentiation, migration and maintaining pluripotency of stem cells. The role of TGFβ signalling in maintaining pluripotency of PSCs is controversial, some studies supporting its role in pluripotency maintenance and others confronting this assumption (83–85). The TGFβ inhibitor SB431542 used in these experiments inhibits signalling mediated by ALK-4, ALK-5 and ALK-7 receptor while leaving ALK1 signalling unaffected (86). Signalling activated by ALK-5 inhibits EC proliferation, tube formation, and migration (87). In line with this, the TGFβ inhibitor has shown to enhance EC differentiation from ESCs and EC growth (35, 50), and it is needed in the maintenance of the vascular identity after EC specification (24). Additionally, it has been shown that TGFβ inhibition functionalizes VEGFR-2 signalling (88). Altogether, TGFβ signalling has multiple roles in several cell types and it it essential to balance between those counteracting functions in EC differentiation protocols. Our results provide evidence that TGFβ inhibitor is most useful in EC differentiation when added after mesodermal induction to promote subsequent EC spesification.

Interestingly, our results indicated high expression of mesodermal genes including *INHBA*, *BMP4*, *GATA2*, *GATA3*, *MEIS1*, *HAND1*, *KLF5* and *TBX3* (57) in the treatment groups receiving BMP-4 at day 5. This is in line with findings that exogenous BMP-4 promotes early mesodermal differentiation (30, 33, 89, 90). The BMP-4 activation, however, did not help in gaining a mature EC phenotype. However, groups RB, RTB and RTCB clustered together at day 15 and exhibited distinct gene signatures exemplified by the induction of a large group of integrins and collagens. This suggest a significant connective role of BMP-4 in these groups although it does not specifically promote mature endothelial differentiation.

In conclusion, we used a simple, serum-free 2D monolayer cell culture method to guide hiPSC into ECs, omitting complicated manufacturing procedures. Using human iPSC as source material and ECs derived from them enables autologous or allogeneic cell preparations to be tested in studies aiming at regenerative vascularization. EC differentiation took approximately 15 days. Differentiated cells showed a typical pattern of EC surface antigens and functional properties, such as tube formation and Ac-LDL uptake. Transcriptomic profiling demonstrated that although the treatment groups were highly similar at day 15, the most potent factors inducing EC phenotype were the cAMP analog 8-Br-cAMP employed at the beginning of EC differentiation and the TGFβ inhibitor SB431542 added after the mesodermal differentiation at day 4. Additionally, the ROCK inhibitor Y-27632 is highly beneficial to EC differentiation and it should be included in the EC culture media. It was also shown that exogenous BMP-4 supplemented from day 1 to day 4 activates early mesodermal differentiation but gives no advantage later in the differentiation process when cells are gaining mature EC phenotype. In summary, this optimized cell culture method provides an improved basis for an efficient EC production from hiPSCs, and offers invaluable information about the transcriptional changes occurring during the EC differentiation that could be employed in the generation of ECs for regenerative therapy applications.

ETHICS APPROVAL

HUVECs were isolated from umbilical cords obtained from the maternity ward of the Kuopio University Hospital under the approval of the Hospital Ethics Committee (permit 341/2015). The samples were anonymous and cannot be traced back to the donor.

AUTHOR CONTRIBUTIONS

HB and JKK designed the study. HB performed experiments and analyzed the data. JKK participated in the research and data analysis and revised the manuscript. TK coordinated research and revised the manuscript. KP provided stem cells, coordinated stem cell work and revised the manuscript. PIM performed flow cytometry analyses and prepared pictures related to them. HN contributed to the RNA-Seq data analyses. JO performed statistical analyses. GW participated in manuscript preparation and revision. JK provided stem cell facilities and enabled research using stem cells. MK coordinated research, analyzed and prepared figures of RNA-Seq data. HB and MK wrote the manuscript. SY-H contributed to the conception and design of the research, critically revised the manuscript for important intellectual content, and supervised the research.

FUNDING

European Research Council (670951), Academy of Finland (257426 to JKK, 287478 and 294073 to MK, 307402 to SY-H), Finnish Foundation for Cardiovascular Research, Jane and Aatos Erkko Foundation, Sigrid Jusélius Foundation, Finnish Medical Foundation, Ida Montin Foundation, Aarne Koskelo Foundation.

ACKNOWLEDGEMENT

We are grateful to Riitta Kauppinen, Marika Ruponen, Elina Reinikainen, Laila Kaskela and Eila Korhonen for helping with stem cells related practical work. We thank the Sequencing Service GeneCore Sequencing Facility (EMBL, http://www.genecore.embl.de) for NGS library sequencing and UEF Bioinformatics Center for server infrastructure.

SUPPLEMENTARY MATERIAL

The Supplementary Material for this article can be found online at: http://journal.frontiersin.org/article/10.3389/fcvm.2018.00016/full#supplementary-material

FIGURE S1 | EC differentiation duration from iPSC was tested by monitoring of ECmarker expression up to 36 days. A presentative diagram of differentiation group RT showing howEC marker expression goes up until differentiation day 15–16 and down after that. ECs lose theirphenotype in a longer culturing period in all tested differentiation groups.

FIGURE S2 | Principal component analysis (PCA) of log-transformed RPKM valuesfrom (A) all RNA-Seq samples (2D plot) and (B) all samples subjected to 15 day differentiationregimen (3D plot).

FIGURE S3 | Heatmap of normalized RPKM values (–1 to 1) of the 50 most highly expressed transcription factors in HUVECs and HAECs. Clustering was performed for genes and samples using Spearman's rank correlation (complete linkage).

FIGURE S4 | Mechanistic networks generated by IPA for transcription factors SMARCA4, GATA6 and KMT2A predicted to be activated from Figure 6B. Blue depicts predicted inhibition and orange activation. The tones of color indicate confidence level (light = low confidence; dark = high confidence).

FIGURE S5 | Mechanistic networks generated by IPA for a chemical compoundtretinoin predicted to be activated. Blue depicts predicted inhibition and orange activation. The tonesof color indicate confidence level (light = low confidence; dark = high confidence).

TABLE S1 | Gene expression analysis comparing hiPSCs to treatment groups on day 5 and day 15. Normalized gene expression values are provided with log2 FC and FDR values for each pairwise comparison.

REFERENCES

1. Mozaffarian D, Benjamin EJ, Go AS, Arnett DK, Blaha MJ, Cushman M , et al. Heart disease and stroke statistics-2016 update: a report from the American Heart Association. *Circulation* (2016) 133(4):e38–60. doi: 10.1161/CIR.0000000000000350
2. Annex BH. Therapeutic angiogenesis for critical limb ischaemia. *Nat Rev Cardiol* (2013) 10(7):387–96. doi: 10.1038/nrcardio.2013.70
3. Ylä-Herttuala S, Bridges C, Katz MG, Korpisalo P. Angiogenic gene therapy in cardiovascular diseases: dream or vision? *Eur Heart J* (2017) 38(18):ehw547–71. doi: 10.1093/eurheartj/ehw547
4. Zhang H, van Olden C, Sweeney D, Martin-Rendon E. Blood vessel repair and regeneration in the ischaemic heart. *Open Heart* (2014) 1(1):e000016. doi: 10.1136/openhrt-2013-000016
5. Fan Y, Shen F, Frenzel T, Zhu W, Ye J, Liu J, et al. Endothelial progenitor cell transplantation improves long-term stroke outcome in mice. *Ann Neurol* (2010) 67(4):488–97. doi: 10.1002/ana.21919
6. Ylä-Herttuala S, Baker AH. Cardiovascular gene therapy: past, present, and future. *Mol Ther* (2017) 25(5):1095–106. doi: 10.1016/j.ymthe.2017.03.027
7. Grunewald M, Avraham I, Dor Y, Bachar-Lustig E, Itin A, Jung S, et al. VEGF-induced adult neovascularization: recruitment, retention, and role of accessory cells. *Cell* (2006) 124(1):175–89. doi: 10.1016/j.cell.2005.10.036
8. You D, Waeckel L, Ebrahimian TG, Blanc-Brude O, Foubert P, Barateau V, et al. Increase in vascular permeability and vasodilation are critical for proangiogenic effects of stem cell therapy. *Circulation* (2006) 114(4):328–38. doi: 10.1161/CIRCULATIONAHA.105.589937
9. Cines DB, Pollak ES, Buck CA, Loscalzo J, Zimmerman GA, Mcever RP, et al. Endothelial cells in physiology and in the pathophysiology of vascular disorders. *Blood* (1998) 91(10):3527–61.
10. Davignon J, Ganz P. Role of Endothelial Dysfunction in Atherosclerosis. *Circulation* (2004) 109(23_suppl_1):III-27–32. doi: 10.1161/01.CIR.0000131515.03336.f8
11. Krispin S, Stratman AN, Melick CH, Stan RV, Malinverno M, Gleklen J, et al. Growth differentiation factor 6 promotes vascular stability by restraining vascular endothelial growth factor signaling. *Arterioscler Thromb Vasc Biol* (2018) 38(2):353–62. doi: 10.1161/ATVBAHA.117.309571
12. Potente M, Carmeliet P. The link between angiogenesis and endothelial metabolism. *Annu Rev Physiol* (2017) 79:43–66. doi: 10.1146/annurev-physiol-021115-105134
13. Davis GE, Senger DR. Endothelial extracellular matrix: biosynthesis, remodeling, and functions during vascular morphogenesis and neovessel stabilization. *Circ Res* (2005) 97(11):1093–107. doi: 10.1161/01.RES.0000191547.64391.e3
14. Zengin E, Chalajour F, Gehling UM, Ito WD, Treede H, Lauke H, et al. Vascular wall resident progenitor cells: a source for postnatal vasculogenesis. *Development* (2006) 133(8):1543–51. doi: 10.1242/dev.02315
15. Asahara T, Murohara T, Sullivan A, Silver M, van der Zee R, Li T, et al. Isolation of putative progenitor endothelial cells for angiogenesis. *Science* (1997) 275(5302):964–6. doi: 10.1126/science.275.5302.964
16. Xu S, Tao J, Yang L, Zhang E, Boriboun C, Zhou J, et al. E2F1 suppresses oxidative metabolism and endothelial differentiation of bone marrow progenitor cells. *Circ Res* (2018):CIRCRESAHA.117.311814. doi: 10.1161/CIRCRESAHA.117.311814
17. Thomson JA, Itskovitz-Eldor J, Shapiro SS, Waknitz MA, Swiergiel JJ, Marshall VS, et al. Embryonic stem cell lines derived from human blastocysts. *Science* (1998) 282(5391):1145–7. doi: 10.1126/science.282.5391.1145
18. Takahashi K, Yamanaka S. Induction of pluripotent stem cells from mouse embryonic and adult fibroblast cultures by defined factors. *Cell* (2006) 126(4):663–76. doi: 10.1016/j.cell.2006.07.024
19. Yu J, Vodyanik MA, Smuga-Otto K, Antosiewicz-Bourget J, Frane JL, Tian S, et al. Induced pluripotent stem cell lines derived from human somatic cells. *Science* (2007) 318(5858):1917–20. doi: 10.1126/science.1151526
20. Hirschi KK, Li S, Roy K. Induced pluripotent stem cells for regenerative medicine. *Annu Rev Biomed Eng* (2014) 16:277–94. doi: 10.1146/annurev-bioeng-071813-105108
21. Singh VK, Kalsan M, Kumar N, Saini A, Chandra R. Induced pluripotent stem cells: applications in regenerative medicine, disease modeling, and drug discovery. *Front Cell Dev Biol* (2015) 3:2. doi: 10.3389/fcell.2015.00002
22. Descamps B, Emanueli C. Vascular differentiation from embryonic stem cells: novel technologies and therapeutic promises. *Vascul Pharmacol* (2012) 56(5-6):267–79. doi: 10.1016/j.vph.2012.03.007
23. Ikuno T, Masumoto H, Yamamizu K, Yoshioka M, Minakata K, Ikeda T, et al. Efficient and robust differentiation of endothelial cells from human induced pluripotent stem cells via lineage control with VEGF and cyclic AMP. *PLoS ONE* (2017) 12(3):e0173271. doi: 10.1371/journal.pone.0173271
24. James D, Nam HS, Seandel M, Nolan D, Janovitz T, Tomishima M, et al. Expansion and maintenance of human embryonic stem cell-derived endothelial cells by TGFbeta inhibition is Id1 dependent. *Nat Biotechnol* (2010) 28(2):161–6. doi: 10.1038/nbt.1605
25. Joo HJ, Choi DK, Lim JS, Park JS, Lee SH, Song S, et al. ROCK suppression promotes differentiation and expansion of endothelial cells from embryonic stem cell-derived Flk1(+) mesodermal precursor cells. *Blood* (2012) 120(13):2733–44. doi: 10.1182/blood-2012-04-421610
26. Kane NM, Xiao Q, Baker AH, Luo Z, Xu Q, Emanueli C. Pluripotent stem cell differentiation into vascular cells: a novel technology with promises for vascular re(generation). *Pharmacol Ther* (2011) 129(1):29–49. doi: 10.1016/j.pharmthera.2010.10.004
27. Liu X, Qi J, Xu X, Zeisberg M, Guan K, Zeisberg EM. Differentiation of functional endothelial cells from human induced pluripotent stem cells: a novel, highly efficient and cost effective method. *Differentiation* (2016) 92(4):225–36. doi: 10.1016/j.diff.2016.05.004
28. Madfis N, Lin Z, Kumar A, Douglas SA, Platt MO, Fan Y, et al. Co-emergence of specialized endothelial cells from embryonic stem cells. *Stem Cells Dev* (2018). doi: 10.1089/scd.2017.0205
29. Narazaki G, Uosaki H, Teranishi M, Okita K, Kim B, Matsuoka S, et al. Directed and systematic differentiation of cardiovascular cells from mouse induced pluripotent stem cells. *Circulation* (2008) 118(5):498–506. doi: 10.1161/CIRCULATIONAHA.108.769562
30. Park SW, Jun Koh Y, Jeon J, Cho YH, Jang MJ, Kang Y, et al. Efficient differentiation of human pluripotent stem cells into functional CD34+ progenitor cells by combined modulation of the MEK/ERK and BMP4 signaling pathways. *Blood* (2010) 116(25):5762–72. doi: 10.1182/blood-2010-04-280719
31. Yurugi-Kobayashi T, Itoh H, Schroeder T, Nakano A, Narazaki G, Kita F, et al. Adrenomedullin/cyclic AMP pathway induces Notch activation and differentiation of arterial endothelial cells from vascular progenitors.

Arterioscler Thromb Vasc Biol (2006) 26(9):1977–84. doi: 10.1161/01.ATV.0000234978.10658.41
32. Zhang J, Chu LF, Hou Z, Schwartz MP, Hacker T, Vickerman V, et al. Functional characterization of human pluripotent stem cell-derived arterial endothelial cells. *Proc Natl Acad Sci USA* (2017) 114(30):E6072–8. doi: 10.1073/pnas.1702295114
33. Zhang P, Li J, Tan Z, Wang C, Liu T, Chen L, et al. Short-term BMP-4 treatment initiates mesoderm induction in human embryonic stem cells. *Blood* (2008) 111(4):1933–41. doi: 10.1182/blood-2007-02-074120
34. Clayton ZE, Sadeghipour S, Patel S. Generating induced pluripotent stem cell derived endothelial cells and induced endothelial cells for cardiovascular disease modelling and therapeutic angiogenesis. *Int J Cardiol* (2015) 197:116–22. doi: 10.1016/j.ijcard.2015.06.038
35. Watabe T, Nishihara A, Mishima K, Yamashita J, Shimizu K, Miyazawa K, et al. TGF-beta receptor kinase inhibitor enhances growth and integrity of embryonic stem cell-derived endothelial cells. *J Cell Biol* (2003) 163(6):1303–11. doi: 10.1083/jcb.200305147
36. Qu C, Puttonen KA, Lindeberg H, Ruponen M, Hovatta O, Koistinaho J, et al. Chondrogenic differentiation of human pluripotent stem cells in chondrocyte co-culture. *Int J Biochem Cell Biol* (2013) 45(8):1802–12. doi: 10.1016/j.biocel.2013.05.029
37. Holmqvist S, Lehtonen Š, Chumarina M, Puttonen KA, Azevedo C, Lebedeva O, et al. Creation of a library of induced pluripotent stem cells from Parkinsonian patients. *NPJ Parkinsons Dis* (2016) 2:16009. doi: 10.1038/npjparkd.2016.9
38. Puttonen KA, Ruponen M, Kauppinen R, Wojciechowski S, Hovatta O, Koistinaho J. Improved method of producing human neural progenitor cells of high purity and in large quantities from pluripotent stem cells for transplantation studies. *Cell Transplant* (2013) 22(10):1753–66. doi: 10.3727/096368912X658764
39. Watanabe K, Ueno M, Kamiya D, Nishiyama A, Matsumura M, Wataya T, et al. A ROCK inhibitor permits survival of dissociated human embryonic stem cells. *Nat Biotechnol* (2007) 25(6):681–6. doi: 10.1038/nbt1310
40. Jaffe EA, Nachman RL, Becker CG, Minick CR. Culture of human endothelial cells derived from umbilical veins. Identification by morphologic and immunologic criteria. *J Clin Invest* (1973) 52(11):2745–56. doi: 10.1172/JCI107470
41. Bertl E, Bartsch H, Gerhäuser C. Inhibition of angiogenesis and endothelial cell functions are novel sulforaphane-mediated mechanisms in chemoprevention. *Mol Cancer Ther* (2006) 5(3):575–85. doi: 10.1158/1535-7163.MCT-05-0324
42. Kaikkonen MU, Niskanen H, Romanoski CE, Kansanen E, Kivelä AM, Laitalainen J, et al. Control of VEGF-A transcriptional programs by pausing and genomic compartmentalization. *Nucleic Acids Res* (2014) 42(20):12570–84. doi: 10.1093/nar/gku1036
43. Heinz S, Benner C, Spann N, Bertolino E, Lin YC, Laslo P, et al. Simple combinations of lineage-determining transcription factors prime cis-regulatory elements required for macrophage and B cell identities. *Mol Cell* (2010) 38(4):576–89. doi: 10.1016/j.molcel.2010.05.004
44. Robinson MD, Mccarthy DJ, Smyth GK. edgeR: a Bioconductor package for differential expression analysis of digital gene expression data. *Bioinformatics* (2010) 26(1):139–40. doi: 10.1093/bioinformatics/btp616
45. de Hoon MJ, Imoto S, Nolan J, Miyano S. Open source clustering software. *Bioinformatics* (2004) 20(9):1453–4. doi: 10.1093/bioinformatics/bth078
46. Saldanha AJ. Java Treeview-extensible visualization of microarray data. *Bioinformatics* (2004) 20(17):3246–8. doi: 10.1093/bioinformatics/bth349
47. Huang Daw, Sherman BT, Lempicki RA. Systematic and integrative analysis of large gene lists using DAVID bioinformatics resources. *Nat Protoc* (2009) 4(1):44–57. doi: 10.1038/nprot.2008.211
48. Eichler GS, Huang S, Ingber DE. Gene expression dynamics inspector (GEDI): for integrative analysis of expression profiles. *Bioinformatics* (2003) 19(17):2321–2.
49. Bai H, Gao Y, Hoyle DL, Cheng T, Wang ZZ. Suppression of transforming growth factor-beta signaling delays cellular senescence and preserves the function of endothelial cells derived from human pluripotent stem cells. *Stem Cells Transl Med* (2017) 6(2):589–600. doi: 10.5966/sctm.2016-0089
50. Park C, Afrikanova I, Chung YS, Zhang WJ, Arentson E, Fong Gh G, et al. A hierarchical order of factors in the generation of FLK1- and SCL-expressing hematopoietic and endothelial progenitors from embryonic stem cells. *Development* (2004) 131(11):2749–62. doi: 10.1242/dev.01130
51. Seghezzi G, Patel S, Ren CJ, Gualandris A, Pintucci G, Robbins ES, et al. Fibroblast growth factor-2 (FGF-2) induces vascular endothelial growth factor (VEGF) expression in the endothelial cells of forming capillaries: An autocrine mechanism contributing to angiogenesis. *J Cell Biol* (1998) 141(7):1659–73.
52. Yamashita J, Itoh H, Hirashima M, Ogawa M, Nishikawa S, Yurugi T, et al. Flk1-positive cells derived from embryonic stem cells serve as vascular progenitors. *Nature* (2000) 408(6808):92–6. doi: 10.1038/35040568
53. Kelly MA, Hirschi KK. Signaling hierarchy regulating human endothelial cell development. *Arterioscler Thromb Vasc Biol* (2009) 29(5):718–24. doi: 10.1161/ATVBAHA.109.184200
54. Adachi H, Tsujimoto M, Arai H, Inoue K. Expression cloning of a novel scavenger receptor from human endothelial cells. *J Biol Chem* (1997) 272(50):31217–20. doi: 10.1074/jbc.272.50.31217
55. Ramirez-Ortiz ZG, Pendergraft WF, Prasad A, Byrne MH, Iram T, Blanchette CJ, et al. The scavenger receptor SCARF1 mediates the clearance of apoptotic cells and prevents autoimmunity. *Nat Immunol* (2013) 14(9):917–26. doi: 10.1038/ni.2670
56. Tamura Y, Osuga J, Adachi H, Tozawa R, Takanezawa Y, Ohashi K, et al. Scavenger receptor expressed by endothelial cells I (SREC-I) mediates the uptake of acetylated low density lipoproteins by macrophages stimulated with lipopolysaccharide. *J Biol Chem* (2004) 279(30):30938–44. doi: 10.1074/jbc.M313088200
57. Waghray A, Saiz N, Jayaprakash AD, Freire AG, Papatsenko D, Pereira CF, et al. Tbx3 controls Dppa3 levels and exit from pluripotency toward mesoderm. *Stem Cell Reports* (2015) 5(1):97–110. doi: 10.1016/j.stemcr.2015.05.009
58. Wang H, Liu C, Liu X, Wang M, Wu D, Gao J, et al. MEIS1 regulates hemogenic endothelial generation, megakaryopoiesis, and thrombopoiesis in human pluripotent stem cells by targeting TAL1 and FLI1. *Stem Cell Reports* (2018) 10(2):447–60. doi: 10.1016/j.stemcr.2017.12.017
59. Laslo P, Spooner CJ, Warmflash A, Lancki DW, Lee HJ, Sciammas R, et al. Multilineage transcriptional priming and determination of alternate hematopoietic cell fates. *Cell* (2006) 126(4):755–66. doi: 10.1016/j.cell.2006.06.052
60. Miranda-Saavedra D, Göttgens B. Transcriptional regulatory networks in haematopoiesis. *Curr Opin Genet Dev* (2008) 18(6):530–5. doi: 10.1016/j.gde.2008.09.001
61. Zhang P, Behre G, Pan J, Iwama A, Wara-Aswapati N, Radomska HS, et al. Negative cross-talk between hematopoietic regulators: GATA proteins repress PU.1. *Proc Natl Acad Sci USA* (1999) 96(15):8705–10. doi: 10.1073/pnas.96.15.8705
62. Chen J, Fu Y, Day DS, Sun Y, Wang S, Liang X, et al. VEGF amplifies transcription through ETS1 acetylation to enable angiogenesis. *Nat Commun* (2017) 8(1):383–017. doi: 10.1038/s41467-017-00405-x
63. de Val S, Black BL. Transcriptional control of endothelial cell development. *Dev Cell* (2009) 16(2):180–95. doi: 10.1016/j.devcel.2009.01.014
64. de Val S. Key transcriptional regulators of early vascular development. *Arterioscler Thromb Vasc Biol* (2011) 31(7):1469–75. doi: 10.1161/ATVBAHA.110.221168
65. Dejana E, Hirschi KK, Simons M. The molecular basis of endothelial cell plasticity. *Nat Commun* (2017) 8:14361. doi: 10.1038/ncomms14361
66. Elcheva I, Brok-Volchanskaya V, Kumar A, Liu P, Lee JH, Tong L, et al. Direct induction of haematoendothelial programs in human pluripotent stem cells by transcriptional regulators. *Nat Commun* (2014) 5:4372. doi: 10.1038/ncomms5372
67. Kanki Y, Nakaki R, Shimamura T, Matsunaga T, Yamamizu K, Katayama S, et al. Dynamically and epigenetically coordinated GATA/ETS/SOX transcription factor expression is indispensable for endothelial cell differentiation. *Nucleic Acids Res* (2017) 45(8):4344–58. doi: 10.1093/nar/gkx159
68. Shah AV, Birdsey GM, Randi AM. Regulation of endothelial homeostasis, vascular development and angiogenesis by the transcription factor ERG. *Vascul Pharmacol* (2016) 86:3–13. doi: 10.1016/j.vph.2016.05.003
69. Shi Y, Inoue H, Wu JC, Yamanaka S. Induced pluripotent stem cell technology: a decade of progress. *Nat Rev Drug Discov* (2017) 16(2):115–30. doi: 10.1038/nrd.2016.245
70. Etienne-Manneville S, Hall A. Rho GTPases in cell biology. *Nature* (2002) 420(6916):629–35. doi: 10.1038/nature01148

71. Wojciak-Stothard B, Ridley AJ. Rho GTPases and the regulation of endothelial permeability. *Vascul Pharmacol* (2002) 39(4-5):187–99. doi: 10.1016/S1537-1891(03)00008-9
72. de Rooij J, Zwartkruis FJ, Verheijen MH, Cool RH, Nijman SM, Wittinghofer A, et al. Epac is a Rap1 guanine-nucleotide-exchange factor directly activated by cyclic AMP. *Nature* (1998) 396(6710):474–7. doi: 10.1038/24884
73. Cullere X, Shaw SK, Andersson L, Hirahashi J, Luscinskas FW, Mayadas TN. Regulation of vascular endothelial barrier function by Epac, a cAMP-activated exchange factor for Rap GTPase. *Blood* (2005) 105(5):1950–5. doi: 10.1182/blood-2004-05-1987
74. Wu Q, Ouyang C, Xie L, Ling Y, Huang T. The ROCK inhibitor, thiazovivin, inhibits human corneal endothelial-to-mesenchymal transition/epithelial-to-mesenchymal transition and increases ionic transporter expression. *Int J Mol Med* (2017) 40(4):1009–18. doi: 10.3892/ijmm.2017.3103
75. Nakagawa T, Li JH, Garcia G, Mu W, Piek E, Böttinger EP, et al. TGF-beta induces proangiogenic and antiangiogenic factors via parallel but distinct Smad pathways. *Kidney Int* (2004) 66(2):605–13. doi: 10.1111/j.1523-1755.2004.00780.x
76. Hogan NT, Whalen MB, Stolze LK, Hadeli NK, Lam MT, Springstead JR, et al. Transcriptional networks specifying homeostatic and inflammatory programs of gene expression in human aortic endothelial cells. *Elife* (2017) 6:e22536. doi: 10.7554/eLife.22536
77. Yamamizu K, Piao Y, Sharov AA, Zsiros V, Yu H, Nakazawa K, et al. Identification of transcription factors for lineage-specific ESC differentiation. *Stem Cell Reports* (2013) 1(6):545–59. doi: 10.1016/j.stemcr.2013.10.006
78. Bohnsack BL, Lai L, Dolle P, Hirschi KK. Signaling hierarchy downstream of retinoic acid that independently regulates vascular remodeling and endothelial cell proliferation. *Genes Dev* (2004) 18(11):1345–58. doi: 10.1101/gad.1184904
79. Lee JY, Mak CP, Wang BJ, Chang WC. Effects of retinoids on endothelial cell proliferation, prostacyclin production and platelet aggregation. *J Dermatol Sci* (1992) 3(3):157–62.
80. Saito A, Sugawara A, Uruno A, Kudo M, Kagechika H, Sato Y, et al. All-trans retinoic acid induces in vitro angiogenesis via retinoic acid receptor: possible involvement of paracrine effects of endogenous vascular endothelial growth factor signaling. *Endocrinology* (2007) 148(3):1412–23. doi: 10.1210/en.2006-0900
81. García-Morales V, Luaces-Regueira M, Campos-Toimil M. The cAMP effectors PKA and epac activate endothelial NO synthase through PI3K/Akt pathway in human endothelial cells. *Biochem Pharmacol* (2017) 145:94–101. doi: 10.1016/j.bcp.2017.09.004
82. Saura M, Zaragoza C, Cao W, Bao C, Rodríguez-Puyol M, Rodríguez-Puyol D, et al. Smad2 mediates transforming growth factor-beta induction of endothelial nitric oxide synthase expression. *Circ Res* (2002) 91(9):806–13. doi: 10.1161/01.RES.0000040397.23817.E5
83. James D, Levine AJ, Besser D, Hemmati-Brivanlou A. TGFbeta/activin/nodal signaling is necessary for the maintenance of pluripotency in human embryonic stem cells. *Development* (2005) 132(6):1273–82. doi: 10.1242/dev.01706
84. Tan F, Qian C, Tang K, Abd-Allah SM, Jing N. Inhibition of transforming growth factor β (TGF-β) signaling can substitute for Oct4 protein in reprogramming and maintain pluripotency. *J Biol Chem* (2015) 290(7):4500–11. doi: 10.1074/jbc.M114.609016
85. Vallier L, Alexander M, Pedersen RA. Activin/Nodal and FGF pathways cooperate to maintain pluripotency of human embryonic stem cells. *J Cell Sci* (2005) 118(Pt 19):4495–509. doi: 10.1242/jcs.02553
86. Inman GJ, Nicolás FJ, Callahan JF, Harling JD, Gaster LM, Reith AD, et al. SB-431542 is a potent and specific inhibitor of transforming growth factor-beta superfamily type I activin receptor-like kinase (ALK) receptors ALK4, ALK5, and ALK7. *Mol Pharmacol* (2002) 62(1):65–74. doi: 10.1124/mol.62.1.65
87. Goumans MJ, Valdimarsdottir G, Itoh S, Lebrin F, Larsson J, Mummery C, et al. Activin receptor-like kinase (ALK)1 is an antagonistic mediator of lateral TGFbeta/ALK5 signaling. *Mol Cell* (2003) 12(4):817–28. doi: 10.1016/S1097-2765(03)00386-1
88. Ginsberg M, James D, Ding BS, Nolan D, Geng F, Butler JM, et al. Efficient direct reprogramming of mature amniotic cells into endothelial cells by ETS factors and TGFβ suppression. *Cell* (2012) 151(3):559–75. doi: 10.1016/j.cell.2012.09.032
89. Chiang PM, Wong PC. Differentiation of an embryonic stem cell to hemogenic endothelium by defined factors: essential role of bone morphogenetic protein 4. *Development* (2011) 138(13):2833–43. doi: 10.1242/dev.061440
90. Nostro MC, Cheng X, Keller GM, Gadue P. Wnt, activin, and BMP signaling regulate distinct stages in the developmental pathway from embryonic stem cells to blood. *Cell Stem Cell* (2008) 2(1):60–71. doi: 10.1016/j.stem.2007.10.011

Conflict of Interest Statement: The authors declare that the research was conducted in the absence of any commercial or financial relationships that could be construed as a potential conflict of interest.

frontiers in Bioengineering and Biotechnology

ORIGINAL RESEARCH
published: 22 January 2018
doi: 10.3389/fbioe.2018.00001

MicroRNA-146a Regulates Perfusion Recovery in Response to Arterial Occlusion *via* Arteriogenesis

*Joshua L. Heuslein[1,2], Stephanie P. McDonnell[2], Ji Song[1], Brian H. Annex[1,2] and Richard J. Price[1,2]**

[1] Department of Biomedical Engineering, University of Virginia, Charlottesville, VA, United States, [2] Robert M. Berne Cardiovascular Research Center, University of Virginia, Charlottesville, VA, United States

The growth of endogenous collateral arteries that bypass arterial occlusion(s), or arteriogenesis, is a fundamental shear stress-induced adaptation with implications for treating peripheral arterial disease. MicroRNAs (miRs) are key regulators of gene expression in response to injury and have strong therapeutic potential. In a previous study, we identified miR-146a as a candidate regulator of vascular remodeling. Here, we tested whether miR-146a regulates *in vitro* angiogenic endothelial cell (EC) behaviors, as well as perfusion recovery, arteriogenesis, and angiogenesis in response to femoral arterial ligation (FAL) *in vivo*. We found miR-146a inhibition impaired EC tube formation and migration *in vitro*. Following FAL, Balb/c mice were treated with a single, intramuscular injection of anti-miR-146a or scramble locked nucleic acid (LNA) oligonucleotides directly into the non-ischemic gracilis muscles. Serial laser Doppler imaging demonstrated that anti-miR-146a treated mice exhibited significantly greater perfusion recovery (a 16% increase) compared mice treated with scramble LNA. Moreover, anti-miR-146a treated mice exhibited a 22% increase in collateral artery diameter compared to controls, while there was no significant effect on *in vivo* angiogenesis or muscle regeneration. Despite exerting no beneficial effects on angiogenesis, the inhibition of mechanosensitive miR-146a enhances perfusion recovery after FAL *via* enhanced arteriogenesis.

Keywords: microRNA, peripheral arterial disease, angiogenesis, arteriogenesis, endothelial cell, shear stress, epigenetics, hindlimb ischemia

OPEN ACCESS

Edited by:
Andrea Banfi,
University of Basel, Switzerland

Reviewed by:
Gaetano Santulli,
Columbia University, United States
Jean-Sébastien Silvestre,
Institut National de la Santé et de la Recherche Médicale, France

****Correspondence:***
Richard J. Price
rprice@virginia.edu

Specialty section:
This article was submitted to Tissue Engineering and Regenerative Medicine, a section of the journal Frontiers in Bioengineering and Biotechnology

Received: *31 October 2017*
Accepted: *03 January 2018*
Published: *22 January 2018*

Citation:
Heuslein JL, McDonnell SP, Song J, Annex BH and Price RJ (2018) MicroRNA-146a Regulates Perfusion Recovery in Response to Arterial Occlusion via Arteriogenesis. Front. Bioeng. Biotechnol. 6:1. doi: 10.3389/fbioe.2018.00001

INTRODUCTION

Peripheral arterial disease (PAD) is caused by blockage(s) of the arteries, in the lower limbs, due to occlusive atherosclerosis (Norgren et al., 2007). There are no medical therapies available to treat PAD and many PAD patients are not amenable to surgical revascularization options or receive little long-term benefit from such surgeries (Annex, 2013). This has led to the rise of new therapeutic strategies that have sought to induce endogenous revascularization *via* stimulation of new capillary growth from preexisting vessels (i.e., angiogenesis) and/or lumen expansion of preexisting arteries (i.e., arteriogenesis) to restore lower limb perfusion. Yet, large-scale therapeutic clinical trials to this end have been largely unsuccessful to date (Seiler et al., 2001; van Royen et al., 2005; Zbinden et al., 2005; Ripa et al., 2006; Subramaniyam et al., 2009). These failures highlight our incomplete understanding of the basic mechanisms of revascularization and underscore the critical need for the continued study of the endogenous regulation of this complex, highly orchestrated process.

MicroRNAs (miRs) have emerged as key regulators of the response to injury including vascular remodeling, comprising of both angiogenesis (Urbich et al., 2008; Neth et al., 2013; Santulli, 2016) and arteriogenesis (Welten et al., 2014; Ganta et al., 2017; Guan et al., 2017). In addition, we reported recently that collateral artery segments exhibit either "moderate" or "amplified" arteriogenesis depending on the hemodynamics to which they are exposed (i.e., non-reversed or reversed flow waveforms, respectively) following femoral arterial ligation (FAL) (Heuslein et al., 2015b). By applying shear stress waveforms biomimetic of these *in vivo* hemodynamics to endothelial cells (ECs) *in vitro*, we identified several mechanosensitive miRs (-100, -199a, and -146a,) as potential negative regulators of arteriogenesis. To this end, inhibition of miR-100 has been shown previously to enhance perfusion recovery following FAL (Grundmann et al., 2011), and we have recently determined that miR-199a inhibition is a potent enhancer of perfusion recovery and arteriogenesis following FAL in Balb/c mice (Heuslein and Price, 2017). Though miR-146a has been shown to be enriched in ECs *in vivo* (Cheng et al., 2013) and to regulate both endothelial activation (Cheng et al., 2013) and *in vitro* angiogenesis (Zhu et al., 2013, 2016; Rau et al., 2014), the role of miR-146a following FAL is unknown. Here, we tested the hypothesis that miR-146a regulates angiogenesis, arteriogenesis, and perfusion recovery after FAL.

MATERIALS AND METHODS

Human Umbilical Vein Endothelial Cell (HUVEC) Culture

Human umbilical vein endothelial cells, purchased from Cell Applications Inc. (San Diego, CA, USA), were thawed and maintained on tissue culture treated flasks in complete endothelial growth medium (Cell Applications). For *in vitro* transfection experiments, HUVECs were transfected at 30 nM for 24 h with miRVana anti-miR-146a (#446084, ThermoFisher Scientific, Waltham, MA, USA) or miR inhibitor negative control (#4464076, ThermoFisher Scientific) using siPORT NeoFX transfection agent (#AM4510, ThermoFisher Scientific) according to the manufacturer's instructions. Twenty-four hours after transfection, cell culture medium was changed. For HUVECs cultured under normal growth condition, culture medium was changed to normal growth medium containing 10% fetal bovine serum (FBS) and cells were incubated for the given experimental time at normoxia conditions (20% O_2). For HUVECs cultured under hypoxia serum starvation (HSS) to simulate ischemia *in vitro*, culture medium was changed to endothelial serum starvation medium (#209-250, Cell Applications) and cells were incubated in a 2% oxygen chamber (BioSpherix, Lacona, NY, USA) for the given experimental duration. For each set of experimental comparisons, cells were used between subculture passages 4 and 7.

Endothelial Matrigel Assay

Following transfection, HUVECs were plated on growth factor reduced Matrigel® (#356231, BD BioSciences, Bedford, MA, USA). A chilled 48-well plate was coated with thawed Matrigel® (200 µL/well) then incubated at 37°C for 30 min to allow gel to form. HUVECs were then plated at 30,000 cells/well and exposed to either normal growth or HSS conditions for 6 h. The 6-h duration was chosen based on similar studies examining formation of capillary-like structures (Hazarika et al., 2013; Rau et al., 2014; Wang et al., 2015). Three fields of view were captured per image using a 4× objective on an Olympus IX50 microscope. Number of loops (i.e., number of meshes or enclosed network of tubes) and number of tubes were quantified using the ImageJ plugin "Angiogenesis Analyzer".

EC Survival

Human umbilical vein endothelial cells were plated at 1×10^4 cells/well in a 96-well plate. Similar to previous studies in our lab (Hazarika et al., 2013; Wang et al., 2015), following transfection, cells were exposed to normal growth conditions (10% FBS, 20% O_2) or HSS conditions for an additional 24 h. During the final 4 h of incubation, tetrazolium salt WST-1/ECS solution (#K301, BioVision, Milpitas, CA, USA) was added to culture medium. At 24 h, cell viability was assessed as the resulting tetrazolium salt cleavage to formazan by mitochondrial dehydrogenases.

EC Permeability

Human umbilical vein endothelial cells were plated and grown until confluent in a 6-well Transwell plate with 0.4-µM pores (#3450, Corning, Tewksbury, MA, USA). Following transfection, HUVECs were cultured in serum-free medium without phenol red and exposed to HSS conditions for an additional 24 h. Rhodamine dextran (1 mg/mL) was added to the HUVEC medium (top Transwell chamber) and HUVECs incubated for an additional 30 min. Following incubation 100 µL samples were drawn from the bottom chamber in triplicate and fluorescence was read at 540ex/615em.

Endothelial Scratch Assay

Human umbilical vein endothelial cells were plated at ~4×10^4 cells/well and grown until confluent. Following transfection, cells were scratched with a p200 pipette tip then washed twice. HUVECs were then cultured in normal growth or HSS conditions for 12 h. Images were captured using a 4× objective on an Olympus IX50 microscope.

Mice

This study was carried out in accordance with the recommendations of the American Heart Association Guidelines for the Use of Animals in Research. The protocol was approved by the Institutional Animal Care and Use Committee at the University of Virginia (Protocol 3814).

Balb/c mice were purchased from Charles River Laboratory (Wilmington, MA, USA). All animals were housed in the animal facilities at the University of Virginia.

FAL Model

We used a previously detailed FAL scheme (Meisner et al., 2012; Heuslein et al., 2015b, 2016, 2017) that produces consistent arteriogenesis in the collateral arteries of the gracilis adductor muscles (Chappell et al., 2008; Distasi et al., 2009; Nickerson et al.,

2009a; Dai and Faber, 2010; Meisner et al., 2013, 2014; Heuslein et al., 2015b, 2016, 2017), along with minimal heterogeneity in the baseline collateral structure with known changes in flow direction from baseline. Male mice, 10–12 weeks of age, were anesthetized (i.p. 120 mg/kg ketamine, 12 mg/kg xylazine, and 0.08 mg/kg atropine), depilated, and prepped for aseptic surgery. On the left leg, an incision was made directly above and along the femoral artery, which was gently dissected from the femoral vein and nerve between the bifurcation of the superior epigastric artery and popliteal artery. Two 6.0 silk sutures were placed immediately distal to the epigastric artery, which served as the origin of the muscular branch artery in all mice, and the artery segment between the two ligatures was then severed with micro dissecting scissors. The surgical site was then closed with 5.0 prolene sutures. A sham surgery, wherein the femoral artery was exposed but not ligated, was performed on the right hindlimb (i.e., on the other leg). Animals received one injection of buprenorphine for analgesia at the time of surgery and a second dose 8–12 h later.

In Vivo miR-146a Antagomir Treatment

Anti-miR-146a-5p (5′-TGGAATTCAGTTCTC-3′) and non-targeting control (5′-ACGTCTATACGCCCA-3′) locked nucleic acid (LNA) oligonucleotides were purchased from Exiqon. Oligonucleotides were reconstituted in sterile TE buffer and stored at 1.2 nmol/μL at −20°C. Prior to use, aliquots of oligonucleotides were thawed and diluted in sterile saline to a final concentration of 0.25 nmol/μL. Immediately following FAL, 7.5 nmol of oligonucleotide was injected into both (ligated and sham-operated) gracilis (thigh) muscles.

Laser Doppler Perfusion Imaging

For monitoring blood flow recovery and post-surgical ischemia, mice were anesthetized *via* 1.5% isoflurane under constant oxygen. Mice were placed in a prone position and the soles of the feet were scanned (PeriCam PSI, PeriMed, Stockholm, Sweden). Mean foot perfusion was used to calculate relative perfusion ratio (ligated/unligated).

Tissue Harvesting for miR and Target Expression

Seven days after FAL, mice were anesthetized (i.p. 120 mg/kg ketamine, 12 mg/kg xylazine, and 0.08 mg/kg atropine) and euthanized *via* an overdose of pentobarbital sodium and phenytoin sodium (Euthasol®, Virbac, Fort Worth, TX, USA). The left ventricle was cannulated with a 23-G catheter (right ventricle was carefully opened to act as a sink for perfusate), and the entire body was perfused with 7 mL of Tris–$CaCl_2$ (0.1 g/L $CaCl_2$) containing 2% heparin, 2 mmol/L adenosine (16404, Fisher Scientific, Pittsburg, PA, USA), and 0.1 mmol/L papaverine (P3510, Sigma-Aldrich, St. Louis, MO, USA) to clear and vasodilate the downstream vasculature at a constant rate of 1.5 mL/min (PHD2000, Harvard Apparatus). Once perfused, we waited 5 min to enable vasodilation. The entire body was then perfused with 14 mL Tris–$CaCl_2$. Both gracilis and gastrocnemius muscles, as well as the liver, spleen, and kidneys were dissected free, placed in RNAlater (Ambion), and stored at −20°C.

RNA Isolation from Tissues and qRT-PCR

Excess RNAlater was removed from tissues. Tissues were then incubated in 450 μL TRIzol reagent for 5 min at room temperature. Tissues were then placed on ice and homogenized using a power homogenizer (Omni International, Kennesaw, GA, USA) in short bursts to avoid overheating. Following homogenization, an additional 550 μL TRIzol reagent was added. Samples were incubated for another 5 min at room temperature to ensure complete lysis. 200 μL of chloroform was added to each sample. Samples were then shaken vigorously for 15 s and incubated for 3 min at room temperature. Following this incubation, samples were centrifuged for 10 min at 12,000 *g* at 4°C. The resulting aqueous layer was carefully removed, place in a new RNA/DNAse-free tube, and an equal volume of 70% ethanol was added to the save aqueous layer. RNA isolation then proceeded using the PureLink total RNA purification system (Life Technologies Inc.) with the on-column DNase protocol (Life Technologies Inc.) according to the manufacturer's instructions. RNA concentration and purity was determined with a NanoDrop spectrophotometer in duplicate.

For miR reverse transcription (Applied Biosystems, #4366596), miR-146a-5p (#000468), miR-539-5p (#001286), and miR-219c-3p (#466357_mat) detection, TaqMan MicroRNA assays (Applied Biosystems) were used. For mRNA reverse transcription, the SuperScript III First Strand Synthesis Super mix (#11752-250), ThermoFisher Scientific was used. TaqMan qPCR primers were used for *Card10* (Mm00459941), *Irak1* (Mm01193538), *Irak2* (Mm01184677), *Smad4* (Mm03023996), and *Nos3* (Mm00435217) qPCR. All quantitative real-time PCRs were done on a BioRad CFX96 detection system using the Bioline SensiMix II Probe Kit (#BIO-83005, Bioline, London, UK). miR expression was normalized to sno-202 (Applied Biosystems, #001232), whereas mRNA expression was normalized to *Hprt* expression (Mm03024075) and the relative expression was determined with the comparative $2^{\Delta\Delta Ct}$ method.

Tissue Harvesting for Whole Mount Vascular Casting and Cross-sectional Analysis

For analysis of lumen diameters in the gracilis collateral arteries and to enable sectioning at specific regions, vascular casting was performed using an opaque polymer that allows for accurate lumen diameter measurements (Distasi et al., 2009). Twenty-one days after FAL, mice were anesthetized (i.p. 120 mg/kg ketamine, 12 mg/kg xylazine, and 0.08 mg/kg atropine), euthanized *via* an overdose of pentobarbital sodium and phenytoin sodium (Euthasol®), and then the abdominal aorta was cannulated. The lower body was then perfused with 7 mL of 2% heparinized saline with 2 mmol/L adenosine (16404, Fisher Scientific) and 0.1 mmol/L papaverine (P3510, Sigma-Aldrich) to clear and vasodilate the downstream vasculature at a constant rate of 1 mL/min (PHD2000, Harvard Apparatus). Once perfused, we waited 5 min to enable vasodilation. Tissues were then perfused with 3 mL of 4% paraformaldehyde solution (19943, Affymetrix, Cleveland, OH, USA) at 1 mL/min and allowed to fix for 10 min. The lower body was then perfused with 0.8 mL Microfil® casting

agent (FlowTech, Inc., Carver, MA, USA) at a constant speed of 0.15 mL/min. The viscosity of Microfil® was adjusted to minimize transport across capillaries. After curing for 1.5 h at room temperature, gracilis muscles were dissected free and then cleared in 50% glycerol in phosphate-buffered saline overnight. Cleared tissues were mounted between two coverslips using 500-μm thick spacers (645501, Grace Bio-Labs Inc.) to keep constant thickness between muscles. Muscles were imaged using transmitted light at 4× magnification on a Nikon TE200 inverted microscope with a CCD camera (Quantifier, Optronics Inc.). Individual fields of view were montaged together (Photoshop CS2, Adobe Systems Inc.).

For analysis of lumen diameters from intact gracilis collateral whole mounts (i.e., vascular casting), collateral entrance regions were defined according to the following method. A cropped portion (560 μm × 560 μm) of the montaged image (previously randomized and de-identified) was taken of the collateral artery at the first visible branch point of a terminal arteriole from the primary collateral as it extended from either the muscular branch or saphenous artery as previously described (Heuslein et al., 2015b, 2016). After each cropped image region was taken, all images were randomized and de-identified. The mean diameter was then taken from 4 to 5 separate diameter measurements along the length of the cropped portion of the collateral artery. Mean collateral artery diameter was taken as the average of both the muscular and saphenous regions for a given mouse.

After imaging, muscles were rehydrated, cut, and paraffin embedded for cross-sectional analysis at the muscular branch and saphenous artery entrance regions to the collateral arteries. Resulting cross-sections were rehydrated and H&E stained for collateral artery structure analysis (day 21 post-FAL).

Cross-sectional Analysis of Collateral Artery Structure

Sections (5-μm thickness) of paraffin embedded muscle from the muscular and saphenous regions were labeled for H&E. Individual fields of view encompassing the collateral vessels were imaged with a 40× water objective on a Zeiss inverted microscope (Zeiss Axioskop, Thornwood, NY, USA) with a CCD camera (Quantifier, Optronics Inc.). All images were randomized and de-identified before analysis. Lumen diameter, wall area, and wall thickness were determined using Fiji (Schindelin et al., 2012).

Cross-sectional Analysis for Gastrocnemius Capillary Density

Sections (5-μm thickness) of paraffin embedded gastrocnemius muscles were deparaffinized, rehydrated, and blocked in Carbofree blocking solution (1:10, Vector Labs). Slides were then incubated with fluorophore conjugated primary antibody (isolectin-IB4-AlexFluor-647, 1:200, Life Technologies Inc.) overnight at 4°C. Nuclei were counterstained with Sytox green (500 μM, Life Technologies Inc.). Slides were washed and sealed with Prolong Gold (Life Technologies Inc.) to minimize photobleaching. Individual fields of view were imaged with a Nikon TE2000 C1 laser scanning confocal microscope with a 10× objective and the same imaging parameters for all fields of view. Fields of view were then montaged together using Fiji (Schindelin et al., 2012). Muscle areas were manually outlined and classified as either viable or non-viable tissue. The number of capillaries (Isolectin-B4$^+$ vessels < 25 μm^2 in diameter) and muscle area (identified from autofluorescence) were determined in each montaged image view using a semi-automated Fiji image analysis.

Cross-sectional Analysis for Gastrocnemius Muscle Morphology

Sections (5-μm thickness) of paraffin embedded muscle from the gastrocnemius muscle were H&E labeled. Individual fields of view were imaged with a 10× objective on a Zeiss inverted microscope (Zeiss Axioskop) with a CCD camera (Quantifier, Optronics Inc.). Individual fields of view were montaged together (Photoshop CS2, Adobe Systems Inc.). All montaged images were randomized and de-identified before analysis. Muscle areas were manually outlined using Fiji (Schindelin et al., 2012). Tissue composition was classified into viable and non-viable, which were defined as:

1. Viable: fibers are present and have centrally located nuclei (regenerating) or fibers are comparable in size, organization, and structure to unligated control with peripheral nuclei (mature) (Meisner et al., 2014).
2. Non-viable: fibers lack nuclei, are rounded and dilated in appearance, have weak eosinophilic cytoplasm (necrotic) or where there is minimal presence of myoblasts and is dominated by fibrous matrix and adipose tissue (fibro-adipose) (Meisner et al., 2014).

Statistical Analyses

All results are reported as mean ± SEM, unless otherwise noted. All data were first tested for normality and equal variance. Statistical significance was then assessed by a Student's *t*-test or a two-way ANOVA followed by a Holm–Sidak multiple comparisons test. Data not following a normal distribution were tested for statistical significance by a Mann–Whitney *U*-test (GraphPad Prism 7.0). Significance was assessed at $p < 0.05$.

RESULTS

miR-146a Inhibition Impairs Endothelial Tube Formation and Migration *In Vitro*

To first determine the effect of miR-146a inhibition on endothelial function, we investigated whether knockdown of miR-146a affected EC capillary-like tube formation, migration, survival, or permeability. HUVECs were transfected with 30 nM anti-miR-146a or scramble controls for 24 h before initiating the assay. Formation of capillary-like tube structures was assessed after 6 h of exposure to either normal growth (20% O_2 and 10% FBS) or HSS (2% O_2) conditions. ECs transfected with anti-miR-146a exhibited a significantly decreased number of EC loops and a trend toward decreased number of tubes compared to scramble in both growth and HSS conditions, suggesting an impact on EC network formation and motility (**Figures 1A,B**). This coincided with impaired

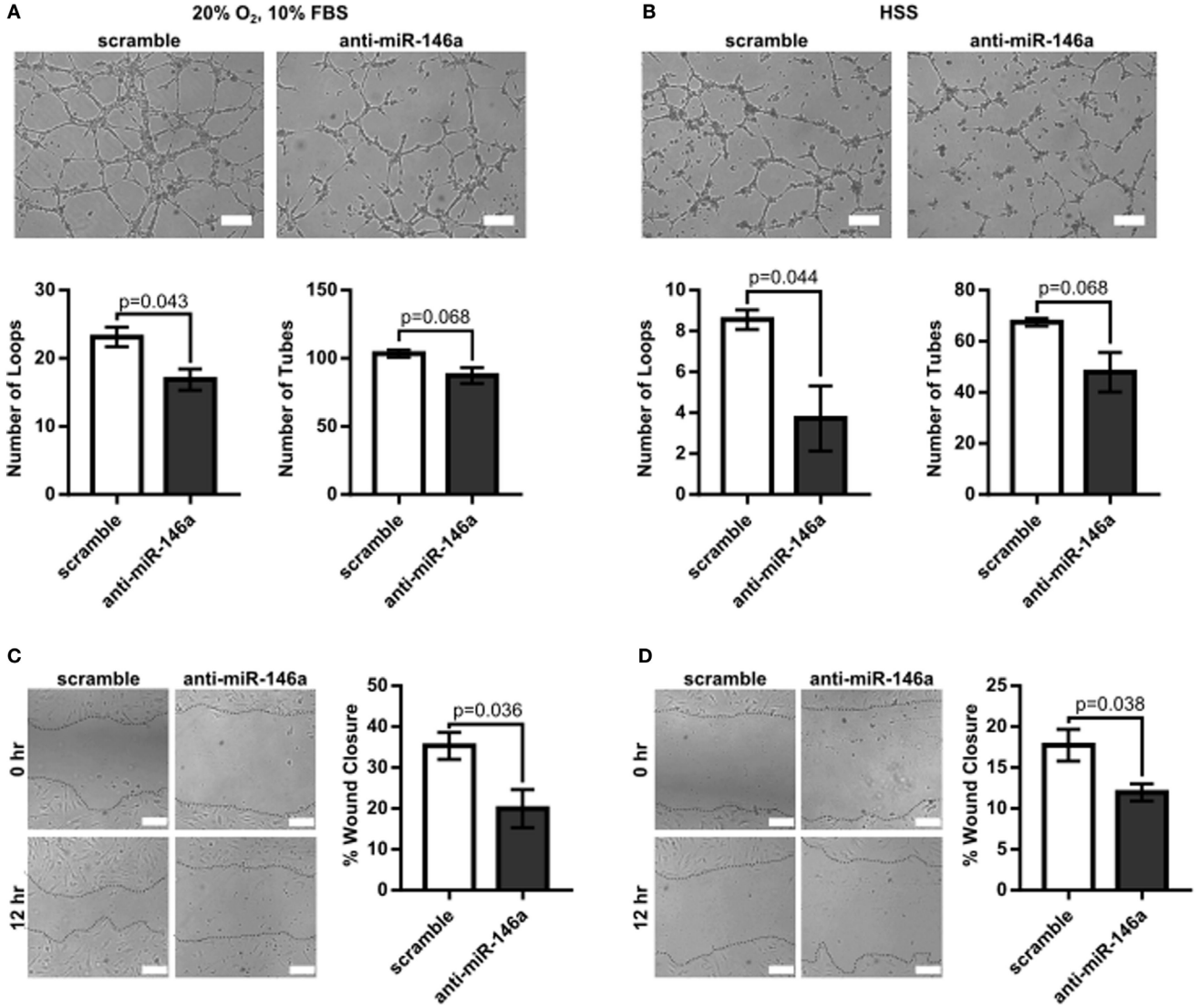

FIGURE 1 | Impaired endothelial tube formation and migration with microRNA (miR)-146a knockdown *in vitro*. **(A,B)** Tube formation of human umbilical vein endothelial cells (HUVECs) transfected with 30 nM scramble or anti-miR-146a oligonucleotides after 6 h of exposure to growth [20% O_2, 10% fetal bovine serum (FBS)] or hypoxia serum starvation (HSS) conditions ($n = 3$). **(C,D)** Endothelial wound closure in HUVECs after 12 h of exposure to either growth [**(C)**, $n = 4$] or HSS [**(D)**, $n = 4$] conditions. Student's *t*-test. Data are mean ± SEM.

EC migration with knockdown of miR-146a, as determined by an endothelial scratch assay, again in both normoxic growth (**Figure 1C**) and HSS (**Figure 1D**) conditions. There were no significant differences in EC survival or EC permeability between scramble and anti-miR-146a treated cells (**Figure 2**).

Perfusion Recovery following FAL Is Improved by miR-146a Inhibition in Balb/c Mice

Next, to test the hypothesis that miR-146a regulates perfusion recovery *in vivo*, we performed FALs on Balb/c mice immediately followed by intramuscular injection of scramble control or anti-miR-146a LNA oligonucleotides directly into each gracilis (i.e., thigh) muscle. We first assessed the efficacy of anti-miR-146a delivery. Local intramuscular injection substantially decreased miR-146a expression (>10-fold) in the gracilis muscle of the ligated limb 7 days post-FAL (**Figure 3A**). Interestingly, despite an intramuscular injection, anti-miR-146a treatment knocked down miR-146a expression in several other tissues including the gastrocnemius muscle ($p < 0.001$), spleen ($p < 0.013$), and liver ($p = 0.06$) (**Figure 3A**). Of note, miR-146a-5p differs in mature sequence from miR-146b-5p by only two nucleotides at their 3′ ends and they share identical seed sequences. We found that while miR-146a primers were specific (no cross-reactivity with miR-146b), miR-146b primers cross-reacted with miR-146a. As such, we could confidently determine miR-146a expression but could not confidently detect miR-146b due to

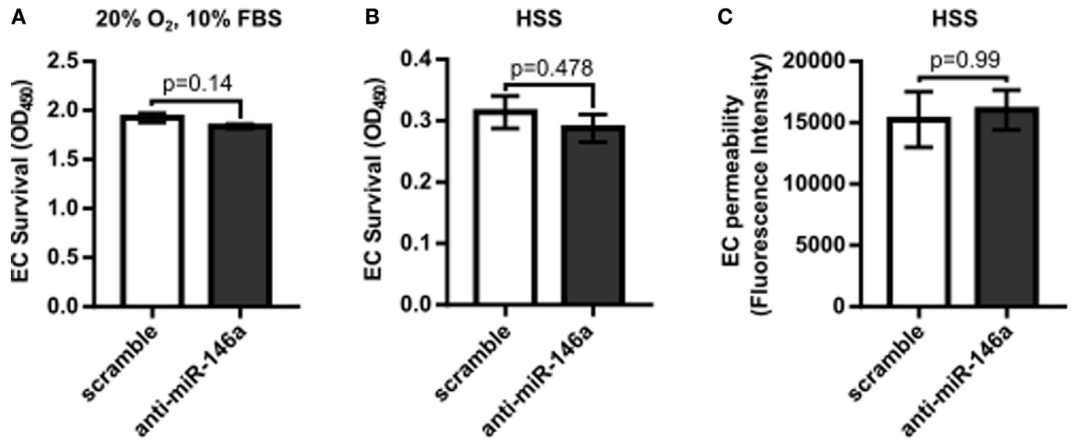

FIGURE 2 | No significant effect on endothelial cell (EC) survival or permeability with microRNA (miR)-146a inhibition *in vitro*. **(A,B)** Twenty-four hours after transfection with 30 nM scramble or anti-miR-146a oligonucleotides, human umbilical vein endothelial cells (HUVECs) were exposed to 24 h of either growth [normoxia, 10% fetal bovine serum (FBS)] or hypoxia serum starvation (HSS) conditions. During the final 4 h, the tetrazolium salt WST-1 was added to the medium. Resulting salt cleavage to formazan by mitochondrial dehydrogenases was used as an indicator of cell viability ($n = 4$). Student's *t*-test. **(C)** Transwell inserts (0.4 μm) were used to assess EC permeability *via* rhodamine dextran (70 kDa), after 24 h of HSS exposure in HUVECs transfected with scramble or anti-miR-146a oligonucleotides ($n = 3$). Mann–Whitney *U*-test. Data are mean ± SEM.

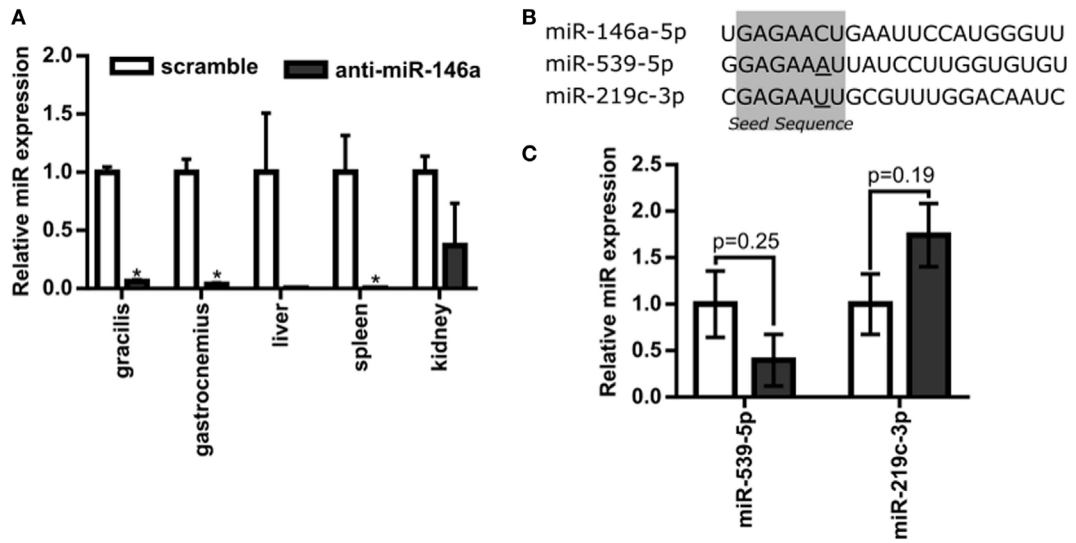

FIGURE 3 | Systemic delivery of anti-microRNA (miR)-146a-5p with single intramuscular injection. **(A)** Relative miR-146a-5p expression in the gracilis and gastrocnemius muscles of ligated limbs as well as the liver, spleen, and kidney 7 days post-femoral arterial ligation (FAL) in Balb/c mice. Mice were treated with a single i.m. injection of 7.5 nmol scramble ($n = 3$) or anti-miR-146a ($n = 4$) locked nucleic acid oligonucleotides immediately post-FAL. *$p < 0.05$, Student's *t*-test except kidney samples which were Mann–Whitney *U*-test. **(B)** Sequence of miR-146a-5p and two additional miRNAs with similar seed sequences, miR-539-5p and miR-219c-3p. Seed sequence is highlighted in gray with nucleotides altered from miR-146a-5p sequence underlined. **(C)** Expression of miR-539-5p and miR-219c-3p in gastrocnemius of ligated limb 7 days post-FAL ($n = 3$–4 for scramble and anti-miR-146a treated mice, respectively). Student's *t*-test. Data are mean ± SEM.

this cross-reactivity. We therefore chose to determine the specificity of anti-miR-146a treatment by assessing the expression of two other miRs (miR-539-5p and miR-219c-3p) that differ in seed sequence from miR-146a-5p by only one nucleotide (**Figure 3B**). Expression of each of these miRs was not significantly altered by anti-miR-146a treatment (**Figure 3C**). We also assessed mRNA expression of several genes previously shown to be direct miR146a targets, including *Card10* (Rau et al., 2014), *Irak1* (Taganov et al., 2006), *Irak2* (Hou et al., 2009), and *Sirt4* to confirm functional knockdown of miR-146a. While it should be noted that these are at the transcript level, anti-miR-146a treatment increased expression of Irak2 as well as decreased eNOS (*Nos3*) mRNA expression, which has been previously shown to be indirectly regulated by miR-146a (Cheng et al., 2013), in the gastrocnemius muscle of anti-miR-146a treated mice (**Figure 4**).

To next assess functional outcomes of anti-miR-146a treatment, we performed FALs and delivered anti-miR-146a or scramble control in a separate cohort of Balb/c mice followed by serial laser Doppler perfusion imaging. Laser Doppler measurements of the plantar surface of the foot indicated moderate ischemia immediately post-FAL, followed by an incomplete perfusion recovery in the scramble-treated control mice. However, anti-miR-146a treated mice exhibited an improved perfusion recovery compared to scramble as early as day 10 post-FAL. By day 21 post-FAL, anti-miR-146a treated mice demonstrated a 16% increase in perfusion recovery vs. scramble-treated controls (**Figures 5A,B**).

miR-146a Inhibition Does Not Regulate Capillary Density following FAL in Balb/c Mice

To determine the mechanism of increased perfusion recovery with anti-miR-146a treatment, we first examined if miR-146a inhibition altered capillary density in the gastrocnemius muscle following FAL. Gastrocnemius muscle cross-sections were labeled using SYTOX green as a nuclear marker and isolectin-B4 as an EC marker. Muscle area autofluorescence was used to determine muscle area (**Figures 6A,B**). We found that there was no significant difference in capillary density determined by percentage of isolectin-B4-positive area per muscle area between anti-miR-146a and scramble-treated mice (**Figure 6C**).

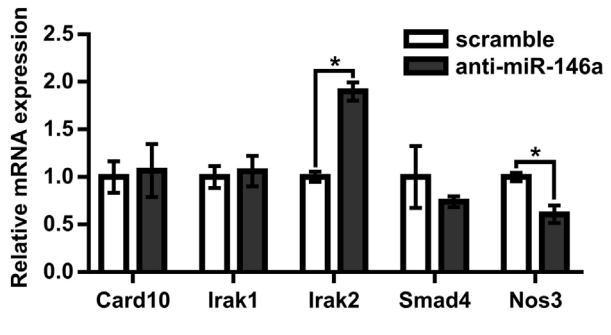

FIGURE 4 | MicroRNA (miR)-146a regulates Irak2 and eNOS expression in ischemic gastrocnemius muscle. Relative mRNA expression of miR-146a targets in gastrocnemius muscle of ligated limb 7 days post-femoral arterial ligation in mice treated with scramble ($n = 3$) or anti-miR-146a ($n = 4$) oligonucleotide. *$p < 0.05$, Student's *t*-test. Data are mean ± SEM.

miR-146a Inhibition Enhances Arteriogenesis following FAL

We next examined whether miR-146a inhibition affected arteriogenesis by measuring luminal diameter growth of gracilis collateral arteries 21 days post-FAL (**Figure 7A**). Both control and anti-miR-146a treated mice experienced significant ($p < 0.001$) arteriogenesis in the ligated limb compared to sham-operated (unligated) controls. However, arteriogenesis was further enhanced with miR-146a inhibition, as collateral artery diameter was 22% greater than in controls (**Figures 7A,B**). Furthermore, cross-sectional analysis of these collateral arteries was used to determine vessel wall area, demonstrating increased wall area in anti-miR-146a treated mice compared to control (**Figures 7C,D**). As we have previously shown that the extent of arteriogenesis varies depending on the flow waveform following FAL (Heuslein et al., 2015b), we analyzed both the muscular (non-reversed flow) and saphenous (reversed flow) collateral segments to determine if miR-146a inhibition led to differences in regional growth. Anti-miR-146a treated mice exhibited a ~35% increase in lumen diameter in muscular (non-reversed flow) segments compared to controls while there was no significant difference in saphenous (reversed flow) segments (**Figures 8A–C**). Wall area was also significantly greater in muscular (non-reversed flow) segments in anti-miR-146a treated mice while there was no significant difference in saphenous (reversed flow) regions compared to controls (**Figures 8D,E**). Finally, we examined the effect of altered

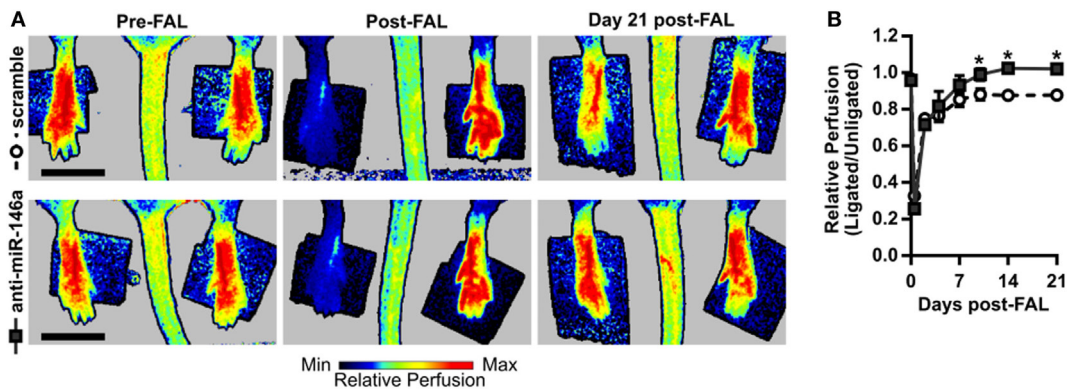

FIGURE 5 | Improved perfusion recovery following femoral arterial ligation (FAL) in Balb/c mice with inhibition of microRNA (miR)-146a. **(A)** Representative images and **(B)** quantification of relative foot perfusion determined by laser Doppler perfusion imaging of mice treated with a single i.m. injection of 7.5 nmol scramble control ($n = 6$) or anti-miR-146a ($n = 4$) LNA oligonucleotides immediately post-FAL. *$p < 0.05$, two-way ANOVA with repeated measures followed by a Holm–Sidak multiple comparisons test. Data are mean ± SEM.

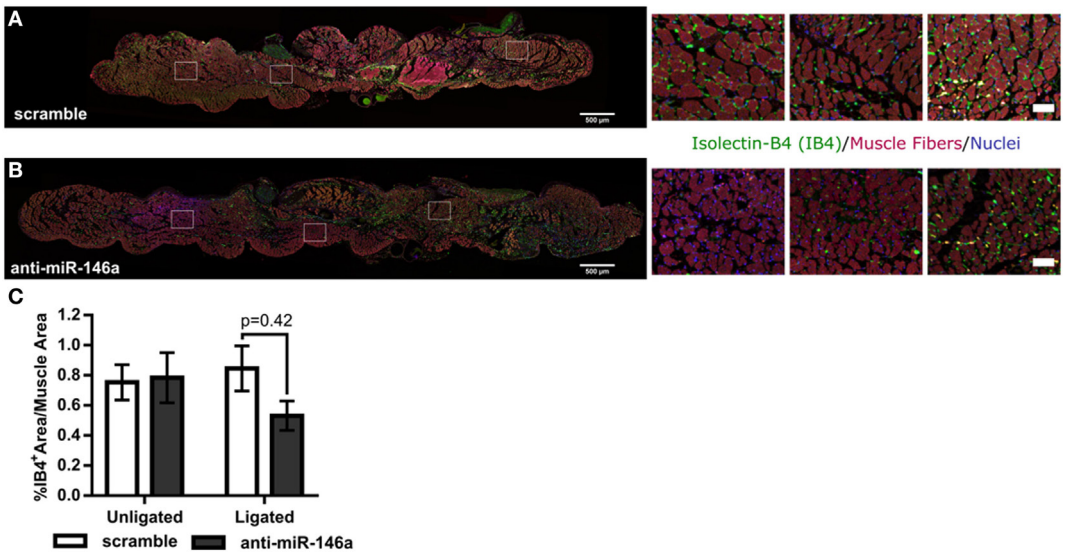

FIGURE 6 | MicroRNA (miR)-146a inhibition does not improve capillary density following femoral arterial ligation (FAL) in Balb/c mice. **(A,B)** Representative images of gastrocnemius muscle labeled for capillaries (isolectin-b4, green), muscle fibers (autofluorescence, red), and nuclei (SYTOX, blue) from ligated limbs 21 days post-FAL. Scale bar = 500 μm. Insets highlight heterogeneous capillary density in viable muscle of anti-miR-146a treated mice. Scale bar = 50 μm. **(C)** Bar graph of percent isolectin-b4 (IB4) positive area per muscle fiber area over entire muscle in ligated and unligated gastrocnemius muscles 21 days post-FAL. $n = 5$ for scramble and $n = 4$ for anti-miR-146a groups.

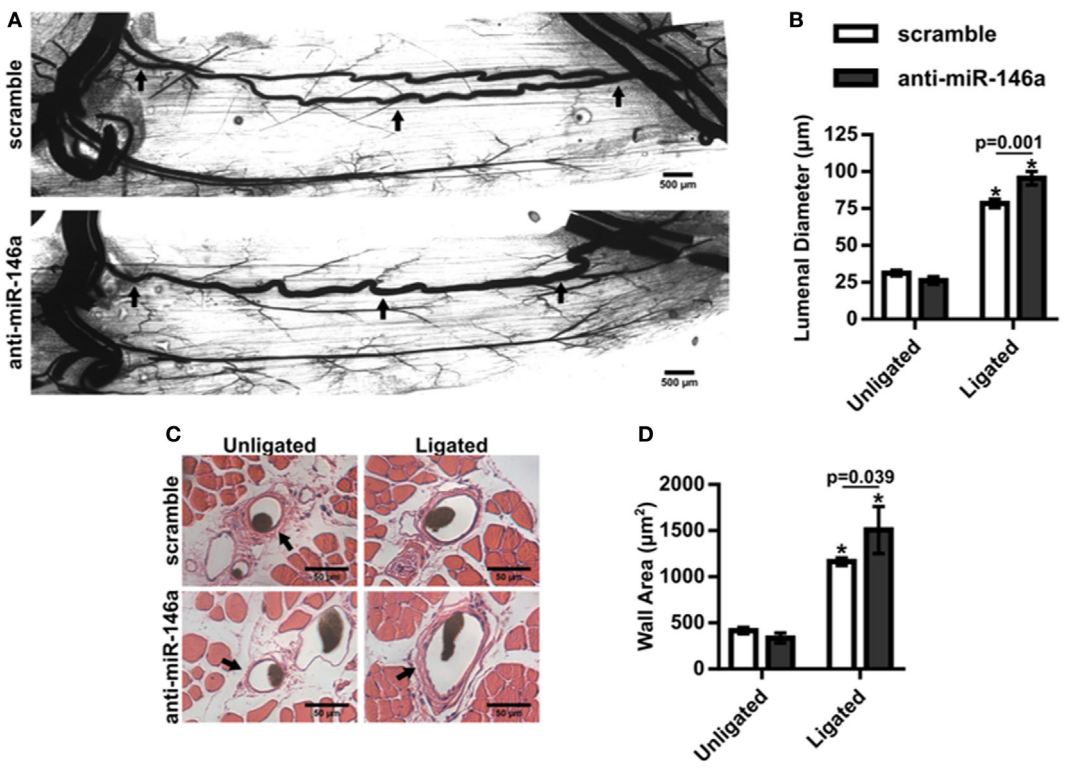

FIGURE 7 | Inhibition of microRNA (miR)-146a enhances collateral artery growth following femoral arterial ligation (FAL). **(A)** Representative whole mount vascular cast images of gracilis collateral arteries 21 days post-FAL in scramble (top) or anti-miR-146a (bottom) treated Balb/c mice. Scale bar = 500 μm. **(B)** Bar graph of mean lumenal diameter along collateral artery length for ligated and unligated limbs of anti-miR-146a ($n = 4$) and scramble-treated mice ($n = 6$). *$p < 0.001$ vs. unligated, two-way ANOVA followed by Holm–Sidak test for multiple comparisons. **(C)** Representative H&E stained cross-sections of collateral arteries from ligated and unligated limbs. Scale bar = 50 μm. **(D)** Bar graph of wall area from H&E stained cross-sections ($n = 4$ or 6 for anti-miR-146a and scramble-treated mice, respectively). *$p < 0.05$ vs. unligated, two-way ANOVA followed by Holm–Sidak test for multiple comparisons. Arrows in **(A,C)** indicate primary collateral artery. Data are mean ± SEM.

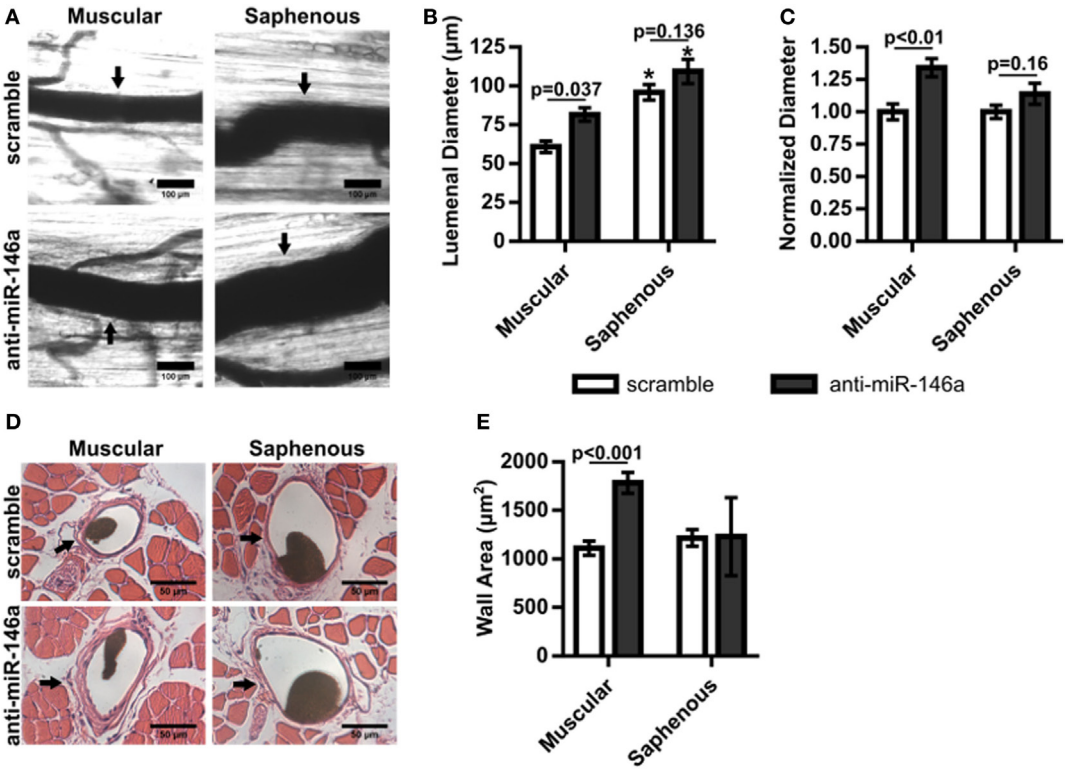

FIGURE 8 | Regional analysis of gracilis collateral arteries. **(A)** Representative vascular cast images from muscular and saphenous collateral artery segments 21 days post-femoral arterial ligation (FAL) in scramble and anti-microRNA (miR)-146a treated Balb/c mice. **(B)** Bar graph of lumenal diameter post-FAL from ligated limb of mice treated with non-targeting control in each region (n = 4 or 6 for anti-miR-146a and control-treated mice, respectively). *$p < 0.05$ vs. muscular region for a given treatment, two-way ANOVA followed by Holm–Sidak test for multiple comparisons. **(C)** Lumenal diameters normalized to the ligated limb of mice treated with scramble in each region (n = 4 or 6 for anti-miR-146a and control-treated mice, respectively). Student's t-test. **(D)** Representative H&E stained cross-sections from muscular and saphenous collateral artery segments 21 days post-FAL. **(E)** Bar graph of wall area from H&E stained cross-sections (n = 4 or 6 for anti-miR-146a and scramble-treated mice, respectively). Two-way ANOVA followed by Holm–Sidak test for multiple comparisons. Arrows indicate the primary collateral artery in **(A,D)**. Data are mean ± SEM.

miR-146a expression on the composition of ischemic muscle tissue downstream of the femoral artery occlusion. Gastrocnemius muscle tissue was categorized as viable (mature and regenerating fibers) or non-viable (necrotic and fibro-adipose tissue) by histological analysis 21 days after FAL (**Figure 9**). There was no significant difference ($p = 0.21$) in muscle composition (i.e., increased viable tissue) between scramble and anti-miR-146a treated mice.

DISCUSSION

In this study, we sought to determine if miR-146a regulates angiogenesis, arteriogenesis, and perfusion recovery following FAL. We first assessed its role in endothelial function and angiogenesis *in vitro* by inhibiting miR-146a in HUVECs and assessing capillary-like tube formation, migration, survival, and permeability. Knockdown of miR-146a attenuated both network-like formation and EC migration while there was no effect on EC survival or permeability. These data would suggest that miR-146a would have no beneficial effect on angiogenesis. To next determine the role of miR-146a *in vivo*, we delivered a single, intramuscular injection of anti-miR-146a LNA oligonucleotides immediately following FAL in Balb/c mice and assessed perfusion recovery, angiogenesis, and arteriogenesis. While control-treated mice exhibited impaired perfusion recovery, miR-146a inhibition elicited a significantly improved recovery. Interestingly, miR-146a inhibition did not significantly affect capillary density or gastrocnemius muscle composition. However, anti-miR-146a was able to significantly enhance collateral artery growth. Together, our results indicate that miR-146a regulates perfusion recovery *via* arteriogenesis without a significant impact on angiogenesis.

Given our previous results in which miR-146a expression was decreased in ECs exposed to an "amplified arteriogenesis" flow waveform, we would have hypothesized that miR-146a inhibition would lead to enhanced collateral artery growth and thus enhanced perfusion recovery (Heuslein and Price, 2017). However, the role of miR-146a in angiogenesis was less clear. One previous report found that inhibition of miR-146a led to increased capillary sprouting in both aortic ring and laser-induced choroidal neovascularization assays (Halkein et al., 2013). In contrast, several previous studies have found that loss of miR-146a impairs angiogenesis *in vitro* (Zhu et al., 2013, 2016; Rau et al., 2014; Li

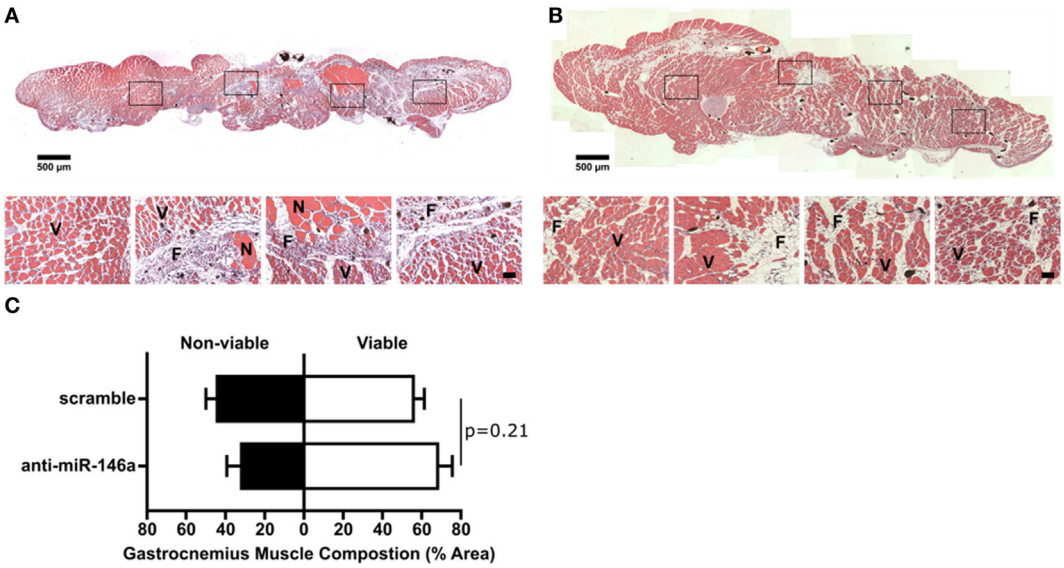

FIGURE 9 | Effect of single dose of anti-microRNA (miR)-146a to gracilis muscle on gastrocnemius muscle composition. **(A,B)** Representative images of H&E staining of gastrocnemius muscle for ligated limb of Balb/c mice treated with scramble **(A)** or anti-miR-146a **(B)** locked nucleic acid oligonucleotide immediately after femoral arterial ligation (FAL) (scale bar = 500 μm, inset scale bar = 50 μm). V, viable muscle; N, necrotic tissue; F, fibro-adipose tissue. **(C)** Bar graph of the percentage of gastrocnemius muscle that is viable (white) or non-viable (black) at day 21 post-FAL in each group (n = 4–5 for anti-miR-146a and scramble groups, respectively). Student's t-test. Data are mean ± SEM.

et al., 2017), which would suggest miR-146a inhibition should impair perfusion recovery. In our hands, *in vitro* miR-146a inhibition attenuated both network-like formation and EC migration while there was no effect on EC survival or permeability. Of note, our assessments of EC function *in vitro* were performed at single time points based on similar studies (Hazarika et al., 2013; Zhu et al., 2013; Rau et al., 2014; Wang et al., 2015). Thus, they do not capture the dynamics of anti-miR-146a treatment. Despite this potential limitation, our *in vitro* results are consistent with later studies wherein miR-146a inhibition attenuated angiogenesis and EC migration *in vitro* (Zhu et al., 2013, 2016; Rau et al., 2014; Li et al., 2017).

We then moved to test the effect of miR-146a inhibition *in vivo* following FAL. Despite the impaired angiogenesis we observed *in vitro*, miR-146a inhibition led to a significantly enhanced perfusion recovery in Balb/c mice *in vivo*. Perfusion recovery following FAL can be dependent on angiogenesis (Meisner et al., 2013), tissue clearance and skeletal muscle regeneration (Meisner et al., 2014), and/or arteriogenesis. To this end, we found no significant difference in capillary density in the gastrocnemius muscle of FAL-operated limbs between anti-miR-146a and scramble-treated mice with a possible trend toward decreased capillary density in anti-miR-146a treated mice. This corresponded to decreased gastrocnemius eNOS expression in FAL-operated limbs (**Figure 4**), which was previously shown to be an indirect target of miR-146a (Cheng et al., 2013), though this was only assessed at the mRNA level whereas phosphorylated eNOS is the main effector of eNOS function. Moreover, there was no significant difference in gastrocnemius muscle composition between anti-miR-146a and scramble control-treated mice. However, mice treated with anti-miR-146a exhibited significantly enhanced collateral artery growth, corresponding to the observed increase in foot perfusion in these mice. Our *in vivo* results indicate that miR-146a regulates perfusion recovery *via* arteriogenesis without a significant impact on angiogenesis.

The lack of observed angiogenesis and muscle regeneration may have several alternative explanations. In this study, capillary density was only examined at day 21. While earlier time points would capture dynamic differences in capillary density between the groups, we chose day 21 as a better representation of the more clinically relevant, steady-state condition. In addition, while anti-miR-146a delivery appeared to systemically inhibit miR-146a expression, angiogenesis is driven by ischemia in the downstream gastrocnemius (i.e., calf) muscle and is a later response to FAL than arteriogenesis. It is therefore possible that a different anti-miR-146a dosing regimen (e.g., timing, amount, number of injections, etc.) may be required to directly induce angiogenesis in addition to arteriogenesis. Furthermore, angiogenesis can also be indirectly induced if the increased blood flow due to arteriogenesis is sufficient to stimulate capillary sprouting. The relatively modest increase in perfusion with anti-miR-146a may not be sufficient to induce additional angiogenesis in this mildly ischemic ligation scheme as opposed to other ligation/excision surgical models which induce significantly greater ischemia in the gastrocnemius. Finally, miR-146a mediated inflammation may lead to different outcomes for arteriogenic and angiogenic processes (i.e., anti-miR-146a be pro-arteriogenic while having no or anti-angiogenic effects in the ischemic gastrocnemius).

MicroRNA-146a's known role as a critical negative regulator of inflammation may help explain its effect on arteriogenesis. In the presence of an inflammatory stimulus (i.e., IL-1β), miR-146a inhibition increases NFκB activity, adhesion molecule (i.e., ICAM-1, VCAM-1) expression, and monocyte adhesion to ECs, whereas miR-146a overexpression blunts EC activation (Cheng et al., 2013). We previously demonstrated a similar phenotype in ECs exposed to pro-arteriogenesis flow waveforms. ECs exposed to a reversed flow ("amplified arteriogenesis") waveform exhibit decreased miR-146a expression as well as increased NFκB activity, ICAM-1 expression, and monocyte adhesion, whereas EC activation is attenuated when exposed to a non-reversed ("moderate arteriogenesis") flow waveform (Heuslein et al., 2015b). Importantly, NFκB signaling is well known to be necessary for arteriogenesis (Tirziu et al., 2012; Sweet et al., 2013) through ICAM-1 (Lan et al., 1994; Nagel et al., 1994) dependent monocyte/macrophage recruitment (Hoefer et al., 2004). Our results are, therefore, consistent with the hypothesis that miR-146a inhibition leads to enhanced arteriogenesis, predominantly in non-reversed flow (i.e., muscular) collateral segments, *via* upregulation of pro-inflammatory (i.e., NFκB) EC activation.

In addition to ECs, miR-146a is also a well-known regulator of inflammatory signaling in leukocytes (Taganov et al., 2006; Boldin et al., 2011; Zhao et al., 2011; Etzrodt et al., 2012). A previous study demonstrated that miR-146a selectively controlled the amplitude of the Ly6C^{hi} monocyte response during an inflammatory challenge. To this end, loss of miR-146a increased Ly6C^{hi} monocyte proliferation and migration, whereas it did not affect Ly6C^{lo} monocytes (Etzrodt et al., 2012). Following FAL, inflammatory monocytes (Ly6C^{hi}/CX3CR1^{lo}/CCR2^{hi}) are recruited to sites of active inflammation, leading to a perivascular accumulation of monocytes/macrophages that is critical for arteriogenesis (Ito et al., 1997; Heil et al., 2004; Shireman, 2007; Capoccia et al., 2008; Nickerson et al., 2009b; Meisner and Price, 2010; Troidl et al., 2013). Our anti-miR-146a intramuscular injections do result in a systemic knockdown of miR-146a and are not cell-specific. It is, therefore, possible that the observed anti-miR-146a mediated enhancement in arteriogenesis is also mediated *via* pericollateral Ly6C^{hi} monocyte proliferation and/or migration.

MicroRNA-146a inhibition is able to stimulate arteriogenesis and improve perfusion recovery; however, given its inability to stimulate angiogenesis and muscle regeneration, its utility as a clinical therapeutic is unclear. Indeed, while it is important to restore the driving pressure to the distal tissue *via* lumen expansion of collateral arteries bypassing the occlusion(s) (i.e., arteriogenesis) in PAD patients (Meisner et al., 2013, 2014; Heuslein et al., 2015a), it is also imperative to stimulate angiogenesis, as capillary density is reduced in these patients (Duscha et al., 2011; Robbins et al., 2011; Annex, 2013). To this end, improved functional outcomes induced by supervised exercise in PAD patients with intermittent claudication are preceded by and correlated with improvement in capillary density within ischemic muscle (Duscha et al., 2011; Robbins et al., 2011). Therapies that utilize a combination of microvascular expansion (i.e., angiogenesis) and restoration of large vessel flow (i.e., stenting, arteriogenesis) are more likely to be an "optimal" treatment (Heuslein et al., 2015a). Further supporting this hypothesis, the ERASE trial found that a combination therapy of revascularization and exercise improved functional outcomes of PAD patients compared to just exercise alone (Fakhry et al., 2015). Overexpression of miR-93 (Ganta et al., 2017) or miR-199a inhibition (Heuslein et al., 2017) have both been shown to be capable of inducing arteriogenesis and improving in the ischemic downstream tissue, demonstrating such miR-based approaches are indeed possible.

In addition, miR-146 inhibition may not be an ideal therapeutic as it could elicit the so-called "Janus phenomenon," wherein pro-arteriogenic therapies also promote atherosclerosis (Epstein et al., 2004). To this end, one study found elevated miR-146a to be atheroprotective, as systemic delivery of miR-146a mimics in Apoe$^{-/-}$Ldlr$^{-/-}$ and Ldlr$^{-/-}$ mice attenuated monocyte/macrophage activation and atherosclerosis (Li et al., 2015). Furthermore, local delivery of anti-miR-146a increased neointimal formation following carotid artery injury in the mouse (Chen et al., 2015). However, miR-146a inhibition may have differential effects on plaque formation depending on the specific cell type. Deletion of endogenous miR-146a within BM-derived cells reduced atherosclerotic plaque formation, whereas miR-146a deletion in the vasculature enhanced EC activation and atherogenesis (Cheng et al., 2017). Future work could determine the cell-specific effect of miR-146a inhibition on arteriogenesis, perfusion recovery, and atherosclerotic plaque stability in an experimental model of PAD with advance atherosclerosis.

ETHICS STATEMENT

This study was carried out in accordance with the recommendations of the American Heart Association Guidelines for the Use of Animals in Research. The protocol was approved by the Institutional Animal Care and Use Committee at the University of Virginia (Protocol 3814).

AUTHOR CONTRIBUTIONS

JH designed and conducted the experiments, analyzed data, and wrote the manuscript. SM and JS helped conduct the experiments and analyze the data. BA and RP supervised the overall study and analyzed data. All authors read and edited the manuscript.

ACKNOWLEDGMENTS

The authors would like to thank the University of Virginia Research Histology Core (under the direction of Sheri VanHoose) for histological tissue processing.

FUNDING

JH received support from a National Science Foundation Graduate Research Fellowship Program Grant No. NSF DGE-1315231 and NIH 4T32HL007284. BA is supported by NIH 1R01 HL116455, 1R01 HL121635, and 2R01 HL101200. RP is supported by NIH R03 EB017927 R21 EB024323 and R01 EB020147.

REFERENCES

Annex, B. H. (2013). Therapeutic angiogenesis for critical limb ischaemia. *Nat. Rev. Cardiol.* 10, 387–396. doi:10.1038/nrcardio.2013.70

Boldin, M. P., Taganov, K. D., Rao, D. S., Yang, L., Zhao, J. L., Kalwani, M., et al. (2011). miR-146a is a significant brake on autoimmunity, myeloproliferation, and cancer in mice. *J. Exp. Med.* 208, 1189–1201. doi:10.1084/jem.20101823

Capoccia, B. J., Gregory, A. D., and Link, D. C. (2008). Recruitment of the inflammatory subset of monocytes to sites of ischemia induces angiogenesis in a monocyte chemoattractant protein-1-dependent fashion. *J. Leukoc. Biol.* 84, 760–768. doi:10.1189/jlb.1107756

Chappell, J. C., Song, J., Burke, C. W., Klibanov, A. L., and Price, R. J. (2008). Targeted delivery of nanoparticles bearing fibroblast growth factor-2 by ultrasonic microbubble destruction for therapeutic arteriogenesis. *Small* 4, 1769–1777. doi:10.1038/nsmb.2010.The

Chen, L. J., Chuang, L., Huang, Y. H., Zhou, J., Lim, S. H., Lee, C. I., et al. (2015). MicroRNA mediation of endothelial inflammatory response to smooth muscle cells and its inhibition by atheroprotective shear stress. *Circ. Res.* 116, 1157–1169. doi:10.1161/CIRCRESAHA.116.305987

Cheng, H. S., Besla, R., Li, A., Chen, Z., Shikatani, E. A., Nazari-Jahantigh, M., et al. (2017). Paradoxical suppression of atherosclerosis in the absence of microRNA-146a. *Circ. Res.* 121, 354–367. doi:10.1161/CIRCRESAHA.116.310529

Cheng, H. S., Sivachandran, N., Lau, A., Boudreau, E., Zhao, J. L., Baltimore, D., et al. (2013). MicroRNA-146 represses endothelial activation by inhibiting pro-inflammatory pathways. *EMBO Mol. Med.* 5, 949–966. doi:10.1002/emmm.201202318

Dai, X., and Faber, J. E. (2010). Endothelial nitric oxide synthase deficiency causes collateral vessel rarefaction and impairs activation of a cell cycle gene network during arteriogenesis. *Circ. Res.* 106, 1870–1881. doi:10.1161/CIRCRESAHA.109.212746

Distasi, M. R., Case, J., Ziegler, M. A., Dinauer, M. C., Yoder, M. C., Haneline, L. S., et al. (2009). Suppressed hindlimb perfusion in Rac2-/- and Nox2-/- mice does not result from impaired collateral growth. *Am. J. Physiol. Heart Circ. Physiol.* 296, H877–H886. doi:10.1152/ajpheart.00772.2008

Duscha, B. D., Robbins, J. L., Jones, W. S., Kraus, W. E., Lye, R. J., Sanders, J. M., et al. (2011). Angiogenesis in skeletal muscle precede improvements in peak oxygen uptake in peripheral artery disease patients. *Arterioscler. Thromb. Vasc. Biol.* 31, 2742–2748. doi:10.1161/ATVBAHA.111.230441

Epstein, S. E., Stabile, E., Kinnaird, T., Lee, C. W., Clavijo, L., and Burnett, M. S. (2004). Janus phenomenon: the interrelated tradeoffs inherent in therapies designed to enhance collateral formation and those designed to inhibit atherogenesis. *Circulation* 109, 2826–2831. doi:10.1161/01.CIR.0000132468.82942.F5

Etzrodt, M., Cortez-Retamozo, V., Newton, A., Zhao, J., Ng, A., Wildgruber, M., et al. (2012). Regulation of monocyte functional heterogeneity by miR-146a and Relb. *Cell Rep.* 1, 317–324. doi:10.1016/j.celrep.2012.02.009

Fakhry, F., Spronk, S., van der Laan, L., Wever, J. J., Teijink, J. A. W., Hoffmann, W. H., et al. (2015). Endovascular revascularization and supervised exercise for peripheral artery disease and intermittent claudication. *JAMA* 314, 1936. doi:10.1001/jama.2015.14851

Ganta, V. C., Choi, M. H., Kutateladze, A., Fox, T. E., Farber, C. R., and Annex, B. H. (2017). A microRNA93-interferon regulatory factor-9-immunoresponsive gene-1-itaconic acid pathway modulates M2-like macrophage polarization to revascularize ischemic muscle. *Circulation* 135, 2403–2425. doi:10.1161/CIRCULATIONAHA.116.025490

Grundmann, S., Hans, F. P., Kinniry, S., Heinke, J., Helbing, T., Bluhm, F., et al. (2011). MicroRNA-100 regulates neovascularization by suppression of mammalian target of rapamycin in endothelial and vascular smooth muscle cells. *Circulation* 123, 999–1009. doi:10.1161/CIRCULATIONAHA.110.000323

Guan, Y., Cai, B., Wu, X., Peng, S., Gan, L., Huang, D., et al. (2017). MicroRNA-352 regulates collateral vessel growth induced by elevated fluid shear stress in the rat hind limb. *Sci. Rep.* 7, 6643. doi:10.1038/s41598-017-06910-9

Halkein, J., Tabruyn, S. P., Ricke-hoch, M., Haghikia, A., Nguyen, N., Scherr, M., et al. (2013). MicroRNA-146a is a therapeutic target and biomarker for peripartum cardiomyopathy. *J. Clin. Invest.* 123, 2143–2154. doi:10.1172/JCI64365

Hazarika, S., Farber, C. R., Dokun, A. O., Pitsillides, A. N., Wang, T., Lye, R. J., et al. (2013). MicroRNA-93 controls perfusion recovery following hind-limb ischemia by modulating expression of multiple genes in the cell cycle pathway. *Circulation* 127, 1818–1828. doi:10.1161/CIRCULATIONAHA.112.000860

Heil, M., Ziegelhoeffer, T., Wagner, S., Fernández, B., Helisch, A., Martin, S., et al. (2004). Collateral artery growth (arteriogenesis) after experimental arterial occlusion is impaired in mice lacking CC-chemokine receptor-2. *Circ. Res.* 94, 671–677. doi:10.1161/01.RES.0000122041.73808.B5

Heuslein, J. L., Gorick, C. M., Song, J., and Price, R. J. (2017). DNMT1-dependent DNA hypermethylation constrains arteriogenesis by augmenting shear stress set-point. *J. Am. Heart Assoc.* doi:10.1161/JAHA.117.007673

Heuslein, J. L., Li, X., Murrell, K. P., Annex, B. H., Peirce, S. M., and Price, R. J. (2015a). Computational network model prediction of hemodynamic alterations due to arteriolar rarefaction and estimation of skeletal muscle perfusion in peripheral arterial disease. *Microcirculation* 22, 360–369. doi:10.1111/micc.12203

Heuslein, J. L., Meisner, J. K., Li, X., Song, J., Vincentelli, H., Leiphart, R. J., et al. (2015b). Mechanisms of amplified arteriogenesis in collateral artery segments exposed to reversed flow direction. *Arterioscler. Thromb. Vasc. Biol.* 35, 2354–2365. doi:10.1161/ATVBAHA.115.305775

Heuslein, J. L., Murrell, K. P., Leiphart, R. J., Llewellyn, R. A., Meisner, J. K., and Price, R. J. (2016). Vascular growth responses to chronic arterial occlusion are unaffected by myeloid specific focal adhesion kinase (FAK) deletion. *Sci. Rep.* 6, 27029. doi:10.1038/srep27029

Heuslein, J. L., and Price, R. J. (2017). Abstract 572: inhibition of microRNA-199a-5p enhances perfusion recovery and arteriogenesis following femoral arterial ligation. *Arterioscler. Thromb. Vasc. Biol.* 36. Available at: http://atvb.ahajournals.org/content/36/Suppl_1/A572

Hoefer, I. E., van Royen, N., Rectenwald, J. E., Deindl, E., Hua, J., Jost, M., et al. (2004). Arteriogenesis proceeds via ICAM-1/Mac-1-mediated mechanisms. *Circ. Res.* 94, 1179–1185. doi:10.1161/01.RES.0000126922.18222.F0

Hou, J., Wang, P., Lin, L., Liu, X., Ma, F., An, H., et al. (2009). MicroRNA-146a feedback inhibits RIG-I-dependent Type I IFN production in macrophages by targeting TRAF6, IRAK1, and IRAK2. *J. Immunol.* 183, 2150–2158. doi:10.4049/jimmunol.0900707

Ito, W. D., Arras, M., Winkler, B., Scholz, D., Schaper, J., and Schaper, W. (1997). Monocyte chemotactic protein-1 increases collateral and peripheral conductance after femoral artery occlusion. *Circ. Res.* 80, 829–837. doi:10.1161/01.RES.80.6.829

Lan, Q., Mercurius, K. O., and Davies, P. F. (1994). Stimulation of transcription factors NFkB and AP1 in ECs subjected to shear stress. *Biochem. Biophys. Res. Commun.* 201, 950–956. doi:10.1006/bbrc.1994.1794

Li, K., Ching, D., Luk, F. S., and Raffai, R. L. (2015). Apolipoprotein E enhances microRNA-146a in monocytes and macrophages to suppress nuclear factor-KB-driven inflammation and atherosclerosis. *Circ. Res.* 117, e1–e11. doi:10.1161/CIRCRESAHA.117.305844

Li, Y., Zhu, H., Wei, X., Li, H., Yu, Z., Zhang, H. M., et al. (2017). LPS induces HUVEC angiogenesis in vitro through miR-146a-mediated TGF-β1 inhibition. *Am. J. Transl. Res.* 9, 591–600.

Meisner, J. K., Annex, B. H., and Price, R. J. (2014). Despite normal arteriogenic and angiogenic responses, hind limb perfusion recovery and necrotic and fibro-adipose tissue clearance are impaired in matrix metalloproteinase 9-deficient mice. *J. Vasc. Surg.* 61, 1583–1594. doi:10.1016/j.jvs.2014.01.038

Meisner, J. K., and Price, R. J. (2010). Spatial and temporal coordination of bone marrow-derived cell activity during arteriogenesis: regulation of the endogenous response and therapeutic implications. *Microcirculation* 17, 583–599. doi:10.1111/j.1549-8719.2010.00051.x.Spatial

Meisner, J. K., Song, J., Annex, B. H., and Price, R. J. (2013). Myoglobin overexpression inhibits reperfusion in the ischemic mouse hindlimb through impaired angiogenesis but not arteriogenesis. *Am. J. Pathol.* 183, 1–10. doi:10.1016/j.ajpath.2013.08.005

Meisner, J. K., Sumer, S., Murrell, K. P., Higgins, T. J., and Price, R. J. (2012). Laser speckle flowmetry method for measuring spatial and temporal hemodynamic alterations throughout large microvascular networks. *Microcirculation* 19, 619–631. doi:10.1111/j.1549-8719.2012.00197.x

Nagel, T., Resnick, N., Atkinson, W. J., Dewey, C. F., and Gimbrone, M. A. (1994). Shear stress selectively upregulates intercellular adhesion molecule-1 expression in cultured human vascular endothelial cells. *J. Clin. Invest.* 94, 885–891. doi:10.1172/JCI117410

Neth, P., Nazari-Jahantigh, M., Schober, A., and Weber, C. (2013). MicroRNAs in flow-dependent vascular remodelling. *Cardiovasc. Res.* 99:294–303. doi:10.1093/cvr/cvt096

Nickerson, M. M., Burke, C. W., Meisner, J. K., Shuptrine, C. W., Song, J., and Price, R. J. (2009a). Capillary arterialization requires the bone-marrow-derived cell (BMC)-specific expression of chemokine (C-C motif) receptor-2, but BMCs do not transdifferentiate into microvascular smooth muscle. *Angiogenesis* 12, 355–363. doi:10.1007/s10456-009-9157-1

Nickerson, M. M., Song, J., Meisner, J. K., Bajikar, S., Burke, C. W., Shuptrine, C. W., et al. (2009b). Bone marrow-derived cell-specific chemokine (C-C motif) receptor-2 expression is required for arteriolar remodeling. *Arterioscler. Thromb. Vasc. Biol.* 29, 1794–1801. doi:10.1161/ATVBAHA.109.194019.Bone

Norgren, L., Hiatt, W. R., Dormandy, J. A., Nehler, M. R., Harris, K. A., and Fowkes, F. G. R. (2007). Inter-society consensus for the management of peripheral arterial disease (TASC II). *Eur. J. Vasc. Endovasc. Surg.* 33, S1–S75. doi:10.1016/j.jvs.2006.12.037

Rau, C.-S., Yang, J. C.-S., Chen, Y.-C., Wu, C.-J., Lu, T.-H., Tzeng, S.-L., et al. (2014). Lipopolysaccharide-induced microRNA-146a targets CARD10 and regulates angiogenesis in human umbilical vein endothelial cells. *Toxicol. Sci.* 140, 315–326. doi:10.1093/toxsci/kfu097

Ripa, R. S., Jørgensen, E., Wang, Y., Thune, J. J., Nilsson, J. C., Søndergaard, L., et al. (2006). Stem cell mobilization induced by subcutaneous granulocyte-colony stimulating factor to improve cardiac regeneration after acute ST-elevation myocardial infarction: result of the double-blind, randomized, placebo-controlled stem cells in myocardial infarc. *Circulation* 113, 1983–1992. doi:10.1161/CIRCULATIONAHA.105.610469

Robbins, J. L., Jones, W. S., Duscha, B. D., Allen, J. D., Kraus, W. E., Regensteiner, J. G., et al. (2011). Relationship between leg muscle capillary density and peak hyperemic blood flow with endurance capacity in peripheral artery disease. *J. Appl. Physiol.* 111, 81–86. doi:10.1152/japplphysiol.00141.2011

Santulli, G. (2016). MicroRNAs and endothelial (Dys) function. *J. Cell. Physiol.* 231, 1638–1644. doi:10.1002/jcp.25276

Schindelin, J., Arganda-Carreras, I., Frise, E., Kaynig, V., Longair, M., Pietzsch, T., et al. (2012). Fiji: an open-source platform for biological-image analysis. *Nat. Methods* 9, 676–682. doi:10.1038/nmeth.2019

Seiler, C., Pohl, T., Wustmann, K., Hutter, D., Nicolet, P. A., Windecker, S., et al. (2001). Promotion of collateral growth by granulocyte-macrophage colony-stimulating factor in patients with coronary artery disease: a randomized, double-blind, placebo-controlled study. *Circulation* 104, 2012–2017. doi:10.1161/hc4201.097835

Shireman, P. (2007). The chemokine system in arteriogenesis and hind limb ischemia. *J. Vasc. Surg.* 45, A48–A56. doi:10.1016/j.jvs.2007.02.030

Subramaniyam, V., Waller, E. K., Murrow, J. R., Manatunga, A., Lonial, S., Kasirajan, K., et al. (2009). Bone marrow mobilization with granulocyte macrophage colony-stimulating factor improves endothelial dysfunction and exercise capacity in patients with peripheral arterial disease. *Am. Heart J.* 158, 53–60. doi:10.1016/j.ahj.2009.04.014

Sweet, D. T., Chen, Z., Givens, C. S., Owens, A. P., Rojas, M., and Tzima, E. (2013). Endothelial Shc regulates arteriogenesis through dual control of arterial specification and inflammation via the Notch and NF-κB pathways. *Circ. Res.* 113, 32–39. doi:10.1161/CIRCRESAHA.113.301407

Taganov, K. D., Boldin, M. P., Chang, K.-J., and Baltimore, D. (2006). NF-kappaB-dependent induction of microRNA miR-146, an inhibitor targeted to signaling proteins of innate immune responses. *Proc. Natl. Acad. Sci. U.S.A.* 103, 12481–12486. doi:10.1073/pnas.0605298103

Tirziu, D., Jaba, I. M., Yu, P., Larrivée, B., Coon, B. G., Cristofaro, B., et al. (2012). Endothelial nuclear factor-κB-dependent regulation of arteriogenesis and branching. *Circulation* 126, 2589–2600. doi:10.1161/CIRCULATIONAHA.112.119321

Troidl, C., Jung, G., Troidl, K., Hoffmann, J., Mollmann, H., Nef, H., et al. (2013). The temporal and spatial distribution of macrophage subpopulations during arteriogenesis. *Curr. Vasc. Pharmacol.* 11, 5–12. doi:10.2174/15701611113090 10005

Urbich, C., Kuehbacher, A., and Dimmeler, S. (2008). Role of microRNAs in vascular diseases, inflammation, and angiogenesis. *Cardiovasc. Res.* 79, 581–588. doi:10.1093/cvr/cvn156

van Royen, N., Schirmer, S. H., Atasever, B., Behrens, C. Y. H., Ubbink, D., Buschmann, E. E., et al. (2005). START Trial: a pilot study on STimulation of ARTeriogenesis using subcutaneous application of granulocyte-macrophage colony-stimulating factor as a new treatment for peripheral vascular disease. *Circulation* 112, 1040–1046. doi:10.1161/CIRCULATIONAHA.104.529552

Wang, T., Cunningham, A., Dokun, A. O., Hazarika, S., Houston, K., Chen, L., et al. (2015). Loss of interleukin-21 receptor activation in hypoxic endothelial cells impairs perfusion recovery after hindlimb ischemia. *Arterioscler. Thromb. Vasc. Biol.* 35, 1218–1225. doi:10.1161/ATVBAHA.115.305476

Welten, S. M., Bastiaansen, A. J., de Jong, R., de Vries, M. R., Peters, E. H., Boonstra, M., et al. (2014). Inhibition of 14q32 microRNAs miR-329, miR-487b, miR-494 and miR-495 increases neovascularization and blood flow recovery after ischemia. *Circ. Res.* 115, 696–708. doi:10.1161/CIRCRESAHA.114.304747

Zbinden, S., Zbinden, R., Meier, P., Windecker, S., and Seiler, C. (2005). Safety and efficacy of subcutaneous-only granulocyte-macrophage colony-stimulating factor for collateral growth promotion in patients with coronary artery disease. *J. Am. Coll. Cardiol.* 46, 1636–1642. doi:10.1016/j.jacc.2005.01.068

Zhao, J. L., Rao, D. S., Boldin, M. P., Taganov, K. D., O'Connell, R. M., and Baltimore, D. (2011). NF-kappaB dysregulation in microRNA-146a-deficient mice drives the development of myeloid malignancies. *Proc. Natl. Acad. Sci. U.S.A.* 108, 9184–9189. doi:10.1073/pnas.1105398108

Zhu, H., Bai, W., Liu, J., Zheng, Z., Guan, H., Zhou, Q., et al. (2016). Up-regulation of FGFBP1 signaling contributes to miR-146a-induced angiogenesis in human umbilical vein endothelial cells. *Sci. Rep.* 6, 25272. doi:10.1038/srep25272

Zhu, K., Pan, Q., Zhang, X., Kong, L. Q., Fan, J., Dai, Z., et al. (2013). miR-146a enhances angiogenic activity of endothelial cells in hepatocellular carcinoma by promoting PDGFRA expression. *Carcinogenesis* 34, 2071–2079. doi:10.1093/carcin/bgt160

Conflict of Interest Statement: The authors declare that the research was conducted in the absence of any commercial or financial relationships that could be construed as a potential conflict of interest.

frontiers in Bioengineering and Biotechnology

ORIGINAL RESEARCH
published: 22 January 2018
doi: 10.3389/fbioe.2018.00002

Localization of Engineered Vasculature within 3D Tissue Constructs

*Shira Landau, Shaowei Guo and Shulamit Levenberg**

Department of Biomedical Engineering, Technion – Israel Institute of Technology, Haifa, Israel

Today, *in vitro* vessel network systems frequently serve as models for investigating cellular and functional mechanisms underlying angiogenesis and vasculogenesis. Understanding the cues triggering the observed cell migration, organization, and differentiation, as well as the time frame of these processes, can improve the design of engineered microvasculature. Here, we present first evidence of the migration of endothelial cells into the depths of the scaffold, where they formed blood vessels surrounded by extracellular matrix and supporting cells. The supporting cells presented localization-dependent phenotypes, where cells adjacent to blood vessels displayed a more mature phenotype, with smooth muscle cell characteristics, whereas cells on the scaffold surface showed a pericyte-like phenotype. Yes-associated protein (YAP), a transcription activator of genes involved in cell proliferation and tissue growth, displayed spatially dependent expression, with cells on the surface showing more nuclear YAP than cells situated deeper within the scaffold.

Keywords: blood vessels, angiogenesis, 3D scaffolds, pericytes, migration

OPEN ACCESS

Edited by:
Andrea Banfi,
University of Basel, Switzerland

Reviewed by:
Arnaud Scherberich,
University Hospital of Basel, Switzerland
Enrico Lucarelli,
Istituto Ortopedico Rizzoli (IRCCS), Italy

***Correspondence:**
Shulamit Levenberg
shulamit@bm.technion.ac.il

Specialty section:
This article was submitted to Tissue Engineering and Regenerative Medicine, a section of the journal Frontiers in Bioengineering and Biotechnology

Received: *24 September 2017*
Accepted: *04 January 2018*
Published: *22 January 2018*

Citation:
Landau S, Guo S and Levenberg S (2018) Localization of Engineered Vasculature within 3D Tissue Constructs. Front. Bioeng. Biotechnol. 6:2. doi: 10.3389/fbioe.2018.00002

INTRODUCTION

Blood vessel growth within engineered tissues is a critical factor in overcoming insufficient blood perfusion in implants (Shandalov et al., 2014; Mirabella et al., 2017). Endothelial and supporting cell cocultures are often used to generate such blood vessels (Koike et al., 2004; Koffler et al., 2011; Freiman et al., 2016; Landau et al., 2017). While this cell combination spontaneously forms microvasculature, the mechanism controlling the process is not well understood.

Endothelial cell migration occurring during angiogenesis is regulated by (1) chemotaxis: the migration of cells in the direction of soluble chemoattractants gradient, (2) haptotaxis: the migration of cells in the direction of tied ligands, and (3) mechanotaxis: the migration of cells in response to mechanical cues. In addition, cell mediated degradation of the extracellular matrix also plays an important role in endothelial cell migration (Lamalice et al., 2007). Distinct differences in vessel network environments exist in the body. For example, single or multiple layers of vascular smooth muscle cells (vSMCs) surround large vessels as opposed to intermediate-sized vessels which are surrounded by mural cells that have shared properties of both vSMCs and pericytes, which in many cases, serve as vSMC progenitors (Holger and Christer Betsholtz, 2003; Bergers and Song, 2005; Volz et al., 2015). Hence, cellular phenotype is influenced by the cell's spatial localization. Thus we hypothesized that during the process of blood vessel formation within engineered constructs, endothelial cells migrate in response to stimulation cues and that the phenotype of supporting cells shifts, in accordance with their spatial localization.

This study was designed to assess ECs migration during angiogenesis and the location-specific characteristics of the cells composing the forming vessels within different three-dimensional (3D)

constructs. While previous studies examined the dynamics of vessel network formation *in vitro* (Blinder et al., 2015; Freiman et al., 2016), the present experimental setup aimed to identify the effect of cellular localization at different layers of the scaffold on vessel formation metrics such as migration, proliferation, protein expression and differentiation of endothelial and supporting cells. Understanding these processes can aid in designing improved vascularized constructs, which will enhance graft integration upon implantation.

MATERIALS AND METHODS

Scaffolds

Gelfoam scaffolds were purchased from Pfizer and were cut into pieces 1 cm long, 0.5 cm wide, and 1.5 mm thick pieces. PLLA/PLGA scaffolds were prepared as followed: 0.4 g NaCl particles were covered with 0.24 ml PLLA/PLGA solution, which was dissolved in chloroform, and evaporated overnight. Salt was then leached out by four washes, leaving behind pores within the scaffold. Scaffolds were then cut into 6 mm diameter circles with the thickness of 0.8 mm. Fibrin gel was obtained by mixing thrombin (20 U/ml, Sigma-Aldrich) with fibrinogen (15 mg/ml, Sigma-Aldrich).

Cell Culture

Human adipose microvascular endothelial cells (HAMECs; ScienceCell), lentivirally transduced with ZsGreen fluorescent protein, were grown in endothelial cell medium (ScienceCell), supplemented with 5% FBS (ScienceCell), and endothelial cell growth supplement (ScienceCell), and used for five to nine passages. Neonatal normal human dermal fibroblasts (HNDFs) (Lonza Walkersville Inc.) were grown in Dulbecco's modified Eagle medium (DMEM) (Gibco), supplemented with 10% FBS (HyClone), 1% non-essential amino acids (NEAAs), 0.2% β-mercaptoethanol (Sigma-Aldrich), and 1% penicillin–streptomycin solution (PEN STREP) (Biological Industries). Dental pulp stem cells (DPSCs) (Lonza) were cultured in low glucose DMEM (Gibco), supplemented with 10% FBS (HyClone), 1% NEAAs, 1% GlutaMAX (Gibco), and 1% penicillin–streptomycin-nystatin solution (Biological Industries). Three dimensional, vascularized constructs were obtained by coseeding endothelial cells (3×10^5 cells) and DPSCs (9×10^5) or fibroblasts (0.6×10^5 cells) in 20 µl medium on the gelfoam or in 7 µl fibrin on the PLLA/PLGA scaffolds followed by incubation of 30 min, before addition of medium. For the mitomycin experiments, 5 ml mitomycin (Sigma-Aldrich) was applied to the fibroblast cells 2 h before seeding, and washed twice with PBS.

Lentivirus Packaging and HAMEC Transduction with ZsGreen and dTomato Fluorescent Proteins

The Lenti-X HTX Packaging System (Clontech, a fourth generation) was used to generate recombinant, replication-incompetent VSV-G pseudotyped lentiviruses, according to the manufacturer's instructions. Transfection of the expression vector into the Lenti-X 293 T packaging cells (Clontech) was performed in a Lenti-X HTX Packaging mix. The supernatants of transfected packaging cells were collected 72 h later and filtered through a 45-µm filter before being added to the HAMECs, with 6 mg/ml polybrene (Sigma-Aldrich). The transduction medium was replaced by culture medium 24 h thereafter, and cells were then cultured for 72 h to allow gene product accumulation in the cells. Cells were then selected using 1 mg/ml puromycin (Takara Bio Company).

Whole-Mount and Cryosection Immunofluorescence Staining

Whole constructs were fixated in paraformaldehyde (4%), for 20 min, and then permeabilized with 0.3% Triton X-100 (Bio Lab Ltd.), for 10 min. Constructs were then washed with PBS and immersed overnight in BSA solution (5%; Millipore). Samples were then incubated with goat antihuman VE-cadherin (1:100; Santa Cruz), mouse antihuman Yes-associated protein (YAP) (1:100; Santa Cruz), mouse antihuman NG2 (1:100; Santa Cruz), rabbit antihuman vWF (1:150; Abcam), rabbit antihuman β-catenin (1:100; Sigma-Aldrich), or mouse antihuman Ki67 (1:20, DAKO) antibodies, overnight, at 4°C. Constructs were then treated with Cy3-labeled (1:100; Jackson Immunoresearch Laboratory), Cy5-labeled (1:100; Jackson Immunoresearch Laboratory), or Alexa-488 (1:400; ThermoFisher Scientific) antibodies, mixed with DAPI (1:1000; Sigma-Aldrich), for 2 h, at room temperature. For the phalloidin staining, constructs were treated with FITC phalloidin (1:100; Sigma-Aldrich) and DAPI for 20 min. For the mitomycin experiment, mitomycin-treated cells and control cells without mitomycin were fixated in paraformaldehyde (4%), for 20 min on day 10 of culture, and then incubated in a 30% (wt/vol) sucrose solution overnight, embedded in optimal cutting temperature compound (Tissue-Tek) and frozen for subsequent cryosectioning (5–20 µm). Standard protocols were used for H&E and Masson's trichrome staining of the sections.

Construct Imaging and Quantification of the Images

Whole vascularized constructs were imaged using a confocal microscope (LSM700, Zeiss), equipped with 20× and 63× oil immersion lenses. Three-dimensional images were projected into 2D images, using maximum intensity projection, and the stacks were then separated into three main regions: the surface (0–10 µm), middle (10–20 µm), and deeper (20 µm-end) areas of the scaffold. Confocal images were then analyzed using a self-written algorithm in MATLAB, for ki67 quantification: images were transformed into binary images and pixel density was calculated. Vessel quality was determined using a self-written algorithm in MATLAB: images were transformed into binary images and the eccentricity parameter, an indicator of the deviation of an element from circularity, was calculated for each separate element in the image. Elongated vessels received a higher eccentricity score, whereas, cells clusters and disrupted vessels, which are more circular, receive lower eccentricity scores. Imaris software (BITPLANE) was used to detect YAP and β-catenin localization through the 3D image.

Statistical Analysis

Presented data include the mean ± SD. Two-way analysis of variance was performed to examine the influence of two independent categorical variables, followed by Bonferroni's multiple comparison tests. Results were considered significant for $p < 0.05$. Statistical analysis was performed using a computerized statistical program (GraphPad Software). Experiments were repeated three times.

RESULTS

Vessel Formation within 3D Constructs

To follow vessel formation dynamics within 3D structures, a coculture of HAMECs and HNDFs was seeded into a gelfoam scaffold. After 7 days of culturing, cells were stained for VE-cadherin and were imaged using a confocal microscope. A sheet-like structure of an endothelial cell monolayer was observed on the surface of the scaffold, whereas in the scaffolds depth, cells began to form microvessels (**Figure 1A**). On day 14 postseeding, the endothelial cell monolayer structure was no longer observed and only microvessels were observed in the scaffolds depth; 3D confocal imaging showed that these vessels were lumenalized. In addition, at the same time point, a dense fibroblast layer was apparent on the scaffold surface and around the vessels (**Figure 1B**; Figures S1 and S2 in Supplementary Material). To confirm that this phenomenon was not limited to a certain scaffold or cell type, dTomato HAMECs were seeded with DPSCs into a PLLA/PLGA scaffold, which was then stained with DAPI and phalloidin. DPSCs were mainly observed on the scaffold surface and endothelial micro-vessels were seen within the scaffold depth (**Figure 2**).

PHD2 Expression throughout the Scaffold

We hypothesize that EC migration toward the scaffolds interior might be due to hypoxia. It is recognized that secretion of VEGF increases in hypoxic conditions (Shweiki et al., 1992) which consequently triggers EC migration. Transversed cryosections were stained with PHD2 (prolyl hydroxylase domain 2), which flags hypoxia inducing factor alpha subunits for ubiquitin-proteasome degradation under normoxic conditions (Carmeliet and Jain, 2011). PHD2 expression was higher at the scaffold surface as compared to the scaffolds depth (**Figures 3A,B**). Hence, the increasing hypoxic conditions at the scaffold depths may have triggered the ECs to form vessels there.

Fibroblast Localization and Proliferation throughout the Scaffold

To examine fibroblast characteristics in the 3D constructs, a HAMEC and HNDF coculture was seeded into the gelfoam scaffold and grown for 14 days, fixated and stained for CD31, to mark the ECs, and for PDGFRβ and αSMA, to mark the pericytes;

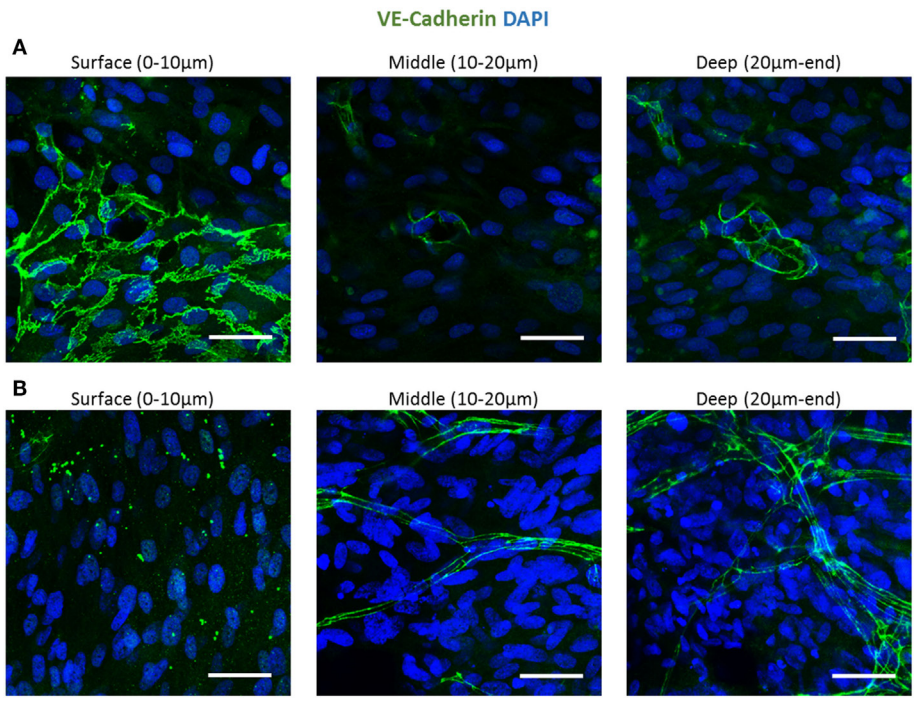

FIGURE 1 | Endothelial cell configuration throughout a 3D gelfoam scaffold. ECs and fibroblasts were seeded into a gelfoam scaffold and were fixated and then stained for VE-cadherin (green) and with DAPI nuclear stain (blue). Images demonstrate the endothelial cell morphology at different depths of the scaffold **(A)** after 7 days in culture. ECs on the scaffold surface formed a sheet and vessels began to form in the depths of the scaffold. **(B)** On day 14 of culturing, a fully developed vessel network was observed in the scaffold depths. Scale bar indicates 50 μm.

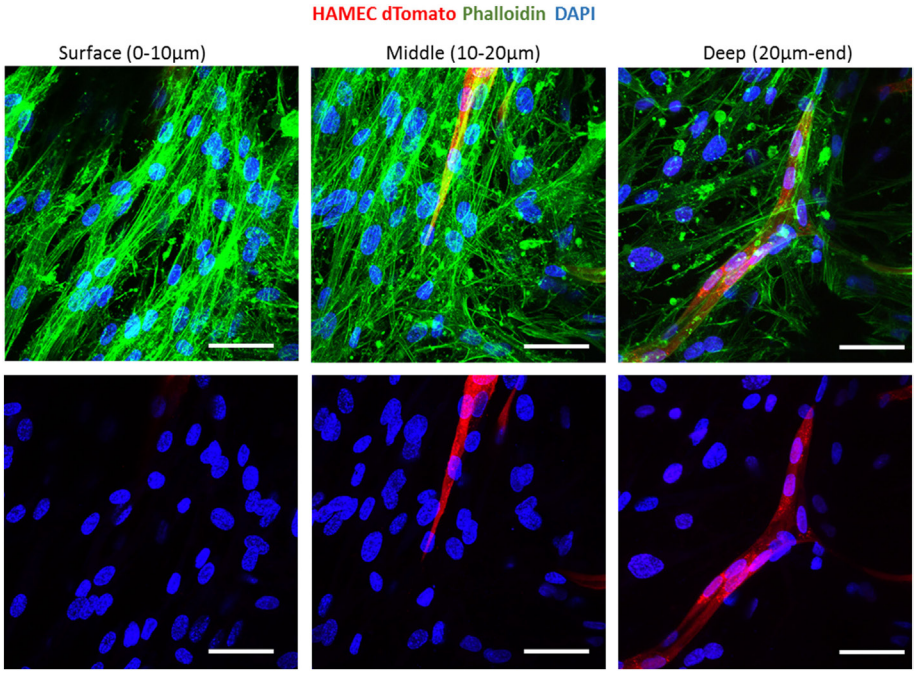

FIGURE 2 | Vessel localization is not limited to a certain scaffold or cell type. Vessel morphogenesis within a PLLA-PLGA scaffold embedded with fibrin, at different depths of the scaffold. Cells were stained with phalloidin (green) and DAPI (blue). ECs were marked with dTomato (red). Scale bar indicates 50 μm.

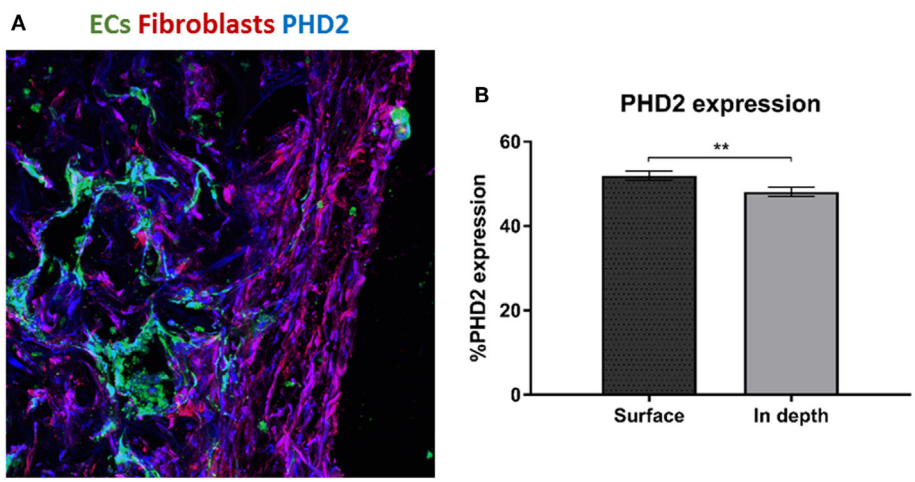

FIGURE 3 | PHD2 expression throughout the scaffold. **(A)** Staining of a transversed cryosection with PHD2 (blue), endothelial cells are marked in green and fibroblasts in red. **(B)** Quantification of PHD2 expression at the scaffold surface and in the scaffold depth. ($n = 3$) $^{**}P$-value <0.01.

expression of the two proteins has been shown to increase during the recruitment of pericytes to stabilize the forming vessels (Welti et al., 2013). Confocal imaging revealed that PDGFRβ-expressing cells were located both on the scaffold surface and in the scaffold depths (**Figure 4**), whereas αSMA-expressing cells were mainly located around the vessel network in the scaffold depth. To assess the degree of cell proliferation at the various scaffold locations, samples were stained for Ki67. Ki67-expressing fibroblasts were significantly more frequent on the scaffold surface compared to the scaffold depth (**Figure 5**), suggesting that cell proliferation decreased within the deeper layers of the scaffold, closer to the forming vessels.

Since canonical Wnt signaling has been implicated in cell proliferation (Clevers, 2006), and is involved in supporting cell recruitment to forming vessel (Reis and Liebner, 2013), we next examined the expression patterns of proteins which play a central

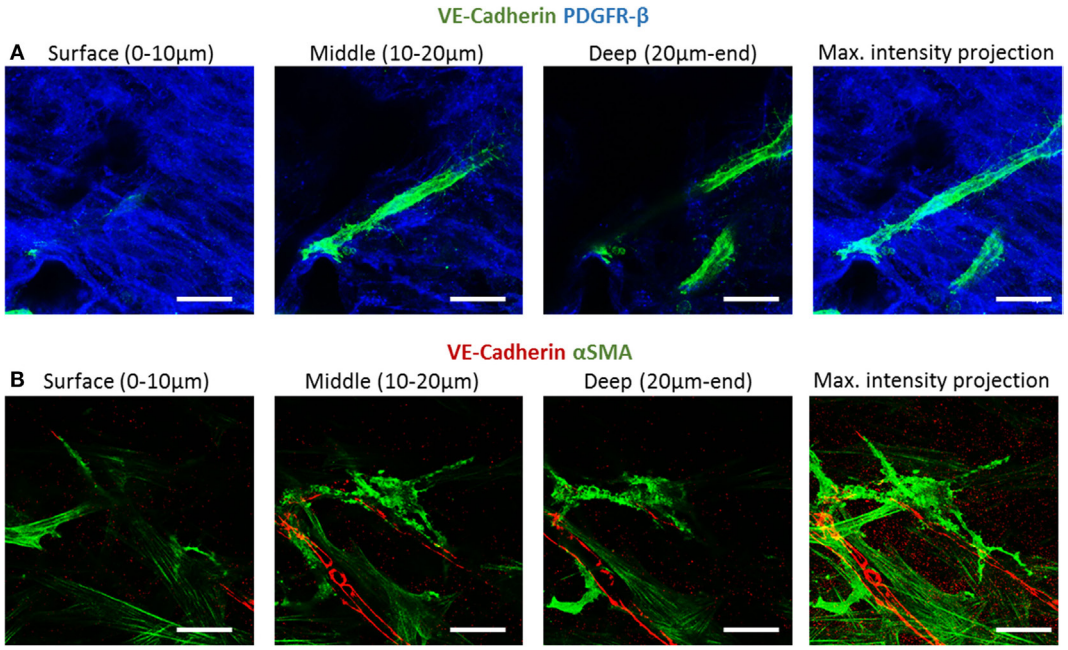

FIGURE 4 | PDGFRβ and αSMA expression across the scaffold. Gelfoam scaffolds seeded with ECs and fibroblast, were cultured for 14 days and then stained for: **(A)** CD31 (green) and PDGFRβ (blue) or **(B)** CD31 (red) and αSMA (green). Expression patterns were assessed at various depths of the scaffolds. Scale bar indicates 50 μm.

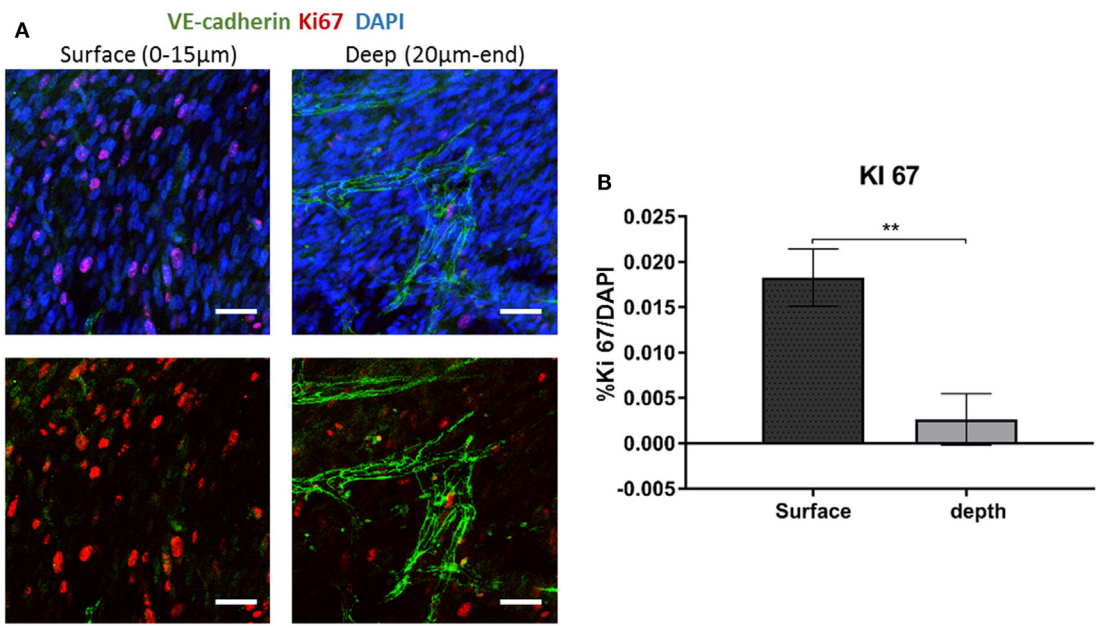

FIGURE 5 | Ki67 expression across the scaffold. **(A)** Gelfoam scaffolds were seeded with ECs and fibroblast, cultured for 14 days, and then stained for Ki67 (red) and VE-cadherin (green). **(B)** Expression patterns were assessed at various depths of the scaffolds. The percentage of Ki67-positive cell on the surface and the depth of the scaffold was quantified. Scale bar indicates 50 μm. ($n = 3$) $^{**}P$-value <0.01.

role in the Wnt canonical pathway within the cells composing the forming vessels. Cells grown on the scaffolds for 14 days were stained for YAP, β-catenin, and VE-cadherin. Localization of YAP in the fibroblast nucleus was only observed in the layers closer to the scaffold surface and its levels decreased with closer proximity to the scaffold core, where the endothelial cells were localized

(**Figure 6A**). Fibroblasts β-catenin showed cytoplasmic localization, which also decreased in the scaffold depths (**Figure 6B**). For the cells grown for 4 days, cytoplasmic β-catenin and nuclear YAP were observed within the ECs sheets located on the surface of the scaffold, which formed at the earlier stages of culturing (**Figure 6C**).

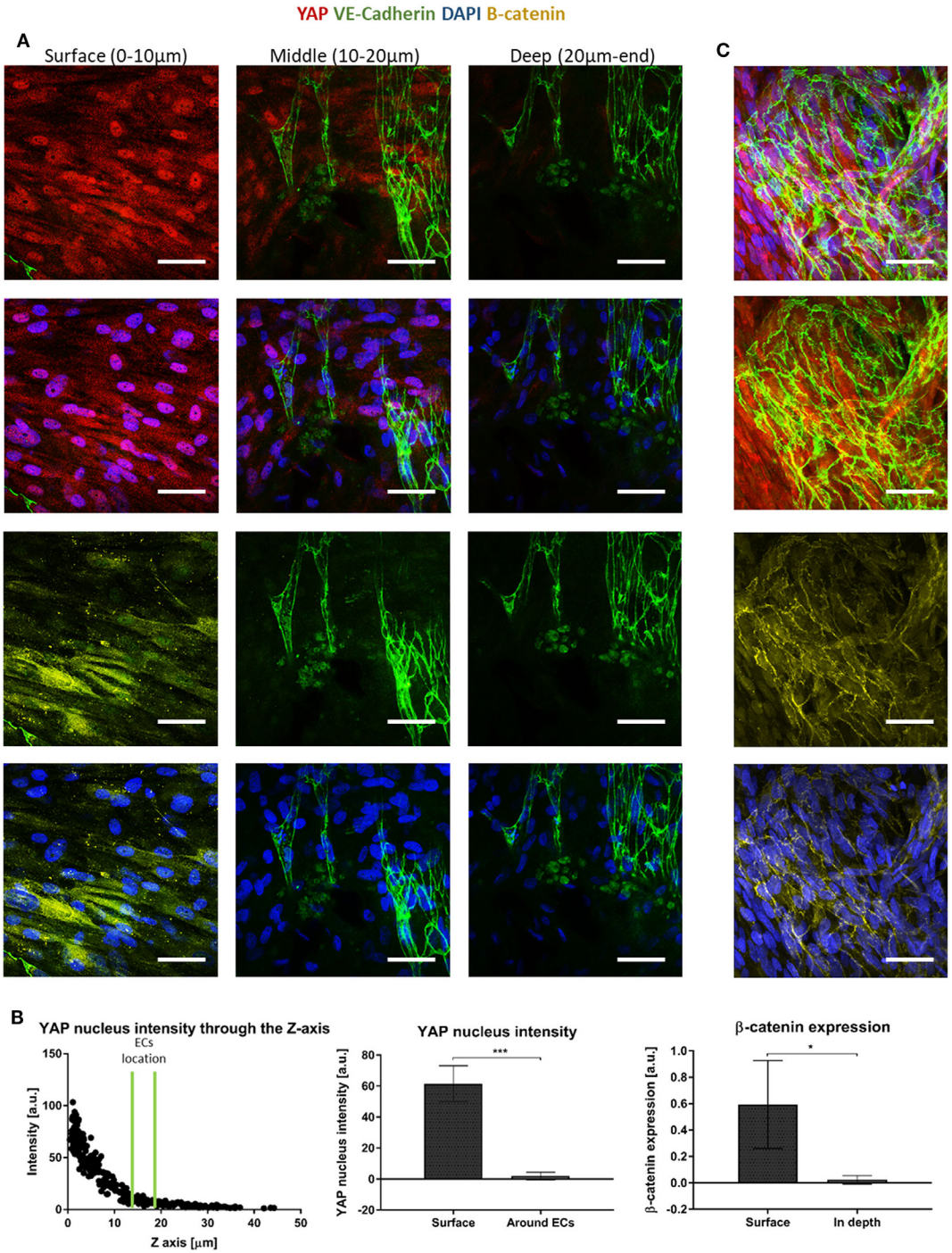

FIGURE 6 | Yes-associated protein (YAP) and β-catenin expression across the scaffold. **(A)** Gelfoam scaffolds seeded with ECs and fibroblasts were stained for YAP (red), DAPI (blue), VE-cadherin (green), and β-catenin (yellow), 14 days after seeding. Various depths of the scaffolds were assessed for expression patterns. **(B)** Left—a representative graph of the distribution of nuclear YAP expression as a function of scaffold depth. EC location is marked by two green lines. Middle—quantification of nuclear YAP fluorescence intensity on the scaffold surface versus in areas in which ECs were observed. ($n = 4$) ***P-value <0.001. Right—quantification of β-catenin fluorescence intensity on the scaffold surface versus in the areas in which ECs were observed. ($n = 3$) *P-value <0.05. **(C)** ECs cultured for 4 days, at the surface of the scaffold formed sheets and expressed cytoplasmic β-catenin (yellow) and nuclear YAP (red). Scale bar indicates 50 μm. *P-value <0.05.

Fibroblast Proliferation Affects Vessel Formation

The heightened expression of nuclear YAP and cytoplasmic β-catenin and more extensive cell proliferation on the scaffold surface, led us to investigate the role of Wnt signaling and specifically, of fibroblast proliferation in vasculogenesis. To this end, fibroblasts were treated with mitomycin prior to seeding and cell-embedded constructs were then grown for 7 or 10 days before being transversely cryosectioned. Confocal images of the various constructs revealed that the ECs seeded with mitomycin-treated fibroblasts, failed to form vessel networks (**Figures 7A,B**). In addition, the ECs in these constructs did not penetrate into the scaffold depths (**Figure 7C**), and remained localized in the same plane as the fibroblasts. Hematoxylin and eosin and trichrome stainings revealed a dense, thick layer of cells and collagen on the surface of scaffolds containing untreated fibroblasts, whereas the constructs with mitomycin-treated cells showed a thin layer, with less collagen deposition (**Figures 8A,B**, dashed box).

ECs Seeding on Scaffolds Precultured with Fibroblasts

Following the observed migration of ECs from the scaffold surface to its depth, when coseeded with fibroblasts, we set out to determine whether this migration occurs in the presence of a preexisting fibroblast layer. To this end, RFP-expressing HNDFs were seeded onto a gelfoam scaffold, and cultured for 12 days before Zs-green-expressing HAMECs were added to the culture. Despite the dense fibroblast layer, the endothelial cells migrated toward the inner part of the scaffold, where they formed a vessel network within 5 days (**Figure 9**). This migration might be due to the previously described hypoxic conditions in the scaffold depth.

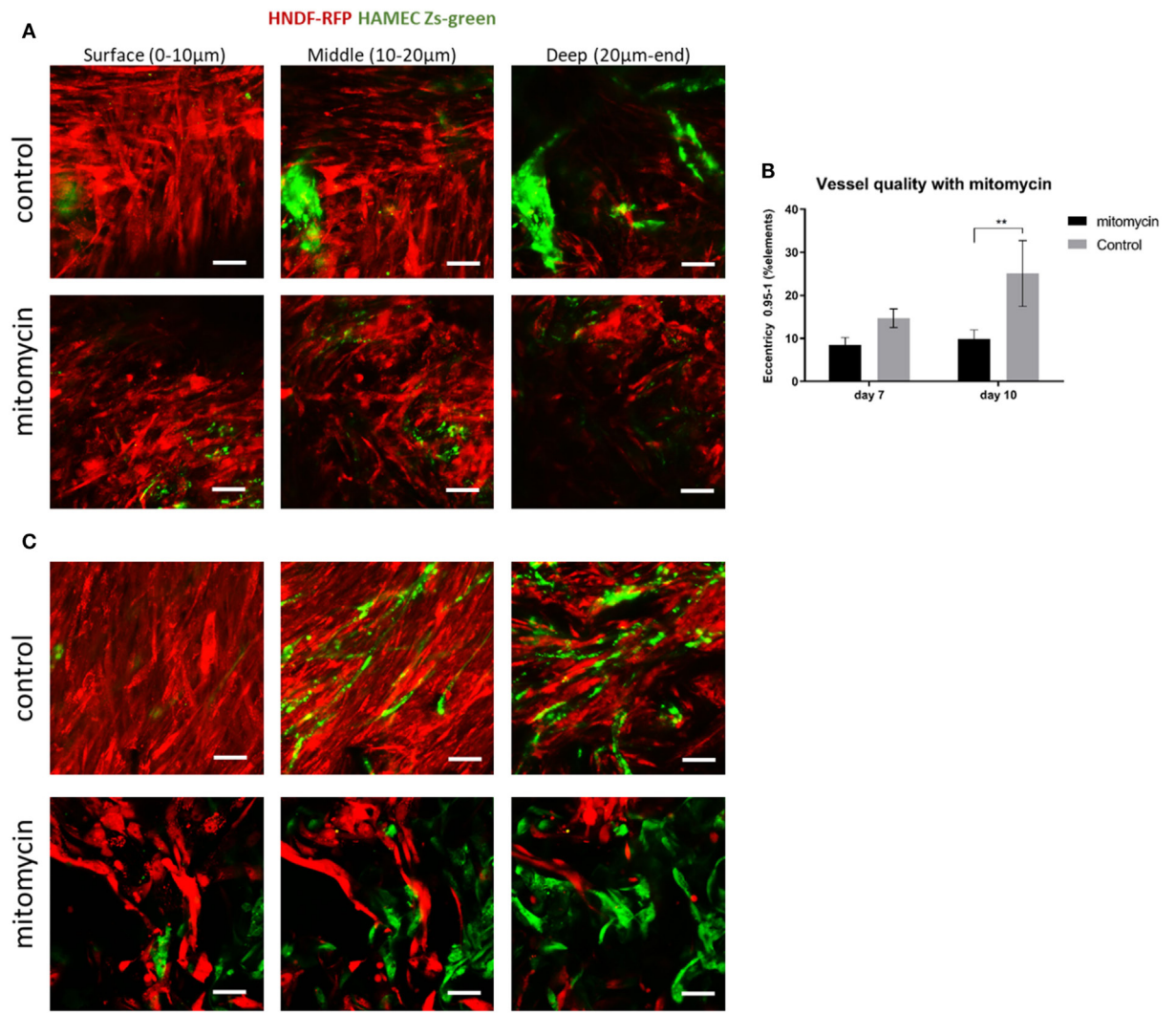

FIGURE 7 | Mitomycin-treated fibroblasts impair blood vessel formation. Fibroblasts (red) treated with mitomycin were cocultured with ECs (green) on scaffolds, for 7 or 10 days. Images of mitomycin-treated and untreated scaffolds on **(A)** day 7 and **(B)** day 10 of culturing, at different depths of the scaffold. ($n = 3$) $^{**}P$-value <0.01. **(C)** Quantification of vessel quality, assessed using the complexity parameter. Scale bar indicates 50 µm.

DISCUSSION

To date, integration of engineered grafts into host tissue remains one of the main obstacles in tissue engineering. Growth of mature and functional blood vessels within the engineered constructs can overcome this problem, by ensuring graft perfusion, thereby preventing localized necrosis, until host-graft composite vessels are established (Shandalov et al., 2014). Biomimetic models designed to investigate vasculogenesis and angiogenesis processes (Nguyen et al., 2013; Landau et al., 2017; Perry et al., 2017) will ultimately empower construction of improved blood vessel networks.

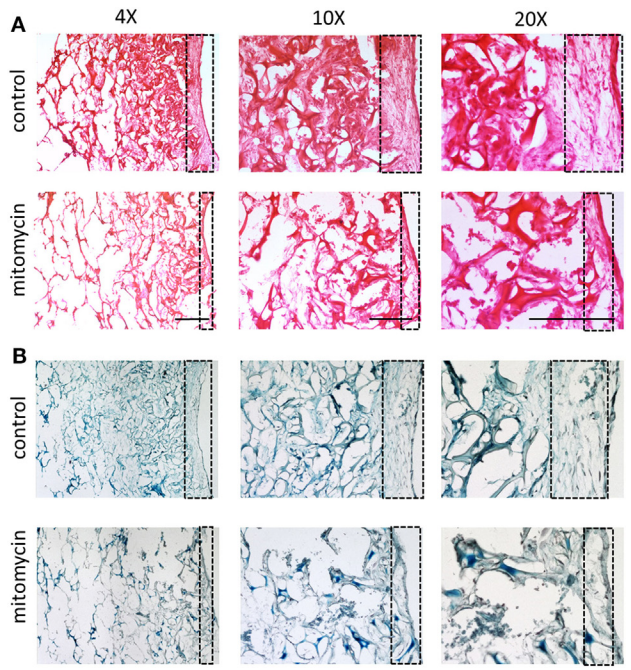

FIGURE 8 | Cell layer and collagen density bearing mitomycin-treated fibroblasts. Scaffolds containing ECs and either untreated or mitomycin-treated fibroblasts, were cultured for 10 days. Transverse cryosections were then stained with **(A)** hematoxylin and eosin or **(B)** Masson's trichrome. Dashed box indicates scaffold surface areas with dense tissue under normal conditions and thin tissue under mitomycin treatment. Scale bar indicates 400 μm.

In this study, tissue engineering techniques were used as a platform to investigate blood vessel development and to investigate cell properties throughout 3D environments of vascular networks. For this purpose, a combination of ECs and fibroblasts or DPSCs was seeded into both PLLA-PLGA scaffolds and gelfoam gelatin sponges. The cell combination formed vessels in a spatially dependent manner, with dense layers of fibroblasts in the surface area and EC-rich vessels, with a thin enveloping fibroblast layer, in the depths of the scaffold. Moreover, the cells showed location-distinct characteristics across the scaffold, with the fibroblasts on the surface appearing to be more proliferative, and expressing more nuclear YAP, while those surrounding the vessels deep within the scaffold, expressed more αSMA.

Mural pericytes impart a nascent vessel stabilizing effect, *via* a process mediated by various cytokines such as, TGF-β1, which promotes mesenchymal precursor cells differentiation into pericytes, and EC-derived platelet-derived growth factor subunit B (PDGF-B), which recruits PDGFR-β-expressing pericytes, which, in turn, migrate toward the forming vessel and surround it (Welti et al., 2013). In the present model, PDGFR-β expression was observed in cells on the scaffold surface and in the cells surrounding the vessels deep within the scaffold, leading us to conclude that PDGFR-β-expressing cells are located all over the scaffolds and are being recruited toward the nascent vessels. In contrast, αSMA expression in vessel supporting cells was rarely detected in cells at the scaffold surface, and distinctly localized around mature vessels, likely mechanically stabilizing the forming vessel. This observation is in keeping with reports of mechanical contractile forces on vessels induced by pericytes enveloping vessels (Bergers and Song, 2005; Volz et al., 2015).

Wnt has been shown to play a significant role in vascular morphogenesis and to promote cell proliferation. When the Wnt pathway is active, cytoplasmic YAP is inhibited, resulting in its accumulation in the nucleus, which, in turn, leads to stabilization of β-catenin in the cell cytoplasm. In contrast, in the absence of Wnt signaling, YAP/TAZ takes part in a destruction complex

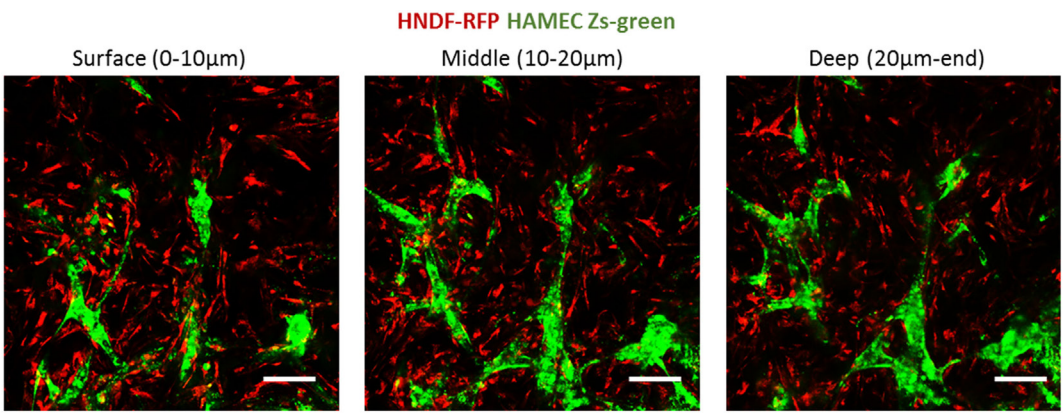

FIGURE 9 | ECs penetration of a precultured fibroblasts layer. ECs (green) were seeded on scaffolds precultured with fibroblasts (red) for 12 days. Images were taken at the different depths of the scaffold, 5 days after reseeding. Scale bar indicates 50 μm.

that degrades β-catenin (Cheng et al., 2003; Azzolin et al., 2014). Thus, we hypothesized that the observed accumulation of nuclear YAP and cytoplasmic β-catenin in the cells located on the scaffold surface, were in a "Wnt ON" state, which could explain the high proliferation rate recorded at the scaffold surface. In contrast, the cells in the inner part of the scaffolds were likely in a "Wnt OFF" state, with lower nuclear YAP and β-catenin levels. When inhibiting fibroblast proliferation, blood vessels failed to form. Thus, we hypothesize that the excessive proliferation of the supporting cells at the scaffold surface, which leads to higher production of ECM, and higher secretion of proangiogenic factors is a prerequisite for blood vessel formation and stabilization.

Additionally, the cells forming the endothelial sheets appeared to express nuclear YAP and cytoplasmic β-catenin. The wnt/β-catenin pathway has been shown to enhance the recruitment of mural cells by PDGF-B and to stabilize the forming vessel (Reis and Liebner, 2013). Thus, we speculate that the endothelial sheets recruit the supporting cells, which then provide mechanical support (Bergers and Song, 2005) and proangiogenic signals (Welti et al., 2013), enabling formation of blood vessels.

The presented model is unique in its reproducibility, independent of the specific cell types or the biomaterials that were used. Coseeding endothelial cells and supporting cells, from different primary cells, within supportive 3D environments allows for the formation of vessel-like structures. The culture conditions for vessel formation, such as cell ratios and media content, may vary according to the specific cell type and specific donor. However, once the vessel network is formed, endothelial cell migration into the scaffold depth and proliferation of supporting cells on the scaffold surface were detected. Though, we cannot exclude that altering the experiment design and the cell type will result in a different phenomenon. The ability to track these processes within 3D environments *in vitro* will enable us to further characterize location-specific cell characteristics.

AUTHOR CONTRIBUTIONS

ShiL performed the research; ShiL, SG, and ShuL designed the research, analyzed the data, and wrote the article.

ACKNOWLEDGMENTS

This work was supported by the European Research Council under the European Union's Seventh Framework Program (FP/2007-2013): ERC Grant Agreement no. [281501 – ENGVASC] and by the I-CORE Program of the Planning and Budgeting Committee and The Israel Science Foundation (Grant # 1902/12). We thank Janette Zavin for her help with cryosections and histology.

SUPPLEMENTARY MATERIAL

The Supplementary Material for this article can be found online at http://www.frontiersin.org/articles/10.3389/fbioe.2018.00002/full#supplementary-material.

FIGURE S1 | NG2 and VWF staining of vessel constructs. ECs and fibroblasts were seeded into a gelfoam scaffold, fixed and then stained for vWF (red, for ECs) and NG2 (green, for fibroblasts). Images present the endothelial cell and fibroblast morphology at different depths of the scaffold on day 14 of culturing.

FIGURE S2 | Lumenized vascular networks. 3D confocal imaging show lumen formation within the vessels, ZY and ZX are transverse views of the vessels.

REFERENCES

Azzolin, L., Panciera, T., Soligo, S., Enzo, E., Bicciato, S., Dupont, S., et al. (2014). YAP/TAZ incorporation in the β-catenin destruction complex orchestrates the Wnt response. *Cell* 158, 157–170. doi:10.1016/j.cell.2014.06.013

Bergers, G., and Song, S. (2005). The role of pericytes in blood-vessel formation and maintenance 1. *Neuro Oncol.* 7, 452–464. doi:10.1215/S1152851705000232

Blinder, Y. J., Freiman, A., Raindel, N., Mooney, D. J., and Levenberg, S. (2015). Vasculogenic dynamics in 3D engineered tissue constructs. *Sci. Rep.* 5, 17840. doi:10.1038/srep17840

Carmeliet, P., and Jain, R. K. (2011). Molecular mechanisms and clinical applications of angiogenesis. *Nature* 473, 298–307. doi:10.1038/nature10144

Cheng, C., Smith, S. K., and Charnock-Jones, D. S. (2003). Wnt-1 signaling inhibits human umbilical vein endothelial cell proliferation and alters cell morphology. *Exp. Cell Res.* 291, 415–425. doi:10.1016/j.yexcr.2003.07.006

Clevers, H. (2006). Wnt/β-catenin signaling in development and disease. *Cell* 127, 469–480. doi:10.1016/j.cell.2006.10.018

Freiman, A., Shandalov, Y., Rozenfeld, D., Shor, E., Segal, S., Ben-David, D., et al. (2016). Adipose-derived endothelial and mesenchymal stem cells enhance vascular network formation on three-dimensional constructs in vitro. *Stem Cell Res. Ther.* 7, 5. doi:10.1186/s13287-015-0251-6

Holger, E. W., and Christer Betsholtz, G. (2003). Endothelial – pericyte interactions in angiogenesis. *Cell Tissue Res.* 314, 15–23. doi:10.1007/s00441-003-0745-x

Koffler, J., Kaufman-Francis, K., Shandalov, Y., Yulia, S., Egozi, D., Dana, E., et al. (2011). Improved vascular organization enhances functional integration of engineered skeletal muscle grafts. *Proc. Natl. Acad. Sci. U.S.A.* 108, 14789–14794. doi:10.1073/pnas.1017825108

Koike, N., Fukumura, D., Gralla, O., Au, P., Schechner, J. S., and Jain, R. K. (2004). Tissue engineering: creation of long-lasting blood vessels. *Nature* 428, 138–139. doi:10.1038/428138a

Lamalice, L., Le Boeuf, F., and Huot, J. (2007). Endothelial cell migration during angiogenesis. *Circ. Res.* 100, 782–794. doi:10.1161/01.RES.0000259593.07661.1e

Landau, S., Szklanny, A. A., Yeo, G. C., Shandalov, Y., Kosobrodova, E., Weiss, A. S., et al. (2017). Tropoelastin coated PLLA-PLGA scaffolds promote vascular network formation. *Biomaterials* 122, 72–82. doi:10.1016/j.biomaterials.2017.01.015

Mirabella, A. T., Macarthur, J. W., Cheng, D., Ozaki, C. K., Yoo, Y. J., and Yang, M. (2017). 3D printed vascular networks direct therapeutic angiogenesis in ischemia. *Nat. Biomed. Eng.* 1. doi:10.1038/s41551-017-0083

Nguyen, D.-H. T., Stapleton, S. C., Yang, M. T., Cha, S. S., Choi, C. K., Galie, P. A., et al. (2013). Biomimetic model to reconstitute angiogenic sprouting morphogenesis in vitro. *Proc. Natl. Acad. Sci. U.S.A* 110, 6712–6717. doi:10.1073/pnas.1221526110

Perry, L., Ben-Shaul, S., Landau, S., and Levenberg, S. (eds) (2017). "Co-culture systems for vasculogenesis," in *Vascularization for Tissue Engineering and Regenerative Medicine* (Cham: Springer International Publishing), 1–29.

Reis, M., and Liebner, S. (2013). Wnt signaling in the vasculature. *Exp. Cell Res.* 319, 1317–1323. doi:10.1016/j.yexcr.2012.12.023

Shandalov, Y., Egozi, D., Koffler, J., Dado-Rosenfeld, D., Ben-Shimol, D., Freiman, A., et al. (2014). An engineered muscle flap for reconstruction of large soft tissue defects. *Proc. Natl. Acad. Sci. U.S.A* 111, 6010–6015. doi:10.1073/pnas.1402679111

Shweiki, D., Itin, A., Soffer, D., and Keshet, E. (1992). Vascular endothelial growth factor induced by hypoxia may mediate hypoxia-initiated angiogenesis. *Nature* 359, 843–845. doi:10.1038/359843a0

Volz, K. S., Jacobs, A. H., Chen, H. I., Poduri, A., McKay, A. S., Riordan, D. P., et al. (2015). Pericytes are progenitors for coronary artery smooth muscle. *Elife* 4, 1–22. doi:10.7554/eLife.10036

Welti, J., Loges, S., Dimmeler, S., and Carmeliet, P. (2013). Recent molecular discoveries in angiogenesis and antiangiogenic therapies in cancer. *J. Clin. Invest.* 123, 3190–3200. doi:10.1172/JCI70212

Conflict of Interest Statement: The authors declare that the research was conducted in the absence of any commercial or financial relationships that could be construed as a potential conflict of interest.

The reviewer AS and handling Editor declared their shared affiliation.

frontiers in Bioengineering and Biotechnology

METHODS
published: 05 February 2018
doi: 10.3389/fbioe.2018.00003

A Low Cost Implantation Model in the Rat That Allows a Spatial Assessment of Angiogenesis

Paul Slezak[1], Cyrill Slezak[2], Joachim Hartinger[1], Andreas Herbert Teuschl[3], Sylvia Nürnberger[4], Heinz Redl[1] and Rainer Mittermayr[1]*

[1] Ludwig Boltzmann Institute for Experimental and Clinical Traumatology, Vienna, Austria, [2] Utah Valley University, Orem, UT, United States, [3] Department of Biochemical Engineering, University of Applied Sciences Technikum Wien, Vienna, Austria, [4] Department of Trauma Surgery, Medical University of Vienna, Vienna, Austria

There is continual demand for animal models that allow a quantitative assessment of angiogenic properties of biomaterials, therapies, and pharmaceuticals. In its simplest form, this is done by subcutaneous material implantation and subsequent vessel counting which usually omits spatial data. We have refined an implantation model and paired it with a computational analytic routine which outputs not only vessel count but also vessel density, distribution, and vessel penetration depth, that relies on a centric vessel as a reference point. We have successfully validated our model by characterizing the angiogenic potential of a fibrin matrix in conjunction with recombinant human vascular endothelial growth factor (rhVEGF165). The inferior epigastric vascular pedicles of rats were sheathed with silicone tubes, which were subsequently filled with 0.2 ml of fibrin and different doses of rhVEGF165, centrically embedding the vessels. Over 4 weeks, tissue samples were harvested and subsequently immunohistologically stained and computationally analyzed. The model was able to detect variations over the angiogenic potentials of growth factor spiked fibrin matrices. Adding 20 ng of rhVEGF165 resulted in a significant increase in vasculature while 200 ng of rhVEGF165 did not improve vascular growth. Vascularized tissue volume increased during the first week and vascular density increased during the second week. Total vessel count increased significantly and exhibited a peak after 2 weeks which was followed by a resorption of vasculature by week 4. In summary, a simple implantation model to study *in vivo* vascularization with only a minimal workload attached was enhanced to include morphologic data of the emerging vascular tree.

Keywords: fibrin, VEGF, animal models, angiogenesis, computational analysis

OPEN ACCESS

Edited by:
Andrea Banfi,
University of Basel, Switzerland

Reviewed by:
Martin Ehrbar,
University of Zurich, Switzerland
Nicolas Rivron,
Hubrecht Institute (KNAW),
Netherlands

****Correspondence:***
Paul Slezak
paul.slezak@trauma.lbg.ac.at

Specialty section:
This article was submitted to Tissue Engineering and Regenerative Medicine, a section of the journal Frontiers in Bioengineering and Biotechnology

Received: *23 September 2017*
Accepted: *15 January 2018*
Published: *05 February 2018*

Citation:
Slezak P, Slezak C, Hartinger J, Teuschl AH, Nürnberger S, Redl H and Mittermayr R (2018) A Low Cost Implantation Model in the Rat That Allows a Spatial Assessment of Angiogenesis. Front. Bioeng. Biotechnol. 6:3. doi: 10.3389/fbioe.2018.00003

BACKGROUND

The ability to understand and manipulate angiogenic processes has become a key element of many therapeutic approaches. Angiogenesis is an essential factor in wound healing and the backbone of any successful tissue engineering attempt (Li et al., 2003; Michlits et al., 2007; Rophael et al., 2007; Lovett et al., 2009; Buehrer et al., 2015). To study the complex system of biomaterials and growth factor stimuli that govern the process of angiogenesis, various *in vivo* and *in vitro* models have been developed (Norrby, 2006; Staton et al., 2009; Poulaki, 2011). Many animal models (Kneser et al., 2006; Arkudas et al., 2007; Malinda, 2009) rely on the concept of implanting biomatrices, which can be loaded with various growth factors or cells and allow the ingrowth of vascular structures.

The emerging vasculature may then be tracked *via* techniques of varying technical complexity. These include *in vivo* perfusion with casting agents and subsequent scanning electron microscopy (Polykandriotis et al., 2008) of the resulting corrosion casts, magnetic resonance angiography (Polykandriotis et al., 2008), photoacoustic imaging (Meiburger et al., 2016), or *in vivo* perfusion with radiopaque contrast agents and *ex vivo* computer tomography scans (Sider et al., 2010). While these methods yield full three-dimensional representations of the vascular trees they usually do not succeed in detecting capillaries as contrast agent perfusion in the smallest of vessels is limited. To include these, histologic staining and counting of vessel cross sections is still commonly performed (Tilkorn et al., 2012; Lilja et al., 2013). The goal of this study was to combine an implantation based model of angiogenesis (Cronin et al., 2004; Rophael et al., 2007; Tilkorn et al., 2012; Lilja et al., 2013) that is time and work efficient with a computational analysis of manually marked vessels. This provides insight into the morphology of newly developed vascular structures that goes beyond simple vessel counting and does not require sophisticated technical equipment. We aim to facilitate the assessment of angiogenic properties of biomaterials and growth factors in conjunction with a characterization of the resulting vascularization, based on a spatial analysis of basic histologic slices, that results in an array of morphological read out parameters that provide a comprehensive representation of newly formed vasculature.

MATERIALS AND METHOD

Study Design

A modified implantation model of biomaterial filled silicone tubes (Cronin et al., 2004; Tilkorn et al., 2012; Lilja et al., 2013) around the inferior epigastric bundle in Sprague Dawley rats weighing between 350 and 450 g was used. The study design consisted of two parts: first, four groups of $N = 10$ samples were set up to study the angiogenic effect of recombinant human vascular endothelial growth factor (rhVEGF165) (PeproTech, Rocky Hill, NJ, USA) inside a fibrin matrix after a time period of 4 weeks. Second, three groups of $N = 6$ samples were set up to study the dynamics of vascularization in a fibrin matrix over time (baseline, 1 week, 2 weeks).

The growth factor treatment groups consisted of a low dose group [0.2 ml fibrin matrix (ARTISS, Baxter AG, Vienna, Austria) loaded with 20 ng rhVEGF165] and a high dose group (0.2 ml fibrin matrix loaded with 200 ng rhVEGF165). A carrier group received 0.2 ml fibrin matrix without the addition of rhVEGF165. A control group received tubes with no biomaterial filling.

The additional groups evaluating the dynamics of the level of vascularization ($N = 6$ samples) received a fibrin matrix with no external growth factor added. Two of these groups consisted of animals sacrificed and evaluated after 1 or 2 weeks, respectively. The group representing the initial time point of surgery (baseline) consisted of animals, which were already dead at the time of implantation. The assessment of the final time point at week 4 was based on the data gained from the fibrin only group described earlier ($N = 10$ samples).

Surgical Procedure

The animals were anesthetized with isoflurane 3% (Forane, Baxter AG, Vienna, Austria) while analgesia was provided by a single shot of buprenorphin, 0.01 mg/kg (Buprenovet, Bayer, Leverkusen, Germany) and meloxicam, 0.1 mg/kg (Metacam, Boeringer Ingelheim, Germany), daily, for a period of 3 days. The animal's inguinal region was shaven and a longitudinal incision of approximately 1.5 cm was made bilaterally (**Figure 1**). The branching of the inferior epigastric bundle from the femoral bundle was exposed and the epigastric vessel trunk was carefully dissected and isolated on each side. Thereafter, custom made silicone tubes were placed around the vascular bundle in order to create a protected niche within the silicone shielding, centrically harboring artery, vein, and nerve. This provided a standardized volume for angiogenesis, in which newly formed vascular structures could be attributed to the specific local conditions and vascular ingrowth from surrounding tissue can be ruled out.

Silicone Tubes

The implanted medical grade silicone tubes measured 1.5 cm in length, with an outer diameter of 6 mm and a wall thickness of 1 mm (**Figure 1**). A silicone membrane was glued onto each end of the tube, with a central aperture, allowing entry of the vascular bundle. The tubes were cut open on their sides in order to slip them around the vascular bundle. Once *in situ*, the tubes were closed with surgical sutures and filled with fibrin matrix and growth factors according to the group setup. They then remained inside the animals for up to 4 weeks before being harvested and analyzed. The implanted tubes were well tolerated by the animals, which showed no signs of pain, discomfort, or physical impairment. Further, no effect on gait was observed.

Histologic Analysis

Each animal yielded two cylindrical tissue samples which were extracted immediately after euthanization. They were fixed with

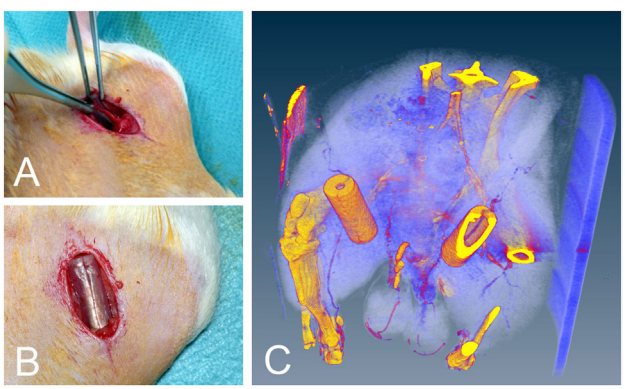

FIGURE 1 | **(A)** Location of the vascular bundle before implantation. **(B)** Implanted silicone tubes. **(C)** Silicone tube *in situ* micro CT image. Note the perfused epigastric vascular bundle passing through the tube. The CT scan was performed in a single animal only to visually present the implantation and was not included in the analysis.

4% neutral buffered formalin and after 24 h rinsed in water for 1 h. The samples were then transferred into 50% ethanol for 1 h and stored in 70% ethanol. Dehydration was completed with further increase of the graded series of alcohol and embedded in paraffin *via* the intermedium xylol. The samples were sectioned in a plane perpendicular to the central axis at the middle of the harvested tissue cylinder at a thickness of 3–4 µm, resulting in circular slices with a centric artery and vein. They were subsequently deparaffinized and stained immunohistochemically for smooth muscle actin (SMA) and the cluster of differentiation 31 (CD31). SMA identifies the contractile cytoskeleton in the pericytes of mature vessels while CD31 stains endothelial cells and therefore additionally identifies emerging vessels and small capillaries (Helfrich et al., 2010) (**Figure 2**). Sections were prepared by blocking the endogenous peroxides with 3% hydrogen peroxide and antibody retrieval with steaming at pH 9.0 in HIER-T EDTA Puffer (ZUC029, Zytomed) or Dako Target Retrieval Solution pH 9.0 (S2367), respectively. SMA antibody (A 2547, Sigma) was then incubated in 1:5,000 and CD31 antibody (sc1506-R Santa Cruz) 1:100, both for 1 h. As secondary antibody, a polymer labeled antibody was used (ImmPRESS™, Vector Laboratories, Burlingame, CA, USA) and incubated for 30 min. Visualization was done with a peroxidase substrate kit (NovaRED™, Vector Laboratories, Burlingame, CA, USA) and counterstaining with hematoxylin.

An Olympus BX61VS scanning microscope was employed to obtain high resolution, full size scans of the samples at a resolution of 644 nm per pixel at a magnification of 200×.

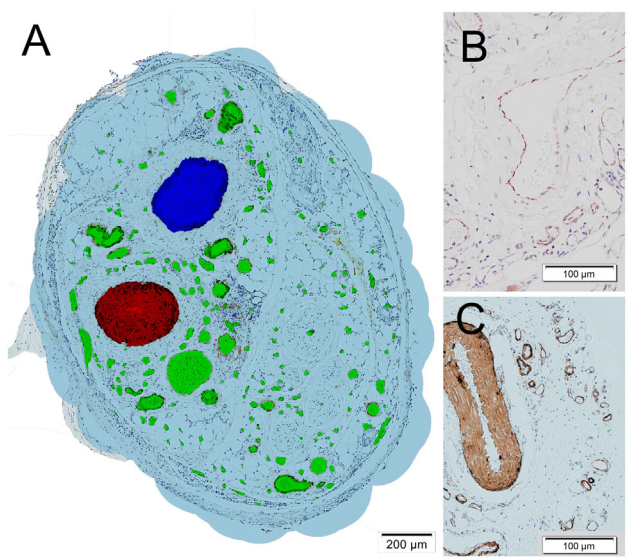

FIGURE 2 | **(A)** Histologic section of a tissue sample obtained from one of the fibrin matrix filled tubes after 4 weeks. The cross sections of vessels were marked manually. The epigastric vein is marked in blue, the epigastric artery in red, other vessels including *de novo* capillaries in green. A virtual oxygen perfusion radius of 150 µm (Lovett et al., 2009) was marked in light blue around each vessel to illustrate and define an area which could potentially be supported by the vascular tree. **(B)** Detail of cluster of differentiation 31 stained vessels. **(C)** Detail of smooth muscle actin stained vessels.

Image Analysis

On the obtained high resolution pictures, all vessel cross section were marked manually in their full extent by experienced researchers in a commercial image editor and color coded to enable automated vessel type detection (central artery red, central vein blue, capillaries green) (**Figure 2**). A vascular wall stained with either SMA or CD31 with a visible lumen or the presence of erythrocytes was used to identify vessel cross sections. The vessel markings were then automatically analyzed using the freely available software tool cell profiler (Carpenter et al., 2006), applying a detection and measuring pipeline in order to detect geometric shape, size, and location of the vessel cross sections.

The tricolored vessel markings were resampled to a size of 2,500 × 2,500 pixels and a color split conversion was performed to produce images only featuring the markings of a specific vessel type. The subsequent standard cell profiler object detection routine was then able to detect the marking of each vessel at 100% accuracy. Vessel center position, vessel area, and vessel major axis lengths were measured. In order to obtain a virtual estimate of perfusion, all detected vessels were then expanded by a radius of 150 µm (Lovett et al., 2009), which was executed within the same analytical routine. Finally, all obtained data were exported and further processed in a custom made Mathematica workflow for image identification, group allocation, and numerical analysis of the measurements including a statistical analysis.

Multi Parameter Analysis

- Total vessel count—the total vessel count represents the total amount of vessel cross sections found in each sample, excluding the central artery and central vein.
- Total perfused area—to quantify the amount of tissue that could potentially be supported by the samples vascular network, a virtual perfusion area was introduced. The cross section of each detected vessels was expanded by a defined radius of 150 µm, representing the potential diffusion of oxygen into the tissue (Lovett et al., 2009). Overlapping perfused areas were single counted. The total of these areas was then calculated to obtain the final result. As such it is the area potentially perfused by the sum of all vessels found in the tissue cross section.
- Perfused area vessel density—the perfused area served as an approximate quantifier for the extent of the tissue surrounding the vascular tree, which in return permitted the calculation of vessels density within this tissue area. Each sample's perfused area vessel density was calculated individually as the ratio of total vessel count and total perfused area.
- Vessel ingrowth distance—to assess the morphology of each vascular tree, the penetration depth of each vessel cross section into the scaffold was calculated. This parameter was obtained by measuring the linear distance from each marked vessels center to the central vein's center. For this calculation, it was assumed that the vessels origin is the central vein according to Polykandriotis et al. (2008). This represents the depth of vascular penetration into the tissue.
- Vessel diameter—to further analyze vascular morphology, we determined the distribution of the vascular diameters in each sample. In our analysis, the vessels diameter was defined to be the minor axis of a vessel's marked elliptical cross sections,

including the vascular wall. This assured a representative diameter in oblique and elliptical cross sections of vessels and minimized the effects of compression artifacts.

Statistical Method

Throughout this paper, all statistical comparisons of means between experimental groups employed one-way analysis of variance (ANOVA) at a 95% confidence level ($\alpha = 0.05$). *Post hoc* comparisons were conducted using a Duncan comparison test with figures indicating level of significance by the number of *'s ($p = 0.05$, 0.01, and 0.001). All uncertainty estimates are SEM.

RESULTS

Vessel Growth Dynamics

Vessel Count and Perfused Area

The longitudinal collection of samples allowed for the consideration of the dynamical processes of angiogenesis (**Figures 3–5**). The implanted sample of week 0 showed a significant SMA (and CD31) stained increase [$F(3,27) = 8.32$, $p = 0.001$] {CD31: [$F(3,27) = 11.37$, $p = 0.000$]} in the number of 54 ± 11 (CD31: 214 ± 55) vessels over the first 2 weeks to a peak value of 208 ± 21 (CD31: 728 ± 114) (**Figure 3**). In the subsequent 2 weeks, we observed the effects of resorption reducing the vessel count to 111 ± 21 (CD31: 308 ± 49) at week 4. Further insight into the underlying dynamic processes was gained by considering the changes in vascularized vessel density and area (**Figures 4** and **5**).

The assessment of SMA vessel growth dynamics revealed a statistically significant [$F(3,27) = 3.64$, $p = 027$] increase in vasculature density to a peak of 101 ± 7 vessels/mm^2 after 2 weeks which had remained constant over prior measurements at 66 ± 8 vessels/mm^2 (**Figure 4**). We further observed that this increase in vascularization density was preceded by a significant [$F(3,27) = 7.09$, $p = 0.001$] increase in vascularized area during the first week from 0.80 ± 0.11 to 2.03 ± 0.17 mm^2 (**Figure 5**), while no concurrent change was observed in vessel density. Subsequently, in the second week, the vascularized area remained constant, while the aforementioned vessel density peaked. Thereafter, we observed the onset of resorption of mature, SMA positive vasculature which is manifested in a significant decrease [$F(3,27) = 3.64$, $p = 0.027$] vessel density while largely maintaining the vascularized area in week 4 (63 ± 10 vessels/mm^2 and 1.74 ± 0.23 mm^2) (**Figures 4** and **5**).

Emerging, CD31-positive vascularization tells a similar story: an initial increase in vascularized area from 1.46 ± 0.40 to 2.60 ± 0.12 mm^2 after 1 week that shows no significant change thereafter [$F(3,27) = 1.97$, $p = 0.145$] (**Figure 5**). Similarly, we observed no concurrent initial change in vascularization density after 1 week over the initial 158 ± 20 vessels/mm^2. Subsequently however, we once again observed a significant spike [$F(3,27) = 6.37$, $p = 0.002$] to a peak density of 412 ± 111 vessels/mm^2 at week 2 before the resorption drop in week 4 to 128 ± 15 vessels/mm^2 (**Figure 4**).

Diameter and Ingrowth Distance

The distribution of mature, SMA positive vessel diameters within the vascular tree remained unaltered over time. The numerically largest changes were observed in the capillary domain, as seen in **Figure 6**. When analyzing the ingrowth distances of the vessels, we saw a trend in accordance with the vascularized area results, with an initial increase in spread and a following decrease in penetration depth after 4 weeks as vascular resorption takes place.

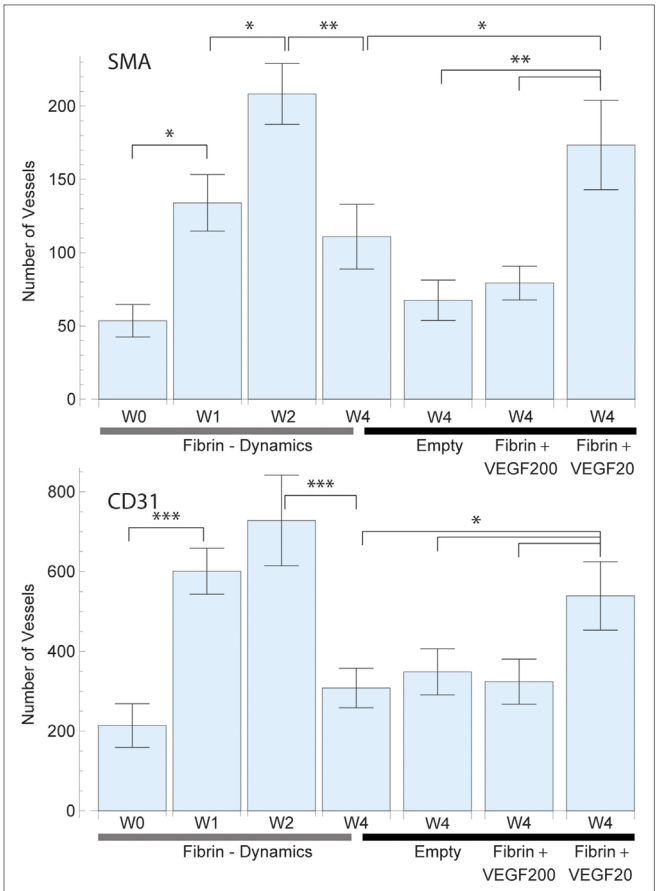

FIGURE 3 | Average total vessel count per sample in each of the study groups for smooth muscle actin (SMA) (top) and CD31 (bottom) staining. The left 4 bars indicate the vascular growth in pure fibrin over a period of 4 weeks. A constant increase in vascularization was observed up to week 2, followed by vascular resorption. The right 4 bars indicate the effect of high dose (200 ng) and low dose (20 ng) recombinant human vascular endothelial growth factor (rhVEGF165) in a fibrin matrix in comparison to pure fibrin and no matrix. A statistical significant difference between the high and low dose rhVEGF165 group was detected. 20 ng rhVEGF165 yielded the best results, while 200 ng was comparable to the empty control.

Growth Factor Effects

Total Vessel Count

Vessel detection was performed for both SMA and CD31 stained sections as shown in **Figure 3**. CD31 staining yielded a higher vessel count throughout the study as expected. After 4 weeks, the average vessel count in SMA stained sliced totaled 111 ± 22 (CD31: 308 ± 49) in the fibrin matrix group, while the empty control group totaled 68 ± 14 (CD31: 349 ± 58) (**Figure 3**). The addition of 20 ng of rhVEGF165 to the fibrin matrix resulted

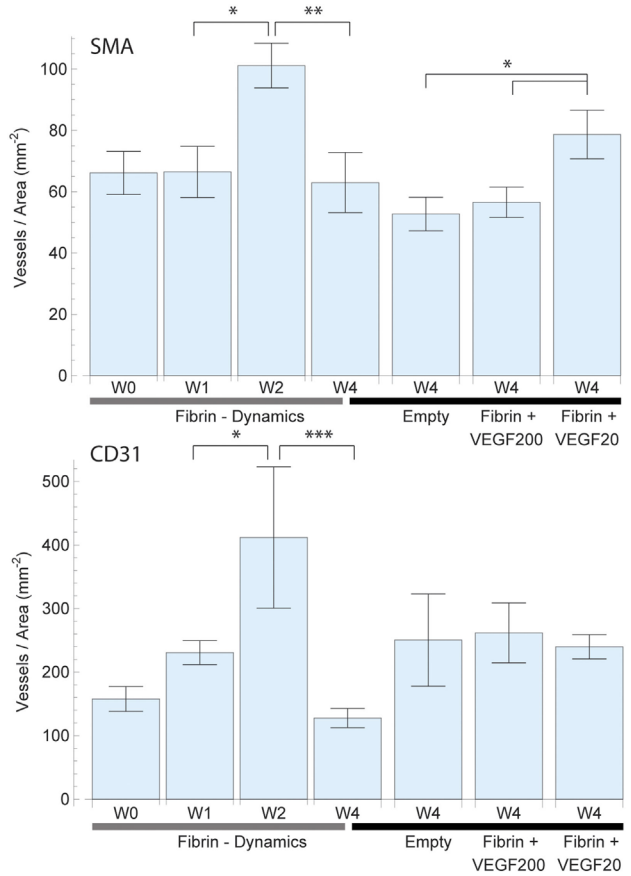

FIGURE 4 | Mean vessel density based on the vascularized area of each individual sample for smooth muscle actin (SMA) (top) and CD31 (bottom) staining. The total vascularized area was calculated by expanding and adding up each vessel cross section by a defined radius of 150 µm representing the potential diffusion of oxygen into the tissue. Overlapping areas were single counted. The left 4 bars indicate the change in vascular density in fibrin over a period of 4 weeks, which peaked at week 2. The right 4 bars indicate the effect of high dose (200 ng) and low dose (20 ng) recombinant human vascular endothelial growth factor (rhVEGF165) in a fibrin matrix in comparison to pure fibrin and no matrix. The 20 ng rhVEGF165 group yielded the best results and a statistical significant difference to the empty control group was detected.

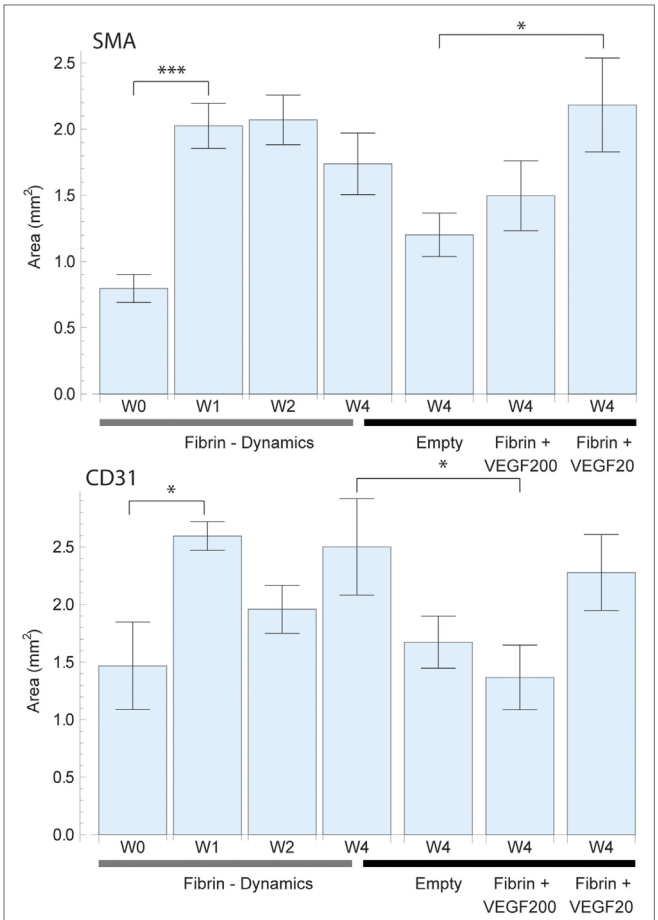

FIGURE 5 | Total perfused area based on a virtual perfusion distance of oxygen which was defined as 150 µm around each vessel for smooth muscle actin (SMA) (top) and CD31 (bottom) staining. The perfused area was calculated by expanding adding up each vessel cross section by 150 µm. Overlapping areas were single counted. The left 4 bars indicate the change in perfused area in pure fibrin over a period of 4 weeks. There was an initially strong increase in vascularized area which then remained constant. The right 4 bars indicate the effect of high dose (200 ng) and low dose (20 ng) recombinant human vascular endothelial growth factor (rhVEGF165) in a fibrin matrix in comparison to pure fibrin and no matrix. The positive effects of fibrin and rhVEGF165 as well as missing effect of excessive rhVEGF165 dosings are confirmed once more.

in an increase of the mean vessel count to 174 ± 31 (CD31: 539 ± 86). At the same time, adding 200 ng of rhVEGF165 diminished vascular growth and resulted in a vessel count of 79 ± 12 (CD31: 324 ± 56) (**Figure 3**). An ANOVA comparison indicates a statistically significant difference among the groups [$F(3,39) = 5.17$, $p = 0.004$] {CD31: [$F(3,39) = 2.82$, $p = 0.05$]}. A further comparison indicates the 20 ng rhVEGF165 group to be statistically different from the other tested groups.

Vessel Density and Total Perfused Area

The vessel density (**Figure 4**) and total perfused area (**Figure 5**) mirrored the trends observed in total vessel count in the SMA stained samples, indicating a similar beneficial effect of rhVEGF165. The addition of 20 ng rhVEGF165 resulted in a vessel density of 78 ± 8 vessels/mm^2 (**Figure 4**) and a perfused area of 2.18 ± 0.35 mm^2 (**Figure 5**). Again, high doses of rhVEGF165 appears to have no angiogenic impact as results in both vessel density of 56 ± 5 vessels/mm^2 and perfused area of 1.50 ± 0.26 mm^2 were in the range of the empty control group (density: 53 ± 5 vessels/mm^2, area: 1.20 ± 0.16 mm^2). No statistical significant difference in perfusion area and density were found [$F(3,39) = 2.48$, $p = 0.07$] and [$F(3,39) = 2.45$, $p = 0.08$].

Similar results were obtained for CD31: the addition of high doses of rhVEGF165 did not improve angiogenesis, resulting in a smaller perfusion area of 1.36 ± 0.28 mm^2 over the fibrin matrix 2.50 ± 0.41 mm^2 (**Figure 5**). No statistical significant difference in perfusion area and density were found [$F(3,39) = 2.66$, $p = 0.06$] and [$F(3,39) = 1.91$, $p = 0.14$].

Vessel Ingrowth

Concerning the morphology of the vascular tree, we were able to follow a trend that the use of a fibrin matrix, and even more so the addition of 20 ng rhVEGF165, would increase the ingrowth distance of mature, SMA positive vessels into the scaffold when compared to the empty control group (**Figure 8**). An equivalent behavior is observed in emerging, CD31 positive vessels.

Vessel Diameter

Analysis of both mature, SMA positive and emerging, CD31 positive vessel diameters showed that the different treatment options had no apparent influence on diameter distribution. While the numerically largest gain in vasculature was detected within the capillary diameter range, the ratio between larger and smaller vessels showed no strong alteration, with a proportionally increase in thicker vessels (**Figure 7**). Furthermore, the model clearly showed that CD31 stained vessels resulted in smaller average diameter than SMA stained vessel.

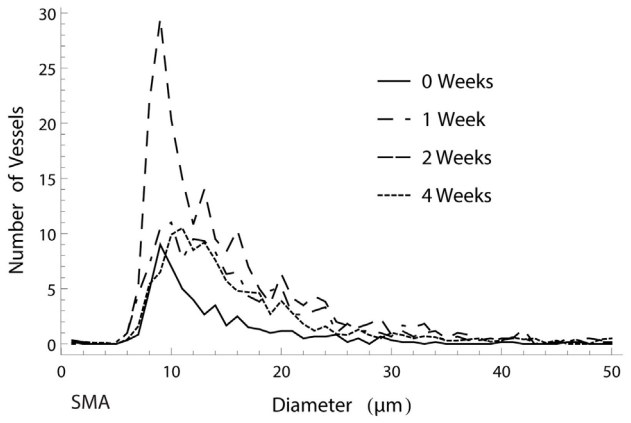

FIGURE 6 | Histogram of the amount of smooth muscle actin (SMA) positive vessels of different diameters over the course of 4 weeks. The numerically largest gain in vessels was observed in week 2 in the capillary range.

DISCUSSION

When establishing our model we meant to optimize it on two levels: first of all, we aimed for a comprehensive evaluation of vascular structures, going beyond a mere vessel count and second, we sought to keep it simple, efficient, and cost effective. Tanaka et al. (2003) have compared different vessel configurations inside implanted biomatrices and have outlined the benefits of an arteriovenous loop setup when creating larger tissue constructs. However, this would include microvascular anastomosis (Kneser et al., 2006; Arkudas et al., 2007; Buehrer et al., 2015) of small vessels and requires a considerable surgical effort. While this is worthwhile when aiming for large tissue quantities (Tanaka et al., 2003), in our analytical approach we favored the symmetrical tissue samples produced by a simple flow through configuration. This provided us with a standardized anatomic reference point (the central vein) needed to determine ingrowth distances. The measured main parameters (position, shape, diameter, vessel count) are then sufficient to calculate a satisfying diversity in parameters like vascular ingrowth distance, vessel density, and spatial distribution as well as diameter distribution, allowing potential comparisons between different growth factors, therapies, materials, and time points.

The model was refined to be a time efficient tool and seeks to keep all tasks involved as time economical and simple as possible. The surgical procedure requires no advanced micosurgical training or operative microscope and is swiftly performed within a few minutes per sample. Analytical procedures consist of basic immunohistologic staining and none of the steps involved, including vessel detection and microscopic scanning takes more than a few minutes per sample.

We validated our model, with a fibrin sealant as it is a frequently used and well-known matrix material (Wong et al., 2003; Arkudas et al., 2007; Mittermayr et al., 2008; Heher et al., 2017) and gives opportunity to portray its angiogenic effect as reference. We showed and detailed this angiogenic effect (Arkudas et al., 2007; Rophael et al., 2007; Mittermayr et al., 2008) in our model,

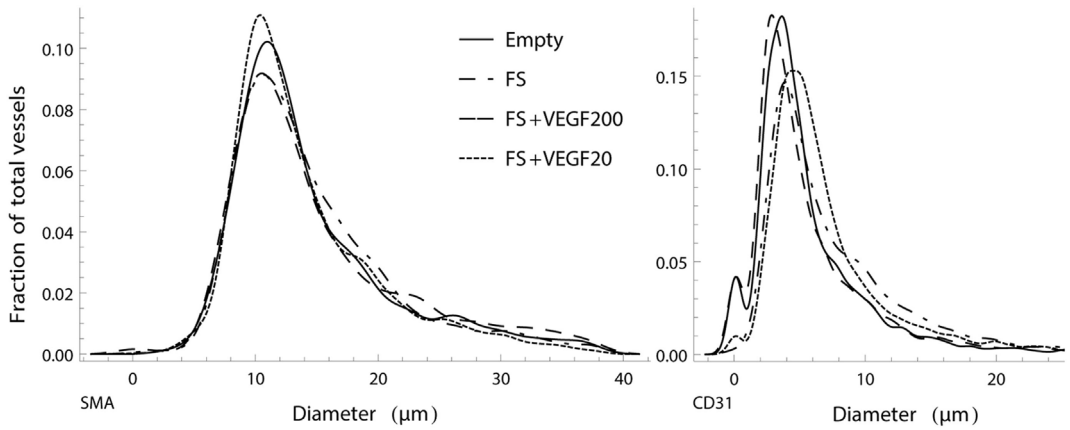

FIGURE 7 | Normalized, smoothed histogram of vessel diameters as a fraction of the total vessels count for smooth muscle actin (SMA) (left) and CD31 (right) staining. The distribution of vessel diameters in the vascular tree is similar between the study groups and suggests that there is no strong influence of the different treatments in regard to ratio of larger to smaller vessels.

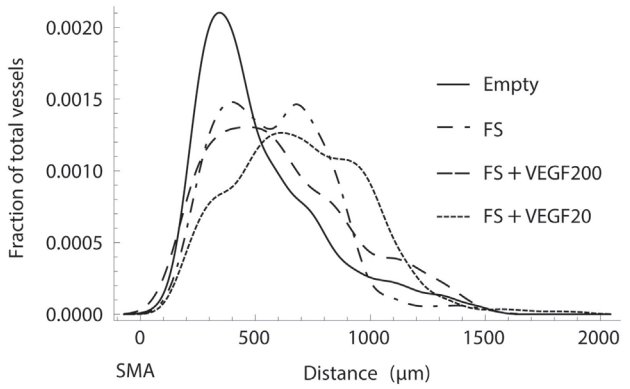

FIGURE 8 | Normalized histogram of the transversal ingrowth distance of vessels into the scaffold as a fraction of the total vessels count. Fibrin with 20 ng of recombinant human vascular endothelial growth factor (rhVEGF165) resulted in the strongest ingrowth while it was severely limited in the absence of a fibrin matrix.

which has led to an increase in newly formed vessels after 4 weeks compared to the control group. We further showed its positive effect in spatial parameters like vessel density, perfused area (which translates into vascularized tissue volume in 3D), vessel penetration depth and assessed vessel diameter. This information is problematic to obtain in standard subcutaneous implantations that lack a standardized reference point and where the specific origin of ingrowing vessels is unknown and where area and density calculations rely on predefined regions of interest which may introduce a certain bias. We also assessed the dynamics of vascularization based on these parameters, depicting a rather high initial vessel count immediately after surgery, which mostly consisted of vessels in the regime of capillaries that where in close proximity to the vascular bundle, which were not removable surgically. This was followed by a gradual outward growth of vessels and their subsequent resorption inside the fibrin biomatrix, in accordance with Arkudas et al. (2007) and Rophael et al. (2007). Through the spatial analysis, we were able to detail the specific parameters in which these changes took place: after 1 week, with the fibrin matrix still in place, we observed an increase in vasculature based on an increase in vascularized volume, while at the same time vessel density remained constant. At the 2 weeks time point however, with the fibrin matrix completely degraded, vascular growth was based on a constant vascularized volume and an increase in vessel density. We attribute this growth pattern to the scaffolding function of the fibrin matrix during the first week and to its ability to bind physiologic growth factors which affects vascular growth during the second week.

To further prove the model as a tool to assess advanced therapeutic effects, rhVEGF165 was added to the fibrin matrix and we validated its efficacy profile (Wong et al., 2003; Mittermayr et al., 2008). Adding 20 ng of rhVEGF165 resulted in an increase in vessel count as well as an increase in both, vascularized volume and vessel density when compared to pure fibrin, proving its angiogenic effect. Again, these changes were also represented in the spatial analysis of mature, SMA positive vessel distribution which revealed an increased ingrowth distance. The analysis of the vascular trees morphology further nicely showed that the numerically largest changes in vasculature took place within the capillary diameter range, with a distinct difference in total capillaries between the study groups. We also included a 10-fold higher dose of the growth factor into our study, in order to show physiological dose boundaries (Ozawa et al., 2004) and the ability of the model to detect such. Here, we saw a decrease in newly grown vasculature after 4 weeks when compared to the low dose rhVEGF165 group and the fibrin biomatrix group. Total vessel count dropped to levels comparable to the empty control group, as did vessel density and vascularized area. In general, SMA stained samples and CD31 stained samples yielded the same overall results, however, it is interesting to point out that for all similarities between SMA and CD31 results, specifically the resorption stage in particular is less likely to show differences in total perfused area in CD31 over SMA. This can be easily explained by the significantly larger number of detected CD31 vessels within a comparable area of potential oxygen diffusion which at this stage spans most of the sample. As such, any change in the number of CD31 vessels will not impact said area (due to the widely overlapping areas of the expanded vessels, data not shown) but will possibly result in a significantly different vessel density in SMA data.

In summary, we have refined an animal model of angiogenesis and tissue engineering to include a more detailed analysis and have validated it by characterizing the efficacy profile of a prominent angiogenic growth factor and a commonly used biomatrix. The setup and procedures involved proved to be efficient, economical and easy to execute, requiring only basic histologic techniques and the same workload attached as traditional vessel counting.

ETHICS STATEMENT

Approval to this study by the Animal Protocol Review Board of the City of Vienna was obtained prior to conducting experiments.

AUTHOR CONTRIBUTIONS

PS conducted and designed the study, wrote the manuscript, conducted the surgeries, and performed data analysis. CS conducted data analysis and conceived and performed the analytical methods and wrote the manuscript. JH performed the surgeries and performed data analysis. AT provided material and participated in writing the manuscript as well as in the review process. SN established and conducted the histologic methods and provided scientific input during data analysis and interpretation. HR participated in the study design, data interpretation, the review process, and provided scientific input. RM conceived the study, participated in the surgeries, data interpretation, the review process, and provided scientific input.

FUNDING

This study was partially funded by ANGIOSCAFF (project 214402) and BIODESIGN (project 262948), part of the European Seventh Framework Program. The financial support by the City of Vienna (MA 23—Project # 18-08) is gratefully acknowledged.

REFERENCES

Arkudas, A., Tjiawi, J., Bleiziffer, O., Grabinger, L., Polykandriotis, E., Beier, J. P., et al. (2007). Fibrin gel-immobilized VEGF and bFGF efficiently stimulate angiogenesis in the AV loop model. *Mol. Med.* 13, 480–487. doi:10.2119/2007-00057.Arkudas

Buehrer, G., Balzer, A., Arnold, I., Beier, J. P., Koerner, C., Bleiziffer, O., et al. (2015). Combination of BMP2 and MSCs significantly increases bone formation in the rat arterio-venous loop model. *Tissue Eng. Part A* 21, 96–105. doi:10.1089/ten.tea.2014.0028

Carpenter, A. E., Jones, T. R., Lamprecht, M. R., Clarke, C., Kang, I. H., Friman, O., et al. (2006). CellProfiler: image analysis software for identifying and quantifying cell phenotypes. *Genome Biol.* 7, R100. doi:10.1186/gb-2006-7-10-r100

Cronin, K. J., Messina, A., Knight, K. R., Cooper-White, J. J., Stevens, G. W., Penington, A. J., et al. (2004). New murine model of spontaneous autologous tissue engineering, combining an arteriovenous pedicle with matrix materials. *Plast. Reconstr. Surg.* 113, 260–269. doi:10.1097/01.PRS.0000095942.71618.9D

Heher, P., Mühleder, S., Mittermayr, R., Redl, H., and Slezak, P. (2017). Fibrin-based delivery strategies for acute and chronic wound healing. *Adv. Drug Deliv. Rev.* doi:10.1016/j.addr.2017.12.007

Helfrich, I., Scheffrahn, I., Bartling, S., Weis, J., von Felbert, V., Middleton, M., et al. (2010). Resistance to antiangiogenic therapy is directed by vascular phenotype, vessel stabilization, and maturation in malignant melanoma. *J. Exp. Med.* 207, 491–503. doi:10.1084/jem.20091846

Kneser, U., Polykandriotis, E., Ohnolz, J., Heidner, K., Grabinger, L., Euler, S., et al. (2006). Engineering of vascularized transplantable bone tissues: induction of axial vascularization in an osteoconductive matrix using an arteriovenous loop. *Tissue Eng.* 12, 1721–1731. doi:10.1089/ten.2006.12.1721

Li, J., Zhang, Y. P., and Kirsner, R. S. (2003). Angiogenesis in wound repair: angiogenic growth factors and the extracellular matrix. *Microsc. Res. Tech.* 60, 107–114. doi:10.1002/jemt.10249

Lilja, H. E., Morrison, W. A., Han, X. L., Palmer, J., Taylor, C., Tee, R., et al. (2013). An adipoinductive role of inflammation in adipose tissue engineering: key factors in the early development of engineered soft tissues. *Stem Cells Dev.* 22, 1602–1613. doi:10.1089/scd.2012.0451

Lovett, M., Lee, K., Edwards, A., and Kaplan, D. L. (2009). Vascularization strategies for tissue engineering. *Tissue Eng. Part B Rev.* 15, 353–370. doi:10.1089/ten.TEB.2009.0085

Malinda, K. M. (2009). In vivo matrigel migration and angiogenesis assay. *Methods Mol. Biol.* 467, 287–294. doi:10.1007/978-1-59745-241-0_17

Meiburger, K. M., Nam, S. Y., Chung, E., Suggs, L. J., Emelianov, S. Y., and Molinari, F. (2016). Skeletonization algorithm-based blood vessel quantification using in vivo 3D photoacoustic imaging. *Phys. Med. Biol.* 61, 7994–8009. doi:10.1088/0031-9155/61/22/7994

Michlits, W., Mittermayr, R., Schafer, R., Redl, H., and Aharinejad, S. (2007). Fibrin-embedded administration of VEGF plasmid enhances skin flap survival. *Wound Repair Regen.* 15, 360–367. doi:10.1111/j.1524-475X.2007.00238.x

Mittermayr, R., Morton, T., Hofmann, M., Helgerson, S., van Griensven, M., and Redl, H. (2008). Sustained (rh)VEGF(165) release from a sprayed fibrin biomatrix induces angiogenesis, up-regulation of endogenous VEGF-R2, and reduces ischemic flap necrosis. *Wound Repair Regen.* 16, 542–550. doi:10.1111/j.1524-475X.2008.00391.x

Norrby, K. (2006). In vivo models of angiogenesis. *J. Cell. Mol. Med.* 10, 588–612. doi:10.1111/j.1582-4934.2006.tb00423.x

Ozawa, C. R., Banfi, A., Glazer, N. L., Thurston, G., Springer, M. L., Kraft, P. E., et al. (2004). Microenvironmental VEGF concentration, not total dose, determines a threshold between normal and aberrant angiogenesis. *J. Clin. Invest.* 113, 516–527. doi:10.1172/JCI18420

Polykandriotis, E., Tjiawi, J., Euler, S., Arkudas, A., Hess, A., Brune, K., et al. (2008). The venous graft as an effector of early angiogenesis in a fibrin matrix. *Microvasc. Res.* 75, 25–33. doi:10.1016/j.mvr.2007.04.003

Poulaki, V. (2011). Angiogenesis assays. *Methods Mol. Biol.* 731, 345–358. doi:10.1007/978-1-61779-080-5_28

Rophael, J. A., Craft, R. O., Palmer, J. A., Hussey, A. J., Thomas, G. P. L., Morrison, W. A., et al. (2007). Angiogenic growth factor synergism in a murine tissue engineering model of angiogenesis and adipogenesis. *Am. J. Pathol.* 171, 2048–2057. doi:10.2353/ajpath.2007.070066

Sider, K. L., Song, J., and Davies, J. E. (2010). A new bone vascular perfusion compound for the simultaneous analysis of bone and vasculature. *Microsc. Res. Tech.* 73, 665–672. doi:10.1002/jemt.20807

Staton, C. A., Reed, M. W., and Brown, N. J. (2009). A critical analysis of current in vitro and in vivo angiogenesis assays. *Int. J. Exp. Pathol.* 90, 195–221. doi:10.1111/j.1365-2613.2008.00633.x

Tanaka, Y., Sung, K. C., Tsutsumi, A., Ohba, S., Ueda, K., and Morrison, W. A. (2003). Tissue engineering skin flaps: which vascular carrier, arteriovenous shunt loop or arteriovenous bundle, has more potential for angiogenesis and tissue generation? *Plast. Reconstr. Surg.* 112, 1636–1644. doi:10.1097/01.PRS.0000086140.49022.AB

Tilkorn, D. J., Davies, E. M., Keramidaris, E., Dingle, A. M., Gerrand, Y. W., Taylor, C. J., et al. (2012). The in vitro preconditioning of myoblasts to enhance subsequent survival in an in vivo tissue engineering chamber model. *Biomaterials* 33, 3868–3879. doi:10.1016/j.biomaterials.2012.02.006

Wong, C., Inman, E., Spaethe, R., and Helgerson, S. (2003). Fibrin-based biomaterials to deliver human growth factors. *Thromb. Haemost.* 89, 573–582.

Conflict of Interest Statement: The authors declare that the research was conducted in the absence of any commercial or financial relationships that could be construed as a potential conflict of interest.

frontiers in Bioengineering and Biotechnology

ORIGINAL RESEARCH
published: 04 April 2018
doi: 10.3389/fbioe.2018.00035

Matrix Metalloproteinase-2 Impairs Homing of Intracoronary Delivered Mesenchymal Stem Cells in a Porcine Reperfused Myocardial Infarction: Comparison With Intramyocardial Cell Delivery

*Katrin Zlabinger[1], Dominika Lukovic[1], Rayyan Hemetsberger[1], Alfred Gugerell[1], Johannes Winkler[1], Ljubica Mandic[1], Denise Traxler[1], Andreas Spannbauer[1], Susanne Wolbank[2], Gerald Zanoni[2], Christoph Kaun[1], Aniko Posa[3], Andrea Gyenes[3], Zsolt Petrasi[4], Örs Petnehazy[4], Imre Repa[4], Renate Hofer-Warbinek[5], Rainer de Martin[5], Florian Gruber[6], Silvia Charwat[1], Kurt Huber[7], Noemi Pavo[1], Imre J. Pavo[1], Noemi Nyolczas[1], Dara L. Kraitchman[8] and Mariann Gyöngyösi[1]**

[1] Department of Cardiology, Medical University of Vienna, Vienna, Austria, [2] Ludwig Boltzmann Institute for Clinical and Experimental Traumatology/AUVA Research Center Austrian Cluster for Tissue Regeneration, Vienna, Austria, [3] Institute of Biophysics, Biological Research Center, Szeged, Hungary, [4] Institute of Diagnostics and Radiation Oncology, University of Kaposvar, Kaposvar, Hungary, [5] Department of Biomolecular Medicine and Pharmacology, Institute of Vascular Biology and Thrombosis Research, Medical University of Vienna, Vienna, Austria, [6] Department of Dermatology, Medical University of Vienna, Vienna, Austria, [7] 3rd Department of Medicine (Cardiology and Emergency Medicine), Wilhelminenhospital, Vienna, Austria, [8] Russell H. Morgan Department of Radiology and Radiological Science, School of Medicine, The Johns Hopkins University, Baltimore, MD, United States

Background: Intracoronary (IC) injection of mesenchymal stem cells (MSCs) results in a prompt decrease of absolute myocardial blood flow (AMF) with late and incomplete recovery of myocardial tissue perfusion. Here, we investigated the effect of decreased AMF on oxidative stress marker matrix metalloproteinase-2 (MMP-2) and its influence on the fate and homing and paracrine character of MSCs after IC or intramyocardial cell delivery in a closed-chest reperfused myocardial infarction (MI) model in pigs.

Methods: Porcine MSCs were transiently transfected with Ad-Luc and Ad-green fluorescent protein (GFP). One week after MI, the GFP-Luc-MSCs were injected either IC (group IC, $11.00 \pm 1.07 \times 10^6$) or intramyocardially (group IM, $9.88 \pm 1.44 \times 10^6$). AMF was measured before, immediately after, and 24 h post GFP-Luc-MSC delivery. *In vitro* bioluminescence signal was used to identify tissue samples containing GFP-Luc-MSCs. Myocardial tissue MMP-2 and CXCR4 receptor expression (index of homing signal) were measured in bioluminescence positive and negative infarcted and border, and non-ischemic myocardial areas 1-day post cell transfer. At 7-day follow-up, myocardial homing

Abbreviations: AMF, absolute myocardial blood flow; CT, computer tomography; FACS, flow cytometry; FGF, fibroblast growth factor; FUP, follow-up; GFP, green fluorescent protein; IC, intracoronary; IM, intramyocardial; LAD, left anterior descending coronary artery; Luc, luciferase; LVEF, left ventricular ejection fraction; MI, myocardial infarction; MMP, matrix metalloproteinase; MRI, magnet resonance image; MSC, mesenchymal stem cell; SDF, stromal derived factor; VEGF, vascular endothelial growth factor.

OPEN ACCESS

Edited by:
Mikaël M. Martino, Monash University, Australia

Reviewed by:
Michela Pozzobon, Istituto di Ricerca Pediatrica, Fondazione Città della Speranza, Italy
Roberta Tasso, Ospedale San Martino (IRCCS), Italy

***Correspondence:**
Mariann Gyöngyösi mariann.gyongyosi@meduniwien.ac.at

Specialty section:
This article was submitted to Tissue Engineering and Regenerative Medicine, a section of the journal Frontiers in Bioengineering and Biotechnology

Received: *26 September 2017*
Accepted: *15 March 2018*
Published: *04 April 2018*

Citation:
Zlabinger K, Lukovic D, Hemetsberger R, Gugerell A, Winkler J, Mandic L, Traxler D, Spannbauer A, Wolbank S, Zanoni G, Kaun C, Posa A, Gyenes A, Petrasi Z, Petnehazy Ö, Repa I, Hofer-Warbinek R, de Martin R, Gruber F, Charwat S, Huber K, Pavo N, Pavo IJ, Nyolczas N, Kraitchman DL and Gyöngyösi M (2018) Matrix Metalloproteinase-2 Impairs Homing of Intracoronary Delivered Mesenchymal Stem Cells in a Porcine Reperfused Myocardial Infarction: Comparison With Intramyocardial Cell Delivery. Front. Bioeng. Biotechnol. 6:35. doi: 10.3389/fbioe.2018.00035

(cadherin, CXCR4, and stromal derived factor-1alpha) and angiogenic [fibroblast growth factor 2 (FGF2) and VEGF] were quantified by ELISA of homogenized myocardial tissues from the bioluminescence positive and negative infarcted and border, and non-ischemic myocardium. Biodistribution of the implanted cells was quantified by using Luciferase assay and confirmed by fluorescence immunochemistry. Global left ventricular ejection fraction (LVEF) was measured at baseline and 1-month post cell therapy using magnet resonance image.

Results: AMF decreased immediately after IC cell delivery, while no change in tissue perfusion was found in the IM group (42.6 ± 11.7 vs. 56.9 ± 16.7 ml/min, $p = 0.018$). IC delivery led to a significant increase in myocardial MMP-2 64 kD expression (448 ± 88 vs. 315 ± 54 intensity × mm^2, $p = 0.021$), and decreased expression of CXCR4 (592 ± 50 vs. 714 ± 54 pg/tissue/ml, $p = 0.006$), with significant exponential decay between MMP-2 and CXCR4 ($r = 0.679$, $p < 0.001$). FGF2 and VEGF of the bioluminescence infarcted and border zone of homogenized tissues were significantly elevated in the IM goups as compared to IC group. LVEF increase was significantly higher in IM group (0.8 ± 8.4 vs 5.3 ± 5.2%, $p = 0.046$) at the 1-month follow up.

Conclusion: Intracoronary stem cell delivery decreased AMF, with consequent increase in myocardial expression of MMP-2 and reduced CXCR4 expression with lower level of myocardial homing and angiogenic factor release as compared to IM cell delivery.

Keywords: mesenchymal stem cells, translational research, cell delivery, oxidative stress, homing, intracoronary, intramyocardial, ischemic injured heart tissue

INTRODUCTION

Since the endogenous cardiac progenitor cells are unable to restore the cardiac function in toto, tissue regeneration of the heart by delivering exogenous reparative cells has been intensively studied. Clinical stem cell therapy was assumed to have beneficial effects on the regeneration of the ischemic injured myocardium; nevertheless, recent clinical studies and meta-analyses revealed that intracoronary (IC) administration of bone marrow-origin mononuclear cells has no impact on left ventricular function and clinical outcome (Gyongyosi et al., 2015).

Mesenchymal stem cells (MSCs) and other progenitor or stem cells secrete various types of cytokines, growth factors, and chemokines under *in vitro* conditions that play an important role in cardiac remodeling, angiogenesis, apoptosis, and survival (Gnecchi et al., 2008). The regenerative mechanism might be attributed to secretion of paracrine factors (Thum et al., 2005); therefore, MSCs are increasingly used in human clinical trials (Roura et al., 2017).

Myocardial engraftment kinetics of cardiac transplanted stem cells play a highly relevant role in the regeneration of cardiac tissue. Impaired homing of the cells may be one reason of the failure of stem cell therapy (Chavakis et al., 2008; Penn and Mangi, 2008; Schoenhard and Hatzopoulos, 2010; Wollert and Drexler, 2010). Our group as well as others have previously reported that due to possible cell sludge formation and microvascular obstruction, experimental IC injection of MSCs results in prompt decrease of absolute myocardial blood flow (AMF) with late and incomplete recovery of tissue perfusion (Vulliet et al., 2004; Gyongyosi et al., 2011). This leads to an increase in intraluminal pressure, inhibiting cell passage distal to the ischemic injured area, and the development of acute local ischemia with enhanced oxidative stress, hampering accumulation, and homing of the cells in the peri-infarcted area (Vulliet et al., 2004; Gyongyosi et al., 2010a,b, 2011).

The stromal cell-derived factor (SDF)-1/chemokine (C-X-C motif) receptor 4 [(SDF)-1/CXCR4] axis is one of the most important factors in stem/progenitor cell homing, chemotaxis, engraftment, and retention into ischemic tissue (Wojakowski et al., 2004). Enhanced expression of matrix metalloproteinase 2 (MMP-2) due to ischemia-induced oxidative stress has been shown to interrupt the SDF/CXCR4 axis due to SDF-1alpha proteolysis, thereby limiting homing (Giricz et al., 2006; Segers et al., 2007; Rota et al., 2008; Lukovic et al., 2016). We have previously demonstrated *in vitro* that MMP-2 directly inhibited the SDF-1 alpha induced migration of CD34+ cells toward cardiomyocytes (Lukovic et al., 2016). The immediate activation of the MMP-2 during ischemia induces local inflammation and degradation of several cellular components *via* NF-kB and NFAT stress signaling pathways. Proteolytic fragments of MMP-2 provoke also autoimmune responses, leading to progressive cardiomyopathy and myocyte contractile dysfunction. MMP-2 plays also a role in pathological processes turning the reversible ischemic events to irreversible injury, contributing to development of heart failure (DeCoux et al., 2014).

In the present experiment, we have investigated the association between decreased myocardial blood flow and the acute oxidative stress marker MMP-2, and the effect of increased MMP-2 on

the homing, biodistribution, and paracrine effect of the cardiac delivered MSCs, in the pig closed-chest, reperfused myocardial infarction (MI) model in a side-by-side comparison of IC and intramyocardial delivery modes.

MATERIALS AND METHODS

Preparation and Transfection of MSC

Bone marrow (100 ml) of farm pigs was harvested from the iliac crest and stored at 4°C (Baxter bag, Baxter Healthcare, Ltd., Thetford, Norfolk, UK). The MSC were selected using Ficoll–Paque (Amersham Biosciences), cultured and transfected as described previously (Gyongyosi et al., 2008). Briefly, buffy coats were plated at 50,000 cells/cm^2 in alpha MEM medium without nucleotides, containing 10% fetal calf serum (FCS), 2 mM L-glutamine, penicillin/streptomycin supplemented with 1 ng/ml fibroblast growth factor 2 (FGF2). The prepared cells were negative for CD45 (Bio-Rad Laboratories, Hercules, CA, USA), CD34 (Thermo Fisher Scientific, Waltham, MA, USA), and positive for CD44, CD90, and CD29 (all EXBIO Praha, Vestec, Czech Republic) expression (see Figure S1 in Supplementary Material).

After reaching the fourth passage, the cultured MSCs were transfected with the combination of Ad-CMV-Luc and Ad-CMV-green fluorescent protein (GFP) (Vector Biolabs, Philadelphia, PA, USA). The AdV was then removed and fresh medium was added. Transfection efficiency was determined by flow cytometry. The viability of the GFP-Luc-MSC was assessed prior to cardiac delivery using trypan blue (Sigma-Aldrich, Saint Louis, MO, USA) staining. A proliferation assay was performed 1, 2, 4, and 8 days after seeding, using an EZ4U kit (Biomedica, Vienna, Austria) according to manufacturer's protocol.

Induction of AMI in Female Pigs

All animal studies were approved by the local Experimental Animal Care Committee of University of Kaposvar, Hungary where the experiments were performed (EC 246/002/SOM2006, MAB-28-2005). The experiments conform to the "Position of the American Heart Association on Research."

Closed-chest, acute reperfused MI was induced in 39 female domestic pigs (23 ± 3 kg) by percutaneous catheter-based balloon occlusion of the left anterior descending coronary artery (LAD), as described previously (Gyongyosi et al., 2011). Briefly, after direct puncture of the right femoral artery and administration of 200 IU/kg of heparin, a 90-min percutaneous balloon (3.0 mm in diameter × 15 mm long, Maverick, Boston Scientific Corp., Natick, MA, USA) occlusion (5 atm) of the mid LAD, beyond the origin of the second major diagonal branch was performed. The complete occlusion of the artery distal to the balloon was confirmed by angiography. After a 90-min LAD occlusion, the balloon was deflated slowly to allow reperfusion. The puncture site was then closed with Angioseal (St. Jude Medical, St. Paul, MN, USA), and the pigs were allowed to recover.

One-week (8 ± 2 days) post-MI, the pigs were randomized to receive either IC infusion or 3D NOGA-guided percutaneous intramyocardial injections of the GFP-Luc-MSC. The study design with different follow-ups (FUPs) is shown in **Figure 1**.

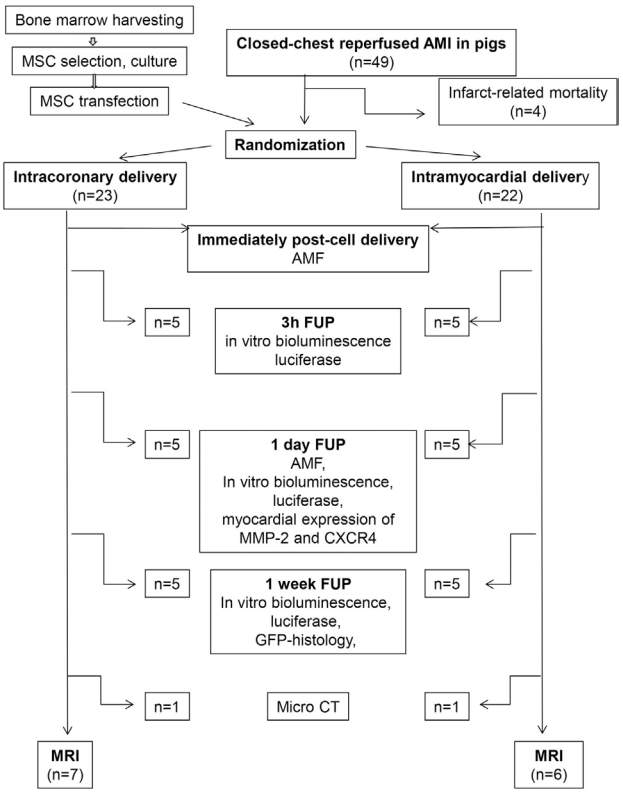

FIGURE 1 | Study design of the experiment. MSC, mesenchymal stem cell; AMF, absolute myocardial blood flow; FUP, follow-up; MMP-2, matrix metalloproteinase; GFP, green fluorescent protein; micro CT, micro computed tomography; MRI, magnet resonance image.

Cardiac Delivery of GFP-Luc-MSCs

For intramyocardial cell administration (group IM), an 8F sheath (Terumo Medical Corporation) was placed in the left femoral artery, and a diagnostic NOGA catheter (Cordis, Johnson & Johnson, Miami Lakes, FL, USA) was advanced through the aortic valve into the left ventricle. Detailed descriptions of the endocardial mapping, injection system components, and principles have been described elsewhere (Ben-Haim et al., 1996; Gepstein et al., 1997). Briefly, the left ventricular endocardial surface was mapped by measuring the local electrical activity and displayed as 3D color-coded map with clear distinction of the viable and nonviable myocardial areas and the border zone of infarction. After replacement of the diagnostic mapping catheter through the Myostar (Cordis, Johnson & Johnson, Miami Lakes, FL, USA) injection catheter, the GFP-Luc-MSCs were injected into the peri-infarct myocardium at 12–13 sites. The injections (0.3 ml cell suspension each) were given slowly (40–45 s) to areas with a unipolar voltage above 6 mV, based on the quality control criteria (Ben-Haim et al., 1996; Gepstein et al., 1997).

For IC cell administration (group IC), a guiding catheter (Medtronic Minneapolis, MN, USA) was introduced into the ostium of the LAD. A Sprinter® Over-the-Wire Semicompliant Balloon Catheter (Medtronic, Minneapolis, MN, USA) was introduced into the LAD, distal to the second diagonal branch

over a guide wire, and a heparin diluted cell suspension (up to 10 ml) of male GFP-Luc-MSCs was slowly injected with stop-flow technique over about 15 min. The patency of the target vessel following the injection was confirmed *via* angiography.

Measurement of AMF

Absolute myocardial blood flow was measured before, immediately after, and at 24 h post-IC and intramyocardial ($n = 5$ of each group) delivery of the GFP-Luc-MSCs.

The measurement of AMF has been described previously (Aarnoudse et al., 2007). Briefly, a 0.014″ pressure wire (Radi Medical Systems, Uppsala, Sweden) was positioned in the distal LAD. A specially designed infusion catheter (Occam Inc., Eindhoven, Netherlands) was advanced over the pressure wire until its tip was just proximal to the flow probe. The infusion catheter was connected to an infusion pump (Stellant D CT Injector, Medrad, Warrendale, PA, USA) and saline (12 ml/min) was infused through this infusion catheter. Maximum hyperemia was induced by continuous intravenous administration of 140 μg/kg/min adenosine. The infusion of saline (20°C) was started and upon reaching a steady-state continuous infusion, the decrease of blood temperature (T) was measured. Volumetric blood flow in the LAD was calculated according to predefined formula.

Tracking of the Cardiac-Delivered GFP-Luc-MSCs: *In Vitro* Bioluminescence Imaging, Luciferase Assay, and Immunohistochemistry

In order to make the injected cells visible in the heart and remote organs, *in vitro* bioluminescence images were performed, as described previously (Gyongyosi et al., 2010a, 2011). Briefly, the hearts and different organs were harvested immediately after euthanasia, cut in 1 cm thick slices, then placed in 20 ml of ATP (200 μM) and luciferin (3 mg/ml) in Ringer solution for 5 min. Photon emission of metabolically active, Luc-expressing cells, close to the tissue surface were captured with a charged-coupled device camera system (IVIS, Xenogen Corp.). Tissue pieces (1–2 mg/each sample) positive for bioluminescence (infarcted and border zona), as well as bioluminescence negative infarcted and border zone and non-ischemic myocardium (remote posterior wall) were cut and prepared for quantitative luciferase measurements and immunohistochemistry.

For measurements of luciferase activity, tissue samples were collected from the infarcted and border zone (bioluminescence positive and negative), and non-ischemic myocardium and different organs of the animals (pericardium, pleura, lung, mediastinal lymphatic nodes, liver, spleen, kidney, skin and bone marrow from the iliac crest) at 3, 24 h, and 7-days post cell delivery. The tissues were processed for measurement of luciferase activity as described previously (Gyongyosi et al., 2011). Luciferase was determined using components of the Dual-Luciferase Reporter Assay System (Promega, Madison, WI, USA) (Gyongyosi et al., 2010b). Results were given in relative light units (RLU) per microgram protein.

Bioluminescence positive tissue samples were fixed in 4% buffered paraformaldehyde and embedded in paraffin for visualization of the GFP+ cells in different organs. Cellular nuclei were counterstained with Hoechst.

Measurement of Oxidative Stress by Cardiac Tissue MMP-2 Activity

To quantify the stem cell infusion-induced increase in oxidative stress, cardiac tissue MMP-2 activities of five myocardial areas (bioluminescence positive infarcted and border zone, bioluminescence negative infarcted and border zone, and non-ischemic myocardium) were measured by zymographic analysis 24 h post cell delivery. Briefly, polyacrylamide gels (8%) were copolymerized with gelatin (2 mg/ml, Sigma-Aldrich), and a constant amount of myocardial tissue homogenate was loaded in each lane. Following electrophoreses at 150 V for 1.5 h, gels were washed with 2.5% Triton X-100 for 3×15 min and incubated for 24–48 h at 37°C in incubation buffer (50 mM Tris–HCl, 150 mM NaCl, 5 mM CaCl2, and 0.05% NaN3, pH 7.4). Gels were then stained with 0.05% Coomassie Brilliant Blue (G-250; Sigma-Aldrich) in a mixture of methanol/acetic acid/water (2.5:1:6.5, v/v) and destained in aqueous 4% methanol/8% acetic acid. Gelatinolytic activities were detected as transparent bands against the dark–blue background. Zymograms were digitally scanned, and band intensities were quantified using Quantity One software (Bio-Rad, Hercules, CA, USA).

Values of 24 h follow-up (FUP) AMF of both groups and MMP-2 64 kD activities of the bioluminescence infarcted area of both IC and IM groups were pooled to investigate the direct effect of decreased AMF on increase in MMP-2 64 kD.

Homing and Paracrine Effect of Cardiac-Delivered GFP-Luc-MSCs

At the 7 days FUP, bioluminescence positive and negative infarcted and infarct-border cardiac tissue samples, as well as samples from the remote non-ischemic myocardium were either processed to immunohistochemistry, or homogenized for tissue ELISA assays.

For immunohistochemistry, myocardial areas were fixed in 4% buffered paraformaldehyde and embedded in paraffin. To investigate the homing of the injected GFP-Luc-MSCs, myocardial expression of cadherin (Abcam, Cambridge, UK), and for angiogenic factors, vascular endothelial growth factor (VEGF) (Cusabio, Cologne, Germany) and FGF2 (Lifespan, Seattle, WA, USA) were displayed by immunofluorescence staining. The following secondary antibodies were used: Dylight 488-conjugated Donkey Anti-Goat IgG (705-485-003), Dylight 549-conjugated Goat Anti-Rabbit IgG (115-505-003), Dylight 549-conjugated Goat Anti-Mouse IgG (115-505-003), Dylight 488-conjugated Donkey Anti-Sheep IgG (713-485-003). Fluorescent images were acquired by an Olympus Provis AX 70 microscope (New Hyde Park, NY, USA).

To quantify the myocardial expression of homing and angiogenic signals, porcine CXCR4 (USCN Life Science, Wuhan, China), SDF-1alpha (Neoscientific, Germany), FGF2 (Neoscientific, Germany), VEGF (Neoscientific, Germany), and cadherin (MyBiosource Inc, San Diego, CA, USA) ELISAs were performed.

Additionally, in order to prove the direct correlation between increased MMP-2 activity and CXCR4 expression, bioluminescence

positive infarcted and border areas were also homogenized and CXCR4 ELISA was performed at the 24 h FUP.

Effect of Cardiac-Delivered GFP-Luc-MSCs on Coronary Microvascularization and Global Cardiac Function

Cardiac magnet resonance image (MRI) was performed using a 1.5-T clinical scanner (Avanto, Siemens, Erlangen, Germany) using a phased array surface coil and a vector ECG system, 1 ± 1 day before, and at the 4-week FUP. Cine MR images were acquired using ECG-gated, steady-state free precession cine MRI in short and long-axis views of the heart (1.2 ms echo time (TE), 40 ms repetition time (TR), 50° flip angle, 300 mm field-of-view, 8 mm slice thickness, and 256 × 256 image matrix). Sixteen short-axis images were acquired by ECG-gated, saturation-recovery true fast imaging with steady state precession (FISP) sequences. Following injection of 0.2 mmol/kg of contrast media, delayed enhancement images were acquired using an inversion recovery-prepared, gradient-echo sequence. Short-axis and long-axis views were obtained 10–15 min after gadolinium injection. Images were analyzed using the Mass 6.1.6 software (Medis, The Netherlands) to calculate end-diastolic and end-systolic volumes and global LV ejection fraction. The LV and infarcted myocardial mass were determined from the cine and delayed enhancement MR images, respectively. The infarct size was expressed relative to LV mass.

To determine microvascularization, micro-computer tomography (MicroCT) of GFP-Luc-MSC-treated infarcted hearts was performed in one animal from each treatment group. The pig hearts were removed and immersed in 4°C Krebs' solution containing heparin and then prepared for microCT to allow quantification of the images of the infarcted area as described previously (Mondy et al., 2009). The coronary arteries were then immediately perfused with an isoosmotic, rinsing solution at 100 mmHg until the fluid ran clearly through the cardiac veins. The heart was placed in a saline bath and Tensol 70 was perfused through the major coronary arteries at 10 ml/h and at a pressure of 100 mmHg until the solution hardened. The cast preparation was completed within 2 h postmortem. The heart was then kept in a water bath at 50°C for 1 day to complete the polymerization process. The myocardial tissue was macerated with 7.5% KOH. The heart images were then captured using a VivaCt75 von Scanco Medical Basserdorf (50 kV, 1 s integration time, 900 projections, 1,024 × 1,024 a-Si flat panel detector, conebeam reconstruction) with a resolution of 80 μm.

Statistics

For semiquantitative determination of luciferase, five samples of each organ and bioluminescence positive (infarct treated) and negative (infarct non-treated), as well as non-ischemic myocardium were measured and the mean values were calculated. Continuous parameters of the groups were compared by using ANOVA supplemented with unpaired *t*-test. Correlation between predefined parameters, such as decrease in AMF with increase in MMP-2 64 kD activity, or MMP-2 64 kD activity with myocardial expression of CXCR4 from the pooled bioluminescence positive infarcted and border area were calculated. In order to prove the direct inhibitory effect of increased MMP-2 64 kD on homing of GFP-Luc-MSCs, the 24 h follow-up data of Luciferase activity of the infarcted and non-infarcted areas were pooled and correlated with MMP-2 64 kD values.

Significance was considered if $p < 0.05$. All statistical tests were performed by using SPSS Mac V24.

RESULTS

Cell Delivery

Proliferation assay indicated a temporary significant decrease in proliferation capacity of the transfected MSC as compared with the native MSC 96 h post-transfection (Figure S2 in Supplementary Material).

A total of 9.88 ± 1.44 × 10^6 GFP-Luc-MSCs (12 ± 2 injection sites, 4.0 ± 0.2 ml cell suspension) was injected intramyocardially in Group IM, while 11.00 ± 1.07 × 10^6 GFP-Luc-MSCs were injected IC in Group IC (12 ± 2 ml cell suspension).

In vitro bioluminescence of the hearts showed less accumulation of the bioluminescence positive (Luc-containing) MSCs in the endocardial surface 24 h post IC delivery, as compared with intramyocardial application (**Figure 2**).

Myocardial Blood Flow and Procedural Ischemia-Induced Changes in MMP-2 Expression

Absolute myocardial blood flow decreased immediately after IC delivery while no significant change in tissue perfusion could be detected using the percutaneous intramyocardial delivery mode (**Table 1**).

Parallel to the decrease of coronary blood flow in the IC group, myocardial expression of MMP-2 was higher in bioluminescence-positive border zones of the infarction as compared to the IM group (MMP-2 72 kD: 338 ± 81 vs 185 ± 38 intensity × mm^2, $p = 0.005$; and MMP-2 64 kD: 448 ± 88 vs 315 ± 54 intensity × mm^2, $p = 0.006$), suggesting the increase in acute oxidative stress due to cell slugging in the microvasculature (**Figure 3**).

In parallel, border zone tissue expression of CXCR4 was significantly lower in the IC delivery group as compared with the IM group (592 ± 50 vs 714 ± 54 pg/mg, $p = 0.006$), indicating decreased level of homing signal (**Figure 3**).

A significant, linear negative correlation was found between the AMF and MMP-2 64 kD myocardial expression (bioluminescence positive infarcted area, pooled data of both groups) ($r = -0.838$, $p < 0.01$, $y = 622 - 5.3\times$) at the 24 h FUP indicating a direct, unfavorable influence of microvascular obstruction on homing signal.

The significant exponential decay of myocardial CXCR4 expression in relation to MMP-2 64 kD intensity in the pooled bioluminescence positive infarcted and border zone proved the direct anti-homing effect of increased MMP-2 activity (**Figure 3**). Additionally, a significant negative logarithmic correlation was found between the MMP-2 64 kD and measured Luciferase activity (number of GFP-Luc-MSCs) in the infarcted treated and infarcted non-treated myocardium (**Figure 3**). Pooling the MMP-2 64 kD and Luciferase data only of the infarcted treated

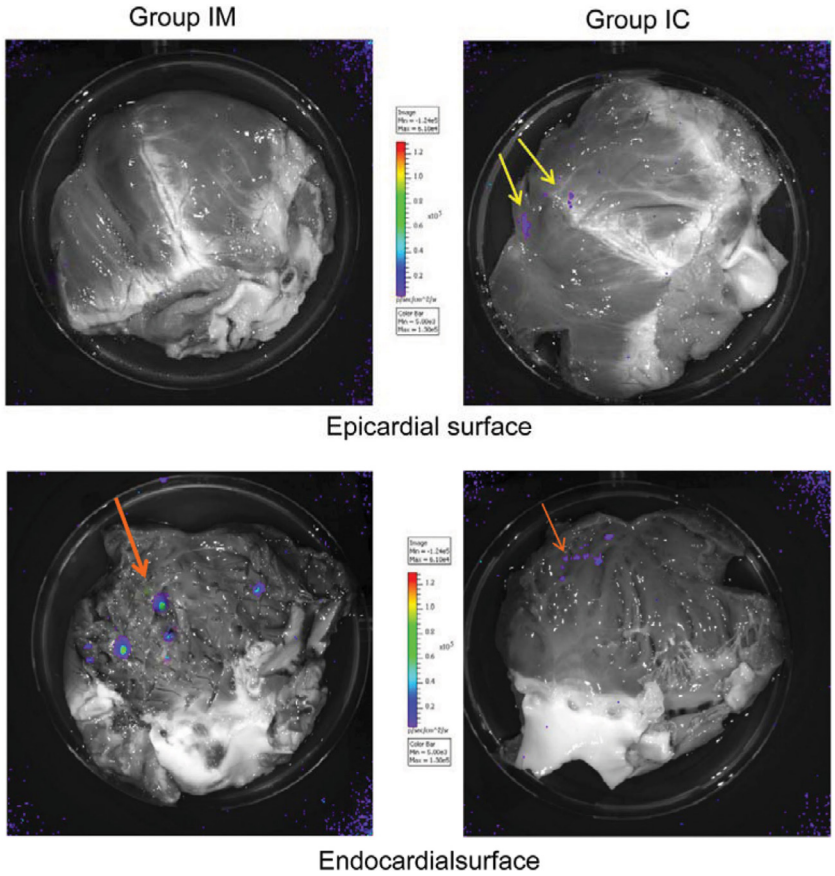

FIGURE 2 | *In vitro* bioluminescence of pig hearts with intracoronary (IC) or intramyocardial delivery of green fluorescent protein (GFP)-Luc-mesenchymal stem cells (MSCs). *In vitro* bioluminescence images of Luc-transfected porcine MSC show epicardial perivascular location of cells after IC injections (upper right) in contrast to intramyocardial delivery (upper left). Highly positive endocardial punctual signals 24 h after intramyocardial GFP-Luc-MSCs delivery (bottom left). Weak confluent signal of GFP-Luc-MSCs on the endocardial surface of the heart after IC delivery (bottom right).

TABLE 1 | Absolute myocardial blood flow before and after GFP-Luc-MSC intracoronary (IC) or percutaneous intramyocardial delivery.

Absolute myocardial blood flow (ml/min)	Intramyocardial group ($n = 5$)	IC group ($n = 5$)	*p*-Value
Pre GFP-Luc-MSC delivery	59.5 ± 11.3	59.9 ± 13.9	n.s.
Immediately after GFP-Luc-MSC delivery	56.9 ± 16.7	42.6 ± 11.7	0.018
24 h post GFP-Luc-MSC delivery	58.9 ± 8.7	45.5 ± 5.2	0.017

GFP, green fluorescent protein; Luc, luciferase; MSC, mesenchymal stem cell.

(injected) area, the coefficient of variation was $r = 0.729$, with a p value of 0.017 (Figure S3 in Supplementary Material).

Expression of Homing Factors in the Myocardium: Differences Between the IC and Intramyocardial Delivery Modes

Trend to higher levels of tissue expressions of homing signals cadherin and SDF-1alpha were seen both in ELISA and immunohistochemistry in the bioluminescence positive areas, supposing that the majority of the secreted paracrine factors were originated from the injected GFP-Luc-MSCs.

At the 7-day FUP, significantly lower CXCR4 was found in the bioluminescence positive infarcted myocardium in the IC group, as compared with the IM group (129 ± 110 vs 411 ± 213 pg/mg, $p = 0.03$) (**Figure 4**), where the cells were injected. Myocardial levels of the angiogenic factors FGF2 were significantly decreased in the IC group in the bioluminescence positive border (710 ± 259 vs 1,390 ± 460 pg/mg, $p = 0.02$) and infarcted areas (1,002 ± 791 vs 2,903 ± 1,609 pg/mg, $p = 0.045$), but also in the bioluminescence negative infarct area (571 ± 127 vs 1,538 ± 479 pg/mg, p = 0.002). In parallel, lower VEGF level was detected in the bioluminescence infarcted (3.17 ± 1.15 vs 5.5 ± 1.6 pg/mg, $p = 0.027$) and border zone (2.89 ± 0.4 vs 4.64 ± 1.0 pg/mg, $p = 0.007$) in IC group vs IM group (**Figure 4**). Fluorescence immunochemistry confirmed the ELISA findings (**Figure 4**).

Biodistribution of GFP-Luc-MSCs in the Heart and Remote Organs

Figure 5 shows the time-dependent accumulation of the injected cells in the heart and remote organs, expressed as the percentage of the originally injected GFP-Luc-MSCs. In accordance with the

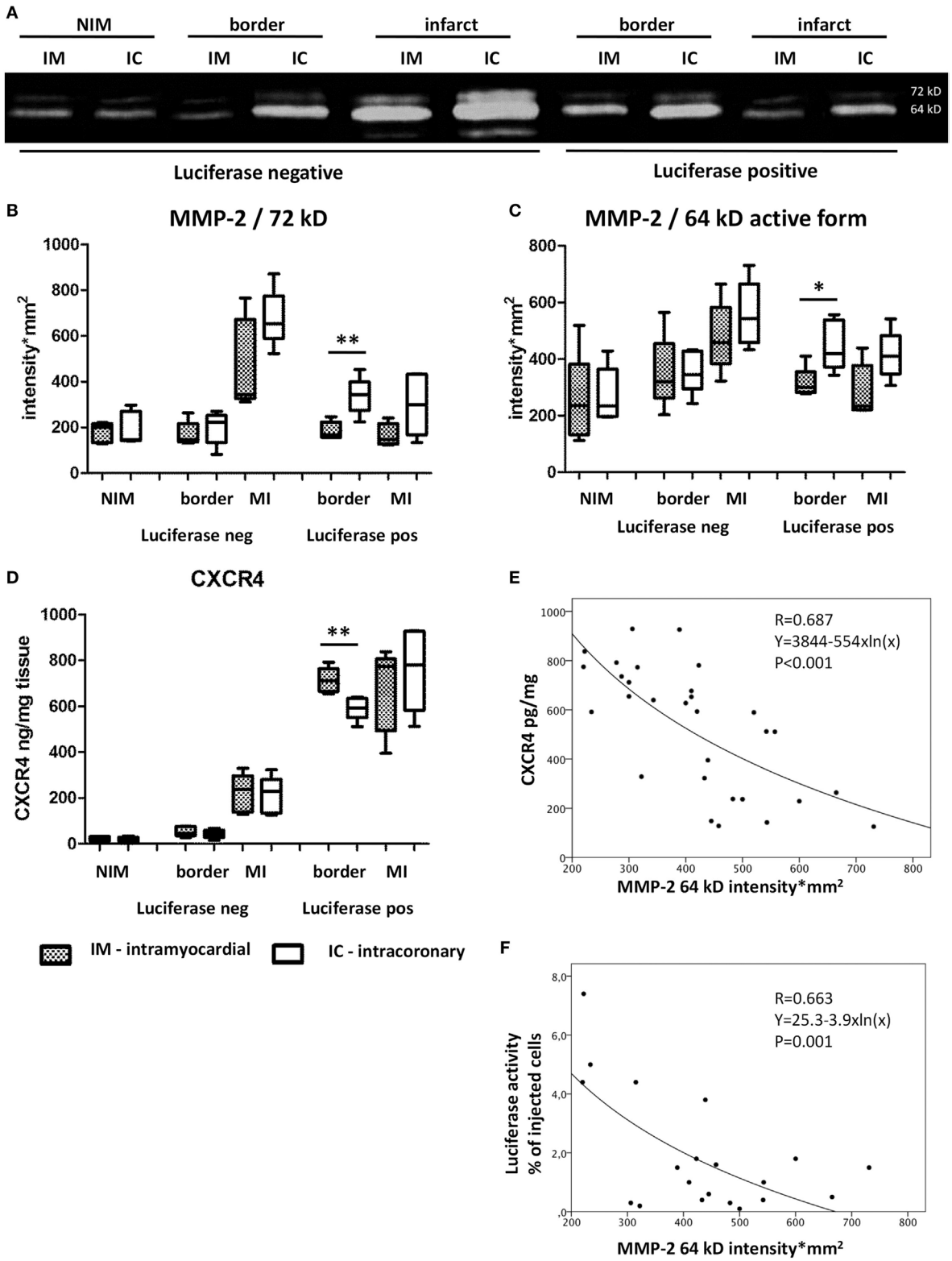

FIGURE 3 | Oxidative stress and homing signals of the myocardium 24 h post acute myocardial infarction. Zymography **(A)** and statistical results **(B,C)** of matrix metalloproteinase-2 (MMP-2), 72 kD and its active form 64 kD expression of the myocardium 1 day after intramyocardial or IC green fluorescent protein (GFP)-Luc-mesenchymal stem cell (MSCs) cell delivery in different location. IM, intramyocardial delivery; IC, intracoronary delivery; NIM, non-ischemic myocardium (remote posterior wall), border, border zone of infarction; MI, infarcted area; **(D)** CXCR4 expression in the myocardial tissues 24 h after cell treatment. **(E)** Exponential decay between MMP-2 and CXCR4. **(F)** Logarithmic correlation between MMP-2 64 kD and luciferase activity (index of number of GFP-Luc-MSCs).

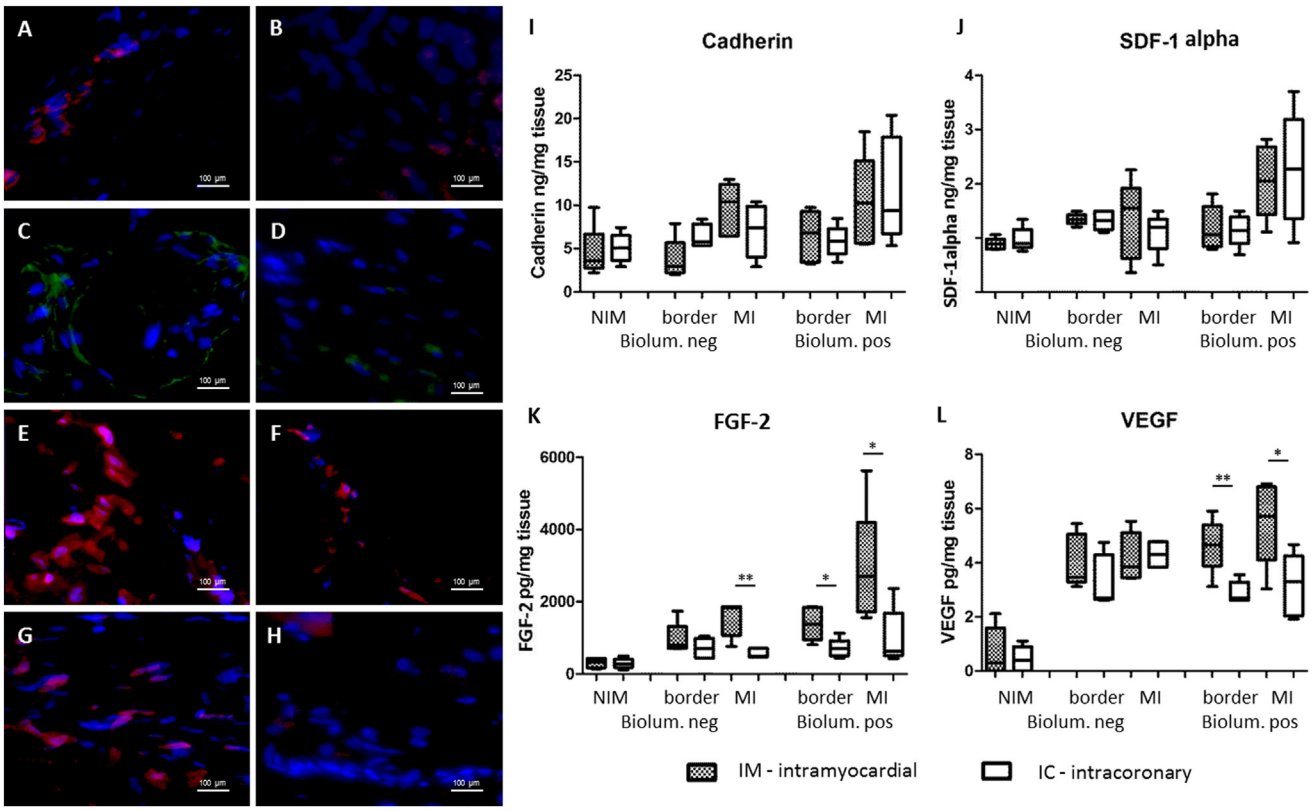

FIGURE 4 | Expression of homing and angiogenic signals of the myocardium 7 days after cardiac transfer of green fluorescent protein (GFP)-Luc-mesenchymal stem cell (MSCs). Fluorescent immunohistochemistry of the bioluminescence positive myocardial areas 7 days after intramyocardial [left panel **(A,C,E,G)**] or intracoronary [right panel **(B,D,F,H)**] GFP-Luc-MSCs delivery shows increased expression of homing signals cadherin **(A,B)**, and angiogenic factors fibroblast growth factor 2 (FGF2) **(C,D)** and vascular endothelial growth factor (VEGF) **(E,F)** in group IM. Infarct area border zone **(G,H)** exhibited higher number of myocardial cells and higher level of VEGF expression in group IM **(G)**. Hoechst staining of the nuclei, 40× magnification. Expression of homing signals cadherin **(I)**, stromal-derived factor-1alpha **(J)**, and angiogenic factors FGF2 **(K)** and VEGF **(L)**.

higher level of CXCR4 homing signal expression of the myocardium, the highest luciferase activity was found in the intramyocardially injected site 3 h post delivery (6.9 ± 5.9%), while IC delivery led to less cell retention (1.7 ± 0.1%) ($p = 0.041$). At 24 h and 7 days FUP, the number of cardiac amount of GFP-Luc-MSCs decreased, but the intramyocardial retention of the cells were still significantly higher in the IM group (**Figure 5**). In accordance with the rapid biodistribution of the cells, higher amount of GFP-Luc-MSCs could be found in bone marrow in the IC group 3 h post-delivery. Each remote organ contained a small amount of GFP-Luc-MSCs, even 1 week after cell delivery, with no difference between the groups.

Fluorescent microscopy confirmed the presence of GFP-positive cells in all sampled organs 1-week post GFP-Luc-MSCs delivery (**Figure 5**).

Microvascularization and LV Function at 1-Month Follow-Up Post IC or Intramyocardial GFP-Luc-MSC Delivery

Magnet resonance image confirmed the significantly higher cardiac output and a significantly improved global ejection fraction in the IM group as compared to IC group (**Table 2**).

MicroCT investigation of one heart of each group showed a higher capillary density in the infarcted area in group IM as compared to a heart of group IC (**Figure 6**).

DISCUSSION

Low coronary blood-flow triggered expression of myocardial MMP-2 followed by decrease of the chemotactic signals for cell homing, resulting in limited homing of injected cells, and lesser degree of angiogenic factor release, with consequent poorer 1-month outcome, as compared with intramyocardial delivery. We could demonstrate a direct relationship between diminished blood flow and increase in myocardial oxidative stress marker MMP-2, as well as a significant association between increase in MMP-2 and decrease of the homing factor CXCR4 in the cell-retention bioluminescence areas. Higher cell entrapment after intramyocardial cell delivery led to higher myocardial tissue levels of FGF2 and VEGF especially in that myocardial areas, where the cells were found.

Retention of Cells After IC or Intramyocardial Delivery

In humans, two main delivery modalities have been utilized in cardiac stem cell clinical trials: IC infusion and intramyocardial

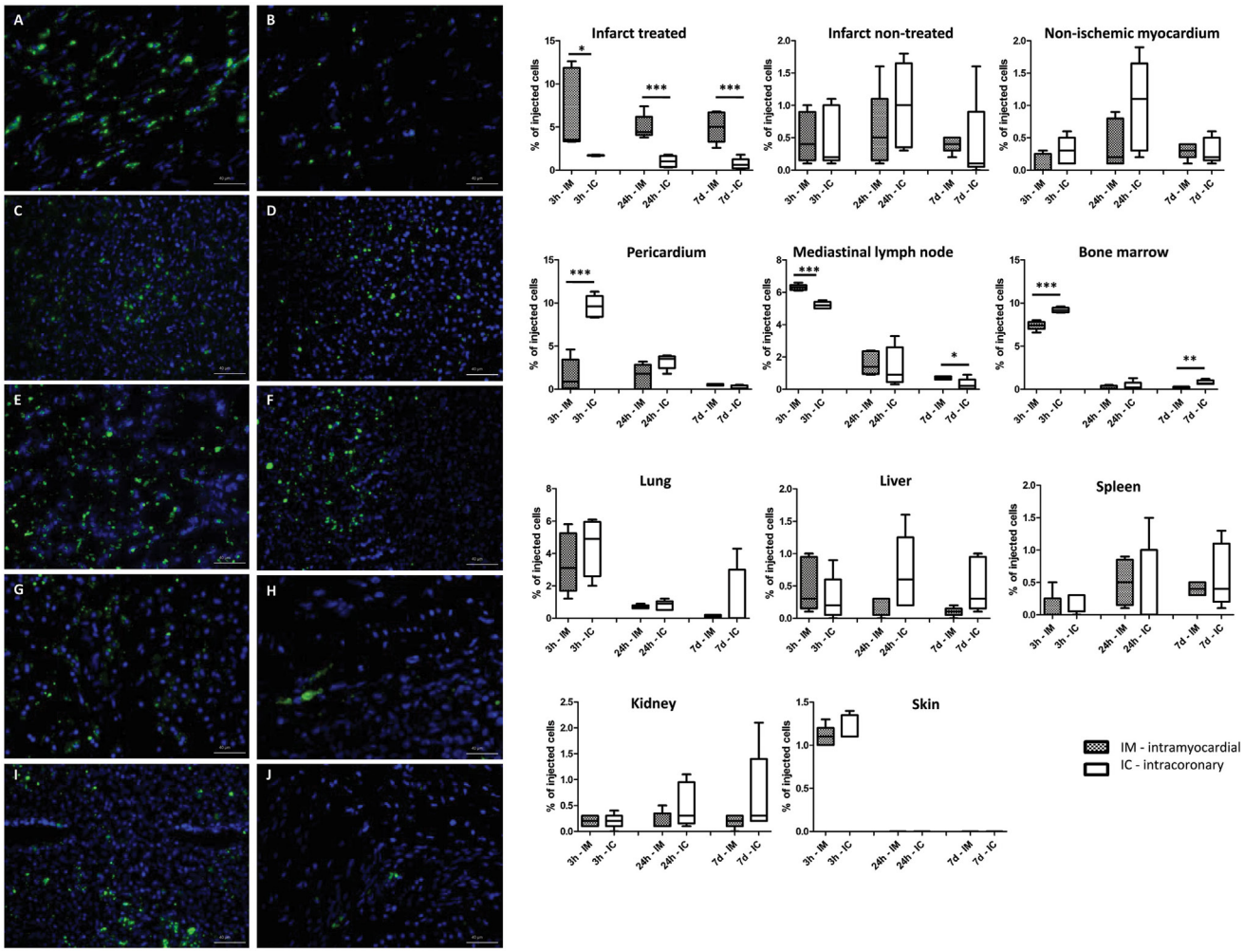

FIGURE 5 | Time-dependent biodistribution of the intramyocardial and intracoronary (IC) delivered green fluorescent protein (GFP)-Luc-mesenchymal stem cell (MSCs). GFP+ positive cells in the infarcted heart tissue **(A,B)**, lung **(C,D)**, mediastinal lymph node **(E,F)**, liver **(G,H)**, and spleen **(I,J)** 7 days after intramyocardial (left panel, group IM) or IC (right panel, group IC) delivery of GFP-Luc-MSCs. Time response of luciferase activity is shown in the graphs on the right side.

TABLE 2 | Magnetic resonance image-derived left ventricular functional results 1 month after green fluorescent protein-Luc-MSC percutaneous intramyocardial or intracoronary (IC) delivery.

	Intramyocardial group ($n = 5$)	IC group ($n = 5$)	*p*-Value
3-days magnet resonance image (MRI)			
End-diastolic volume (ml)	65.8 ± 17.8	61.5 ± 20.6	n.s.
End-systolic volume (ml)	42.6 ± 13.1	37.6 ± 12.3	n.s.
Stroke volume (ml)	23.3 ± 5.2	23.8 ± 9.1	n.s.
Cardiac output (l/min)	1.6 ± 0.3	1.6 ± 0.3	n.s.
Ejection fraction (%)	36.2 ± 4.3	38.7 ± 5.2	n.s.
1-month follow-up MRI			
End-diastolic volume (ml)	78.9 ± 30.7	78.3 ± 33.6	n.s.
End-systolic volume (ml)	47.5 ± 22.7	47.5 ± 24.0	n.s.
Stroke volume (ml)	31.4 ± 9.3	30.9 ± 16.7	n.s.
Cardiac output (l/min)	2.3 ± 0.2	1.9 ± 0.5	0.049
Ejection fraction (%)	41.5 ± 5.9	39.4 ± 11.7	n.s.
Change in ejection fraction (%)	5.3 ± 5.2	0.8 ± 8.4	0.046

delivery. Both routes have their advantages, and have shown moderate efficacy in cardiac regeneration therapy (Ben-Haim et al., 1996; Gepstein et al., 1997; Aarnoudse et al., 2007; Gyongyosi et al., 2008; DeCoux et al., 2014; Lukovic et al., 2016). Because intramyocardial cell transfer represents a more invasive procedure, IC cell delivery is more attractive for routine clinical use. However, despite the simplicity, acute ischemia due to stop-flow cell injection technique (repeated occlusion/reperfusion of the infarct-related artery) and the potential for intravascular cell clustering and distal embolization is a concern (Gyongyosi et al., 2010a, 2011). Our results are in line with the observations that higher myocardial accumulation of injected cells with consequent better efficacy profile could be demonstrated if the transplanted cells were injected intramyocardially (Collantes et al., 2017; Kanelidis et al., 2017). In addition to the previous works, we have revealed that intramyocardial injections led to less biodistribution

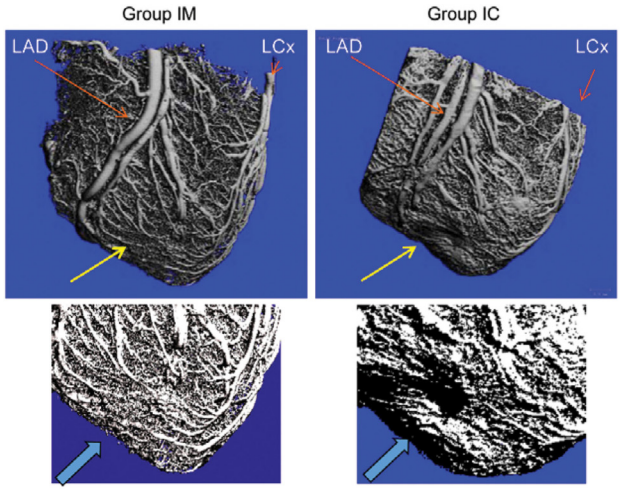

FIGURE 6 | MicroCT of the infarcted and green fluorescent protein-Luc-mesenchymal stem cell (MSCs)-treated hearts. Microvascularization in the infarcted area (yellow arrow) 1 month after intramyocardial (group IM) or intracoronary (group IC) delivery of MSCs. Repeated micro CT image focusing on the anterior apical area of infarction (arrow).

in remote organs, and that intramyocardial injections resulted in higher expression of angiogenic substances in that myocardial areas, where the cells were injected and retained.

Increased Oxidative Stress After IC Injection of Regenerative Cells

In accordance with the decreased blood flow and induced oxidative stress, myocardial expression of MMP-2 was increased in our experiment with diminished CXCR4-mediated homing signal in the IC group, with consequently diminished number of homed stem cells. Increased MMP-2 (both the 72 kD and its 64 kD activated form) expression has already been shown in injured carotid artery, which was remarkably enhanced and dominated by low-flow conditions (Bassiouny et al., 1998). In contrast with the carotid artery, where increased MMP-2 contributes to migration of smooth muscle cells to injury site, the increased expression of MMP-2 in the infarcted heart cleaves the SDF-1alpha/CXCR4 axis, resulting in accumulation of toxic proteolytic remnants, causing also reduced CXCR4-mediated homing signal, as our experiment showed (Giricz et al., 2006; Segers et al., 2007; Rota et al., 2008).

Homogenized myocardial tissue samples from the bioluminescence area (where the GFP-Luc-MSCs were found) showed higher expression of cadherin, SDF1alpha and CXCR4, as well as FGF2 and VEGF in the both groups, suggesting that the secretion of the homing and angiogeneic substances can be at least partly attributed to the injected GFP-Luc-MSCs. However, according to cross-talk of the transplanted stem and host myocardial cells, it is not possible to separate, which cells are responsible for the paracrine activity found in the myocardial areas, where the stem cells were retained.

Engrafted MSC secrete a variety of soluble trophic factors that mediate beneficial paracrine effects in the surrounding cells, especially proangiogenic factors (Bussche and Van de Walle, 2014) and, therefore, creating a favorable microenvironment. MSC may achieve protection by paracrine effects through released mediators rather than direct cardiac regeneration. In addition, less cardiomyocyte apoptosis (Nguyen et al., 2010) and attenuation of the myofibroblast transition in response to reduced oxygen and mechanical stress (Galie and Stegemann, 2014) greatly contribute to cardiac repair. Therefore, MSC and their secretome can reduce tissue injury, protect tissue from further adverse effects, and enhance tissue repair (Gnecchi et al., 2012; Gallina et al., 2015). Considering the limited homing and enhanced cell biodistribution after cell-based cardiac therapies, cell-free therapy injecting the paracrine factors released by stem cells *in vitro* came to foreground in the last years. However, up to now, neither single factor, nor combination of factors or survival cocktail could achieve similar reparative effect as did the stem cells.

Several investigators reported separate results on oxidative stress-induced MMP-2, or homing and biodistribution of injected cells or paracrine effect, to best of our knowledge, our study is the first to demonstrate the role of MMP-2 in cell homing, biodistribution, and paracrine effect of the retained cells, in its entire complexity. By using the *in vitro* bioluminescesce technology, we could localize macroscopically the injected living cells, and investigate the fingerprint of the cells on the myocardium and the additive influence of the local milieu on the injected cells, in terms of release of local paracrine factors.

Imaging of the Cardiac Delivered Stem Cells

In order to investigate the direct effect of the cells in the tissue of our porcine model, we made the cells visible with *in vitro* bioluminescence imaging (Gyongyosi et al., 2010a, 2011). In accordance with the delivery technique, relatively high focal intensity signal could be seen after intramyocardial delivery, while obviously weaker signal was displayed post-IC delivery. Our results confirm previous radiolabeling studies showing poorer retention of stem cells after IC delivery compared to intramyocardial delivery (Hou et al., 2005). Similar to our results, Hale et al. have detected transplanted MSCs in the untreated myocardial areas 1 week after intravenous or intramyocardial delivery, which may reflect the movement of these cells from the infarct zone into the surrounding infarcted and the non-ischemic areas (Hale et al., 2008). We have also observed a widespread distribution of cells into non-target organs such as the liver, spleen, kidney, mediastinal lymph node, pericardium, and bone marrow with mild accumulation of the GFP-Luc-MSCs after 7 days mainly in liver, spleen, and bone marrow. With the exception of the lymph nodes, MSCs were found in organs of the reticuloendothelial system or the bone marrow, the latter being the expected site for "homing" of MSCs. Whether the decreased homing signal in the myocardium contributed to higher level of biodistribution of cells into remote organs remains to be elucidated.

Limitations

We have not included normal, healthy animals as control group, because we intended to compare the differential effects

of the two delivery modes on homing, paracrine function, and biodistribution of the injected cells. Additionally, we and other groups have already published data of control animals without MI and also MI without cell delivery, in comparison with cell-treated animals. Indeed, we have followed the 3R principles of the EU Commission (reduction, refinement and replacement) by reducing the number of the animals to the obligatory minimum. We have measured the myocardial MMP-2, CXCR4, cadherin, SDF-1alpha, FGF2, and VEGF also in the non-ischemic myocardium and compared the measured values to the ischemic infarcted and border areas. Even if it is known that the non-ischemic myocardium undergoes also certain biological processes [intrinsic remote ischemic conditioning by Pavo et al. (2017)], we assume that the expression levels of these factors in the remote areas may reflect the non-ischemic status, close to normal conditions.

We did not block MMP-2 activity by giving TIMP, since this was not the aim of our study. Preclinical studies have already been performed to investigate the cardioprotective effect of different MMP inhibitors, but unexpected systemic toxic effect has been observed by using TIMP (DeCoux et al., 2014): clinical development of most of the MMP inhibitors have been discontinued due to safety reasons (Dorman et al., 2007). Moreover, MMP-blocking in humans did not show beneficial effects on LV remodeling or clinical outcomes (Hudson et al., 2006). Constructing a specific MMP-2-inhibitor releasing system with biodegradable hydrogel for controlled release (CCT40CS), Fan et al. could overcome the pharmacological pitfalls of the MMP-2 inhibitors, namely the poor selectivity, toxicity, and fibrosis-inducing activity. Rats were subjected to anterior MI, and after randomization, animals of the respective groups received direct intramyocardial injections of CCT40CS 30 min post infarction. Results were compared with sham and infarction groups with no MMP-2 inhibitors. In these experiments, the authors have convincingly proven the role of MMP-2 in the infarcted rodent model, and the beneficial effects of a specific construct MMP-2 inhibitor on prevention of cardiac extracellular matrix degradation, cardiac remodeling, fibrosis and improvement of the cardiac function (Fan et al., 2017).

We have not counted the GFP-positive cells and the immunofluorecent stained cells because the quantification of the cell number in different areas of the heart and the remote organs are much more exact by using luciferase assay and ELISA from larger tissue samples (up to 5 mg) than the 4 μm thick limited size of microscopic pictures.

In conclusion, we have demonstrated IC stem cell delivery-associated decrease in myocardial blood flow and the consequent increase in myocardial MMP-2 and decreased CXCR4 expression with less cell homing and less angiogenic substance release. These led to diminished functional improvement of the infarcted left ventricle when compared with intramyocardial stem cell transfer, in the early phase of acute MI in pigs.

ETHICS STATEMENT

All animal studies were approved by the local Experimental Animal Care Committee of University of Kaposvar, Hungary where the experiments were performed (EC 246/002/SOM2006, MAB-28-2005). The experiments conform to the "Position of the American Heart Association on Research."

AUTHOR CONTRIBUTIONS

Planning of study: KZ, DL, RH, and MG. Conducting of experiments: all. Analysis: AG, JW, LM, DT, AS, SW, GZ, CK, AP, AG, ZP, ÖP, IR, RH-W, RM, FG, SC, KH, NP, IP, NN, and DK. Review: all.

FUNDING

This study was supported by the Boltzmann Institute of Cardiovascular Research and the Verein zur Förderung der Forschung (ATVB).

SUPPLEMENTARY MATERIAL

The Supplementary Material for this article can be found online at https://www.frontiersin.org/articles/10.3389/fbioe.2018.00035/full#supplementary-material.

FIGURE S1 | Flow cytometry analysis of mesenchymal stem cells: cells are negative for CD 34 and CD 45 and positive for CD 29, CD 44, CD 90.

FIGURE S2 | Cell proliferation assay post transfection of MSCs with Ad- green fluorescent protein (GFP) and Ad-Luc. Proliferation assay of the transfected and non-transfected porcine mesenchymal stem cells (MSCs). Transient transfection with adenovirus-associated luciferase and GFP resulted in a temporarily significant decrease in proliferation capacity.

FIGURE S3 | Significant logarithmic correlation between marker matrix metalloproteinase-2 (MMP-2) 64 kD intensity and luciferase activity (index of green fluorescent protein-Luc-mesenchymal stem cell number) in the infarcted injected area.

REFERENCES

Aarnoudse, W., Van't Veer, M., Pijls, N. H., Ter Woorst, J., Vercauteren, S., Tonino, P., et al. (2007). Direct volumetric blood flow measurement in coronary arteries by thermodilution. *J. Am. Coll. Cardiol.* 50, 2294–2304. doi:10.1016/j.jacc.2007.08.047

Bassiouny, H. S., Song, R. H., Hong, X. F., Singh, A., Kocharyan, H., and Glagov, S. (1998). Flow regulation of 72-kD collagenase IV (MMP-2) after experimental arterial injury. *Circulation* 98, 157–163. doi:10.1161/01.CIR.98.2.157

Ben-Haim, S. A., Osadchy, D., Schuster, I., Gepstein, L., Hayam, G., and Josephson, M. E. (1996). Nonfluoroscopic, in vivo navigation and mapping technology. *Nat. Med.* 2, 1393–1395. doi:10.1038/nm1296-1393

Bussche, L., and Van de Walle, G. R. (2014). Peripheral blood-derived mesenchymal stromal cells promote angiogenesis via paracrine stimulation of vascular endothelial growth factor secretion in the equine model. *Stem Cells Transl. Med.* 3, 1514–1525. doi:10.5966/sctm.2014-0138

Chavakis, E., Urbich, C., and Dimmeler, S. (2008). Homing and engraftment of progenitor cells: a prerequisite for cell therapy. *J. Mol. Cell. Cardiol.* 45, 514–522. doi:10.1016/j.yjmcc.2008.01.004

Collantes, M., Pelacho, B., Garcia-Velloso, M. J., Gavira, J. J., Abizanda, G., Palacios, I., et al. (2017). Non-invasive in vivo imaging of cardiac stem/progenitor cell biodistribution and retention after intracoronary and intramyocardial delivery in a swine model of chronic ischemia reperfusion injury. *J. Transl. Med.* 15, 56. doi:10.1186/s12967-017-1157-0

DeCoux, A., Lindsey, M. L., Villarreal, F., Garcia, R. A., and Schulz, R. (2014). Myocardial matrix metalloproteinase-2: inside out and upside down. *J. Mol. Cell. Cardiol.* 77, 64–72. doi:10.1016/j.yjmcc.2014.09.016

Dorman, G., Kocsis-Szommer, K., Spadoni, C., and Ferdinandy, P. (2007). MMP inhibitors in cardiac diseases: an update. *Recent Pat. Cardiovasc. Drug Discov.* 2, 186–194. doi:10.2174/157489007782418964

Fan, Z., Fu, M., Xu, Z., Zhang, B., Li, Z., Li, H., et al. (2017). Sustained release of a peptide-based matrix metalloproteinase-2 inhibitor to attenuate adverse cardiac remodeling and improve cardiac function following myocardial infarction. *Biomacromolecules* 18, 2820–2829. doi:10.1021/acs.biomac.7b00760

Galie, P. A., and Stegemann, J. P. (2014). Injection of mesenchymal stromal cells into a mechanically stimulated in vitro model of cardiac fibrosis has paracrine effects on resident fibroblasts. *Cytotherapy* 16, 906–914. doi:10.1016/j.jcyt.2014.01.416

Gallina, C., Turinetto, V., and Giachino, C. (2015). A new paradigm in cardiac regeneration: the mesenchymal stem cell secretome. *Stem Cells Int.* 2015, 765846. doi:10.1155/2015/765846

Gepstein, L., Hayam, G., and Ben-Haim, S. A. (1997). A novel method for nonfluoroscopic catheter-based electroanatomical mapping of the heart. In vitro and in vivo accuracy results. *Circulation* 95, 1611–1622.

Giricz, Z., Lalu, M. M., Csonka, C., Bencsik, P., Schulz, R., and Ferdinandy, P. (2006). Hyperlipidemia attenuates the infarct size-limiting effect of ischemic preconditioning: role of matrix metalloproteinase-2 inhibition. *J. Pharmacol. Exp. Ther.* 316, 154–161. doi:10.1124/jpet.105.091140

Gnecchi, M., Danieli, P., and Cervio, E. (2012). Mesenchymal stem cell therapy for heart disease. *Vascul. Pharmacol.* 57, 48–55. doi:10.1016/j.vph.2012.04.002

Gnecchi, M., Zhang, Z., Ni, A., and Dzau, V. J. (2008). Paracrine mechanisms in adult stem cell signaling and therapy. *Circ. Res.* 103, 1204–1219. doi:10.1161/CIRCRESAHA.108.176826

Gyongyosi, M., Blanco, J., Marian, T., Tron, L., Petnehazy, O., Petrasi, Z., et al. (2008). Serial noninvasive in vivo positron emission tomographic tracking of percutaneously intramyocardially injected autologous porcine mesenchymal stem cells modified for transgene reporter gene expression. *Circ. Cardiovasc. Imaging.* 1, 94–103. doi:10.1161/CIRCIMAGING.108.797449

Gyongyosi, M., Hemetsberger, R., Wolbank, S., Kaun, C., Posa, A., Marian, T., et al. (2010a). Imaging the migration of therapeutically delivered cardiac stem cells. *JACC Cardiovasc. Imaging* 3, 772–775. doi:10.1016/j.jcmg.2010.04.012

Gyongyosi, M., Hemetsberger, R., Posa, A., Charwat, S., Pavo, N., Petnehazy, O., et al. (2010b). Hypoxia-inducible factor 1-alpha release after intracoronary versus intramyocardial stem cell therapy in myocardial infarction. *J. Cardiovasc. Transl. Res.* 3, 114–121. doi:10.1007/s12265-009-9154-1

Gyongyosi, M., Hemetsberger, R., Wolbank, S., Pichler, V., Kaun, C., Posa, A., et al. (2011). Delayed recovery of myocardial blood flow after intracoronary stem cell administration. *Stem Cell. Rev.* 7, 616–623. doi:10.1007/s12015-010-9213-7

Gyongyosi, M., Wojakowski, W., Lemarchand, P., Lunde, K., Tendera, M., Bartunek, J., et al. (2015). Meta-analysis of cell-based CaRdiac stUdiEs (ACCRUE) in patients with acute myocardial infarction based on individual patient data. *Circ. Res.* 116, 1346–1360. doi:10.1161/CIRCRESAHA.116.304346

Hale, S. L., Dai, W., Dow, J. S., and Kloner, R. A. (2008). Mesenchymal stem cell administration at coronary artery reperfusion in the rat by two delivery routes: a quantitative assessment. *Life Sci.* 83, 511–515. doi:10.1016/j.lfs.2008.07.020

Hou, D., Youssef, E. A., Brinton, T. J., Zhang, P., Rogers, P., Price, E. T., et al. (2005). Radiolabeled cell distribution after intramyocardial, intracoronary, and interstitial retrograde coronary venous delivery: implications for current clinical trials. *Circulation* 112(9 Suppl.), I150–I156. doi:10.1161/CIRCULATIONAHA.104.526749

Hudson, M. P., Armstrong, P. W., Ruzyllo, W., Brum, J., Cusmano, L., Krzeski, P., et al. (2006). Effects of selective matrix metalloproteinase inhibitor (PG-116800) to prevent ventricular remodeling after myocardial infarction: results of the PREMIER (Prevention of Myocardial Infarction Early Remodeling) trial. *J. Am. Coll. Cardiol.* 48, 15–20. doi:10.1016/j.jacc.2006.02.055

Kanelidis, A. J., Premer, C., Lopez, J., Balkan, W., and Hare, J. M. (2017). Route of delivery modulates the efficacy of mesenchymal stem cell therapy for myocardial infarction: a meta-analysis of preclinical studies and clinical trials. *Circ. Res.* 120, 1139–1150. doi:10.1161/CIRCRESAHA.116.309819

Lukovic, D., Zlabinger, K., Gugerell, A., Spannbauer, A., Pavo, N., Mandic, L., et al. (2016). Inhibition of CD34+ cell migration by matrix metalloproteinase-2 during acute myocardial ischemia, counteracted by ischemic preconditioning. *F1000Res.* 5, 2739. doi:10.12688/f1000research.9957.1

Mondy, W. L., Cameron, D., Timmermans, J. P., De Clerck, N., Sasov, A., Casteleyn, C., et al. (2009). Micro-CT of corrosion casts for use in the computer-aided design of microvasculature. *Tissue Eng. Part C Methods* 15, 729–738. doi:10.1089/ten.TEC.2008.0583

Nguyen, B. K., Maltais, S., Perrault, L. P., Tanguay, J. F., Tardif, J. C., Stevens, L. M., et al. (2010). Improved function and myocardial repair of infarcted heart by intracoronary injection of mesenchymal stem cell-derived growth factors. *J. Cardiovasc. Transl. Res.* 3, 547–558. doi:10.1007/s12265-010-9171-0

Pavo, N., Lukovic, D., Zlabinger, K., Zimba, A., Lorant, D., Goliasch, G., et al. (2017). Sequential activation of different pathway networks in ischemia-affected and non-affected myocardium, inducing intrinsic remote conditioning to prevent left ventricular remodeling. *Sci. Rep.* 7, 43958. doi:10.1038/srep43958

Penn, M. S., and Mangi, A. A. (2008). Genetic enhancement of stem cell engraftment, survival, and efficacy. *Circ. Res.* 102, 1471–1482. doi:10.1161/CIRCRESAHA.108.175174

Rota, M., Padin-Iruegas, M. E., Misao, Y., De Angelis, A., Maestroni, S., Ferreira-Martins, J., et al. (2008). Local activation or implantation of cardiac progenitor cells rescues scarred infarcted myocardium improving cardiac function. *Circ. Res.* 103, 107–116. doi:10.1161/CIRCRESAHA.108.178525

Roura, S., Galvez-Monton, C., Mirabel, C., Vives, J., and Bayes-Genis, A. (2017). Mesenchymal stem cells for cardiac repair: are the actors ready for the clinical scenario? *Stem Cell Res Ther.* 8, 238. doi:10.1186/s13287-017-0695-y

Schoenhard, J. A., and Hatzopoulos, A. K. (2010). Stem cell therapy: pieces of the puzzle. *J. Cardiovasc. Transl. Res.* 3, 49–60. doi:10.1007/s12265-009-9148-z

Segers, V. F., Tokunou, T., Higgins, L. J., MacGillivray, C., Gannon, J., and Lee, R. T. (2007). Local delivery of protease-resistant stromal cell derived factor-1 for stem cell recruitment after myocardial infarction. *Circulation* 116, 1683–1692. doi:10.1161/CIRCULATIONAHA.107.718718

Thum, T., Bauersachs, J., Poole-Wilson, P. A., Volk, H. D., and Anker, S. D. (2005). The dying stem cell hypothesis: immune modulation as a novel mechanism for progenitor cell therapy in cardiac muscle. *J. Am. Coll. Cardiol.* 46, 1799–1802. doi:10.1016/j.jacc.2005.07.053

Vulliet, P. R., Greeley, M., Halloran, S. M., MacDonald, K. A., and Kittleson, M. D. (2004). Intra-coronary arterial injection of mesenchymal stromal cells and microinfarction in dogs. *Lancet* 363, 783–784. doi:10.1016/S0140-6736(04)15695-X

Wojakowski, W., Tendera, M., Michalowska, A., Majka, M., Kucia, M., Maslankiewicz, K., et al. (2004). Mobilization of CD34/CXCR4+, CD34/CD117+, c-met+ stem cells, and mononuclear cells expressing early cardiac, muscle, and endothelial markers into peripheral blood in patients with acute myocardial infarction. *Circulation* 110, 3213–3220. doi:10.1161/01.CIR.0000147609.39780.02

Wollert, K. C., and Drexler, H. (2010). Cell therapy for the treatment of coronary heart disease: a critical appraisal. *Nat. Rev. Cardiol.* 7, 204–215. doi:10.1038/nrcardio.2010.1

Conflict of Interest Statement: The research was conducted in the absence of any commercial or financial relationships that could be construed as a potential conflict of interest.

frontiers in Bioengineering and Biotechnology

REVIEW
published: 14 May 2018
doi: 10.3389/fbioe.2018.00056

Whole Organ Tissue Vascularization: Engineering the Tree to Develop the Fruits

Alessandro F. Pellegata[1], *Alfonso M. Tedeschi*[1] *and Paolo De Coppi*[1,2]*

[1] *Stem Cells and Regenerative Medicine, Great Ormond Street Institute of Child Health, University College London, London, United Kingdom,* [2] *SNAPS, Great Ormond Street Hospital for Children NHS Foundation Trust, University College London, London, United Kingdom*

Tissue engineering aims to regenerate and recapitulate a tissue or organ that has lost its function. So far successful clinical translation has been limited to hollow organs in which rudimental vascularization can be achieved by inserting the graft into flaps of the omentum or muscle fascia. This technique used to stimulate vascularization of the graft takes advantage of angiogenesis from existing vascular networks. Vascularization of the engineered graft is a fundamental requirement in the process of engineering more complex organs, as it is crucial for the efficient delivery of nutrients and oxygen following *in-vivo* implantation. To achieve vascularization of the organ many different techniques have been investigated and exploited. The most promising results have been obtained by seeding endothelial cells directly into decellularized scaffolds, taking advantage of the channels remaining from the pre-existing vascular network. Currently, the main hurdle we need to overcome is achieving a fully functional vascular endothelium, stable over a long time period of time, which is engineered using a cell source that is clinically suitable and can generate, *in vitro*, a yield of cells suitable for the engineering of human sized organs. This review will give an overview of the approaches that have recently been investigated to address the issue of vascularization in the field of tissue engineering of whole organs, and will highlight the current caveats and hurdles that should be addressed in the future.

Keywords: organ, tissue engineering, vascularization, stem cells, regenerative medicine, decellularization, angiogenesis, endothelial cells

OPEN ACCESS

Edited by:
Andrea Banfi,
Universität Basel, Switzerland

Reviewed by:
Pedro M. Baptista,
Instituto de Investigación Sanitaria Aragón (IIS Aragón), Spain
Andrea Peloso,
Policlinico San Matteo Fondazione (IRCCS), Italy

***Correspondence:**
Paolo De Coppi
p.decoppi@ucl.ac.uk

Specialty section:
This article was submitted to Tissue Engineering and Regenerative Medicine, a section of the journal Frontiers in Bioengineering and Biotechnology

Received: *31 January 2018*
Accepted: *23 April 2018*
Published: *14 May 2018*

Citation:
Pellegata AF, Tedeschi AM and De Coppi P (2018) Whole Organ Tissue Vascularization: Engineering the Tree to Develop the Fruits. Front. Bioeng. Biotechnol. 6:56. doi: 10.3389/fbioe.2018.00056

INTRODUCTION

The availability of whole organs for transplantation still represents a significant burden, while the clinical demand continues to increase. Indeed, the number of patients that are eligible for transplant therapy is likely to grow further in the future. This is thanks to the continued development of medical technologies that can preserve life, allowing patients to live with chronic conditions which were previously fatal. Various congenital and acquired pathologies result in organ failure, for which the only cure is organ transplantation. Donor organ shortages, and complications associated with life-long immunosuppression related to allogeneic transplantation, result in significant morbidity and mortality (Orlando et al., 2012).

Regenerative medicine, in particular tissue engineering aims to regenerate a tissue or organ that has lost its function. This field of research takes advantage of cells, scaffolds and stimuli, delivered through a bioreactor to the growing organ *in vitro* (Tresoldi et al., 2015). Tissue engineering as an approach could represent the best route available to overcome the hurdles related to organ transplantation. Over the last years, interest in this topic has grown, as demonstrated by the numerous studies addressing tissue engineering of whole organs (**Figure 1**). To restore the function of an organ it is vital that all compartments are engineered (Badylak et al., 2011), since the overall function of an organ is due to the synergy of its individual compartments e.g., epithelia, mesoderm, parenchyma and vasculature. It can be argued that the vasculature, in particular, is of great importance in whole organ engineering, and represents the major point of communication between the organ and the rest of the body. For example in organs that exert an endocrine function chemicals are released into the blood stream, while more importantly, the vasculature delivers oxygen and nutrients to the organ, essential for survival. This latter aspect is fundamental in the process of whole organ tissue engineering since the delivery of oxygen in an avascular tissue would be limited to a few hundreds μm by gas diffusion (Jain et al., 2005). This would certainly result in necrosis which would hamper the *in vitro* growth of organs and limit survival post-transplantation. Ideally, the vasculature of the tissue engineered organ should be directly connected to the host vasculature, optimally this would take place at the time of organ grafting by direct anastomosis. Alternatively, the graft could be subjected to an environment that promotes angiogenesis, if rapid ingrowth of host vasculature could be stimulated, over a period short enough to avoid tissue necrosis of the graft, this may provide a vascular network capable of sustaining graft survival.

Blood vessel function is not only limited to the above mentioned functions, indeed endothelial cells play an active role in orchestrating the processes involved in tissue repair (Ding et al., 2011; Takebe et al., 2013; Hu et al., 2014; Pellegata et al., 2015; Poulos et al., 2015; Ramasamy et al., 2015). This aspect is crucial in the regeneration and engraftment processes of whole organ engineering and can be easily demonstrated by the parallel interest in whole organ tissue engineering (**Figure 1**) and angiogenesis in tissue engineering (**Figure 2**).

In order to engineer whole organs that can function and survive upon grafting, it is essential to incorporate a functional endothelium. Establishing a properly organized vascular network that features vessels of the correct size, protruding evenly throughout the whole organ will have a huge impact on translation of tissue engineered organs into clinical practice. The optimal scenario would be for researchers to establish techniques for the development of endothelial layers, thus providing a barrier with vasomotility and a site for perfusion which matches the specific typology of the target organ in terms of endothelial pattern, such as normal, fenestrated or sinusoidal (Rafii et al., 2016).

Although organ vascularization represents a significant bottleneck to clinical translation, many different and promising approaches have been investigated. This review will provide an overview of the different strategies that have been employed, analyzing the state of the art techniques applied to the major organs of the body.

WHOLE ORGANS DECELLULARIZATION

Decellularization is the complete removal of all cellular and nuclear material from a tissue while preserving its extracellular matrix (Gilpin and Yang, 2017). The process is usually achieved by means of detergents and enzymes, coupled with physical stress. Nearly every tissue of the human body has been decellularized, and very recently, whole human limbs have been used to produce acellular scaffolds (Gerli et al., 2018). This technique has the unique advantage of generating a

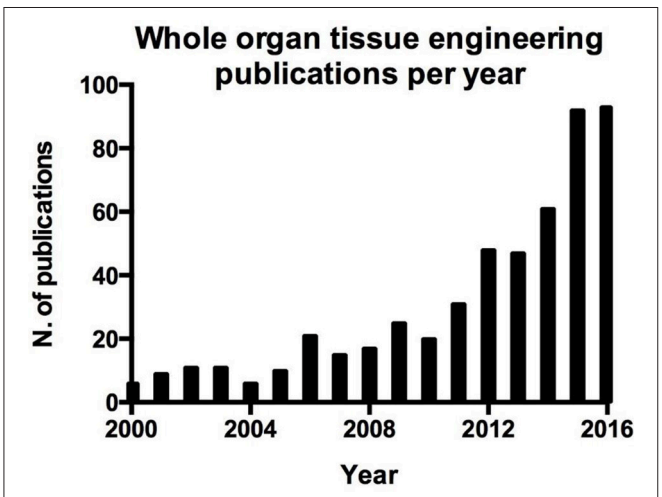

FIGURE 1 | Number of publication per year on whole organ tissue engineering resulting from a search on Pubmed.

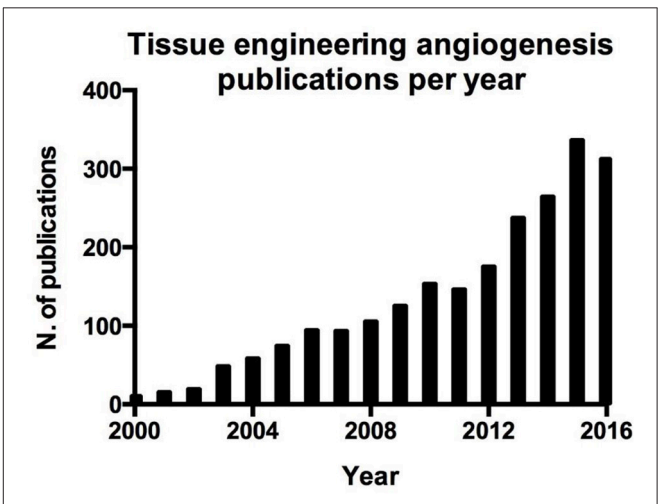

FIGURE 2 | Number of publication per year on angiogenesis in tissue engineering resulting from a search on Pubmed.

scaffold that closely resembles the native environment from both a biochemical and anatomical point of view (Crapo et al., 2011). Acellular matrices allow cellular growth and functional differentiation without triggering an immune response, even in the case of xenogeneic transplantation (Fishman et al., 2013).

The natural and obvious evolution of this technique has been the decellularization of whole organs (Scarritt et al., 2015). This approach represents the easiest way to obtain a scaffold which exactly mimics the complex structure of an organ, an aspect that is crucial to rebuild the organ and restore its function. Moreover, organs that are deemed medically unsuitable for transplantation due to poor condition, could represent a potential source of organs for the generation of decellularized scaffolds for tissue engineering (Peloso et al., 2015; Verstegen et al., 2017).

Interestingly, it has been shown that among the different compartments preserved within decellularized organs, the extracellular matrix of the vasculature is unaltered and retains its structure, resulting an easy route to deliver cells evenly throughout the whole organ. Preservation of the vasculature has been demonstrated in different organs such as intestine (Totonelli et al., 2012), lung (Maghsoudlou et al., 2013), liver (Maghsoudlou et al., 2016), heart (Ott et al., 2008), and kidney (Song et al., 2013; Bonandrini et al., 2014).

CELLS FOR WHOLE ORGAN TISSUE ENGINEERING

The microvasculature is an essential feature of the organ, needed to transport nutrients, blood cells, oxygen and waste products. This network of complex vessels is formed by a process of angiogenesis and neovascularization. It is composed of different interacting cell types, endothelial cells (ECs) lining the vessel wall, and perivascular cells or mural cells, mainly composed by pericytes (PC) and vascular smooth muscle cells (vSMC). These processes are crucial during growth and development, injury, repair, and remodeling, since these rely on the interactions between the microvasculature and its microenvironment (Bergers and Song, 2005).

When considering the vasculature that must be regenerated during whole organ tissue engineering, the most crucial and difficult part to engineer is the microvasculature which is composed of ECs and PCs. Moreover larger vessels are surrounded by a layer of vSMCs which regulates the blood afflux to the organ. Determining the best cell source to deliver the different anatomical structures of the vasculature within a whole organ is a crucial step. This section, will focus on the different strategies that have been published in the literature and that have shown potential for use in whole organ tissue engineering.

Endothelial Cells

Finding a suitable endothelial cell source still remains a significant hurdle toward the delivery of vascularized tissue engineered organs. This is particularly significant because adult endothelial cells show an impaired proliferative potential after expansion. In tissue engineering the key aim is to harvest primary cells with minimum invasion, to culture and expand these cells returning a high yield sufficient to colonize the organ. Cells should retain their basic functions, for example endothelial cells should inhibit blood clotting while promoting anastomosis to the host vasculature. With this aim in mind, different cell sources have been investigated ranging from primary isolated adult cells, to cells differentiated from stem or progenitor cell populations.

Classical adult endothelial cell harvesting requires the involvement of large diameter vessels. For this reason, harvesting ECs from patients remains a problem of great concern with significant complications. The only non-invasive sources of adult human ECs remains cadaveric vessels and the umbilical vein (Bourke et al., 1986). Human umbilical vein endothelial cells (HUVECs) have so far been the gold standard in EC research due to their relative ease of accessibility and high yield following isolation. However, HUVECs have shown poor engraftment and anastomosis when transplanted into various animal models. In 2004, with the aim of creating long lasting blood vessels, HUVECs and mesenchymal cells were seeded in a three-dimensional fibronectin-type 1 collagen gel, then implanted into mice. In this experiment, HUVECs were able to form tubes that connected to the host vasculature allowing perfusion. However, HUVECs alone showed limited capacity to form vessels and failed to survive in the long term, although the functionality of the vasculature over a long period of time was not assessed in this study (Koike et al., 2004). More recently Mummery's group observed that HUVECs were not able to incorporate into the vasculature of *zebrafish* xenograft model, but rather attached to the vasculature or migrated throughout the embryo. Therefore, alone HUVECs are an inadequate source of cells for vascular tissue engineering, making it necessary to investigate other options (Orlova et al., 2014).

Endothelial progenitor cells (EPC) can be isolated from the peripheral blood, offering a potential source of autologous cells that can be easily harvested. EPCs were firstly described by Asahara et al. who identified a hematopoietic population capable of eliciting postnatal vasculogenesis in adult peripheral blood (Asahara et al., 1997).

Blood-derived EPCs have already been used to endothelialize synthetic vascular grafts in several studies (He et al., 2003; Shirota et al., 2003). Grafts lined with these EPCs have been implanted *in vivo* into a canine carotid model. After 30 days, 11 out of 12 grafts remained patent, with cells lining the surface showing features of a mature EC phenotype (He et al., 2003). Umbilical cord blood (Murga et al., 2004) and bone marrow (Hamilton et al., 2004) could represent additional sources of autologous vascular progenitor cells. Indeed, several studies have shown that bone marrow–derived cells functionally contribute to neoangiogenesis during wound healing and limb ischemia (Majka et al., 2003), endothelialization of vascular grafts (Shi et al., 1998), and organ vascularization (Otani et al., 2002). Differentiated human umbilical cord blood derived EPCs seeded on vascular scaffolds formed neotissue in both biomimetic and static *in vitro* environments. These tissues were characterized as endothelial monolayers with related functions (e.g., the production of eNOS indicating features of functional endothelium) (Schmidt et al., 2004).

However, significant controversies exist over the identity and role of EPCs in vascular repair, cord blood is not available from all individuals and the rarity and expansion potential of these cells make them unsuitable for scaled-up production. For this reason, alternative sources for patient-specific ECs would be of value.

More recently induced pluripotent stem cells (iPSC) have been broadly investigated as a promising cell source for ECs. Mummery's group found that human iPSC-derived ECs are able to form blood vessels and anastomose to the host vasculature when injected into a zebrafish model (Orlova et al., 2014). Moreover, iPSC-derived ECs were able to outperform HUVECs, which were so far considered the gold standard in EC research. While promising, the clinical use of ECs derived from iPSC is still associated to concerns regarding the tumourogenic potential of pluripotent cells and their limited clinical use for macular degeneration in the retina (Cossu et al., 2017).

It would be advantageous to overcome both the limited yield and availability of adult cells and the tumorougenic potential of EC-iPSC. For this reason, it is possible that the work proposed by Rafii's group would be extremely relevant to the field. In particular, they described the direct conversion of somatic cells to functional endothelium. Interestingly, the approach has been performed with human mid-gestation lineage-committed amniotic fluid derived cells which have been converted into a phenotypically stable and expandable population of vascular ECs without transition through a pluripotent state (Ginsberg et al., 2015).

Recently, the idea that ECs only serve to line simple passive "tubing" systems is slowly coming to an end, their role is more complex than simply delivering oxygen and nutrients, and includes modulating the coagulation of blood, regulating the transportation of inflammatory cells and serving as gatekeepers of cellular metabolism (Carmeliet and Jain, 2011; Ghesquière et al., 2014). Tissue-specific microvascular networks of capillaries can perform complex physiological tasks such as sustaining the homeostasis of resident stem cells and guiding the regeneration and repair of adult organs avoiding fibrosis. Further evidence exists to support the idea that ECs produce angiocrine factor, providing inhibitory and stimulatory tissue-specific signals for stem cell renewal (Butler et al., 2010; Nolan et al., 2013). With this in mind, tissue engineering processes reliant on the use of stem cells could benefit from the establishment of an appropriate endothelial niche. This could provide the ideal environment to recapitulate the complex signaling networks able to instruct organ regeneration.

Pericytes

ECs are the main component of the vasculature which have been extensively studied and characterized, while pericytes are now coming into focus as key regulators of angiogenesis. Although paternity of pericytes is generally assigned to Rouget in 1874 (Rouget, 1874). Rouget cells have since then been re-named pericytes, referring to their anatomical localization in close proximity to the endothelial layer by Zimmermann in 1923 (Zimmermann, 1923). The periendothelial location of pericytes is frequently confused with the periendothelial location of vascular smooth muscle cells, fibroblast and macrophages (Armulik et al., 2011). Although everyone adopted the view that pericytes belong to the same lineage of vSMCs, it is widely accepted that there is no singular molecular marker that enables us to distinguish them unequivocally from vSMCs or other mesenchymal cells. In addition, the expression of markers used to identify pericytes is transient and is not consistent, indeed different perycites can express different sets of markers and this expression can change throughout the life of the same cell (Armulik et al., 2011). Due to this heterogeneity, and marker promiscuity, it has been impossible to fully establish pericyte identity, and the only clear definition refers to their anatomical location. Currently cells defined as pericytes are localized in the vascular basal membrane as seen via electron microscopy (Miller and Sims, 1986).

However, this definition loses strength in conditions of active angiogenesis, such as during embryogenesis and tissue regeneration, where clear identification of these pericytes becomes even more difficult. It is also widely accepted that pericytes are more frequent in the proximity of micro-vessels (capillaries, venules, and terminal arterioles), where they share the basal membrane with endothelial cells, and are connected by tight, gap, and adherent junctions. Indeed, a single pericyte can be connected with several endothelial cells by cell protrusions that wrap around, and along the blood vessel (Gerhardt and Betsholtz, 2003; Kovacic and Boehm, 2009). However, even this definition has been challenged by the observations of sub-endothelial pericyte-like cells in large vessels (Díaz-Flores et al., 2009). Although many controversial aspects exist in the field, an increasing number of studies suggest that perycites may be the progenitor of vSMCs, and may constitute multipotent progenitor cells like adipocyte progenitors (Olson and Soriano, 2011), osteoblast, chondrocytes (Collett and Canfield, 2005), and skeletal muscle stem cells (Dellavalle et al., 2007). This resembles the behavior of mesenchymal stem cells (MSCs) and therefore it has led to the concept of a perivascular niche of MSCs (Armulik et al., 2011).

Paolo Bianco's laboratory has argued in support of this theory, and on the widely shared view that MSCs are ubiquitous in human connective tissue, defined by common *in vitro* phenotype and coinciding with ubiquitous pericytes. They reported that ubiquitous MSCs with identical capacities do not exist, but that "tissue-specific" mesodermal progenitors are capable of being recruited to a mural cell fate, providing a plausible mechanism by which pericytes are formed, and how they serve as a source of local progenitor cells (Sacchetti et al., 2016). Together these considerations provide evidence to suggest that pericytes are a powerful tool for tissue regeneration since they can contribute to restoration of the vascular smooth muscle layer, known to be essential for a functional and mature endothelium (Bergers and Song, 2005), as well as the mesodermal compound of the tissue from which they originate. Nevertheless, it is not possible to exclude the theory that these cells can contribute to regeneration of the smooth muscle compound of organs due to their default capacity to differentiate into vSMCs, which does not have a clear distinction from non-vascular smooth muscle cells.

Regardless their origin, it is largely accepted that perivascular cells play an important role during the early phases of angiogenesis. Although initial endothelial cell sprouts may form

without pericyte involvement, pericytes are among the first cells to invade newly vascularized tissues, and are found to be located at the growing front of endothelial sprouts. Pericytes can suppress endothelial growth, migration and microvessel stabilization (Bergers and Song, 2005; von Tell et al., 2006), moreover, pericyte involvement has also been directly implicated in conferring capillary resistance to regression *in-vivo*. For this reason, an increasing number of studies are focusing on these cells type for the purpose of vascular tissue engineering. As a source of pericytes for tissue engineering, a pioneering study from the groups of Bianco and Cossu reported that cells isolated from the embryonic murine dorsal aorta, and ascribed to the perivascular lineage (by the expression of CD34, Flk-1, SMA and c-Kit), are able to generate *in-vivo* both vascular and extravascular mesodermal derivatives. For this reason, these cells have been named mesoangioblasts (MAB) (Minasi et al., 2002). However, MABs derived from adult tissue lose their endothelial features, and are therefore considered "pericyte derived" cells. Cells with similar features can be isolated from skeletal muscle biopsies, and they are able to differentiate down the smooth muscle lineage (default function of a pericyte) and skeletal muscle (as mesodermal lineage of origin) (Dellavalle et al., 2011). Similarly to what we have discussed above, pericytes could be derived from pluripotent stem cells. A protocol for deriving MAB-like stem/progenitor cells from human and murine iPSCs has been recently established (Gerli et al., 2014). Relevantly, defined conditions for simultaneous derivation of ECs and PCs from hiPSCs of different tissue origin with high efficiency have also been defined (Orlova et al., 2014).

Vascular Smooth Muscle Cells

From a whole organ tissue engineering perspective, the overall range of differently sized vessels which form the vascular tree must be regenerated because microvasculature alone cannot support organ function. Indeed, smooth muscle cells, which represent the main difference between microvasculature and larger vessels, have a crucial role in delivering vasculature function. They deliver vasomotiliy and contribute to the biomechanical blood flow response (Neff et al., 2011). Consequently, derivation and culture of vascular smooth muscle cells represent a significant step toward regeneration of the whole vasculature.

Different approaches have been exploited in order to find a suitable and reliable cell source that could give rise to the vascular smooth muscle compartment. However, while in the specific field of blood vessels tissue engineering, intended to regenerate a single vascular graft, a lot of efforts have been put into engineering the smooth muscle layer (Tresoldi et al., 2015), the field of whole organ revascularization has mainly addressed pericytes regeneration to provide a stable microvasculature.

Mesenchymal stem or stromal cells are one of the most widely investigated sources to derive VSMCs. A seminal paper which combined decellularized scaffold and MSCs was published by Zhao et al. They were able to derive ECs and vSMCs from bovine MSCs to fully develop tissue engineered arteries which were transplanted into a sheep model as a carotid artery interposition which remained patent over 5 months (Zhao et al., 2010a). Another example is provided in the work by Jung et al. where human MSCs were used to create a scaffold-free graft which featured a mature smooth muscle layer (Jung et al., 2015).

Beside MSC, adipose derived stem cells (ADSCs) represent another broadly exploited VSMCs source because of their easy harvesting. Indeed this cell type is able, under the right biochemical and biomechanical conditions, to give rise to a mature smooth muscle phenotype that features contractility (Harris et al., 2011). The principal pathway involved seems to be transforming growth factor-beta 1 (TGF-β1). Indeed, in a similar study, ADSCs were induced to differentiate into VSMCs through TGF-β1 and bone morphogenic growth factor. The human VSMCs derived from ADSCs were seeded on small-caliber vascular graft. The resulting vessel wall had a dense and well-organized structure similar to the one of physiological vessels (Wang et al., 2010).

A remarkable example of delivering the smooth muscle layer in a whole organ is represented by the promising results that have been achieved by Ott's laboratory. In their work, the co-seeding of HUVECs and human MSCs, as perivascular supporting cells, in decellularized rat lung scaffolds resulted in a broad re-endotheliasation, but more interestingly, in the same work, they regenerated the lung vasculature using both endothelium and vSMCs with cells derived from human inducible pluripotent stem cells, showing how these cells can represent another valuable source of vSMCs (Ren et al., 2015).

Furthermore, vSMCs, as mentioned above, are supposed to feature a common ancestry with pericytes, making the sources of PCs presented in the previous paragraph a potential cell population for the derivation of the smooth muscle phenotype. In particular, mesoangioblasts, which are an easily accessible cell population are already used in the clinic (Cossu et al., 2015), and can give rise to a smooth muscle phenotype (Tagliafico et al., 2004), making them an ideal candidate for regeneration of the smooth muscle vascular layer. Another option which has been investigated, is the direct recruitment of VSMC *in-vivo*. This approach worked for blood vessels of 5–6 mm in diameter (Pellegata et al., 2015; Syedain et al., 2017).

To summarize, a fully functional and mature vasculature requires both endothelial and mural cells. Many studies focused on blood vessel tissue engineering have demonstrated the importance of this coexistence. However, the majority of the attempts to regenerate the vasculature in whole organs have been carried out using only ECs as discussed in the next sections of this review. The results achieved in the last years, using different cell types together, definitely suggest that the co-culture approach is more appropriate to address whole organ revascularization.

LIVER AND PANCREAS

Within the field of whole organ tissue engineering, liver is the most widely investigated organ of all, with one third of studies published on the liver including the issue of vascularization. Indeed, there is a relevant clinical need dictated by the shortage of available organs for transplant. Moreover, the anatomy of the liver lends itself well to decellularization, a process that has been established for both animal and human liver (Mazza et al.,

2015). Subsequent recellularization can be obtained through the portal vein, even in small animal models. Indeed, the portal vein together with suprahepatic vein represents the most relevant vasculature since a liver can survive without its arterial supply. Hepatic tissue engineering still remains a significant challenge and to date the derivation of mature hepatocytes is an unmet goal (Hannan et al., 2013; Leclerc et al., 2017), however the environment, in particular the decellularized matrix seems to favor this process (Lorvellec et al., 2017). Potentially endothelial cells could play an active part in liver tissue engineering, since they are known to control liver regeneration (Ding et al., 2010), indeed Taniguchi's group described in a pioneering study that the transplantation of vascularized liver buds were able to recapitulate the organ function (Takebe et al., 2013).

From an organ tissue engineering perspective, the main strategy adopted is the injection of endothelial cells, mainly HUVECs (Baptista et al., 2011; Shirakigawa et al., 2013; Takebe et al., 2014; Bao et al., 2015; Verstegen et al., 2017). Pioneering work was performed by Soker's group in 2011 where they reported decellularization of whole livers from different species. In addition, the group cultured HUVECs together with fetal cells in ferret liver scaffolds and demonstrated that the regenerated endothelium does not leak when perfused with labeled dextran (Baptista et al., 2011). Bao et al. cultured HUVECs in pig decellularized scaffolds functionalized with heparin over 3 days, showing a good engraftment of the cells, furthermore they showed how the functionalized decellularized liver does not elicit sudden thrombosis when grafted in the infra-hepatic space of piglets (Bao et al., 2015). Orthotopic liver transplant has been performed also by Atala's group, in their study MS1 re-endothelialized porcine livers sustained blood perfusion *in-vivo* for 24 h avoiding thrombi formation and resulting in patent vessels as confirmed by ultrasound monitoring (Ko et al., 2015). HUVECs were used also in another study, in which endothelial cells were dynamically cultured for 3 days on decellularized rat livers, interestingly the cells prevented blood leakage upon *in-vitro* reperfusion (Shirakigawa et al., 2013). HUVECs were also tested on human decellularized livers, specifically Verstegen et al. seeded HUVECs on 250 μm scaffold slices achieving a good recellularization and highlighting how the matrix instructed cells to locate in the vascular tissue (Verstegen et al., 2017). Furthermore, in another study the endothelial cell line EA HY926 was used to recellularize an acellular pig liver lobe, coated with heparin gel which promoted cell adhesion and engraftment. Dynamic culture for 10 days resulted in an even cell distribution of cells, and the scaffold did not elicit thrombosis when heterotopically grafted in pigs for 1 h (Hussein et al., 2016). It should be remarked that in the studies by Hussein et al. and Bao et al. the addition of heparin immobilized on the scaffold enhanced the blood perfusion over time *in-vivo* (Bao et al., 2015; Hussein et al., 2016). Perfusion over the long term still remains the main hurdle, indeed these studies showed a limited time frame of up to 3 days post-implantation, while patency over a long period should be established to deliver a clinically relevant hepatic graft. Kadota et al. proposed an approach in which bone marrow derived mesenchymal stem cells seeded in a rat liver produced pro-angiogenic factors and sustained an orthotopic transplantation for 60 min (Kadota et al., 2014). This represents a reversed approach in which the strategy is to promote the ingrowth of host vasculature, similar to what is described in similar studies using collagen gel, and showing ingrowth of host blood vessels. In particular, in the study by Zhao et al. the collagen gel was embedded with hepatocytes before subcutaneous implantation for 7 days (Takimoto et al., 2003; Zhao et al., 2010b). However, this approach limits the size of the graft as the ingrowth of blood vessels cannot be fast enough to sustain human sized tissues while avoiding necrosis.

The pancreas, which shares many key endocrine and exocrine functions with the liver, has been decellularized as a whole organ to address the possibility of islet transplantation. Two reports have been published which have addressed recellularization with endothelial cells. Peloso et al. reported the dynamic culture of human decellularized pancreas with human primary pancreatic endothelial cells (Peloso et al., 2016). Results showed engraftment of cells which maintained a CD31 positive phenotype, half of the cells seeded continued to proliferate. Furthermore, Guo et al. recently performed re-endothelialization of decellularized rat pancreas with EPCs (Guo et al., 2018). The repopulated scaffolds were subcutaneously implanted in mice showing anastomosis with host vasculature resulting in a higher density of blood vessels in the graft compared to unseeded scaffolds.

To go progress liver and pancreas tissue engineering for translation into clinical care, it will be necessary to deliver pre-vascularized engineered organs which could sustain long-term orthotopical engraftment. Focus should be given to engineer specialized liver endothelium which features a very particular and site specific vasculature that should be recapitulated.

KIDNEY

The kidney contains clear vascular access from both arterial and venous vessels. As a filtration organ, vasculature plays a key role in organ function, making the vasculature necessary not only for the survival of the engineered graft, but also to deliver its function. Different cellular sources have been used to engineer the renal vasculature, with the renal artery being the main route of cell delivery.

The first attempt at whole kidney tissue engineering was described by Ott's group. In their study they described the decellularization of kidneys from different species, such as rat, pig and human. They were able to repopulate rat kidneys using HUVECs and rat neonatal kidney cells, achieving a spatial distribution that resembled the native glomerula. Dynamic culture of the seeded cells resulted in a drop in vascular resistance and evidence of vascular function. The group performed a short-term orthotopic implantation of the engineered kidney by anastomosis of both vascular pedicles. They reported evidence of a distinct vasculature which avoided the formation of blood clots, although it was not clearly stated for how long the graft was in place (Song et al., 2013). Interestingly, they reported that the extracellular matrix was able to spatially instruct the cells and drive them toward the correct anatomical location.

The notion of an instructive ECM has been also described by Remuzzi's group. In their work they showed that murine

embryonic stem cell fate is influenced by the decellularized scaffold. In this experiment, cells seeded through the renal artery of a decellularized rat kidney became distributed evenly in capillary structures. Within 72 h of seeding the cells had lost their pluripotency, and were shown to differentiate into mesoderm-derived endothelial precursors (Bonandrini et al., 2014). The instruction of embryonic stem cells has also been demonstrated in large animal studies. In a study proposed by Batchelder and colleagues, human ESCs were seeded on decellularized rhesus monkey kidneys. After 7 days, the cells differentiated into kidney specific cell types comprehensive of a CD31+ cell fraction (Batchelder et al., 2015). To further describe how endothelial cells could orchestrate cell fate, Du et al. seeded a mouse decellularized kidney with iPSC-derived Pax-2+ progenitors and iPSC-derived endothelial cells. They showed how the presence of endothelial cells regulated the expression of renal genes in the progenitor cells. The scaffolds were subcutaneously implanted in SCID mice for 12 weeks. Results showed that only in the presence of endothelial cells were the glomeruli recellularized. Moreover, they showed *in-vitro* how endothelial cells improved glomerular barrier function (Du et al., 2016). Very recently Bombelli et al. derived human nephrospheres, the spheres were shown to contain renal stem cell like cells. Interestingly, when cultured on decellularized tissue slices they showed that the ECM is again able to instruct the nephrospheres and drive their differentiation toward endothelial cells and tubular structures in 30 days (Bombelli et al., 2017). Overall kidney revascularization has been investigated using a wide range of different cell sources, demonstrating that the extracellular matrix can provide the cues required for cell differentiation. Alternatively, Atala's group has focused on primary cells, providing evidence which suggest that primary cells can be used to replace human size renal function and they have developed a method that allows the efficient expansion of primary cells which can maintain a normal renal phenotype (Abolbashari et al., 2016).

INTESTINE

Decellularization has proven to be an effective technique to provide acellular intestinal scaffolds, with preserved native vasculature (Totonelli et al., 2012). Preserving vascular access such as the mesenteric artery and the mesenteric vein facilitates transplantation of the organ, providing vessels that can be anastomosed in the host, providing immediate perfusion to the organ, essential for survival of the graft upon transplantation (Zhu et al., 2008). To date, a very limited number of papers have addressed the vasculature of the intestine. Very recently, decellularized rat intestinal segments were engineered with iPSC-derived epithelial cells for 14 days and HUVECs for 3 days. The intestine was subsequently implanted in a heterotopic model consisting of a subcutaneous graft in the neck, anastomosed to the vasculature and provided with two-end stomas. The graft was maintained for 4 months, results reported graft functionality, and nutrients delivered into the lumen of the engineered intestine, via the stoma, were adsorbed into the rat blood stream. However, patency of the engineered blood vessels wasn't directly assessed (Kitano et al., 2017). A similar approach was taken by MacNeil's group, who injected human dermal microvascular endothelial cells, and human dermal fibroblasts, into the vasculature of decellularized rat intestines. They demonstrated successful delivery and engraftment of the cells in the decellularized vasculature, in addition to ongoing sprouting angiogenesis featuring DLL4 positive cells (Dew et al., 2016). To date there have been few reports investigating the topic of intestine re-endotehlialization. Intestinal tissue engineering is being studies by many groups but the development of intestinal vasculature still remains an open field that deserves attention. The intestinal epithelium is a complex environment in which there exists a complex crosstalk between many different cell types, it will thus be fundamental to unveil how epithelium and endothelium interact in orchestrating this particular epithelium. Finally, it is relevant to remark that in order to achieve a functional intestine, engineering of the lymphatic tissue is essential and this has only be partially explored (Koike et al., 2004).

LUNG

Lung function depends on the presence of a functional vasculature to achieve optimal gas exchange. Therefore it is not surprising that nearly half of the work related to whole lung engineering is focussed on engineering of the vasculature. Early studies demonstrated the feasibility of whole lung decellularization (Maghsoudlou et al., 2013). Cortiella et al. reported the first attempt to decellularize a whole lung. In this study, they showed how the pulmonary extracellular matrix was able to instruct mouse ESCs to differentiate into site-specific cells such as CD31+ cells, similarly to what has been seen in ECMs derived from other organs (Cortiella et al., 2010). The same group recently reported the decellularization of human pediatric lungs, with subsequent seeding of primary adult human epithelial and vascular cells, and dynamic bioreactor culture (Nichols et al., 2017). Interestingly, they reported a good distribution of cells throughout the scaffold, with proper recellularization of the blood vessel. Type 1 and 2 epithelium were present, and were shown to have the capacity to produce surfactant.

In 2010, Niklason's team decellularized rat lungs and seeded them with pulmonary epithelium and vascular endothelium utilizing a custom-made bioreactor. Interestingly, the seeded epithelium displayed remarkable hierarchical organization within the matrix, and the seeded endothelial cells efficiently repopulated the vascular compartment. Moreover, mechanical characteristics of the engineered lungs were similar to those of native lung tissue, and when implanted into rats the engineered lungs participated in gas exchange (Petersen et al., 2010). Ott's group has a long history of work addressing whole lung engineering; in 2014 they reported decellularization of rat, pig and human lungs, and the cytocompatibility of these matrices by seeding either epithelial cells or HUVECs on slices (Gilpin et al., 2014). In a subsequent study, they introduced the concept of addressing both the endothelial and the perivascular compartments, and introduced seeding through both arterial and venous routes (Ren et al., 2015). They co-seeded either HUVECs and hMSC, or iPSC-derived ECs and PCs, reaching a

75% endothelial coverage that resulted in a good barrier function. Re-endothelialized lungs were orthotopically transplanted into rats for 3 days, *in-vivo* characterization was limited to showing the presence of cells and perfusability of the HUVECs-hMSC seeded grafts. Finally, in the same study they showed scalability, up to human lung size. Scalability was improved in two later studies in which the same group showed the recellularization of human and pig lungs with both epithelial and endothelial cells (Gilpin et al., 2016; Zhou et al., 2017). However, the latter were orthotopically transplanted for only 1 h showing a poor degree of gas exchange. Other published studies have been able to reach an even cellular distribution throughout whole decellularized rat lungs, following seeding using rat microvascular endothelial cells (Calle et al., 2016; Stabler et al., 2016). Niklason's group exploited the concept of regenerating the vessel mural compartment by re-endothelializing decellularized rat lungs using rat endothelial cells supported by rat adipose-derived stem/stromal cells which gave rise to pericytes. The re-endothelialized lungs showed improved vascular resistance comparable to native lungs, moreover they were orthotopically transplanted in rats for 3 h showing how the presence of perivascular cells avoided oedema formation (Doi et al., 2017).

Finally, a slightly different approach was proposed by Wagner et al. (2014). In their study, they isolated bronchovascular bundles and coated these with sodium alginate showing how this increases cellular adhesion toward scaling up, however, they report variability in the decellularization outcomes that failed to be standardized. Taken together studies focused on the lung show how seeding through both arterial and vascular vessels is necessary in order to reach an even distribution of cells, that can potentially support organ function. Results are encouraging, however, lung re-endothelialization still lacks *in-vivo* transplantation results which exceed 3 days.

HEART

In the context of the heart, endothelial cells play a double role, both lining the coronary vasculature, providing nutrients to the hearth muscle, as well as covering the valves and chambers of the heart. Whole heart re-endothelialization has been firstly investigated in the rat by Taylor's team. Rat aortic endothelial cells were seeded onto decellularized rat hearts via perfusion of the aorta. After 1 week of dynamic culture in a bioreactor, cells repopulated coronaries and showed metabolic activity (Ott et al., 2008). A similar approach was described by Yasui et al. who reported 30 days of successful dynamic co-culture when scaffolds were seeded with rat neonatal endothelial cells alongside rat neonatal cardiomyocytes and fibroblasts. These results showed that, although they achieved contraction, cells were randomly distributed in the organ ECM (Yasui et al., 2014). From a methodological perspective, other studies have compared different seeding approaches. Robertson et al. demonstrated that when rat aortic endothelial cells are seeded onto a decellularized rat heart, better cell distribution is achieved when perfusion is via the inferior vena cava and brachiocephalic artery compared to the aorta. After 7 days, of bioreactor culture cells are shown to retain their phenotype, were able to produce nitric oxide, and reduced thrombosis in an *in-vitro* assay. Finally, they performed a heterotopic transplantation by anastomosis to the aorta and inferior vena cava of the recipient, transplanting unseeded scaffolds as control. After 1 week, re-endothelialized hearts showed clear vessel formation with reduced incidence of blood clotting (Robertson et al., 2014).

Scaling up of techniques has been described in two studies using pig and human hearts. Weymann et al. seeded HUVECs and murine neonatal cardiac cells onto the decellularized scaffold of a pig heart, and cultured the organ in a bioreactor for 3 weeks. After 10 days a homogeneous re-endothelialization of the coronary tract was reported (Weymann et al., 2014). Sanchez et al. reported the decellularization of a whole human heart (Sánchez et al., 2015) followed by recellularization of tissue slices. Recellularization was tested by culturing HUVECs with different cell types on scaffold slices for 21 days. Endothelial cell migration was reported and cells were shown to line the endocardium and vasculature, demonstrating again that the ECM can direct cells to their correct location during engraftment. To successfully engineer a whole heart for clinical translation, scaling up of techniques is essential. Studies to date are limited to the use of HUVECs and rat aortic cells, making it necessary to find a more suitable primary cell source, especially because endothelium is needed also for atria, ventriculi, and valves. Heart orthotopic engineering poses incredible challenges, heterotypical implants in addition to proper functional evaluation of the *in-vitro* engineered vasculature are required to proceed to the next step.

DISCUSSION AND FUTURE DIRECTIONS

To date, there is significant interest in the field of whole organ tissue engineering. The growing demand for a solution to the availability of transplant organs is high on the agenda for patients, clinicians and health care providers. The field of whole organ engineering is an innovative and exciting area of research with the potential to overcome, and provide a solution to the availability of transplantable organs. There are some organs and tissues for which the vasculature does not play a prominent role, as demonstrated by successful transplantation of engineered tracheas which were supported by an omental wrap at orthotopic transplantation (Elliott et al., 2012). As discussed above however, it is clear that the vasculature is a fundamental feature of more complex organs.

The majority of studies on-going in the field of whole organ tissue engineering take advantage of decellularized organs as the basis, providing a scaffold on which the complex multicellular organ can be built. This is not surprising as, to date, no other manufacturing method can deliver a scaffold that can recapitulate the complex structure and anatomy of a human organ. It can be speculated that in the near future innovations in manufacturing techniques, such as 3D printing or stereolithography, will be able to provide complex structures using bioactive materials. Indeed, the advances in 3D bioprinting may directly benefit the field of tissue engineering by allowing the direct printing of cells onto a scaffold.

TABLE 1 | Summary of the studies presented in the review addressing revascularization in whole organs.

Organ	Cells	Scaffold	Seeding method	*In-vitro* culture	*In-vivo*	References
Liver	EA HY926 endothelial cell line and HepG2	Decellularized pig lobe	Perfusion in portal vein and hepatic artery	Dynamic 10d	Heterotopic 1 h	Hussein et al., 2016
Liver	HUVECs	Decellularized pig scaffold	Perfusion in portal vein	Static 3d	Orthotopic in infrahepatic space for 1 h	Bao et al., 2015
Liver	Endothelial progenitor cells	Decellularized rat liver	Perfusion in portal vein	Dynamic 3d	Subcutaneous 21d	Zhou et al., 2017
Liver	HUVECs and human fetal liver cells	Decellularized mouse, rat, ferret, rabbit and piglet livers	Perfusion in portal vein an vena cava	Dyanmic 7d	Scaffold reperfusion in terminal anesthesia	Baptista et al., 2011
Liver	MS1	Decellularized pig liver	Perfusion in portal vein	Dynamic 3d	Orthotopic 24 h	Ko et al., 2015
Liver	HUVECs	Decellularized human liver slices	Top seeding	Static 5d	–	Verstegen et al., 2017
Liver	Bone marrow MSC and hepatocytes	Decellularized rat liver	Perfusion in portal vein	Dynamic 6d	Orthotopic 60 min	Kadota et al., 2014
Liver	HUVECs and hepatocytes	Decellularized rat liver right lobe	Perfusion in portal vein	Dynamic 3d	–	Shirakigawa et al., 2013
Pancreas	Human primary pancreatic endothelial cells	Decellularized human pancreas	Perfusion in superior mesenteric artery and splenic artery	Dynamic 6d	–	Peloso et al., 2016
Pancreas	Rat EPC	Decellularized rat pancreas	Perfusion in inferior vena cava	Dynamic 3d	Subcutaneous in mice 20d	Guo et al., 2018
Kidney	Mouse ESC	Decellularized rat kidney	Perfusion in renal artery	Dynamic 72 h	–	Bonandrini et al., 2014
Kidney	HUVECs and rat neonatal kidney cells	Decellularized rat, pig and human kidneys	Vacuum assisted perfusion in renal artery	Dynamic 5d	Orthotopic in rats	Song et al., 2013
Kidney	iPSC derived Pax-2 progenitors and endothelial cells	Decellularized mouse kidney	Perfusion in renal artery	Static 16 h	Subcutaneous in SCID mice for 12 weeks	Du et al., 2016
Kidney	Human neurospheres	Decellularized human kidney slices	Top seeding	Static 30d	–	Bombelli et al., 2017
Kidney	Human ESC	Decellularized rhesus monkey kidney	Perfusion in renal artery	Dynamic 7d	–	Batchelder et al., 2015
Lung	Human lung epithelial and pulmonary endothelial cells	Decellularized rat and human lung	Perfusion in pulmonary artery	Dynamic 7d	–	Gilpin et al., 2016
Lung	HUVECs and human epithelial cells	Decellularized rat, pig and human lung slices	Top seeding	Static 5d	–	Gilpin et al., 2014
Lung	HUVECs and hMSC or iPSC derived endothelial cells and perivascular cells	Decellularized rat lung and human lung single lobe	Perfusion in pulmonary artery and vein	Dynamic 6d	Orhotopic in rats for 3 days	Ren et al., 2015
Lung	HUVECs and human airway epithelial progenitors	Decellularized pig lung	Perfusion in pulmonary artery and vein	Dynamic 6d	Orhotopic in pigs for 1 h	Zhou et al., 2017
Lung	Mixed rat neonatal lung population and rat lung microvascular endothelial cells	Decellularized rat lung	Perfusion in pulmonary artery and vein	Dynamic 4d	–	Calle et al., 2016
Lung	Rat microvascular endothelial cells	Decellularized rat lung	Perfusion in pulmonary artery	Dynamic 7d	–	Stabler et al., 2016
Lung	Human mixed lung population	Decellularized human pediatric lung pieces	Top seeding	Dynamic 7d	–	Nichols et al., 2017
Lung	Rat ECs and ADSC	Decellularized rat lung	Perfusion in pulmonary artery and vein	Dynamic 16d	Orhotopic in rats for 3 h	Doi et al., 2017
Lung	Human adult cells	Bronchovascular bundles isolated from decellularized pig lung and human lobe	Perfusion in the bundle	Static 28d	–	Wagner et al., 2014
Lung	Mouse ESC	Decellularized rat lung	Perfusion in the bronchi	Dynamic 21d	–	Cortiella et al., 2010

(Continued)

TABLE 1 | Continued

Organ	Cells	Scaffold	Seeding method	*In-vitro* culture	*In-vivo*	References
Heart	Rat aortic endothelial cells and rat neonatal cardiac cells	Decellularized rat heart	Injection	Dynamic 7d	–	Ott et al., 2008
Heart	Rat neonatal endothelial cells, cardiomyocytes and fibroblasts	Decellularized rat heart	Perfusion in the aorta	Dynamic 30d	–	Yasui et al., 2014
Heart	Rat aortic endothelial cells	Decellularized rat heart	Retrograde aortic, brachiocephalic artery or IVC and brachiocephalic artery perfusion	Dynamic 7d	Heterotopic 7d	Robertson et al., 2014
Heart	HUVECs, human cardiac progenitors, hMSC or cardiomyocytes	Decellularized human heart slices	Top seeding	Static 21d	–	Sánchez et al., 2015
Heart	HUVECs and murine neonatal cardiac cells	Decellularized pig heart	Perfusion in the aorta	Dynamic 21d	–	Weymann et al., 2014

Nevertheless, current decellularization techniques are able to preserve the architecture of whole organs, particularly the vasculature, resulting in the possibility of delivering the endothelial cells directly through perfusion, allowing for the creation of a vascular network that is similar to the primary organ.

In contrast to a synthetic scaffold, naturally derived scaffolds maintain the extracellular matrix which has been shown to have a positive influence on cell seeding, promoting cell engraftment, migration and differentiation. This feature of the ECM has been demonstrated by different groups internationally, and represents one of the most powerful tools in the hands of researchers. Currently, we do not fully understand the biochemical and topological cues that drive this process, however cells can be organized and moved to the right location even in complex and highly tissue-specific sites. From a methodological perspective, exploiting this feature of the extracellular matrix researchers can deliver different cell populations to a decellularized scaffold simultaneously, relying on self-arrangement.

The main hurdle to tissue engineering complex multicellular organs is the culture environment. Different cell types require different biochemical environments and stimuli, identifying a culture medium that is well tolerated by a variety of cells of different origins, without influencing differentiation pathways poses a significant challenge.

Beside biochemical and topological cues, a dynamic environment plays a crucial role in tissue engineering, this is demonstrated by the benefit provided by bioreactor based dynamic culture. This is particularly important for the vasculature and it is mandatory to provide perfusion to engineer blood vessels. Endothelial cells strongly benefit from shear stress, to grow and express the correct phenotype. Calculating the amount of shear stress provided in an intricate blood vessel network such as that of a whole organs is complex. The beneficial effect of perfusion is clear, at least in term of providing an even distribution of nutrients. Complex computational models, coupled with particle tracking, could be applied to this field to precisely tune the amount of shear stress the endothelial cells need to be exposed to. Moreover, providing a dynamic perfusion avoids the formation of cell clumps during culture.

Taken together the studies reviewed here hold great potential that require further exploitation and scale up. However, there is still a significant gap toward real clinical translation of engineered revascularized organs. Many studies to date, only exploit one vascular access route and do not investigate whether both venous and arterial networks are recellularized. The few groups who have exploited the infusion of cells through both arterial and vascular accesses showed a more homogeneous distribution of the cells throughout the scaffold and to the authors this looks like the path to follow in future seeding strategies. Besides cell seeding, no studies have demonstrated the ability of long-term perfusion in orthotopic models, current studies report short time points limited to a few hours or days, mainly because of blood clotting. Furthermore, studies should focus on providing reliable and reproducible methods to assess vasculature function and patency. Active methods that show perfusion of the organ should be used and patency assessed *in-vivo*. To date no studies have achieved a fully confluent regenerated endothelium, and this remains a significant hurdle in demonstrating functionality resembling the normal physiological state.

In order to reach long term patency of the blood vessel network, researchers should focus on delivering *ex-vivo*, a stable and functional vasculature that provides an adequate and confluent endothelial layer. Research has been hampered by the availability of clinically relevant endothelial cell sources. Almost the majority of the studies presented in this review use HUVECs, but adult endothelial cells have a limited proliferative potential and are not stable over long time periods (**Table 1**). This largely limits the application of normal adult cells for human sized tissue. iPSCs can be a powerful alternative, but limited by the current concerns on safety and the difficultly in achieving a functional, stable, and homogenous differentiation. Conversely, the direct reprograming of adult cells, taking advantage of the expression of fetal factors, holds a great potential with less

procedural concerns. As it has been highlighted, perivascular cells exert a fundamental role in the development and stabilization of vasculature. Considering that reliable and non-invasive sources of perivascular cells, such as mesoangioblasts are available, tissue engineering studies should put efforts into developing strategies that take advantage of using perivascular cells to support endothelial cells.

In conclusion, the fields of whole organ tissue engineering has reached the time of scaling up to develop functional human sized preclinical models. Vascularization will be the cornerstone essential for the generation of fully functional, tissue engineered organs which will survive and function post-transplantation.

AUTHOR CONTRIBUTIONS

AFP, AMT, and PDC contributed with conception and writing of the paper.

ACKNOWLEDGMENTS

PDC is supported by the NIHR Professorship RP 2014-04-046; AFP is funded by INTENS H2020 grant 668294; AMT is supported by GSK- BBSRC iCASE Studentship, we thanks Dr. Gemma Molyneux for the critical review of the manuscript.

REFERENCES

Abolbashari, M., Agcaoili, S. M., Lee, M. K., Ko, I. K., Aboushwareb, T., Jackson, J. D., et al. (2016). Repopulation of porcine kidney scaffold using porcine primary renal cells. *Acta Biomater.* 29, 52–61. doi: 10.1016/j.actbio.2015.11.026

Armulik, A., Genove, G., and Betsholtz, C. (2011). Pericytes: developmental, physiological, and pathological perspectives, problems, and promises. *Dev. Cell* 21, 193–215. doi: 10.1016/j.devcel.2011.07.001

Asahara, T., Murohara, T., Sullivan, A., Silver, M., van der Zee, R., Li, T., et al. (1997). Isolation of putative progenitor endothelial cells for angiogenesis. *Science* 275, 964–967. doi: 10.1126/science.275.5302.964

Badylak, S. F., Taylor, D., and Uygun, K. (2011). Whole-organ tissue engineering: decellularization and recellularization of three-dimensional matrix scaffolds. *Annu. Rev. Biomed. Eng.* 13, 27–53. doi: 10.1146/annurev-bioeng-071910-124743

Bao, J., Wu, Q., Sun, J., Zhou, Y. J., Wang, Y. J., Jiang, X., et al. (2015). Hemocompatibility improvement of perfusion-decellularized clinical-scale liver scaffold through heparin immobilization. *Sci. Rep.* 5:10756. doi: 10.1038/srep10756

Baptista, P. M., Siddiqui, M. M., Lozier, G., Rodriguez, S. R., Atala, A., and Soker, S. (2011). The use of whole organ decellularization for the generation of a vascularized liver organoid. *Hepatology* 53, 604–617. doi: 10.1002/hep.24067

Batchelder, C. A., Martinez, M. L., and Tarantal, A. F. (2015). Natural scaffolds for renal differentiation of human embryonic stem cells for kidney tissue engineering. *PLoS ONE* 10:e0143849. doi: 10.1371/journal.pone.0143849

Bergers, G., and Song, S. (2005). The role of pericytes in blood-vessel formation and maintenance. *Neuro Oncol.* 7, 452–464. doi: 10.1215/S1152851705000232

Bombelli, S., Meregalli, C., Scalia, C., Bovo, G., Torsello, B., and De Marco, S. (2017). Nephrosphere-derived cells are induced to multilineage differentiation when cultured on human decellularized kidney scaffolds. *Am. J. Pathol.* 188, 184–195. doi: 10.1016/j.ajpath.2017.09.012

Bonandrini, B., Figliuzzi, M., Papadimou, E., Morigi, M., Perico, N., Casiraghi, F., et al. (2014). Recellularization of well-preserved acellular kidney scaffold using embryonic stem cells. *Tissue Eng. Part A* 20, 1486–1498. doi: 10.1089/ten.tea.2013.0269

Bourke, B. M., Roche, W. R., and Appleberg, M. (1986). Endothelial-cell harvest for seeding vascular prostheses - the influence of technique on cell-function, viability, and number. *J. Vasc. Surg.* 4, 257–263. doi: 10.1016/0741-5214(86)90195-3

Butler, J. M., Kobayashi, H., and Rafii, S. (2010). Instructive role of the vascular niche in promoting tumour growth and tissue repair by angiocrine factors. *Nat. Rev. Cancer* 10, 138–146. doi: 10.1038/nrc2791

Calle, E. A., Hill, R. C., Leiby, K. L., Le, A. V., Gard, A. L., Madri, J. A., et al. (2016). Targeted proteomics effectively quantifies differences between native lung and detergent-decellularized lung extracellular matrices. *Acta Biomater.* 46, 91–100. doi: 10.1016/j.actbio.2016.09.043

Carmeliet, P., and Jain, R. K. (2011). Molecular mechanisms and clinical applications of angiogenesis. *Nature* 473, 298–307. doi: 10.1038/nature10144

Collett, G. D., and Canfield, A. E. (2005). Angiogenesis and pericytes in the initiation of ectopic calcification. *Circ. Res.* 96, 930–938. doi: 10.1161/01.RES.0000163634.51301.0d

Cortiella, J., Niles, J., Cantu, A., Brettler, A., Pham, A., Vargas, G., et al. (2010). Influence of acellular natural lung matrix on murine embryonic stem cell differentiation and tissue formation. *Tissue Eng. Part A* 16, 2565–2580. doi: 10.1089/ten.tea.2009.0730

Cossu, G., Birchall, M., Brown, T., De Coppi, P., Culme-Seymour, E., Gibbon, S., et al. (2017). Lancet commission: stem cells and regenerative medicine. *Lancet* 391, 883–910. doi: 10.1016/S0140-6736(17)31366-1

Cossu, G., Previtali, S. C., Napolitano, S., Cicalese, M. P., Tedesco, F. S., Nicastro, F., et al. (2015). Intra-arterial transplantation of HLA-matched donor mesoangioblasts in Duchenne muscular dystrophy. *EMBO Mol. Med.* 7, 1513–1528. doi: 10.15252/emmm.201505636

Crapo, P. M., Gilbert, T. W., and Badylak, S. F. (2011). An overview of tissue and whole organ decellularization processes. *Biomaterials* 32, 3233–3243. doi: 10.1016/j.biomaterials.2011.01.057

Dellavalle, A., Maroli, G., Covarello, D., Azzoni, E., Innocenzi, A., Perani, L., et al. (2011). Pericytes resident in postnatal skeletal muscle differentiate into muscle fibres and generate satellite cells. *Nat. Commun.* 2:e50532. doi: 10.1038/ncomms1508

Dellavalle, A., Sampaolesi, M., Tonlorenzi, R., Tagliafico, E., Sacchetti, B., Perani, L., et al. (2007). Pericytes of human skeletal muscle are myogenic precursors distinct from satellite cells. *Nat. Cell Biol.* 9, 255–267. doi: 10.1038/ncb1542

Dew, L., English, W. R., Chong, C. K., and MacNeil, S. (2016). Investigating neovascularization in rat decellularized intestine: an *in vitro* platform for studying angiogenesis. *Tissue Eng. Part A* 22, 1317–1326. doi: 10.1089/ten.tea.2016.0131

Díaz-Flores, L., Gutierrez, R., Madrid, J. F., Varela, H., Valladares, F., Acosta, E., et al. (2009). Pericytes. morphofunction, interactions and pathology in a quiescent and activated mesenchymal cell niche. *Histol. Histopathol.* 24, 909–969. doi: 10.14670/HH-24.909

Ding, B. S., Nolan, D. J., Butler, J. M., James, D., Babazadeh, A. O., Rosenwaks, Z., et al. (2010). Inductive angiocrine signals from sinusoidal endothelium are required for liver regeneration. *Nature* 468, 310–U240. doi: 10.1038/nature09493

Ding, B. S., Nolan, D. J., Guo, P. P., Babazadeh, A. O., Cao, Z. W., Rosenwaks, Z., et al. (2011). Endothelial-derived angiocrine signals induce and sustain regenerative lung alveolarization. *Cell* 147, 539–553. doi: 10.1016/j.cell.2011.10.003

Doi, R., Tsuchiya, T., Mitsutake, N., Nishimura, S., Matsuu-Matsuyama, M., Nakazawa, Y., et al. (2017). Transplantation of bioengineered rat lungs recellularized with endothelial and adipose-derived stromal cells. *Sci. Rep.* 7:8447. doi: 10.1038/s41598-017-09115-2

Du, C., Narayanan, K., Leong, M. F., Ibrahim, M. S., Chua, Y. P., Khoo, V. M., et al. (2016). Functional kidney bioengineering with pluripotent stem-cell-derived renal progenitor cells and decellularized kidney scaffolds. *Adv. Healthc. Mater.* 5, 2080–2091. doi: 10.1002/adhm.201600120

Elliott, M. J., De Coppi, P., Speggiorin, S., Roebuck, D., Butler, C. R., Samuel, E., et al. (2012). Stem-cell-based, tissue engineered tracheal replacement in a child: a 2-year follow-up study. *Lancet* 380, 994–1000. doi: 10.1016/S0140-6736(12)60737-5

Fishman, J. M., Lowdell, M. W., Urbani, L., Ansari, T., Burns, A. J., Turmaine, M., et al. (2013). Immunomodulatory effect of a decellularized skeletal muscle

scaffold in a discordant xenotransplantation model. *Proc. Natl. Acad. Sci. U.S.A.* 110, 14360–14365. doi: 10.1073/pnas.1213228110

Gerhardt, H., and Betsholtz, C. (2003). Endothelial-pericyte interactions in angiogenesis. *Cell Tissue Res.* 314, 15–23. doi: 10.1007/s00441-003-0745-x

Gerli, M. F, Maffioletti, S. M., Millet, Q., and Tedesco, F. S. (2014). Transplantation of induced pluripotent stem cell-derived mesoangioblast-like myogenic progenitors in mouse models of muscle regeneration. *J. Vis. Exp.* 20:e50532. doi: 10.3791/50532

Gerli, M. F. M., Guyette, J. P., Evangelista-Leite, D., Ghoshhajra, B. B., and Ott, H. C. (2018). Perfusion decellularization of a human limb: a novel platform for composite tissue engineering and reconstructive surgery. *PLoS ONE* 13:e0191497. doi: 10.1371/journal.pone.0191497

Ghesquière, B., Wong, B. W., Kuchnio, A., and Carmeliet, P. (2014). Metabolism of stromal and immune cells in health and disease. *Nature* 511, 167–176. doi: 10.1038/nature13312

Gilpin, A., and Yang, Y. (2017). Decellularization strategies for regenerative medicine: from processing techniques to applications. *Biomed Res. Int.* 2017:9831534. doi: 10.1155/2017/9831534

Gilpin, S. E., Charest, J. M., Ren, X., Tapias, L. F., Wu, T., Evangelista-Leite, D., et al. (2016). Regenerative potential of human airway stem cells in lung epithelial engineering. *Biomaterials* 108, 111–119. doi: 10.1016/j.biomaterials.2016.08.055

Gilpin, S. E., Guyette, J. P., Gonzalez, G., Ren, X., Asara, J. M., Mathisen, D. J., et al. (2014). Perfusion decellularization of human and porcine lungs: bringing the matrix to clinical scale. *J. Heart Lung. Transplant.* 33, 298–308. doi: 10.1016/j.healun.2013.10.030

Ginsberg, M., Schachterle, W., Shido, K., and Rafii, S. (2015). Direct conversion of human amniotic cells into endothelial cells without transitioning through a pluripotent state. *Nat. Protoc.* 10, 1975–1985. doi: 10.1038/nprot.2015.126

Guo, Y., Wu, C., Xu, L., Xu, Y., Xiaohong, L., and Hui, Z. (2018). Vascularization of pancreatic decellularized scaffold with endothelial progenitor cells. *J. Artif. Organs*. doi: 10.1007/s10047-018-1017-6. [Epub ahead of print].

Hamilton, D. W., Maul, T. M., and Vorp, D. A. (2004). Characterization of the response of bone marrow-derived progenitor cells to cyclic strain: implications for vascular tissue-engineering applications. *Tissue Eng.* 10, 361–369. doi: 10.1089/107632704323061726

Hannan, N. R., Segeritz, C. P., Touboul, T., and Vallier, L. (2013). Production of hepatocyte-like cells from human pluripotent stem cells. *Nat. Protoc.* 8, 430–437. doi: 10.1038/nprot.2012.153

Harris, L. J., Abdollahi, H., Zhang, P., McIlhenny, S., Tulenko, T. N., and DiMuzio, P. J. (2011). Differentiation of adult stem cells into smooth muscle for vascular tissue engineering. *J. Surg. Res.* 168, 306–314. doi: 10.1016/j.jss.2009.08.001

He, H., Shirota, T., Yasui, H., and Matsuda, T. (2003). Canine endothelial progenitor cell-lined hybrid vascular graft with nonthrombogenic potential. *J. Thorac. Cardiov. Surg.* 126, 455–464. doi: 10.1016/S0022-5223(02)73264-9

Hu, J., Srivastava, K., Wieland, M., Runge, A., Mogler, C., Besemfelder, E., et al. (2014). Endothelial cell-derived Angiopoietin-2 controls liver regeneration as a spatiotemporal rheostat. *Science* 343, 416–419. doi: 10.1126/science.1244880

Hussein, K. H., Park, K. M., Kang, K. S., and Woo, H. M. (2016). Heparin-gelatin mixture improves vascular reconstruction efficiency and hepatic function in bioengineered livers. *Acta Biomater.* 38, 82–93. doi: 10.1016/j.actbio.2016.04.042

Jain, R. K., Au, P., Tam, J., Duda, D. G., and Fukumura, D. (2005). Engineering vascularized tissue. *Nat. Biotechnol.* 23, 821–823. doi: 10.1038/nbt0705-821

Jung, Y., Ji, H. Y., Chen, Z. Z., Chan, H. F., Atchison, L., Klitzman, B., et al. (2015). Scaffold-free, human mesenchymal stem cell-based tissue engineered blood vessels. *Sci. Rep.* 5:15116. doi: 10.1038/srep15116

Kadota, Y., Yagi, H., Inomata, K., Matsubara, K., Hibi, T., Abe, Y., et al. (2014). Mesenchymal stem cells support hepatocyte function in engineered liver grafts. *Organogenesis* 10, 268–277. doi: 10.4161/org.27879

Kitano, K., Schwartz, D. M., Zhou, H. Y., Gilpin, S. E., Wojtkiewicz, G. R., Ren, X., et al. (2017). Bioengineering of functional human induced pluripotent stem cell-derived intestinal grafts. *Nat. Commun.* 8:765. doi: 10.1038/s41467-017-00779-y

Ko, I. K., Peng, L., Peloso, A., Smith, C. J., Dhal, A., Deegan, D. B., et al. (2015). Bioengineered transplantable porcine livers with re-endothelialized vasculature. *Biomaterials* 40, 72–79. doi: 10.1016/j.biomaterials.2014.11.027

Koike, N., Fukumura, D., Gralla, O., Au, P., Schechner, J. S., and Jain, R. K. (2004). Tissue engineering: creation of long-lasting blood vessels. *Nature* 428, 138–139. doi: 10.1038/428138a

Kovacic, J. C., and Boehm, M. (2009). Resident vascular progenitor cells: an emerging role for non-terminally differentiated vessel-resident cells in vascular biology. *Stem Cell Res.* 2, 2–15. doi: 10.1016/j.scr.2008.05.005

Leclerc, E., Kimura, K., Shinohara, M., Danoy, M., Le Gall, M., Kido, T., et al. (2017). Comparison of the transcriptomic profile of hepatic human induced pluripotent stem like cells cultured in plates and in a 3D microscale dynamic environment. *Genomics* 109, 16–26. doi: 10.1016/j.ygeno.2016.11.008

Lorvellec, M., Scottoni, F., Crowley, C., Fiadeiro, R., Maghsoudlou, P., and Pellegata, A. F. (2017). Mouse decellularised liver scaffold improves human embryonic and induced pluripotent stem cells differentiation into hepatocyte-like cells. *PLoS ONE* 12:e0189586. doi: 10.1371/journal.pone.0189586

Maghsoudlou, P., Georgiades, F., Smith, H., Milan, A., Shangaris, P., Urbani, L., et al. (2016). Optimization of liver decellularization maintains extracellular matrix micro-architecture and composition predisposing to effective cell seeding. *PLoS ONE* 11:e0155324. doi: 10.1371/journal.pone.0155324

Maghsoudlou, P., Georgiades, F., Tyraskis, A., Totonelli, G., Loukogeorgakis, S. P., Orlando, G., et al. (2013). Preservation of micro-architecture and angiogenic potential in a pulmonary acellular matrix obtained using intermittent intra-tracheal flow of detergent enzymatic treatment. *Biomaterials* 34, 6638–6648. doi: 10.1016/j.biomaterials.2013.05.015

Majka, S. M., Jackson, K. A., Kienstra, K. A., Majesky, M. W., Goodell, M. A., and Hirschi, K. K. (2003). Distinct progenitor populations in skeletal muscle are bone marrow derived and exhibit different cell fates during vascular regeneration. *J. Clin. Invest.* 111, 71–79. doi: 10.1172/JCI16157

Mazza, G., Rombouts, K., Hall, A. R., Urbani, L., Luong, T. V., Al-Akkad, W., et al. (2015). Decellularized human liver as a natural 3D-scaffold for liver bioengineering and transplantation. *Sci Rep.* 5:13079. doi: 10.1038/srep13079

Miller, F. N., and Sims, D. E. (1986). Contractile elements in the regulation of macromolecular permeability. *FASEB J.* 45, 84–88.

Minasi, M. G., Riminucci, M., De Angelis, L., Borello, U., Berarducci, B., Innocenzi, A., et al. (2002). The meso-angioblast: a multipotent, self-renewing cell that originates from the dorsal aorta and differentiates into most mesodermal tissues. *Development* 129, 2773–2784.

Murga, M., Yao, L., and Tosato, G. (2004). Derivation of endothelial cells from CD34(-) umbilical cord blood. *Stem Cells* 22, 385–395. doi: 10.1634/stemcells.22-3-385

Neff, L. P., Tillman, B. W., Yazdani, S. K., Machingal, M. A., Yoo, J. J., Soker, S., et al. (2011). Vascular smooth muscle enhances functionality of tissue-engineered blood vessels *in vivo*. *J. Vasc. Surg.* 53, 426–434. doi: 10.1016/j.jvs.2010.07.054

Nichols, J. E., La Francesca, S., Vega, S. P., Niles, J. A., Argueta, L. B., Riddle, M., et al. (2017). Giving new life to old lungs: methods to produce and assess whole human paediatric bioengineered lungs. *J. Tissue Eng. Regen. Med.* 11, 2136–2152. doi: 10.1002/term.2113

Nolan, D. J., Ginsberg, M., Israely, E., Palikuqi, B., Poulos, M. G., James, D., et al. (2013). Molecular signatures of tissue-specific microvascular endothelial cell heterogeneity in organ maintenance and regeneration. *Dev. Cell* 26, 204–219. doi: 10.1016/j.devcel.2013.06.017

Olson, L. E., and Soriano, P. (2011). PDGFR beta signaling regulates mural cell plasticity and inhibits fat development. *Dev. Cell* 20, 815–826. doi: 10.1016/j.devcel.2011.04.019

Orlando, G., Wood, K. J., De Coppi, P., Baptista, P. M., Binder, K. W., Bitar, K. N., et al. (2012). Regenerative medicine as applied to general surgery. *Ann. Surg.* 255, 867–880. doi: 10.1097/SLA.0b013e318243a4db

Orlova, V. V., van den Hil, F. E., Petrus-Reurer, S., Drabsch, Y., ten Dijke, P., and Mummery, C. L. (2014). Generation, expansion and functional analysis of endothelial cells and pericytes derived from human pluripotent stem cells. *Nat. Protoc.* 9, 1514–1531. doi: 10.1038/nprot.2014.102

Otani, A., Kinder, K., Ewalt, K., Otero, F. J., Schimmel, P., and Friedlander, M. (2002). Bone marrow-derived stem cells target retinal astrocytes and can promote or inhibit retinal angiogenesis. *Nat. Med.* 8, 1004–1010. doi: 10.1038/nm744

Ott, H. C., Matthiesen, T. S., Goh, S. K., Black, L. D., Kren, S. M., Netoff, T. I., et al. (2008). Perfusion-decellularized matrix: using nature's platform to engineer a bioartificial heart. *Nat. Med.* 14, 213–221. doi: 10.1038/nm1684

Pellegata, A. F., Dominioni, T., Ballo, F., Maestroni, S., Asnaghi, M. A., Zerbini, G., et al. (2015). Arterial decellularized scaffolds produced using an innovative automatic system. *Cells Tissues Organs* 200, 363–373. doi: 10.1159/000439082

Peloso, A., Petrosyan, A., Da Sacco, S., Booth, C., Zambon, J. P., O'Brien, T., et al. (2015). Renal extracellular matrix scaffolds from discarded kidneys maintain glomerular morphometry and vascular resilience and retains critical growth factors. *Transplantation* 99, 1807–1816. doi: 10.1097/T.P.0000000000000811

Peloso, A., Urbani, L., Cravedi, P., Katari, R., Maghsoudlou, P., Fallas, M. E., et al. (2016). The human pancreas as a source of protolerogenic extracellular matrix scaffold for a new-generation bioartificial endocrine pancreas. *Ann. Surg.* 264, 169–179. doi: 10.1097/SLA.0000000000001364

Petersen, T. H., Calle, E. A., Zhao, L. P., Lee, E. J., Gui, L. Q., Raredon, M. B., et al. (2010). Tissue-engineered lungs for *in vivo* implantation. *Science* 329, 538–541. doi: 10.1126/science.1189345

Poulos, M. G., Crowley, M. J. P., Gutkin, M. C., Ramalingam, P., Schachterle, W., et al. (2015). Vascular platform to define hematopoietic stem cell factors and enhance regenerative hematopoiesis. *Stem Cell Rep.* 5, 881–894. doi: 10.1016/j.stemcr.2015.08.018

Rafii, S., Butler, J. M., and Ding, B. S. (2016). Angiocrine functions of organ-specific endothelial cells. *Nature* 529, 316–325. doi: 10.1038/nature17040

Ramasamy, S. K., Kusumbe, A. P., and Adams, R. H. (2015). Regulation of tissue morphogenesis by endothelial cell-derived signals. *Trends Cell Biol.* 25, 148–157. doi: 10.1016/j.tcb.2014.11.007

Ren, X., Moser, P. T., Gilpin, S. E., Okamoto, T., Wu, T., Tapias, L. F., et al. (2015). Engineering pulmonary vasculature in decellularized rat and human lungs. *Nat. Biotechnol.* 33, 1097–1102. doi: 10.1038/nbt.3354

Robertson, M. J., Dries-Devlin, J. L., Kren, S. M., Burchfield, J. S., and Taylor, D. A. (2014). Optimizing recellularization of whole decellularized heart extracellular matrix. *PLoS ONE* 9:e90406. doi: 10.1371/journal.pone.0090406

Rouget, C. (1874). Note sur le developpement de la tunique contractile des vaisseaux. *Compt. Rend Acad. Sci.* 59, 559–562.

Sacchetti, B., Funari, A., Remoli, C., Giannicola, G., Kogler, G., Liedtke, S., et al. (2016). No identical "Mesenchymal Stem Cells" at different times and sites: human committed progenitors of distinct origin and differentiation potential are incorporated as adventitial cells in microvessels. *Stem Cell Rep.* 6, 897–913. doi: 10.1016/j.stemcr.2016.05.011

Sánchez, P. L., Fernandez-Santos, M. E., Costanza, S., Climent, A. M., Moscoso, I., Gonzalez-Nicolas, M. A., et al. (2015). Acellular human heart matrix: a critical step toward whole heart grafts. *Biomaterials* 61, 279–289. doi: 10.1016/j.biomaterials.2015.04.056

Scarritt, M. E., Pashos, N. C., and Bunnell, B. A. (2015). A review of cellularization strategies for tissue engineering of whole organs. *Front. Bioeng. Biotechnol.* 30, 43. doi: 10.3389/fbioe.2015.00043

Schmidt, D., Breymann, C., Weber, A., Guenter, C. I., Neuenschwander, S., Zund, G., et al. (2004). Umbilical cord blood derived endothelial progenitor cells for tissue engineering of vascular grafts. *Ann. Thorac. Surg.* 78, 2094–2098. doi: 10.1016/j.athoracsur.2004.06.052

Shi, Q., Rafii, S., Wu, M. H., Wijelath, E. S., Yu, C., Ishida, A., et al. (1998). Evidence for circulating bone marrow-derived endothelial cells. *Blood* 92, 362–367.

Shirakigawa, N., Takei, T., and Ijima, H. (2013). Base structure consisting of an endothelialized vascular-tree network and hepatocytes for whole liver engineering. *J. Biosci. Bioeng.* 116, 740–745. doi: 10.1016/j.jbiosc.2013.05.020

Shirota, T., He, H. B., Yasui, H., and Matsuda, T. (2003). Human endothelial progenitor cell-seeded hybrid graft: proliferative and antithrombogenic potentials *in vitro* and fabrication processing. *Tissue Eng.* 9, 127–136. doi: 10.1089/107632703762687609

Song, J. J., Guyette, J. P., Gilpin, S. E., Gonzalez, G., Vacanti, J. P., and Ott, H. C. (2013). Regeneration and experimental orthotopic transplantation of a bioengineered kidney. *Nat. Med.* 19, 646–651. doi: 10.1038/nm.3154

Stabler, C. T., Caires, L. C., Mondrinos, M. J., Marcinkiewicz, C., Lazarovici, P., Wolfson, M. R., et al. (2016). Enhanced Re-endothelialization of decellularized rat lungs. *Tissue Eng. Part C Methods* 22, 439–450. doi: 10.1089/ten.tec.2016.0012

Syedain, Z. H., Graham, M. L., Dunn, T. B., O'Brien, T., Johnson, S. L., Schumacher, R. J., et al. (2017). A completely biological "off-the-shelf" arteriovenous graft that recellularizes in baboons. *Sci. Transl. Med.* 9:eaan4209. doi: 10.1126/scitranslmed.aan4209

Tagliafico, E., Brunelli, S., Bergamaschi, A., De Angelis, L., Scardigli, R., Galli, D., et al. (2004). TGF beta/BMP activate the smooth muscle/bone differentiation programs in mesoangioblasts. *J. Cell Sci.* 117, 4377–4388. doi: 10.1242/jcs.01291

Takebe, T., Koike, N., Sekine, K., Fujiwara, R., Amiya, T., Zheng, Y. W., et al. (2014). Engineering of human hepatic tissue with functional vascular networks. *Organogenesis* 10, 260–267. doi: 10.4161/org.27590

Takebe, T., Sekine, K., Enomura, M., Koike, H., Kimura, M., Ogaeri, T., et al. (2013). Vascularized and functional human liver from an iPSC-derived organ bud transplant. *Nature* 499, 481–484. doi: 10.1038/nature12271

Takimoto, Y., Dixit, V., Arthur, M., and Gitnick, G. (2003). De novo liver tissue formation in rats using a novel collagen-polypropylene scaffold. *Cell Transplant.* 12, 413–421. doi: 10.3727/000000003108746966

Totonelli, G., Maghsoudlou, P., Garriboli, M., Riegler, J., Orlando, G., Burns, A. J., et al. (2012). A rat decellularized small bowel scaffold that preserves villus-crypt architecture for intestinal regeneration. *Biomaterials* 33, 3401–3410. doi: 10.1016/j.biomaterials.2012.01.012

Tresoldi, C., Pellegata, A. F., and Mantero, S. (2015). Cells and stimuli in small-caliber blood vessel tissue engineering. *Regen. Med.* 10, 505–527. doi: 10.2217/rme.15.19

Verstegen, M. M. A., Willemse, J., van den Hoek, S., Kremers, G. J., Luider, T. M., van Huizen, N. A., et al. (2017). Decellularization of whole human liver grafts using controlled perfusion for transplantable organ bioscaffolds. *Stem Cells Dev.* 26, 1304–1315. doi: 10.1089/scd.2017.0095

von Tell, D., Armulik, A., and Betsholtz, C. (2006). Pericytes and vascular stability. *Exp. Cell Res.* 312, 623–629. doi: 10.1016/j.yexcr.2005.10.019

Wagner, D. E., Bonenfant, N. R., Sokocevic, D., DeSarno, M. J., Borg, Z. D., Parsons, C. S., et al. (2014). Three-dimensional scaffolds of acellular human and porcine lungs for high throughput studies of lung disease and regeneration. *Biomaterials* 35, 2664–2679. doi: 10.1016/j.biomaterials.2013.11.078

Wang, C., Cen, L., Yin, S., Liu, Q. H., Liu, W., Cao, Y. L., et al. (2010). A small diameter elastic blood vessel wall prepared under pulsatile conditions from polyglycolic acid mesh and smooth muscle cells differentiated from adipose-derived stem cells. *Biomaterials* 31, 621–630. doi: 10.1016/j.biomaterials.2009.09.086

Weymann, A., Patil, N. P., Sabashnikov, A., Jungebluth, P., Korkmaz, S., Li, S. L., et al. (2014). Bioartificial heart: a human-sized porcine model - the way ahead. *PLoS ONE* 9:e111591. doi: 10.1371/journal.pone.0111591

Yasui, H., Lee, J. K., Yoshida, A., Yokoyama, T., Nakanishi, H., Miwa, K., et al. (2014). Excitation propagation in three-dimensional engineered hearts using decellularized extracellular matrix. *Biomaterials* 35, 7839–7850. doi: 10.1016/j.biomaterials.2014.05.080

Zhao, Y., Zhang, S., Zhou, J. Y., Wang, J. L., Zhen, M. C., Liu, Y., et al. (2010a). The development of a tissue-engineered artery using decellularized scaffold and autologous ovine mesenchymal stem cells. *Biomaterials* 31, 296–307. doi: 10.1016/j.biomaterials.2009.09.049

Zhao, Y., Xu, Y., Zhang, B., Wu, X., Xu, F., Liang, W., et al. (2010b). *In vivo* generation of thick, vascularized hepatic tissue from collagen hydrogel-based hepatic units. *Tissue Eng Part C Methods* 16, 653–659. doi: 10.1089/ten.tec.2009.0053

Zhou, H., Kitano, K., Ren, X., Rajab, T. K., Wu, M., and Gilpin, S. E. (2017). Bioengineering human lung grafts on porcine matrix. *Ann. Surg.* 267, 590–598. doi: 10.1097/SLA.0000000000002129

Zhu, L., Gong, D., Zou, Y., Li, Y., Wu, Y., Yuan, B., et al. (2008). Cervical heterotopic small intestinal transplantation in rats using artery sleeve anastomosis. *Transplant. Proc.* 40, 1645–1649. doi: 10.1016/j.transproceed.2008.03.146

Zimmermann, K. W. (1923). Der feinere bau der blutkapillaren. *Z. Anat. Entwicklungsgesch* 68, 29–109. doi: 10.1007/BF02593544

Conflict of Interest Statement: The authors declare that the research was conducted in the absence of any commercial or financial relationships that could be construed as a potential conflict of interest.

frontiers in Bioengineering and Biotechnology

REVIEW
published: 17 April 2018
doi: 10.3389/fbioe.2018.00041

Current Strategies for the Manufacture of Small Size Tissue Engineering Vascular Grafts

*Michele Carrabba and Paolo Madeddu**

School of Clinical Sciences, Bristol Heart Institute, University of Bristol, Bristol, United Kingdom

Occlusive arterial disease, including coronary heart disease (CHD) and peripheral arterial disease (PAD), is the main cause of death, with an annual mortality incidence predicted to rise to 23.3 million worldwide by 2030. Current revascularization techniques consist of angioplasty, placement of a stent, or surgical bypass grafting. Autologous vessels, such as the saphenous vein and internal thoracic artery, represent the gold standard grafts for small-diameter vessels. However, they require invasive harvesting and are often unavailable. Synthetic vascular grafts represent an alternative to autologous vessels. These grafts have shown satisfactory long-term results for replacement of large- and medium-diameter arteries, such as the carotid or common femoral artery, but have poor patency rates when applied to small-diameter vessels, such as coronary arteries and arteries below the knee. Considering the limitations of current vascular bypass conduits, a tissue-engineered vascular graft (TEVG) with the ability to grow, remodel, and repair *in vivo* presents a potential solution for the future of vascular surgery. Here, we review the different methods that research groups have been investigating to create TEVGs in the last decades. We focus on the techniques employed in the manufacturing process of the grafts and categorize the approaches as scaffold-based (synthetic, natural, or hybrid) or self-assembled (cell-sheet, microtissue aggregation and bioprinting). Moreover, we highlight the attempts made so far to translate this new strategy from the bench to the bedside.

Keywords: tissue engineering, vascular conduits, myocardial ischemia, regenerative medicine, stem cells

OPEN ACCESS

Edited by:
Andrea Banfi,
Universität Basel, Switzerland

Reviewed by:
Alberto Rainer,
Università Campus Bio-Medico, Italy
Deirdre Anderson,
Oregon Health & Science University, United States

***Correspondence:**
Paolo Madeddu
mdprm@bristol.ac.uk

Specialty section:
This article was submitted to Tissue Engineering and Regenerative Medicine, a section of the journal Frontiers in Bioengineering and Biotechnology

Received: *19 December 2017*
Accepted: *23 March 2018*
Published: *17 April 2018*

Citation:
Carrabba M and Madeddu P (2018) Current Strategies for the Manufacture of Small Size Tissue Engineering Vascular Grafts. Front. Bioeng. Biotechnol. 6:41. doi: 10.3389/fbioe.2018.00041

INTRODUCTION

Cardiovascular disease is the principal cause of death worldwide. Common manifestations are coronary heart disease (CHD) and peripheral arterial disease (PAD), which develop as a consequence of the critical atherosclerotic narrowing of supplying arteries. The worldwide annual incidence of deaths related to cardiovascular disease, is expected to rise to 23.3 million by 2030 (Criqui and Aboyans, 2015). In the UK alone, more than 2 million people suffer from CHD. Moreover, there are 188,000 hospital episodes attributed to a myocardial infarction (MI) each year. Approximately 12 to 20% of people over the age of 60 develop PAD and many of them manifest critical limb ischemia, which is associated with a poor quality of life and high risk of amputation and death (Townsend et al., 2015).

Prompt restoration of tissue perfusion is pivotal for preventing heart failure in patients with CHD and for helping the repair of ischemic limbs. Current revascularization techniques consist

of angioplasty, placement of a stent, or surgical bypass grafting. In the United States, an average of 400,000 coronary artery bypass grafting (CABG) interventions are recorded annually (Epstein et al., 2011; Pashneh-Tala et al., 2015). Moreover, the number of invasive lower-extremity vascular procedures for patients with PAD has doubled over the last decade. The surgical bypass grafting mostly involves the use of autologous vessels, such as the saphenous vein and internal thoracic artery. Though representing the gold standard for small-diameter (<6 mm) vascular replacement, these vessels require invasive harvesting and are often unsuitable for use. For instance, in patients needing primary revascularization of the lower extremities, as many as 30% lack a suitable autogenous vein. This number increases to 50% in those patients requiring a secondary bypass procedure. Furthermore, venous grafts can develop neointimal hyperplasia in the peri-anastomotic regions. Patency rates for saphenous vein grafting remain limited, with both coronary and femoro-popliteal reconstructions showing failure rates of approximately 50% at 10 years (Goldman et al., 2004; van Dijk et al., 2007; Collins et al., 2008; Kim et al., 2008; Schwann et al., 2009; Harskamp et al., 2013).

Surgical revascularization with implantation of conduits made of non-biodegradable polymers, including Polytetrafluoroethylene (PTFE), Gore-Tex, and Dacron, prove to be effective when replacing large vessels. However, when used in the application of small-diameter vascular grafts, they were complicated by the occurrence of thrombotic occlusions (Jackson et al., 2000; van Det et al., 2009; Takagi et al., 2010).

Considering the limitations of current vascular bypass conduits (Gui and Niklason, 2014), a tissue-engineered vascular graft (TEVG) embedded with cells to generate a living material capable of physiological remodeling represents a potential solution for the future of vascular surgery. In this review, we provide a summary of methodologies and solutions adopted in recent years that aim to create functional small-diameter TEVGs.

TISSUE ENGINEERING

Halfway through the twentieth century, the first autologous saphenous vein was used as a vascular graft in a clinical application by Kunlin (1951). By the end of the 1970s, synthetic material such as Dacron (De Bakey et al., 1958) and PTFE (Soyer et al., 1972; Campbell et al., 1976; Tellis et al., 1979), were introduced for aortic and lower extremity bypass, respectively. As mentioned above, the low patency rate over a long period of implantation was the common limitation of these vascular grafts.

Tissue engineering aims to provide alternative and innovative solutions for small diameter vascular replacement, and an interdisciplinary approach could offer the chance to design a graft for any specific target tissue and clinical needs.

The first commercially available acellular TEVG from bovine and human origin, such as Artegraft (North Brunswick, NJ) (Hutchin et al., 1975), Procol (Hancock Jaffe Laboratories Inc., Irvine, CA) (Hatzibaloglou et al., 2004), and Cryovein (CryoLife, Kennesaw, GA) (Madden et al., 2004), appeared on the market toward the end of the 1970s. Nevertheless, the flourishing number of techniques and innovative approaches finds its definitive turning point with Weinberg and Bell in 1986, who first tried to fabricate a biological vascular graft with xenogenic cells embedded to circumvent the limited availability of autologous cells (Weinberg and Bell, 1986). A collagen gel was used as a substrate on which they cultured bovine fibroblasts, vascular smooth muscle cells (VSMCs) and endothelial cells (ECs), thereby recreating the adventitia, media and intima layers of the vessel, respectively. This attempt led to the fabrication of a vessel-like structure with poor mechanical properties, that required a Dacron mesh to act as a structural support. Despite its apparent failure, this pioneering study drew a new path in TEVG development. From then on, many attempts have been made, ultimately leading to a standardized set of quality control criteria for TEVG fabrication, that is based on the performance of the actual "gold standard" [for example the saphenous vein (SV) or internal mammary artery (IMA)]. The ideal TEVG, therefore, should have anti-thrombogenic properties preferentially conferred by a fully autologous endothelium. Another important quality requisite is the similarity of TEVG mechanical properties to the native tissue, with a recommended minimum burst pressure of 1700 mmHg (Konig et al., 2010; Wise et al., 2011), together with a fatigue resistance of 30 days to cyclic loading *in vitro* (L'Heureux et al., 2007) and a level of compliance necessary to avoid excessive stress. A mechanical mismatch is acknowledged as a key determinant in the loss of long-term patency, resulting in aneurysm formation and implant at failure. The living cell component within the TEVG is critical to provide remodeling potential and biochemical signaling (G et al., 2015) while being devoid of immunogenic activity. To achieve clinically valuable outcomes, the manufacturing process has to take into account other fundamental aspects, such as the capability of the TEVG to be stored and delivered ready for the intervention as well as to be easily manipulated during the implantation.

TEVGs can be mainly categorized into self-assembled vascular grafts and scaffold-based approaches, using synthetic, natural or hybrid materials. Natural polymers, can then be further categorized into extracellular matrix (ECM)-based material and decellularized natural matrices.

Scaffold-Based Tevgs

The scaffold-based approach represents the most diffuse strategy to build TEVGs. The popularity of this methodology is justified by the fact that the presence of physical support enables the cells to follow a pathway during their colonization and proliferation. As introduced previously, the study performed by Weinberg and Bell pioneered the development of the scaffold-based methodology which during the last 30 years, saw the introduction of many variables and the use of a great variety of manufacturing techniques and materials.

Synthetic Materials

Synthetic polymers have been widely used for the fabrication of TEVGs. The advantage is that the final properties of the graft can be tuned to meet the clinical needs, choosing the appropriate fabrication technique and specific material. However, the required higher level of technologies and the long period

involved in the process of manufacturing constitute significant obstacles to clinical translation. Other prominant disadvantages shown by these materials are the lack of cell binding sites and the necessity to ensure an anti-thrombogenic property of the lumen, as required in the case of PLGA. A variety of polymers and copolymers have been tested. The most studied comprise degradable polyesters, like polyglycolic acid (PGA) (Niklason and Langer, 1997; Hoerstrup et al., 2006), poly-lactic acid (PLA), poly-l-lactic acid (PLLA) (Yokota et al., 2008), their copolymer poly (lactide-co-glycolide) (PLGA) (In Jeong et al., 2007), and polycaprolactone. Among the biodegradable polymers, polyurethanes (PU) (Hashi et al., 2007; Nieponice et al., 2010; Sharifpoor et al., 2011) and Poly(glycerol-sebacate) (PGS) (Wu et al., 2012), which are bioabsorbable elastomers, possess good biocompatibility properties allowing proliferation of endothelial cells (ECs) onto the luminal side and parietal infiltration of VSMCs (Gao et al., 2006; Rai et al., 2012). Hemocompatibility testing sees PGS having a low platelet adhesion and inflammation (Motlagh et al., 2006) and stimulating the production of elastin (Lee et al., 2011). However, the main issue was represented by the lack of mechanical properties, with a burst pressure of 200 mmHg (Lee et al., 2011). Various TEVG models fabricated with synthetic polymers have been assessed in preclinical small and large animal models. Both PU (Nieponice et al., 2010) seeded with mouse-derived MSCs and bone marrow-derived stem cells (BMDSCs) seeded onto PLA (Hashi et al., 2007) vascular grafts were used in a rat model and showed patency rates of 50 and 100% respectively, after several weeks from implantation. PGA is the most extensively explored material having been used in sheep (Brennan et al., 2008; Cummings et al., 2012), dogs, pigs (Quint et al., 2011) and primate models. Acellular electrospun PCL conduits, implanted into a mouse carotid model, allowed complete endothelium formation in 28 days. However, neointimal formation was detected, in particular at the anastomoses (Chan et al., 2017). Electrospinning microfabrication technique is often used to generate tubular structures composed of nanofibers from different polymers. Composite scaffolds made of PCL/poly(ethylene oxide) (Wang et al., 2016) and PCL/PLGA (Ong et al., 2017) have been tested in animal models with the later acellular graft having been evaluated in an ovine bilateral arteriovenous shunt model. Such a model showed good results in term of patency (66%) and endothelialization of the lumen after 4 weeks of implantation, but the graft eventually dilated as a consequence of inadequate elastin content (Ong et al., 2017).

Despite the great variety of preclinical studies, very few assessed the clinical utility of this type of TEVGs. One key study involving synthetic biodegradable polymers has been carried out by Niklason et al. using PGA seeded with VSMCs to create a small diameter TEVG (Niklason and Langer, 1997). The graft was conditioned with pulsatile flow for 8 weeks to achieve full maturation, through deposition of collagen matrix. At the end of the *in vitro* culturing, the structure showed a burst pressure of 2150 mmHg (Niklason, 1999; Niklason et al., 2001). These engineered blood vessels, named Humacyte (Humacyte Incorporated, RTP, NC), were tested in a series of small and large animals models, showing 100% patency after 24 days and 88% after 6 months in dogs and baboons, respectively (Dahl et al., 2011, 2013). These promising results led to a clinical trial that got underway in 2012, in which the acellular PGA scaffolds were used for vascular access in patients with end-stage renal disease (Gui and Niklason, 2014; Lawson et al., 2016). This study involved 60 patients recruited in Poland and the US with an average of follow-up period of 16 months, during which 4 patients died, although none were associated with the failure of the graft (Lawson et al., 2016) (**Table 1**). Additionally no immune response or aneurysm formation was detected. In term of efficacy, the TEVGs were successfully patent (63%) at 6 months, while the patency rate dropped to 28% after 12 months. This led to numerous interventions of thrombectomy to restore the patency (Lawson et al., 2016).

Natural Materials

ECM based grafts

The lack of bio-activity of synthetic scaffolds prompted researchers to investigate natural polymers obtained from ECM as a possible alternative option. Proteins derived from the ECM have the benefit of maintaining the natural binding sites for cell adhesion, improving biomimetic and biocompatibility properties of the material and stimulating the colonization and proliferation of recruited cells. Collagen, gelatin, elastin, fibrin, and silk-fibroin are the most extensively used in tissue engineering. Different manufacturing techniques can be selected to produce a TEVG of this kind. Typical fabrications procedures consist of electrospinning (Soffer et al., 2008), freeze-drying (Engbers-Buijtenhuijs et al., 2006; Zhang et al., 2006), and mold casting (Boccafoschi et al., 2007; Schutte et al., 2010) (**Figure 1C**). Electrospun meshes of gelatin (Elsayed et al., 2016) have been used, usually in combination with a polymeric structure, to improve the surface conjugation with cells, while silk-fibroin nanofibers tubes have been used alone (Marelli et al., 2010) or as a support matrix for coating hydrogel such as collagen (Marelli et al., 2012) and gelatin (Marcolin et al., 2017). The feasibility of the approach has been proven *in vitro*, with the tubular scaffold showing encouraging mechanical properties (burst pressure of 1075 ± 444 mmHg) (Marcolin et al., 2017).

Following the Weinberg and Bell study in 1986, most of the studies focusing on natural materials have used a gel-based approach. This consists of casting a mixture of the desired gel and cell suspension in a tubular mold made of a polypropylene tube. The first period of incubation and cell growth is followed by a period of maturation in dynamic conditions to confer properties of a vascular tissue (Weinberg and Bell, 1986). Tranquillo et al. achieved the fabrication of a tubular structure using a fibrin gel with human dermal fibroblasts, but the burst pressure after 3 weeks was still far below (543 mmHg) the SV values (Huynh and Tranquillo, 2010). Natural gels, based on collagen and fibrin, have been evaluated as a possible artificial arterial conduit in animal models. The above mentioned fibrin-based structure with fibroblasts was implanted into the femoral artery of sheep. Cyclic deformation in addition to pulsatile flow conditioning improved mechanical properties of the graft (Syedain et al., 2011). To further improve the mechanical properties of the TEVG, a suspension of ovine dermal fibroblasts were added to

TABLE 1 | TEVG applied in human studies.

Approaches	Applications	Scaffold materials and fabrication methods	Groups
Natural material-based TEVG	Graft as an extrahepatic portal vein bypass.	Decellularized human iliac vein seeded with autologous cells **No commercial product**	Sumitran-Holgersson and colleagues (Olausson et al., 2012)
	Lower extremity bypass surgery	Decellularized bovine carotid artery graft **Commercial name**: Artegraft, (North Brunswick, NJ)	Lin and colleagues (Lindsey et al., 2017)
Synthetic material-based TEVG	Arteriovenous (AV) shunt for heamodyalisis	Decellularization of PGA scaffolds seeded with cadaver SMCs. **Commercial name**: Humacyte, (Humacyte Incorporated, RTP, NC)	Dahl/Niklason and colleagues (Lawson et al., 2016)
Self-assembled TEVG	AV shunt for heamodyalisis access	Cell-sheet of human fibroblast in a shape of conduit. ECs were seeded in the graft after devitalization of the luminal side. **Commercial name**: Cytograft, (Cytograft Tissue Engineering, Inc.)	L'Heureux and colleagues (Wystrychowski et al., 2011)
	AV shunts for hemodialysis access	Cell-sheet of human fibroblast in a shape of conduit, without further endothelialization. Dehydrated and stored (−80°C) before clinical application. **Commercial name**: LifeLine^{TM}, (Cytograft Tissue Engineering, Inc.)	L'Heureux and colleagues (Wystrychowski et al., 2014)

the fibrin and the gelled structure was cultured for a total period of 5 weeks (the first 2 in static conditions and the remaining 3 under pulsatile flow stimulation) (Syedain et al., 2014). At the end of the conditioning period, the structure was decellularized. This process led to obtaining a TEVG with around 4200 mmHg burst pressure, able to remain patent for 24 weeks and with a concentration of collagen and elastin close to the natural values (Syedain et al., 2014). In another study, VSMCs were used to colonialize the fibrin gel and ECs were seeded on to the luminal side before implantation into an ovine model (Swartz, 2004; Liu et al., 2007). This graft showed good results in terms of integration with the native vessel but, on the other hand, it displayed poor mechanical properties.

Silk fibroin-based materials were considered as an alternative (Enomoto et al., 2010) and Kaplan et al. implanted a graft of this kind in the abdominal aorta of rats (Lovett et al., 2010). No thrombosis was seen and implants remained patent, with the absence of occlusion or ischemia detected at the 1 month follow-up.

Collagen-based vascular grafts were recently tested *in vivo* and assessed for the feasibility of the system to hold microsurgical sutures. Dehydration of crosslinked collagen allowed to create a small-diameter TEVG (diameter $\leq$ 1 mm) with a burst pressure of approximately 1313 mmHg, compliance of 1.7%/100 mmHg (comparable with mammalian vein), but the strength of the anastomosis at the interface between the rat femoral artery and TEVG was still lower than the one between two portions of explanted rat femoral artery (Li et al., 2017). Natural polymers are acknowledged to be valid alternatives in the production of small diameter TEVGs, due to their higher biocompatibility and capability to remodel *in vivo*. Nonetheless, natural polymers generally offer reduced mechanical strength compared to their synthetic counterparts and can be more susceptible to degradation, which, if not carefully controlled, may lead to rupture and aneurysm formation.

Decellularized natural matrices

The mismatch of mechanical properties, in terms of strength, elasticity, long-term resistance, and fatigue, between the fabricated scaffold and the native vessel led to development of grafts with a structure more similar to the biological ones, but available as an off-the-shelf product. This need was reflected by further attempts to employ decellularization of tissues harvested from allogenic or xenogeneic sources (**Figure 1**). The elimination of cells is needed to avoid an immunological reaction from the recipient, but agents employed to this scope should have properties allowing preservation of the structure and function of the ECM. These techniques typically use detergents, like sodium dodecyl sulfate, octylglucoside, sodium deoxycholate, and enzymes, like dispase II, nucleases, phospholipase, and thermolysin, often in combination with mechanical and physical methods to accelerate the process (Crapo et al., 2011).

The approach based on natural matrices to obviate the problems associated with autologous grafts, led to the commercialization of a variety of decellularized products, such as Procol (Hancock Jaffe Laboratories Inc., Irvine, CA), the SG 100 SynerGraft® vascular graft, (CryoLife, Kennesaw, Georgia, USA) and the already mentioned Artegraft (North Brunswick, NJ). To improve the properties of these grafts, autologous ECs and VSMCs obtained from differentiation

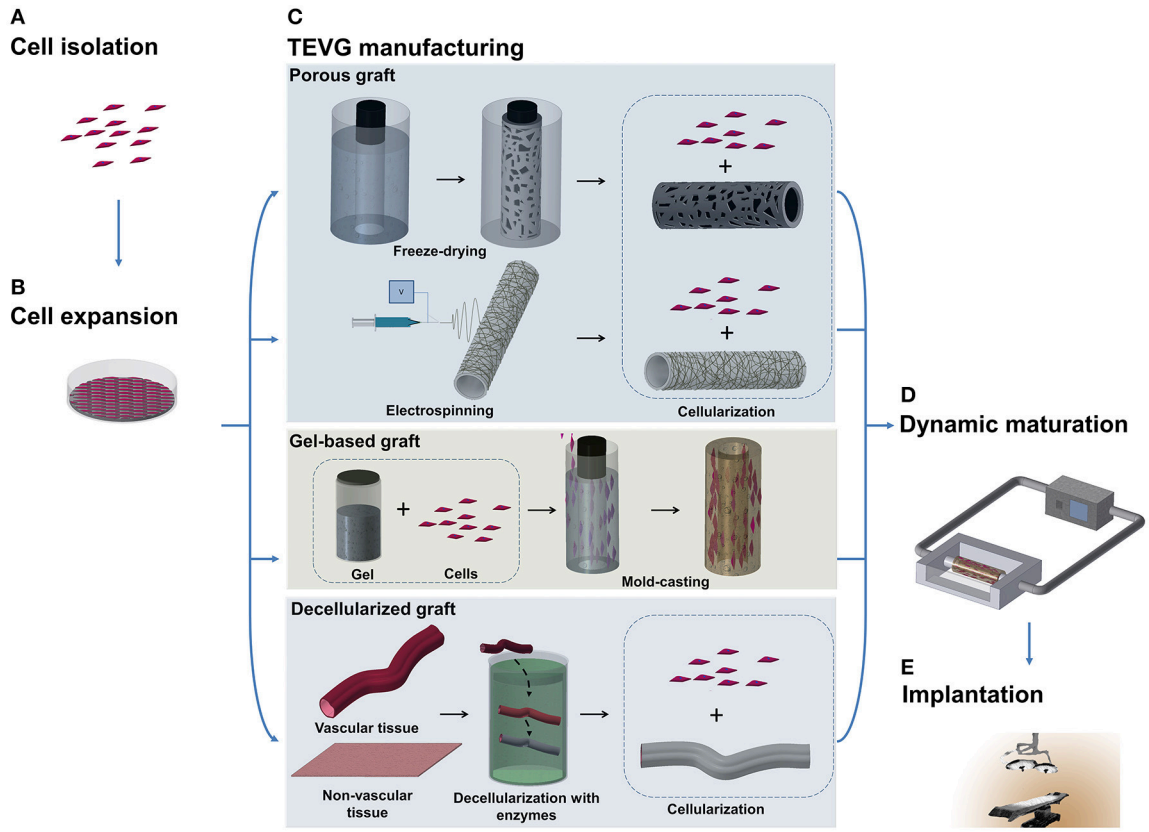

FIGURE 1 | Schematic illustration of TEVG manufacturing process. **(A,B)** Tissues obtained from biopsies of patients are treated and cells are isolated and expanded *in vitro*. **(C)** Microfabrication techniques, such as freeze-drying and electrospinning, can be used to treat natural and synthetic materials in order to obtain a porous scaffold. Another approach sees the casting of a suspension of gel and cells into a mold to produce a tubular structure. Vascular and non-vascular tissues, obtained from allogeneic or xenogeneic sources, are used as TEVGs after being decellularized by using detergents and enzymes. **(D)** The TEVG undergoes cellularization with the expanded autologous cells before moving to dynamic conditioning into bioreactor which allows the maturation of the structure. **(E)** The manufactured TEVG is implanted into the patient.

of bone marrow-derived cells were seeded in decellularized matrices and then tested in ovine (Tillman et al., 2012) and canine models (Cho et al., 2005).

Decellularized vascular grafts derived from bovine have been widely experimented in clinical trials (Katzman et al., 2005; Chemla and Morsy, 2009) in which their performance was compared with the classical PTFE graft in arteriovenous fistula (AVF) and bypass procedures (Butler et al., 1977). Despite the investments, the grafts maintained high costs, showed low patency and multiple cases of immunogenic response due to the inefficacy in the decellularization process. Sumitran-Holgersson et al. performed the first human study on a single pediatric patient (**Table 1**), using a decellularized human iliac vein seeded with autologous cells (Olausson et al., 2012). The outcomes were promising, with patency up to 2 years even if applied in a low-flow district. A recent long-term study (2002–2017) showed the application of a bovine carotid artery graft (Artegraft) in lower extremity bypass surgery (Lindsey et al., 2017). Follow-up of 5 years of primary endpoints showed positive results for patency (66.7%) and salvage limb rates (81% of treated cases) (**Table 1**).

Among the non-vascular tissues, swine or bovine pericardium have been tested in the past, but porcine small intestinal submucosa (SIS) was the first to be assessed as a valid tissue source (Sandusky et al., 1995). SIS, used as an arteriovenous shunt in a sheep model, showed burst pressure of around 1200 mmHg and the cellularization of the graft improved the anticoagulation properties with a lower rate of platelet aggregate formation (Peng et al., 2011). The decellularization process has many disadvantages. In fact, the main cause of failure is related to immune response induced by leftovers of foreign cellular material. Although the biological origin of the tissue reduced the gap between the properties of the native vessel and the built graft, a persistent limitation consists of the divergent behavior under long-term stress. This difference leads to failure of the graft and possible creation of an aneurysm. In addition, decellularized grafts originating from non-vascular tissue, even if more reliable, are unsuitable for applications in which the scaffold has the necessity to adapt and grow with the patient, as in the case of correction of congenital vascular defects. In these patients, atherosclerotic and fibrotic remodeling and calcification are the

most common consequences of poor integration of the graft with the surrounding tissue, resulting in stenosis and graft failure and requiring multiple interventions for substitution (Shetty et al., 2009; Gössl et al., 2012; Woo et al., 2016).

Hybrid Scaffolds

Natural and synthetic polymers can be used together to create a composite scaffold in order to improve the characteristics that each category possess on its own. In recent years, initially positive results led to investment in this approach. A three-layered TEVG has been fabricated overlapping nanofibers of PCL, collagen, and PLLA (Haghjooy Javanmard et al., 2016). PCL has also been used blended with collagen (Tillman et al., 2009; Bertram et al., 2017), gelatin (Jiang et al., 2017) and elastin (Wise et al., 2011) to improve surface adhesion features, while a PLCL porous scaffold was coated with nanofibers of silk fibroin (Henry et al., 2017) or alternatively with a layer of hMSCs/ECs (Ahn et al., 2015; Pangesty et al., 2017).

PEG-fibrin hydrogel, with murine smooth muscle progenitor cells, was reinforced with an inner layer of electrospun PU fibers (McMahon et al., 2011). *in vivo* experiments with composite TEVGs were performed in the last decade demonstrating the feasibility of the hybrid approach. Murine models have been used to evaluate TEVGs composed of nanofibers of PCL blended with spider silk and chitosan (Zhao et al., 2013), and the scaffold showed maintenance of the patency for up to 8 weeks. A more recent experiment involved a decellularized rat aortic vessel in which the lumen was coated with heparin. Aiming at preventing the vessel weakening and consequent aneurysm formation, the decellularized structure was externally reinforced with PCL (Gong et al., 2016). This hybrid scaffold was easily sutured and displayed improved mechanical properties compared to rat autografts, with a burst pressure of 2060 mmHg and patency rate of 100% after 10 weeks implantation. In a large animal model, Poly(L/D)lactide (P(L/DL)LA) coated with fibrin gel was used as an interposed carotid artery graft in sheep (Koch et al., 2010). Autologous ECs, VSMCs, and fibroblasts were encapsulated in the fibrin gel and cast around the synthetic polymer before the bioreactor conditioning for 21 days to allow for the maturation of the cells. The TEVG was then implanted and after 6 months it showed the absence of thrombus and full patency. A study was recently performed on a large animal, grafting a PCL/collagen scaffold seeded with autologous ECs and VSMCs as arterial interposition. Computed tomography (CT) scan and ultrasonography showed no stenosis and structural integrity of the TEVG at 6 months follow-up (Ju et al., 2017). Though the hybrid approach offers an opportunity of exploiting the qualities of natural and synthetic polymers, a typical drawback is a need for long conditioning and the requirement of high technological skills during the manufacturing process.

Self-Assembled Tevg

Despite the improvements achieved in fabricating TEVGs based on scaffolds, some research groups believed that scaffolds would force the cells to grow in an unnatural assembly, and therefore decided to test the tissue engineered self-assembled (TESA) approach. Self-assembled TEVGs are based on the concept that cells, placed in a 3D environment and with the right stimuli, would be able to organize themselves in a complex tissue. Currently, three main strategies have been investigated: cell-sheet assembly, micro-tissue aggregation, and cell printing (**Figure 2**). Different cell sources have been considered suitable to generate a cell-sheet tissue engineered graft. Human adipose-derived stromal cells (Vallières et al., 2015) and dermal or SV fibroblasts (Bourget et al., 2012) were used to create a scaffold-free graft and, after *in vitro* characterization, displayed good mechanical properties and the ability to produce ECM proteins, including collagen type I, III, and IV, laminin and fibronectin, which are necessary to give structural support to the vessel. The development of this novel scaffold-free approach finds its origin in the success of the first trial by the pioneer L'Heureux. In 1998, L'Heureux et al. first documented the feasibility of implanting a cell-sheet graft in a canine model (L'Heureux et al., 1998). The technique consisted of peeling off a confluent culture of VSMCs and fibroblasts and carefully shaping the cell sheet with all the released ECM into a tubular structure (**Figure 2A**). Conditioning in a bioreactor represents a crucial step to allow the maturation of the cells by fusion of the wrapped layers in a unique vascular structure. After the extended conditioning (8 weeks) under dynamic conditions, the graft showed a burst pressure of around 2600 mmHg, which is higher than that of SV. Relevant to the physiological maturation of the graft, the authors showed the production of ECM proteins typical of the vasculature and the recruitment of ECs onto the luminal surface. Nonetheless, at 7 days post-implantation, the grafts exhibited bleeding and detachment of the layers leading to the failure of the implant. To overcome these limitations, a new study to fabricate scaffold-free TEVGs was performed, involving only human fibroblasts and increasing the period in dynamic culture (L'Heureux et al., 2006). The new grafts showed greater performances from the point of view of mechanical properties (burst pressure of 3468 mmHg) and were used as an arterial interposition in primate models. The grafts were shown to be resistant, did not form aneurysms and were fully patent after 8 weeks. Overall, the main limitation of the technique is the time to produce the graft which, considering the duration between the formation of a confluent sheet and the fusion throughout the bioreactor conditioning, was assessed to be around 28 weeks (L'Heureux et al., 2006). Scaffold-free grafts, containing autologous mesenchymal stem cells (MSCs), were tested by Zhao et al. during pre-clinical studies in a rabbit model (Zhao et al., 2012). The TEVG, used to replace a section of carotid artery 1 cm in length, was fully patent and completely endothelialized after the 4 weeks from implantation. An assessment of histology showed a full integration of the cell-sheet graft and a more complex remodeling in the laminated structure after the period of implantation.

In the meantime, the scaffold-free engineered graft developed by L'Heureux et al., patented with the name of Cytograft (Cytograft Tissue Engineering, Inc., Novato, CA), was used at the beginning of the 2000s in a clinical trial involving 10 patients that suffered from end-stage renal disease (McAllister et al., 2009). Fibroblasts obtained from biopsies of the patient were used to create the autologous TEVG. The fabrication procedure, illustrated above, was completed with the devitalization of the

luminal side of the graft, and subsequent seeding of autologous ECs. The period of time required to produce these grafts turned out to be around 7.5 months. Excluding one patient that died for a cause not related to the graft, the other 3 failures of the self-assembled blood vessel were related to dilatation, thrombosis, and aneurysms. After the 20 month trial, the overall results of the study were promising. Grafts had 78% patency rate at the time point of 1 month and 60% at 6 months. In this study, McAllister et al. demonstrated the feasibility of long distance graft delivery after fabrication in insulated and sealed conditions for long distance (McAllister et al., 2009). L'Heureux's group further improved the production of an off-the-shelf graft attempting to define a procedure to store the graft after the manufacturing process. The cell-sheet based scaffolds were devitalized to be frozen and at the moment in which the patient required the implantation they were thawed, rehydrated and autologous ECs were finally seeded on the luminal side (Wystrychowski et al., 2011). The new allogenic Lifeline™ (Cytograft Tissue Engineering, Inc.), without the seeding of the autologous ECs, was also used in patients as shunts for hemodialysis (**Table 1**). The mechanical properties of the graft were not affected by the thawing procedure and no immune response was detected (Wystrychowski et al., 2014).

Microtissue aggregation represents a variation among the TESA strategies, in which, to circumvent mechanical stress, the cells are not peeled from the culture surface and the post-culturing manipulation to shape the graft is avoided using a growing template. In this approach, a temperature–responsive poly(N-isopropylacrylamide) is used as culturing surface, allowing the easy detachment of the cell aggregate when the culture is confluent (Asakawa et al., 2010). Alternatively, high density hanging drop cells are deposited in the mold for *in situ* merging by secretion of ECM, representing building blocks for vascular-like structures (Marga et al., 2012). Kelm et al. obtained a tubular structure by the aggregation of human artery-derived fibroblasts and HUVECs (Kelm et al., 2010) (**Figure 2B**). Fourteen days of conditioning with dynamic pulsatile flow allowed the fusion of the multiple blocks in a unique tissue with layered tissue formation.

One typical constraint of the TESA technique is the limited shape that the graft can assume. In fact, the inability of the cell aggregation to self-sustain, forced the researcher to keep the geometry as simple as possible. The possibility to rectify this limitation was recently proposed by the use of Bioprinting, which may have the refined capability to build a patient-specific arterial vessel (**Figure 2C**). Bioprinting is currently used to create constructs for growth factor delivery (Gao et al., 2015), *in vitro* microvacularized constructs (Kamei et al., 2006; Cui and Boland, 2009; Miller et al., 2012; Bertassoni et al., 2014; Kolesky et al., 2014; Gao et al., 2015) and myocardial patches (Gaebel et al., 2011; Gaetani et al., 2012, 2015). Some studies have focused on providing a proof-of-concept for manufacturing vascular structures with the intention to be used as small-diameter TEVGs (Borovjagin et al., 2017; Duan, 2017). A novel approach exploited the concept of self-assembly through the fusion of cell spheroids forming a unique tubular structure (Mironov et al., 2009). Norette et al. performed an initial study attempting to bioprint a complex vascular tree (Norotte, 2009). The high flexibility of this approach allowed the fabrication of tubular structures by aggregation of spheroids, with connected branches of accurate diameter and wall thickness. On the other hand, this strategy showed limitations in terms of sterility and its time-consuming nature. Maintaining the integrity of the environment during the assembling of the vascular tree is challenging, and a minimum of 7 days is required to allow for the fusion of the spheroids on to the tubular surface. To overcome some of these disadvantages, Norette et al. reduced the complexity of the system and succeeded in the creation of a tubular structure by deposition of human umbilical vein VSMCs and skin fibroblasts (Norotte, 2009). Additionally, mouse embryonic fibroblasts have been used by Kucukgul et al. to fabricate a scaffold-free arterial construct (Kucukgul et al., 2015). A bioprinted vascular graft suitable for implantation and delivery to any large *in vivo* model or clinical trial has not been developed, mainly due to the lack of mechanical properties and the long period required to produce a stable structure.

CONCLUSIONS

The necessity to find an alternative to autologous vascular grafts led to the development of TEVG, which, exploiting the combination of multiple approaches, holds promise to match the minimal requirement of current autologous vessels. Many improvements have been awarded in the recent past and results from *in vivo* experiments showed encouraging outcomes. Nevertheless, initial clinical trials did not always confirm the experimental findings, thus suggesting there is still room for improvements in the translational process.

Failure of TEVG could occur at different time points after the implantation and, accordingly, can be classified as early, midterm and late failures (Pashneh-Tala et al., 2015). Acute thrombosis is the main cause of early failure (within 3 months after implantation) and it is a coagulation reaction driven by platelet adhesion on collagen, which in the native vasculature is avoided by the anti-thrombotic properties of the endothelium. Acellular and decellularized TEVGs are mostly affected by this issue. Biodegradable TEVGs, cellularized or based on hybrid approach, shielding the scaffold lumen from the bloodstream, show a reduction in thrombus events. Multiple solutions have been explored, combining different synthetic and natural materials and performing chemical functionalization of the surface to improve anti-thrombogenic properties (Seifu et al., 2013; Tara et al., 2014). Furthermore, biodegradable polymers offer the possibility for the cells to colonialize the porous structure and thereby stimulate the production of ECM proteins. On the other hand, if the properties of the polymers are not well tuned, the intimal thickening can reduce the patency caused by the excessive migration and proliferation of cells. Lumen occlusion due to anastomotic intimal hyperplasia typically characterizes the midterm failures (from 3 months to 2 years). Late term failure is associated, instead, to recurrent atherosclerotic disease and is a common problem with all the current approaches. It is

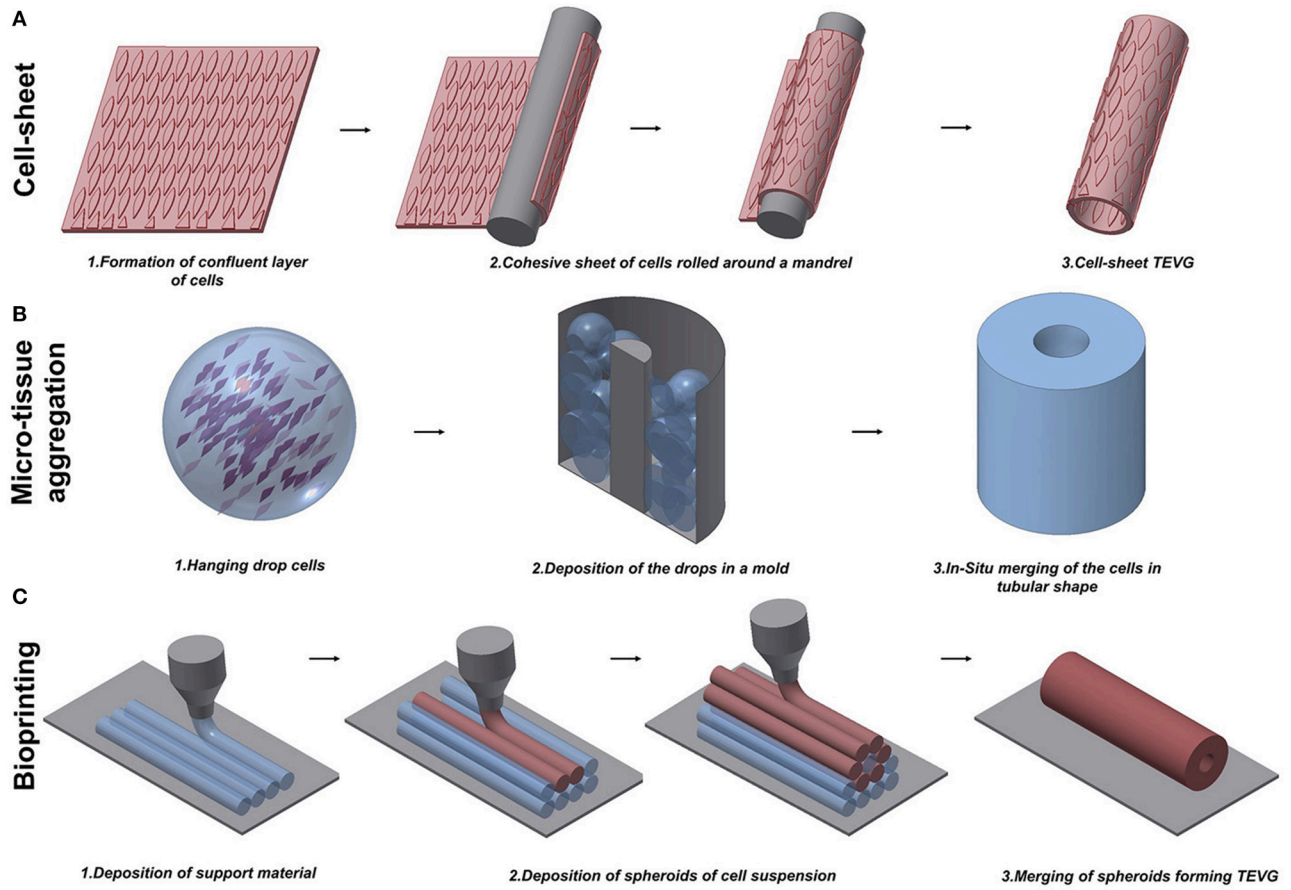

FIGURE 2 | Schematic representation of techniques to manufacture scaffold-free vascular grafts. **(A)** Cell-sheet TEVG approach involves the use of a dense and cohesive sheet of cells to create a tubular structure. The sheet is rolled around a mandrel and matured under dynamic conditions to develop vessel-like properties. **(B)** Hanging drop cells are accurately positioned into a mold in the microtissue aggregation approach **(B)**. The production of ECM allows the merging of the aggregates in a complex structure. **(C)** Bioprinting exploits the extrusion of support material to increase the flexibility of the fabrication. An accurate design of support material and cells extruded in spheroids allows the creation of tubular structures.

mainly due to the loss in consistency of the graft or poor *in vivo* integration.

So far, decellularized native tissues are the most successful *in vivo* approach, although post-implantation thrombus events are the main limitation for low long-term patency. Moreover, decellularization is still a topic of debate because the incompleteness of the process may lead to an immunogenic reaction by the recipient, whereas an excessive chemical treatment can provoke the loss of mechanical properties and aneurysmal dilatation (Shojaee and Bashur, 2017).

On the other hand, recent improvements in biodegradable TEVG production, offering a wider range of physical properties and the capability to remodel *in vivo*, might represent a potential solution to generate a valid TEVG. New microfabrication technologies allow patient-specific manufacturing of the TEVG, eliminating the dimension mismatch at the anastomosis site. This approach is particularly suitable for correction of congenital related diseases. Nevertheless, patency rate is still drastically lower than autologous grafts, with *in vivo* animal experiments no longer than 2 years.

For the category of cellularized TEVGs, the cell source represents a much discussed topic. As described in this review, an extensive variety of cells have been tested, both to build the core of the graft (in the case of a scaffold-free approach) and to cellularize the scaffold in the pre-implantation stage. Autologous mature vascular cells, like VSMCs, ECs, and fibroblasts, have been used to cellularize TEVGs with success. Here, the main limitation is represented by the extraction from a patient biopsy, thereby leading to insufficient expansion (G et al., 2015). Adult stem cells, such as BM-MSCs have been used in consideration of their high proliferative property. The time-consuming process of fabrication, cellularization or chemical treatment is often not compatible with the urgent need of patients suffering severe pathology. This can only be solved through the adoption of an off-the-shelf TEVGs. In this approach, standardization of the fabrication process, preservation of sterile conditions and delivery represent the main challenges. However, the potential of having a ready to use graft, with advantages for patients and clinicians, is becoming an attracting prospective.

Owing to the growing target-population for tissue engineering technologies/products under development for cardiac and vascular indications, as well as the major healthcare costs associated with existing treatments, the potential financial figure for these products is in the range of multibillion-dollar volume. In the U.S. alone, the total potential market for tissue engineering and cell transplantation technologies is expected to exceed USD 22.8 billion in the year 2019. Furthermore, the global vascular graft market is expected to reach USD 3,626 million by 2022, according to a new study by Grand View Research, Inc. There is a positive prospect that rising healthcare expenditure, favorable reimbursement policies, and technological breakthroughs will boost growth in the vascular graft market over the next 10 years. At present, TEVGs contribute a minimal part of these financial figures, however, a number of positive factors indicate that this new technology will be successfully translated from research into medical practice.

AUTHOR CONTRIBUTIONS

MC: searched the literature and drafted the manuscript; PM: critically revised the work.

FUNDING

This work has been supported by a Ph.D. studentship entitled Perivascular delivery of bioengineered scaffold for treatment of limb ischemia (MC) supervised by PM and an MRC grant (MR/N027086/1) entitled *in vitro* and *in vivo* preclinical testing of pericyte-engineered grafts for correction of congenital heart defects.

REFERENCES

Ahn, H., Ju, Y. M., Takahashi, H., Williams, D. F., Yoo, J. J., Lee, S. J., et al. (2015). Engineered small diameter vascular grafts by combining cell sheet engineering and electrospinning technology. *Acta Biomater.* 16, 14–22. doi: 10.1016/j.actbio.2015.01.030

Asakawa, N., Shimizu, T., Tsuda, Y., Sekiya, S., Sasagawa, T., Yamato, M., et al. (2010). Pre-vascularization of *in vitro* three-dimensional tissues created by cell sheet engineering. *Biomaterials* 31, 3903–3909. doi: 10.1016/j.biomaterials.2010.01.105

Bertassoni, L. E., Cecconi, M., Manoharan, V., Nikkhah, M., Hjortnaes, J., Cristino, A. L., et al. (2014). Hydrogel bioprinted microchannel networks for vascularization of tissue engineering constructs. *Lab. Chip* 14, 2202–2211. doi: 10.1039/C4LC00030G

Bertram, U., Steiner, D., Poppitz, B., Dippold, D., Köhn, K., Beier, J. P., et al. (2017). Vascular tissue engineering: effects of integrating collagen into a PCL based nanofiber material. *Biomed Res. Int.* 2017:9616939. doi: 10.1155/2017/9616939

Boccafoschi, F., Rajan, N., Habermehl, J., and Mantovani, D. (2007). Preparation and characterization of a scaffold for vascular tissue engineering by direct-assembling of collagen and cells in a cylindrical geometry. *Macromol. Biosci.* 7, 719–726. doi: 10.1002/mabi.200600242

Borovjagin, A. V., Ogle, B. M., Berry, J. L., and Zhang, J. (2017). From microscale devices to 3D printing: advances in fabrication of 3D cardiovascular tissues. *Circ. Res.* 120, 150–165. doi: 10.1161/CIRCRESAHA.116.308538

Bourget, J. M., Gauvin, R., Larouche, D., Lavoie, A., Labbé, R., Auger, F. A., et al. (2012). Human fibroblast-derived ECM as a scaffold for vascular tissue engineering. *Biomaterials* 33, 9205–9213. doi: 10.1016/j.biomaterials.2012.09.015

Brennan, M. P., Dardik, A., Hibino, N., Roh, J. D., Nelson, G. N., Papademitris, X., et al. (2008). Tissue engineered vascular grafts demonstrate evidence of growth and development when implanted in a juvenile animal model. *Annu. Surg.* 248, 370–377. doi: 10.1097/SLA.0b013e318184dcbd

Butler, H. G., Baker, L. D., and Johnson, J. M. (1977). Vascular access for chronic hemodialysis: polytetrafluoroethylene (PTFE) versus bovine heterograft. *Am. J. Surg.* 134, 791–793. doi: 10.1016/0002-9610(77)90326-9

Campbell, C. D., Brooks, D. H., Webster, M. W., and Bahnson, H. T. (1976). The use of expanded microporous polytetrafluoroethylene for limb salvage: a preliminary report. *Surgery* 79, 485–491.

Chan, A. H., Tan, R. P., Michael, P. L., Lee, B. S., Vanags, L. Z., Ng, M. K., et al. (2017). Evaluation of synthetic vascular grafts in a mouse carotid grafting model. *PLoS ONE* 12:e0174773. doi: 10.1371/journal.pone.0174773

Chemla, E. S., and Morsy, M. (2009). Randomized clinical trial comparing decellularized bovine ureter with expanded polytetrafluoroethylene for vascular access. *Br. J. Surg.* 96, 34–39. doi: 10.1002/bjs.6434

Cho, S.-W., Lim, S. H., Kim, I.-K., Hong, Y. S., Kim, S.-S., Yoo, K. J., et al. (2005). Small-diameter blood vessels engineered with bone marrow- derived cells. *Ann. Surg.* 241, 506–515. doi: 10.1097/01.sla.0000154268.12239.ed

Collins, P., Webb, C. M., Chong, C. F., and Moat, N. E. (2008). Radial artery versus saphenous vein patency randomized trial: five-year angiographic follow-up. *Circulation* 117, 2859–2864. doi: 10.1161/CIRCULATIONAHA.107.736215

Crapo, P. M., Gilbert, T. W., and Badylak, S. F. (2011). An overview of tissue and whole organ decellularization processes. *Biomaterials* 32, 3233–3243. doi: 10.1016/j.biomaterials.2011.01.057

Criqui, M. H., and Aboyans, V. (2015). Epidemiology of peripheral artery disease. *Circ. Res.* 116, 1509–1526. doi: 10.1161/CIRCRESAHA.116.303849

Cui, X., and Boland, T. (2009). Human microvasculature fabrication using thermal inkjet printing technology. *Biomaterials* 30, 6221–6227. doi: 10.1016/j.biomaterials.2009.07.056

Cummings, I., George, S., Kelm, J., Schmidt, D., Emmert, M. Y., Weber, B., et al. (2012). Tissue-engineered vascular graft remodeling in a growing lamb model: Expression of matrix metalloproteinases. *Eur. J. Cardio-thoracic Surg.* 41, 167–172. doi: 10.1016/j.ejcts.2011.02.077

Dahl, L. S., Lawson, J. H., Prichard, H. L., Manson, R. J., Tente, W. E., Kypson, A. P., et al. (2013). Abstracts from the emerging science series, April 24, 2013. *Circulation* 127, 2071–2072. doi: 10.1161/CIR.0b013e318295baf5

Dahl, S. L., Kypson, A. P., Lawson, J. H., Blum, J. L., Strader, J. T., Li, Y., et al. (2011). Readily available tissue-engineered vascular grafts. *Sci. Transl. Med.* 3:68ra9. doi: 10.1126/scitranslmed.3001426

De Bakey, M. E., Cooley, D., A., Crawford, E. S., and Morris Jr, G. C. (1958). Clinical application of a new flexible knitted dacron arterial substitute. *Am. Surg.* 24, 862–869. doi: 10.1001/archsurg.1958.01290040061008

Duan, B. (2017). State-of-the-art review of 3D bioprinting for cardiovascular tissue engineering. *Ann. Biomed. Eng.* 45, 195–209. doi: 10.1007/s10439-016-1607-5

Elsayed, Y., Lekakou, C., Labeed, F., and Tomlins, P. (2016). Fabrication and characterisation of biomimetic, electrospun gelatin fibre scaffolds for tunica media-equivalent, tissue engineered vascular grafts. *Mater. Sci. Eng. C* 61, 473–483. doi: 10.1016/j.msec.2015.12.081

Engbers-Buijtenhuijs, P., Buttafoco, L., Poot, A. A., Dijkstra, P. J., de Vos, R. A., Sterk, L. M., et al. (2006). Biological characterisation of vascular grafts cultured in a bioreactor. *Biomaterials* 27, 2390–2397. doi: 10.1016/j.biomaterials.2005.10.016

Enomoto, S., Sumi, M., Kajimoto, K., Nakazawa, Y., Takahashi, R., Takabayashi, C., et al. (2010). Long-term patency of small-diameter vascular graft made from fibroin, a silk-based biodegradable material. *J. Vasc. Surg.* 51, 155–164. doi: 10.1016/j.jvs.2009.09.005

Epstein, A. J., Polsky, D., Yang, F., Yang, L., and Groeneveld, P. W. (2011). Coronary revascularization trends in the United States, 2001-2008. *JAMA* 305, 1769–1776. doi: 10.1001/jama2011.551

G, N., Tan, A., Gundogan, B., Farhatnia, Y., Nayyer, L., Mahdibeiraghdar, S., et al. (2015). Tissue engineering vascular grafts a fortiori: looking

back and going forward. *Expert Opin. Biol. Ther.* 15, 231–244. doi: 10.1517/14712598.2015.980234

Gaebel, R., Ma, N., Liu, J., Guan, J., Koch, L., Klopsch, C., et al. (2011). Patterning human stem cells and endothelial cells with laser printing for cardiac regeneration. *Biomaterials* 32, 9218–9230. doi: 10.1016/j.biomaterials.2011.08.071

Gaetani, R., Doevendans, P. A., Metz, C. H., Alblas, J., Messina, E., Giacomello, A., et al. (2012). Cardiac tissue engineering using tissue printing technology and human cardiac progenitor cells. *Biomaterials* 33, 1782–1790. doi: 10.1016/j.biomaterials.2011.11.003

Gaetani, R., Feyen, D. A., Verhage, V., Slaats, R., Messina, E., Christman, K. L., et al. (2015). Epicardial application of cardiac progenitor cells in a 3D-printed gelatin/hyaluronic acid patch preserves cardiac function after myocardial infarction. *Biomaterials* 61, 339–348. doi: 10.1016/j.biomaterials.2015.05.005

Gao, J., Crapo, P. M., and Wang, Y. (2006). Macroporous elastomeric scaffolds with extensive micropores for soft tissue engineering. *Tissue Eng.* 12, 917–925. doi: 10.1089/ten.2006.12.917

Gao, Q., He, Y., Fu, J. Z., Liu, A., and Ma, L. (2015). Coaxial nozzle-assisted 3D bioprinting with built-in microchannels for nutrients delivery. *Biomaterials* 61, 203–215. doi: 10.1016/j.biomaterials.2015.05.031

Goldman, S., Zadina, K., Moritz, T., Ovitt, T., Sethi, G., Copeland, J. G., et al. (2004). Long-term patency of saphenous vein and left internal mammary artery grafts after coronary artery bypass surgery: results from a department of veterans affairs cooperative study. *J. Am. Coll. Cardiol.* 44, 2149–2156. doi: 10.1016/j.jacc.2004.08.064

Gong, W., Lei, D., Li, S., Huang, P., Qi, Q., Sun, Y., et al. (2016). Hybrid small-diameter vascular grafts: anti-expansion effect of electrospun poly ε-caprolactone on heparin-coated decellularized matrices. *Biomaterials* 76, 359–370. doi: 10.1016/j.biomaterials.2015.10.066

Gössl, M., Khosla, S., Zhang, X., Higano, N., Jordan, K. L., Loeffler, D., et al. (2012). Role of circulating osteogenic progenitor cells in calcific aortic stenosis. *J. Am. Coll. Cardiol.* 60, 1945–1953. doi: 10.1016/j.jacc.2012.07.042

Gui, L., and Niklason, L. E. (2014). Vascular tissue engineering: building perfusable vasculature for implantation. *Curr. Opin. Chem. Eng.* 3, 68–74. doi: 10.1016/j.coche.2013.11.004

Haghjooy Javanmard, S., Anari, J., Zargar Kharazi, A., and Vatankhah, E. (2016). *in vitro* hemocompatibility and cytocompatibility of a three-layered vascular scaffold fabricated by sequential electrospinning of PCL, collagen, and PLLA nanofibers. *J. Biomater. Appl.* 31, 438–449. doi: 10.1177/0885328216652068

Harskamp, R. E., Lopes, R. D., Md, P., Baisden, C. E., de Winter, R. J., Alexander, J. H., et al. (2013). Saphenous vein graft failure after coronary artery bypass surgery: pathophysiology, management, and future directions. *Ann. Surg.* 257, 824–833. doi: 10.1097/SLA.0b013e318288c38d

Hashi, C. K., Zhu, Y., Yang, G.-Y., Young, W. L., Hsiao, B. S., Wang, K., et al. (2007). Antithrombogenic property of bone marrow mesenchymal stem cells in nanofibrous vascular grafts. *Proc. Natl. Acad. Sci. U.S.A.* 104, 11915–11920. doi: 10.1073/pnas.0704581104

Hatzibaloglou, A., Velissaris, Y., Kaitzis, D., Grekas, D., Avdelidou, A., and Kiskinis, D. (2004). ProCol® vascular bioprosthesis for vascular access: midterm results. *J. Vasc. Access* 5, 16–18. doi: 10.1177/112972980400500104

Henry, J. J. D., Yu, J., Wang, A., Zhang, Y., Li, X. S., Guex, A. G., et al. (2017). A compliant and biomimetic three-layered vascular graft for small blood vessels *Biofabrication* 9:025010. doi: 10.1088/1758-5090/aa6bae.

Hoerstrup, S. P., Cummings Mrcs I., Lachat, M., Schoen, F. J., Jenni, R., Leschka, S., et al. (2006). Functional growth in tissue-engineered living, vascular grafts: Follow-up at 100 weeks in a large animal model. *Circulation* 114, 159–167. doi: 10.1161/CIRCULATIONAHA.105.001172

Hutchin, P., Jacobs, J. R., Devin, J. B., and Roland, A. S. (1975). Bovine graft arteriovenous fistulas for maintenance hemodialysis. *Surg. Gynecol. Obstet.* 141, 255–258.

Huynh, T. N., and Tranquillo, R. T. (2010). Fusion of concentrically layered tubular tissue constructs increases burst strength. *Ann. Biomed. Eng.* 38, 2226–2236. doi: 10.1007/s10439-010-0045-z

In Jeong, S., Kim, S. Y., Cho, S. K., Chong, M. S., Kim, K. S., Kim, H., et al. (2007). Tissue-engineered vascular grafts composed of marine collagen and PLGA fibers using pulsatile perfusion bioreactors. *Biomaterials* 28, 1115–1122.

Jackson, M. R., Belott, T. P., Dickason, T., Kaiser, W. J., Modrall, J. G., Valentine, R. J., et al. (2000). The consequences of a failed femoropopliteal bypass grafting: comparison of saphenous vein and PTFE grafts. *J. Vasc. Surg.* 32, 498–505. doi: 10.1016/j.biomaterials.2006.10.025

Jiang, Y. C., Jiang, L., Huang, A., Wang, X. F., Li, Q., and Turng, L. S. (2017). Electrospun polycaprolactone/gelatin composites with enhanced cell-matrix interactions as blood vessel endothelial layer scaffolds. *Mater. Sci. Eng. C* 71, 901–908. doi: 10.1016/j.msec.2016.10.083

Ju, Y. M., Ahn, H., Arenas-Herrera, J., Kim, C., Abolbashari, M., Atala, A., et al. (2017). Electrospun vascular scaffold for cellularized small diameter blood vessels: a preclinical large animal study. *Acta Biomater.* 59, 58–67. doi: 10.1016/j.actbio.2017.06.027

Kamei, M., Brian Saunders, W., Bayless, K. J., Dye, L., Davis, G. E., and Weinstein, B. M. (2006). Endothelial tubes assemble from intracellular vacuoles *in vivo*. *Nature* 442, 453–456. doi: 10.1038/nature04923

Katzman, H. E., Glickman, M. H., Schild, A. F., Fujitani, R. M., and Lawson, J. H. (2005). Multicenter evaluation of the bovine mesenteric vein bioprostheses for hemodialysis access in patients with an earlier failed prosthetic graft. *J. Am. Coll. Surg.* 201, 223–230. doi: 10.1016/j.jamcollsurg.2005.03.040

Kelm, J. M., Lorber, V., Snedeker, J. G., Schmidt, D., Broggini-Tenzer, A., Weisstanner, M., et al. (2010). A novel concept for scaffold-free vessel tissue engineering: self-assembly of microtissue building blocks. *J. Biotechnol.* 148, 46–55. doi: 10.1016/j.jbiotec.2010.03.002

Kim, K. B., Cho, K. R., and Jeong, D. S. (2008). Midterm angiographic follow-up after off-pump coronary artery bypass: serial comparison using early, 1-year, and 5-year postoperative angiograms. *J. Thorac. Cardiovasc. Surg.* 135, 300–307. doi: 10.1016/j.jtcvs.2007.09.044

Koch, S., Flanagan, T. C., Sachweh, J. S., Tanios, F., Schnoering, H., Deichmann, T., et al. (2010). Fibrin-polylactide-based tissue-engineered vascular graft in the arterial circulation. *Biomaterials* 31, 4731–4739. doi: 10.1016/j.biomaterials.2010.02.051

Kolesky, D. B., Truby, R. L., Gladman, A. S., Busbee, T. A., Homan, K. A., and Lewis, J. A. (2014). 3D bioprinting of vascularized, heterogeneous cell-laden tissue constructs. *Adv. Mater. Weinheim.* 26, 3124–3130. doi: 10.1002/adma.201305506

Konig, G., Mcallister, T. N., Dusserre, N., Garrido, S. A., Iyican, C., Marini, A., et al. (2010). Mechanical properties of completely autologous human tissue engineered blood vessels compared to human saphenous vein and mammary artery. *Biomaterials* 30, 1542–1550. doi: 10.1016/j.biomaterials.2008.11.011

Kucukgul, C., Ozler, S. B., Inci, I., Karakas, E., Irmak, S., Gozuacik, D., et al. (2015). 3D bioprinting of biomimetic aortic vascular constructs with self-supporting cells. *Biotechnol. Bioeng.* 112, 811–821. doi: 10.1002/bit.25493

Kunlin, J. (1951). Long vein transplantation in treatment of ischemia caused by arteritis. *Rev. Chir.* 70, 206–235.

L'Heureux, N., Dusserre, N., Konig, G., Victor, B., Keire, P., Wight, T. N., et al. (2006). Human tissue-engineered blood vessels for adult arterial revascularization. *Nat. Med.* 12, 361–365. doi: 10.1038/nm1364

L'Heureux, N., Dusserre, N., Marini, A., Garrido, S., de la Fuente, L., and McAllister, T. (2007). Technology Insight: the evolution of tissue-engineered vascular grafts—from research to clinical practice. *Nat. Clin. Pract. Cardiovasc. Med.* 4, 389–395. doi:10.1038/ncpcardio0930.

L'Heureux, N., Pâquet, S., Labbé, R., Germain, L., and Auger, F. A. (1998). A completely biological tissue-engineered human blood vessel. *FASEB J.* 12, 47–56.

Lawson, J. H., Glickman, M. H., Ilzecki, M., Jakimowicz, T., Jaroszynski, A., Peden, E. K., et al. (2016). Bioengineered human acellular vessels for dialysis access in patients with end-stage renal disease: two phase 2 single-arm trials. *Lancet* 387, 2026–2034. doi: 10.1016/S0140-6736(16)00557-2

Lee, K.-W., Stolz, D. B., and Wang, Y. (2011). Substantial expression of mature elastin in arterial constructs. *Proc. Natl. Acad. Sci. U.S.A.* 108, 2705–2710. doi: 10.1073/pnas.1017834108

Li, X., Xu, J., Nicolescu, C. T., Marinelli, J. T., and Tien, J. (2017). Generation, endothelialization, and microsurgical suture anastomosis of strong 1-mm-diameter collagen tubes. *Tissue Eng. Part A* 23, 335–344. doi: 10.1089/ten.tea.2016.0339

Lindsey, P., Echeverria, A., Cheung, M., Kfoury, E., Bechara, C. F., and Lin, P. H. (2017). Lower extremity bypass using bovine carotid artery graft (artegraft): an analysis of 124 cases with long-term results. *World J. Surg.* 42, 295–301. doi: 10.1007/s00268-017-4161-x

Liu, J. Y., Swartz, D. D., Peng, H. F., Gugino, S. F., Russell, J. A., and Andreadis, S. T. (2007). Functional tissue-engineered blood vessels from bone marrow progenitor cells. *Cardiovasc. Res.* 75, 618–628. doi: 10.1016/j.cardiores.2007.04.018

Lovett, M., Eng, G., Kluge, J., Cannizzaro, C., Vunjak-novakovic, G., and Kaplan, D. L. (2010). Tubular silk sca olds for small diameter vascular grafts. *Organogenesis* 6, 217–224. doi: 10.4161/org.6.4.13407

Madden, R. L., Lipkowitz, G. S., Browne, B. J., and Kurbanov, A. (2004). Experience with cryopreserved cadaveric femoral vein allografts used for hemodialysis access. *Ann. Vasc. Surg.* 18, 453–458. doi: 10.1007/s10016-004-0055-0

Marcolin, C., Draghi, L., Tanzi, M. C., and Faré, S. (2017). Electrospun silk fibroin–gelatin composite tubular matrices as scaffolds for small diameter blood vessel regeneration. *J. Mater. Sci. Mater. Med.* 28, 1–12. doi: 10.1007/s10856-017-5884-9

Marelli, B., Achilli, M., Alessandrino, A., Freddi, G., Tanzi, M. C., Far, S., et al. (2012). Collagen-reinforced electrospun silk fibroin tubular construct as small calibre vascular graft. *Macromol. Biosci.* 12, 1566–1574. doi: 10.1002/mabi.201200195

Marelli, B., Alessandrino, A., Farè, S., Freddi, G., Mantovani, D., and Tanzi, M. C. (2010). Compliant electrospun silk fibroin tubes for small vessel bypass grafting. *Acta Biomater.* 6, 4019–4026. doi: 10.1016/j.actbio.2010.05.008

Marga, F., Jakab, K., Khatiwala, C., Shepherd, B., Dorfman, S., Hubbard, B., et al. (2012). Toward engineering functional organ modules by additive manufacturing. *Biofabrication* 4:022001. doi: 10.1088/1758-5082/4/2/022001

McAllister, T. N., Maruszewski, M., Garrido, S. A., Wystrychowski, W., Dusserre, N., Marini, A., et al. (2009). Effectiveness of haemodialysis access with an autologous tissue-engineered vascular graft: a multicentre cohort study. *Lancet* 373, 1440–1446. doi: 10.1016/S0140-6736(09)60248-8

McMahon, R. E., Qu, X., Jimenez-Vergara, A. C., Bashur, C. A., Guelcher, S. A., Goldstein, A. S., et al. (2011). Hydrogel–electrospun mesh composites for coronary artery bypass grafts. *Tissue Eng. Part C Methods* 17, 451–461. doi: 10.1089/ten.tec.2010.0427

Miller, J. S., Stevens, K. R., Yang, M. T., Baker, B. M., Nguyen, D. H., Cohen, D. M., et al. (2012). Rapid casting of patterned vascular networks for perfusable engineered three-dimensional tissues. *Nat. Mater.* 11, 768–774. doi: 10.1038/nmat3357

Mironov, V., Visconti, R. P., Kasyanov, V., Forgacs, G., Drake, C. J., and Markwald, R. R. (2009). Organ printing: tissue spheriods as building blocks. *Biomaterials* 30, 2164–2174. doi: 10.1016/j.biomaterials.2008.12.084

Motlagh, D., Yang, J., Lui, K. Y., Webb, A. R., and Ameer, G. A. (2006). Hemocompatibility evaluation of poly(glycerol-sebacate) *in vitro* for vascular tissue engineering. *Biomaterials* 27, 4315–4324. doi: 10.1016/j.biomaterials.2006.04.010

Nieponice, A., Soletti, L., Guan, J., Hong, Y., Gharaibeh, B., Maul, T. M., et al. (2010). *in vivo* assessment of a tissue-engineered vascular graft combining a biodegradable elastomeric scaffold and muscle-derived stem cells in a rat model. *Tissue Eng. Part A* 16, 1215–1223. doi: 10.1089/ten.tea.2009.0427

Niklason, L. E., and Langer, R. S. (1997). Advances in tissue engineering of blood vessels and other tissues. *Transpl. Immunol.* 5, 303–306. doi: 10.1016/S0966-3274(97)80013-5

Niklason, L. E. (1999). Functional arteries grown *in vitro*. *Science* 284, 489–493. doi: 10.1126/science.284.5413.489

Niklason, L. E., Abbott, W., Gao, J., Klagges, B., Hirschi, K. K., Ulubayram, K., et al. (2001). Morphologic and mechanical characteristics of engineered bovine arteries. *J. Vasc. Surg.* 33, 628–638. doi: 10.1067/mva.2001.111747

Norotte, C. (2009). Scaffold-free vascular tissue engineering using bioprinting. *Biomaterials* 30, 5910–5917. doi: 10.1016/j.biomaterials.2009.06.034

Olausson, M., Patil, P. B., Kuna, V. K., Chougule, P., Hernandez, N., Methe, K., et al. (2012). Transplantation of an allogeneic vein bioengineered with autologous stem cells: a proof-of-concept study. *Lancet* 380, 230–237. doi: 10.1016/S0140-6736(12)60633-3

Ong, C. S., Fukunishi, T., Liu, R. H., Nelson, K., Zhang, H., Wieczorek, E., et al. (2017). Bilateral arteriovenous shunts as a method for evaluating tissue engineered vascular grafts in large animal models. *Tissue Eng. Part C Methods* 23, 728–735. doi: 10.1089/ten.tec.2017.0217

Pangesty, A. I., Arahira, T., and Todo, M. (2017). Development and characterization of hybrid tubular structure of PLCL porous scaffold with hMSCs/ECs cell sheet. *J. Mater. Sci. Mater. Med.* 28:165. doi: 10.1007/s10856-017-5985-5

Pashneh-Tala, S., MacNeil, S., and Claeyssens, F. (2015). The Tissue-engineered vascular graft—past, present, and future. *Tissue Eng. Part B Rev.* 22, 68–100. doi: 10.1089/ten.teb.2015.0100

Peng, H., Schlaich, E. M., Row, S., Andreadis, S. T., and Swartz, D. D. (2011). A novel ovine *ex vivo* arteriovenous shunt model to test vascular implantability. *Cells Tissues Organs* 195, 108–121. doi: 10.1159/000331415

Quint, C., Kondo, Y., Manson, R. J., Lawson, J. H., Dardik, A., and Niklason, L. E. (2011). Decellularized tissue-engineered blood vessel as an arterial conduit. *Proc. Natl. Acad. Sci. U.S.A.* 108, 9214–9219. doi: 10.1073/pnas.1019506108

Rai, R., Tallawi, M., Grigore, A., and Boccaccini, A. R. (2012). Synthesis, properties and biomedical applications of poly(glycerol sebacate) (PGS): A review. *Prog. Polym. Sci.* 37, 1051–1078. doi: 10.1016/j.progpolymsci.2012.02.001

Sandusky, G. E., Lantz, G. C., and Badylak, S. F. (1995). Healing Comparison of small intestine submucosa and ePTFE grafts in the canine carotid artery. *J. Surg. Res.* 58, 415–420. doi: 10.1006/jsre.1995.1064

Schutte, S. C., Chen, Z., Brockbank, K. G., and Nerem, R. M. (2010). Cyclic strain improves strength and function of a collagen-based tissue-engineered vascular media. *Tissue Eng. Part A* 16, 3149–3157. doi: 10.1089/ten.tea.2010.0009

Schwann, T. A., Zacharias, A., Riordan, C. J., Durham, S. J., Shah, A. S., and Habib, R. H. (2009). Sequential radial artery grafts for multivessel coronary artery bypass graft surgery: 10-year survival and angiography results. *Ann. Thorac. Surg.* 88, 31–39. doi: 10.1016/j.athoracsur.2009.03.081

Seifu, D. G., Purnama, A., Mequanint, K., and Mantovani, D. (2013). Small-diameter vascular tissue engineering. *Nat. Rev. Cardiol.* 10, 410–421. doi: 10.1038/nrcardio.2013.77

Sharifpoor, S., Simmons, C. A., Labow, R. S., and Paul Santerre, J. (2011). Functional characterization of human coronary artery smooth muscle cells under cyclic mechanical strain in a degradable polyurethane scaffold. *Biomaterials* 32, 4816–4829. doi: 10.1016/j.biomaterials.2011.03.034

Shetty, R., Pibarot, P., Audet, A., Janvier, R., Dagenais, F., Perron, J., et al. (2009). Lipid-mediated inflammation and degeneration of bioprosthetic heart valves. *Eur. J. Clin. Invest.* 39, 471–480. doi: 10.1111/j.1365-2362.2009.02132.x

Shojaee, M., and Bashur, C. A. (2017). Compositions including synthetic and natural blends for integration and structural integrity: engineered for different vascular graft applications. *Adv. Healthc. Mater.* 6:1700001. doi: 10.1002/adhm.201700001

Soffer, L., Wang, X., Zhang, X., Kluge, J., Dorfmann, L., Kaplan, D. L., et al. (2008). Silk-based electrospun tubular scaffolds for tissue-engineered vascular grafts. *J. Biomater. Sci. Polym. Ed.* 19, 653–664. doi: 10.1163/156856208784089607

Soyer, T., Lempinen, M., Cooper, P., Norton, L., and Eiseman, B. (1972). A new venous prosthesis. *Surgery* 72, 864–872.

Swartz, D. D. (2004). Engineering of fibrin-based functional and implantable small-diameter blood vessels. *AJP Hear. Circ. Physiol.* 288, H1451–H1460. doi: 10.1152/ajpheart.00479.2004

Syedain, Z. H., Meier, L. A., Bjork, J. W., Lee, A., and Tranquillo, R. T. (2011). Implantable arterial grafts from human fibroblasts and fibrin using a multi-graft pulsed flow-stretch bioreactor with noninvasive strength monitoring. *Biomaterials* 32, 714–722. doi: 10.1016/j.biomaterials.2010.09.019

Syedain, Z. H., Meier, L. A., Lahti, M. T., Johnson, S. L., and Tranquillo, R. T. (2014). Implantation of completely biological engineered grafts following decellularization into the sheep femoral artery. *Tissue Eng. Part A* 20, 1726–1734. doi: 10.1089/ten.tea.2013.0550

Takagi, H., Goto, S. N., Matsui, M., Manabe, H., and Umemoto, T. (2010). A contemporary meta-analysis of Dacron versus polytetrafluoroethylene grafts for femoropopliteal bypass grafting. *J. Vasc. Surg.* 52, 232–236. doi: 10.1016/j.jvs.2010.02.010

Tara, S., Rocco, K. A., Hibino, N., Sugiura, T., Kurobe, H., Breuer, C. K., et al. (2014). Vessel bioengineering. *Circ. J.* 78, 12–19. doi: 10.1253/circj.CJ-13-1440

Tellis, V. A., Kohlberg, W. I., Bhat, D. J., Driscoll, B., and Veith, F. J. (1979). Expanded polytetrafluoroethylene graft fistula for chronic hemodialysis. *Ann. Surg.* 189, 101–105. doi: 10.1097/00000658-197901000-00019

Tillman, B. W., Yazdani, S. K., Lee, S. J., Geary, R. L., Atala, A., and Yoo, J. J. (2009). The *in vivo* stability of electrospun polycaprolactone-collagen scaffolds in vascular reconstruction. *Biomaterials* 30, 583–588. doi: 10.1016/j.biomaterials.2008.10.006

Tillman, B. W., Yazdani, S. K., Neff, L. P., Corriere, M. A., Christ, G. J., Soker, S., et al. (2012). Bioengineered vascular access maintains structural integrity in response to arteriovenous flow and repeated needle puncture. *J. Vasc. Surg.* 56, 783–793. doi: 10.1016/j.jvs.2012.02.030

Townsend, N., Bhatnagar, P., Wilkins, E., Wickramasinghe, K., and Rayner, M. (2015). *Cardiovascular Disease Statistics (Ber)*. Oxford: Nuffield Department of Population Health, University of Oxford.

Vallières, K., Laterreur, V., Tondreau, M. Y., Ruel, J., Germain, L., Fradette, J., et al. (2015). Human adipose-derived stromal cells for the production of completely autologous self-assembled tissue-engineered vascular substitutes. *Acta Biomater.* 24, 209–219. doi: 10.1016/j.actbio.2015.06.011

van Det, R. J., Vriens, B. H. R., van der Palen, J., and Geelkerken, R. H. (2009). Dacron or ePTFE for femoro-popliteal above-knee bypass grafting: short- and long-term results of a multicentre randomised trial. *Eur. J. Vasc. Endovasc. Surg.* 37, 457–463. doi: 10.1016/j.ejvs.2008.11.041

van Dijk, D., Spoor, M., Hijman, R., Nathoe, H. M., Borst, C., Jansen, E. W., et al. (2007). Cognitive and cardiac outcomes 5 years after off-pump vs on-pump coronary artery bypass graft surgery. *JAMA* 297:701. doi: 10.1001/jama.297.7.701

Wang, K., Zheng, W., Pan, Y., Ma, S., Guan, Y., Liu, R., et al. (2016). Three-layered PCL grafts promoted vascular regeneration in a rabbit carotid artery model. *Macromol. Biosci.* 16, 608–918. doi: 10.1002/mabi.201500355

Weinberg, C. B., and Bell, E. (1986). A blood vessel model constructed from collagen and cultured vascular cells. *Science* 231, 397–400. doi: 10.1126/science.2934816

Wise, S. G., Byrom, M. J., Waterhouse, A., Bannon, P. G., Ng, M. K., and Weiss, A. S. (2011). A multilayered synthetic human elastin/polycaprolactone hybrid vascular graft with tailored mechanical properties. *Acta Biomater.* 7, 295–303. doi: 10.1016/j.actbio.2010.07.022

Woo, J. S., Fishbein, M. C., and Reemtsen, B. (2016). Histologic examination of decellularized porcine intestinal submucosa extracellular matrix (CorMatrix) in pediatric congenital heart surgery. *Cardiovasc. Pathol.* 25, 12–17. doi: 10.1016/j.carpath.2015.08.007

Wu, W., Allen, R. A., and Wang, Y. (2012). Fast-degrading elastomer enables rapid remodeling of a cell-free synthetic graft into a neoartery. *Nat. Med.* 18, 1148–1153. doi: 10.1038/nm.2821

Wystrychowski, W., Cierpka, L., Zagalski, K., Garrido, S., Dusserre, N., Radochonski, S., et al. (2011). Case study: first implantation of a frozen, devitalized tissue-engineered vascular graft for urgent hemodialysis access. *J. Vasc. Access* 12, 67–70. doi: 10.5301/JVA.2011.6360

Wystrychowski, W., McAllister, T. N., Zagalski, K., Dusserre, N., Cierpka, L., and L'Heureux, N. (2014). First human use of an allogeneic tissue-engineered vascular graft for hemodialysis access. *J. Vasc. Surg.* 60, 1353–1357. doi: 10.1016/j.jvs.2013.08.018

Yokota, T., Ichikawa, H., Matsumiya, G., Kuratani, T., Sakaguchi, T., Iwai, S., et al. (2008). *In situ* tissue regeneration using a novel tissue-engineered, small-caliber vascular graft without cell seeding. *J. Thorac. Cardiovasc. Sur.* 136, 900–907. doi: 10.1016/j.jtcvs.2008.02.058

Zhang, L., Ao, Q., Wang, A., Lu, G., Kong, L., Gong, Y., et al. (2006). A sandwich tubular scaffold derived from chitosan for blood vessel tissue engineering. *J. Biomed. Mater. Res. Part A* 77, 277–284. doi: 10.1002/jbm.a.30614

Zhao, J., Liu, L., Wei, J., Ma, D., Geng, W., Yan, X., et al. (2012). A novel strategy to engineer small-diameter vascular grafts from marrow-derived mesenchymal stem cells. *Artif. Organs* 36, 93–101. doi: 10.1111/j.1525-1594.2011.01231.x

Zhao, J., Qiu, H., Chen, D. L., Zhang, W. X., Zhang, D. C., and Li, M. (2013). Development of nanofibrous scaffolds for vascular tissue engineering. *Int. J. Biol. Macromol.* 56, 106–113. doi: 10.1016/j.ijbiomac.2013.01.027

Conflict of Interest Statement: The authors declare that the research was conducted in the absence of any commercial or financial relationships that could be construed as a potential conflict of interest.

frontiers in Bioengineering and Biotechnology

ORIGINAL RESEARCH
published: 18 April 2017
doi: 10.3389/fbioe.2017.00025

Engineering Blood and Lymphatic Microvascular Networks in Fibrin Matrices

*Lea Knezevic[1,2,3†], Mira Schaupper[1,2†], Severin Mühleder[1,2], Katharina Schimek[4,5], Tobias Hasenberg[5], Uwe Marx[5], Eleni Priglinger[1,2], Heinz Redl[1,2] and Wolfgang Holnthoner[1,2]**

[1] Ludwig Boltzmann Institute for Experimental and Clinical Traumatology, Vienna, Austria, [2] Austrian Cluster for Tissue Regeneration, Vienna, Austria, [3] Department of Cardiology, Division of Heart and Lungs, University Medical Center Utrecht, Utrecht, Netherlands, [4] Technische Universität Berlin, Medical Biotechnology, Berlin, Germany, [5] TissUse GmbH, Berlin, Germany

OPEN ACCESS

Edited by:
Bruno Peault,
University of California
Los Angeles, USA

Reviewed by:
Andriana Margariti,
Queen's University Belfast, Ireland
Giovanni Vozzi,
University of Pisa, Italy

***Correspondence:**
Wolfgang Holnthoner
wolfgang.holnthoner@trauma.lbg.ac.at

†These authors have contributed equally to this work.

Specialty section:
This article was submitted to Tissue Engineering and Regenerative Medicine, a section of the journal Frontiers in Bioengineering and Biotechnology

Received: 14 February 2017
Accepted: 28 March 2017
Published: 18 April 2017

Citation:
Knezevic L, Schaupper M, Mühleder S, Schimek K, Hasenberg T, Marx U, Priglinger E, Redl H and Holnthoner W (2017) Engineering Blood and Lymphatic Microvascular Networks in Fibrin Matrices. Front. Bioeng. Biotechnol. 5:25. doi: 10.3389/fbioe.2017.00025

Vascular network engineering is essential for nutrient delivery to tissue-engineered constructs and, consequently, their survival. In addition, the functionality of tissues also depends on tissue drainage and immune cell accessibility, which are the main functions of the lymphatic system. Engineering both the blood and lymphatic microvasculature would advance the survival and functionality of tissue-engineered constructs. The aim of this study was to isolate pure populations of lymphatic endothelial cells (LEC) and blood vascular endothelial cells (BEC) from human dermal microvascular endothelial cells and to study their network formation in our previously described coculture model with adipose-derived stromal cells (ASC) in fibrin scaffolds. We could follow the network development over a period of 4 weeks by fluorescently labeling the cells. We show that LEC and BEC form separate networks, which are morphologically distinguishable and sustainable over several weeks. In addition, lymphatic network development was dependent on vascular endothelial growth factor (VEGF)-C, resulting in denser networks with increasing VEGF-C concentration. Finally, we confirm the necessity of cell–cell contact between endothelial cells and ASC for the formation of both blood and lymphatic microvascular networks. This model represents a valuable platform for *in vitro* drug testing and for the future *in vivo* studies on lymphatic and blood microvascularization.

Keywords: lymphatics, endothelial cells, coculture, fibrin, tissue engineering

INTRODUCTION

Survival of tissue-engineered constructs following implantation is inherently dependent on adequate oxygen and nutrient supply. The diffusion range of oxygen is generally limited to ~200 µm (Carmeliet and Jain, 2000), meaning that thick tissues require a vascular network to deliver a sufficient amount of nutrients and, thus, promote cell survival (Frerich et al., 2001; Costa-Almeida et al., 2014). Consequently, adequate oxygen and nutrient supply is a prerequisite for survival of tissue-engineered constructs *in vivo*. Therefore, the success of scaffold inclusion relies greatly on efficient vascularization. While a lot of attention has been dedicated to the engineering of blood vasculature, substantially fewer studies have focused on the engineering of lymphatic vessels. Lymphatic research gained a

boost with the identification of markers that distinguish blood and lymphatic endothelial cells (LEC) [blood vascular endothelial cells (BEC) and LEC, respectively]. The lymphatic system is an essential component of nearly all tissues; its main functions being drainage and recycling of interstitial fluid, and immune cell and lipid transport (Tammela and Alitalo, 2010). Tissues with damaged lymphatic networks are characterized by lymphedema and persistent infections (Petrek et al., 2001; Beesley et al., 2007; Hayes et al., 2008; Weitman et al., 2013). Consequently, incorporation of a lymphatic network into tissue-engineered constructs is likely to improve their integration and functionality *in vivo* by enabling appropriate tissue drainage and substantial immune cell accessibility.

A large body of research has focused on overcoming the issue of insufficient vascularization (Rouwkema et al., 2008; Baldwin et al., 2014). Pre-vascularization strategies assume the development of a vascular network *in vitro* prior to implantation of the tissue-engineered construct. Coculturing endothelial cells together with supporting cells was shown to result in the formation of a vascular network *in vitro* (Rivron et al., 2008; Baldwin et al., 2014; Costa-Almeida et al., 2014). Furthermore, supporting cells are needed for stabilization of the vessels in networks, and for the restriction of permeability and prevention of vessel regression (Kunz-Schughart et al., 2006; Rivron et al., 2008; Duttenhoefer et al., 2013). The supporting cells most commonly used include fibroblasts (Grainger and Putnam, 2011), mesenchymal stromal cells, such as adipose-derived stromal cells (ASC) and bone marrow-derived stromal cells [reviewed by Pill et al. (2015)], and smooth muscle cells (Elbjeirami and West, 2006). A source of endothelial cells commonly used is human umbilical vein endothelial cells (HUVEC) (Siow, 2012), which have been shown to form vascular networks when cocultured with supporting cell types *in vitro* (Sorrell et al., 2007; Verseijden et al., 2010a; Holnthoner et al., 2015). On the other hand, human dermal microvascular endothelial cells (HDMEC) represent a more appealing source, since the majority of endothelial cells in a human body are found in microvascular structures, making this cell type suitable for studying many physiological and pathological conditions (Hewett and Murray, 1993). These cells have also been found to form vascular networks when cocultured with mural cells (Sorrell et al., 2007; Unger et al., 2010), but their behavior resembles that of *in vivo* cells more closely than it does of HUVEC (Swerlick et al., 1991; Cornelius et al., 1995). In addition to being a valuable source of BEC, HDMEC also contain LEC (Kriehuber et al., 2001; Marino et al., 2014; Gibot et al., 2016). For a potential clinical application, circulating endothelial colony-forming cells (ECFC) are a promising source of BEC, since they can be isolated from peripheral blood (Siow, 2012) and show tube-forming capacity and the ability to form vascular networks *in vitro* (Fuchs et al., 2009; Medina et al., 2010; Holnthoner et al., 2015). Moreover, they have been shown to contain a subset of lymphatic ECFC (DiMaio et al., 2016) and could also offer the possibility of engineering an autologous vascular network for future clinical use.

A few approaches for lymphatic tissue engineering have been developed in response to the necessity for tissue drainage and immune cell surveillance of tissue constructs (Schaupper et al., 2016). Lymphatic capillary-like structures, for example, were established in collagen and fibrin matrices with interstitial flow applied (Helm et al., 2007). Similarly, lymphatic capillary formation was achieved in a skin regeneration model implanted into mouse tails, simulating the influence of interstitial flow (Boardman and Swartz, 2003). Lymphatic capillaries were successfully formed in fibrin-collagen hydrogels and integrated into a rat model of dermo-epidermal skin grafts (Marino et al., 2014). Another model shows the development of lymphatic capillaries in an *in vitro* scaffold-free three-dimensional (3D) coculture of LEC and fibroblasts (Gibot et al., 2016).

The functionality of tissue-engineered constructs could be greatly improved by the simultaneous engineering of a lymphatic vascular network as well as a blood vascular network. The aim of this study was to investigate the network-forming capacities of the two endothelial cell populations isolated from the HDMEC population and to explore the differences between the two cell types in vascular network formation *in vitro*. Consequently, we have established a 3D coculture model consisting of ASC and fluorescently labeled LEC and BEC in fibrin hydrogels and showed the effect of vascular endothelial growth factor (VEGF)-C and supporting cells on the development of blood and lymphatic networks.

MATERIALS AND METHODS

Cell Culture and Isolation

The isolation of human ASC was approved by the ethics committee of the state of Upper Austria (#200). ASC were obtained from liposuction materials as described previously (Wolbank et al., 2007) and cultured in Endothelial Cell Growth Medium (EGM™-2 BulletKit™, Lonza) supplemented with additional FCS (Sigma-Aldrich, St. Louis, MO, USA) to a final concentration of 5% (referred to as EGM-2 unless stated otherwise). The cells were used in passages 2–10. HDMEC were isolated from human foreskin, according to protocol described previously (Schimek et al., 2013). Juvenile prepuce was obtained in compliance with the relevant laws, with informed consent and ethics approval (Ethic Committee Charité University Medicine, Berlin, Germany), from a pediatric surgery after routine circumcisions. LEC were isolated from HDMEC populations using immunomagnetic cell sorting with anti-podoplanin antibody and magnetic beads (Dynabeads, M280 goat anti-rabbit, ThermoFisher), following the manufacturer's instructions. The podoplanin-negative population, representing BEC, were obtained from the negative fraction by a second negative immunomagnetic selection with anti-podoplanin antibody, to remove the remaining podoplanin positive cells. BEC were cultured in EGM-2 medium, while LEC were propagated in EGM-2 medium supplemented with 50 ng/mL VEGF-C. All cells derived from HDMEC were used between passages 6 and 9.

Plasmids and Retroviral Infection

Isolated LEC and BEC populations were retrovirally infected with fluorescent proteins to visualize network formation. The cDNA encoding pLV-EGFP, pLV-mCherry, and pBMN-Z was purchased

from Addgene (Cambridge, MA, USA). The pcDNA3-EYFP-HIS was purchased from Invitrogen (ThermoFisher, Waltham, MA, USA). The eGFP and mCherry were subcloned into the pBMN backbone after digestion with *Bam*HI and *Sal*I. The EYFP-HIS was subcloned into pBMN after digestion with *Bam*HI and *Eco*RI. Phoenix Ampho cells were a kind gift from Regina Grillari (University of Natural Resources and Life Sciences, Vienna, Austria) and cultured in DMEM 10% FCS. Virus particle generation was performed by transfecting Phoenix cells at 80% confluency using Lipofectamine 2000 or TurboFect (ThermoFisher, Waltham, MA, USA), following the manufacturer's instructions. The supernatants containing virus particles were transferred onto 80% confluent LEC and BEC, and virus particles were centrifuged onto the cells at 800 × *g* for 60 min. The supernatant was then removed, and the cells were incubated overnight in EGM-2. Retrovirally infected cells were then expanded in new flasks and used for subsequent experiments.

Two-dimensional (2D) Cocultures

Two-dimensional cocultures were prepared in 8-well chamber slides by seeding a total number of 48,000 cells/well. The cultures prepared contained equal ratios of ASC, LEC, and BEC, cultured in EGM-2 medium, with or without VEGF-C (25 ng/mL).

Embedding of the Cells in Fibrin Matrices

Fibrin matrix was prepared, as described elsewhere (Rohringer et al., 2014), to address the question whether lymphatic capillaries can be built within the fibrin hydrogel. LEC and BEC used in these cultures were fluorescently labeled as described above. Briefly, 3D matrices were prepared on 15-mm diameter round coverslips (Paul Marienfeld, Lauda Königshofen, Germany) and are subsequently referred to as "clots." The clots were prepared by diluting thrombin (human thrombin 4, Baxter, Vienna, Austria; 4 U/mL) 1:10 in calcium chloride ($CaCl_2$, Baxter, Vienna, Austria or Fresenius Kabi GmbH, Graz, Austria; 40 μmol/mL solution), and fibrinogen (Baxter, Vienna, Austria; 100 mg/mL) 1:20 in EGM-2. A total of 100,000 cells/cell type were used in each clot. The clot suspension contained a final concentration of 0.2 U/mL thrombin and 2.5 mg/mL fibrinogen. All clots were prepared in duplicate. After placing the suspensions on the cover slides, the clots were incubated for 20 min at 37°C prior to the addition of medium. An amount of 2 mL of EGM-2 medium or EGM-2 medium supplemented with VEGF-C at indicated concentrations was added to the clots and exchanged every 2–3 days.

LEC and BEC 3D Cocultures with Varying VEGF-C

Either LEC or BEC were cocultured with ASC and placed into fibrin matrices, as indicated above. Clots were cultured in EGM-2 with different VEGF-C concentrations (0, 10, 25, and 50 ng/mL). Fluorescence images of the cultures were taken once a week for 4 weeks.

LEC and BEC 3D Tricultures

Lymphatic endothelial cells and BEC were embedded in fibrin matrices, as indicated above and cultured separately (with or without ASC) or together (with or without ASC) in EGM-2 or, for LEC, in EGM-2 medium containing VEGF-C (25 ng/mL). The cultures were photographed once a week for 4 weeks.

Generation of ASC-Conditioned Medium (ASC-CM) and 3D Coculture

A total of 100,000 ASC were seeded in a tissue culture flask with the surface area of 75 cm^2. The cells were cultured for 48 h prior to the removal of supernatant. The supernatant was removed and centrifuged for 15 min at 500 × *g*. The cells were then split and cultured for the next supernatant generation. As a control, EGM-2 medium was incubated in a tissue culture flask for the same time period as the ASC-CM. The 3D fibrin matrices were prepared as indicated earlier. LEC and BEC were cultured alone or with ASC. When cultured alone, the cells were either incubated in control EGM-2 medium or with ASC-conditioned EGM-2 medium (2 mL/clot). When cultured with ASC, the cells were cultured in a 1:1 ratio (100,000 cells of each) and grown in EGM-2 medium. When indicated, the medium was supplemented with VEGF-C at a concentration of 25 ng/mL. Images of the cultures were taken once a week.

Network Quantification

The images were first processed in ImageJ software. The networks were quantified using Adobe Photoshop (Adobe Systems, San Jose, CA, USA) and Angiosys (Buckingham, UK) software. The standardization of images was performed in Adobe Photoshop, as described previously (Charwat et al., 2015). Briefly, the images of the LEC and BEC 3D tricultures were taken after 7 days from four different positions in each clot. One image was taken from each sample (including the duplicates) for three separate experiments (with cells from three donors) at day 28 for the quantification of the LEC networks at different VEGF-C concentrations.

Antibodies and Flow Cytometry

Antibodies used in flow cytometry measurements were as follows: anti-rabbit PE (Poly4064) and anti-mouse PE (Poly4053) from BioLegend (San Diego, CA, USA); mouse antihuman podoplanin from Santa Cruz Biotechnology (Dallas, TX, USA); rabbit antihuman podoplanin, rabbit antihuman LYVE-1, and mouse antihuman vascular endothelial growth factor receptor 3 (VEGFR3) from Reliatech (Wolfenbüttel, Germany); and anti-rabbit and anti-mouse Alexa Fluor 488 from ThermoFisher Scientific (Waltham, MA, USA). The analysis was performed on a Beckman Coulter CytoFlex Flow Cytometer (Brea, CA, USA), and the data were analyzed using FlowJo software (FlowJo LLC, Ashland, OR, USA).

Statistical Analysis

The statistical analysis for LEC and BEC cocultures was performed with GraphPad software using the Student's *t*-test, with a level of significance set at $p < 0.05$. The data were logarithmically transformed and statistical analysis performed using one-way ANOVA with Dunnett's *post hoc* analysis for the quantification of the networks at different VEGF-C concentrations. Level of significance was set at $p < 0.05$.

RESULTS

Isolation and Characterization of LEC and BEC from HDMEC Cultures

Lymphatic endothelial cells and BEC were firstly isolated from mixed populations of HDMEC obtained from neonatal foreskins of three donors with the aim of obtaining both LEC and BEC from the same tissue source. The populations of LEC and BEC could be distinguished upon microscopic observation, where LEC are visible as island-forming cells within BEC populations (**Figure 1A**). In addition, the two cell types could be distinguished by the presence or absence of podoplanin (**Figure 1A**). After immunomagnetic cell sorting into podoplanin-positive (LEC) (**Figure 1B**) and podoplanin-negative (BEC) cells (**Figure 1C**), the purity of the populations was confirmed with flow cytometry showing >96% podoplanin-positive and -negative populations, respectively. In addition, BEC and LEC could be distinguished by lymphatic vessel endothelial hyaluronic acid receptor (LYVE)-1 expression, while both populations expressed VEGFR3 (**Figures 1B,C**). Populations of LEC and BEC were

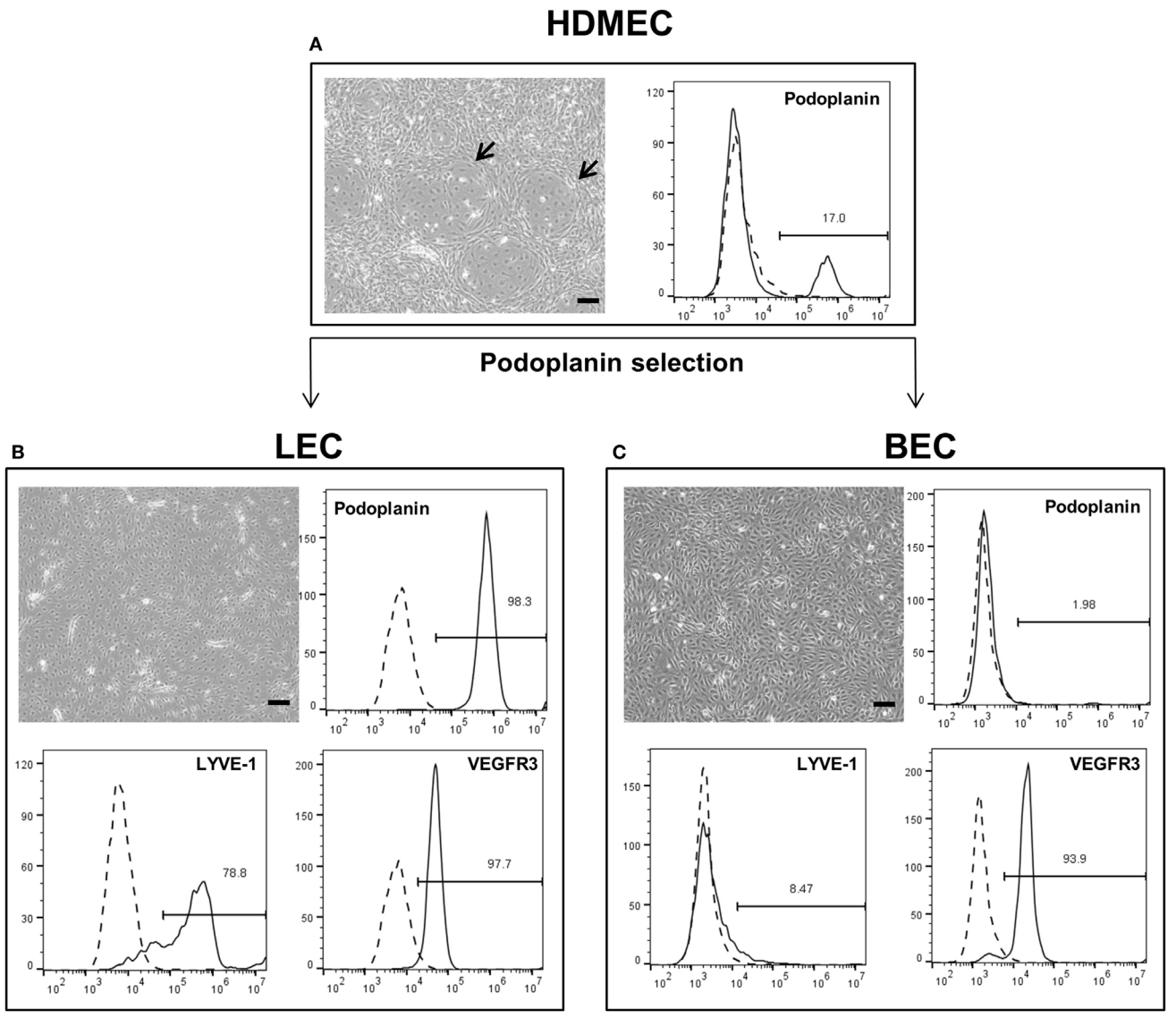

FIGURE 1 | Schematic representation of the separation of human dermal microvascular endothelial cells (HDMEC) into lymphatic endothelial cells (LEC) and blood vascular endothelial cells (BEC). Scale bar represents 100 μm. **(A)** Brightfield microscopy image of HDMEC before MACS with representative FACS plot showing the presence of podoplanin-positive cells. Arrows indicate LEC islands within BEC populations. **(B)** Brightfield microcopy images and representative FACS plots of a pure LEC population. The population is positive for lymphatic markers podoplanin, LYVE-1, and vascular endothelial growth factor receptor 3 (VEGFR3). **(C)** Brightfield microcopy images and representative FACS plots of a pure BEC population. The population is largely negative for lymphatic markers podoplanin and LYVE-1, but positive for VEGFR3.

transduced with retroviral vectors for stable expression of GFP, YFP, or mCherry with the aim of tracking network development over several weeks.

2D Cultures of LEC, BEC, and ASC Show Separate LEC and BEC Vascular-Like Structures

The three cell types were mixed in equal ratios and observed for a period of 1 week to analyze whether LEC and BEC form vascular-like structures when cocultured with ASC. The cells organized into islands of LEC (green), surrounded by BEC (red) (**Figure 2A**). Both LEC and BEC formed elongated tube-like structures that differed in morphology, with LEC forming wide structures and BEC thinner ones (**Figures 2B,C**). In addition, the LEC and BEC structures appeared separate from one another.

LEC Respond to Increased VEGF-C Concentrations with Increased Network Densities

We next aimed to determine whether LEC cocultured with ASC can form networks in fibrin hydrogels. LEC were integrated into fibrin matrices together with ASC and cultured for the period of 28 days. Due to previous observations of our group that VEGF-C is not secreted by ASC (Rohringer et al., 2014), different concentrations of VEGF-C were added to the culture medium to determine the optimal concentration of VEGF-C for network development of LEC. LEC did not form network-like structures without any exogenously added VEGF-C (**Figure 3A**). Some of the structures formed were elongated and resembled primitive LEC tubes, but the structures were not interconnected. An extensive network was already present at day 7 with 10 ng/mL, and the vessel-like structures were easily distinguishable. With concentrations of 25 and 50 ng/mL, the network was dense from day 7, with only subtle differences in network density between the two conditions. In addition, we observed that the structure morphology is dependent on the VEGF-C concentration. At a concentration of 10 and 25 ng/mL, the network consists of wider vessel-like structures, while at 50 ng/mL, the network contains thinner structures and these are already present at day 7. The statistical analysis shows that the concentration of 10 ng/mL increases the number of tubes and junctions significantly compared to the control condition of no exogenously added VEGF-C, while this effect was even further enhanced at concentrations of 25 and 50 ng/mL (**Figure 3B**). The mean number of tubules and junctions at 0 ng/mL was 72 (±59.22) and 35 (±31.97), at 10 ng/mL was 182 (±79.92) and 95 (±44.65), at 25 ng/mL was 217 (±88.98) and 119 (±55.97), and at 50 ng/mL was 218 (±125.9) and 121 (±75.31), respectively. In contrast to LEC, culturing BEC with increasing concentrations of VEGF-C did not enhance network formation (data not shown).

Tricultures of LEC, BEC, and ASC in Fibrin Gels Show VEGF-C-Dependent Separate Network Formation of LEC and BEC

Considering the observation that LEC form vascular-like networks when cultured with ASC in fibrin hydrogels, we next aimed to determine whether LEC and BEC can form separate networks and tube-like structures when cocultured together in fibrin matrices. Since the concentration of 50 ng/mL of VEGF-C did not result in significantly denser networks compared to 25 ng/mL (**Figure 3B**), LEC were further cultured in fibrin gels with EGM-2 supplemented with 25 ng/mL of VEGF-C. BEC and LEC were integrated, either as monocultures, as cocultures with ASC or as tricultures containing LEC, BEC, and ASC. The duplicate samples were cultured in EGM-2 medium supplemented with VEGF-C. In the absence of ASC, neither BEC nor LEC could form tube-like structures or networks (**Figure 4A**), and the cells grew in monolayers. Without VEGF-C, BEC (red) were more prevalent, while with the addition of VEGF-C, the LEC (green) and BEC formed clearly separated clusters of cells. Both LEC and BEC formed networks in the presence of ASC, whereas LEC network formation was more prominent with the addition of exogenous VEGF-C. While the mean numbers of LEC tubules and junctions per field in the absence of VEGF-C were 87 (±6.417) and 31 (±5.266), respectively, with the addition of VEGF-C, the mean numbers of tubules and junctions increased to 450 (±25.94) and 240 (±15.84), respectively. Without VEGF-C,

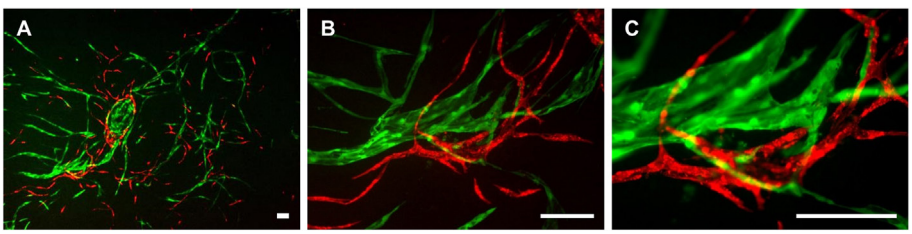

FIGURE 2 | Two-dimensional culture of lymphatic endothelial cells (LEC) (green), blood vascular endothelial cells (BEC) (red), and adipose-derived stromal cells (non-fluorescent). Scale bar represents 200 μm. **(A)** An overview of the culture showing elongated structures formed by LEC and BEC, and an LEC island surrounded by BEC. **(B)** The same image in larger magnification depicting the different morphologies of BEC and LEC structures, with BEC forming thin, uniform projections, and LEC forming both wide and thin structures. **(C)** The same image in higher magnification showing that structures formed by BEC and LEC are separate from each other. LEC were transduced with GFP and BEC with mCherry. LEC and BEC originate from the same human dermal microvascular endothelial cells (HDMEC) donor in a single experiment. Images are representative of three experiments with three HDMEC donors.

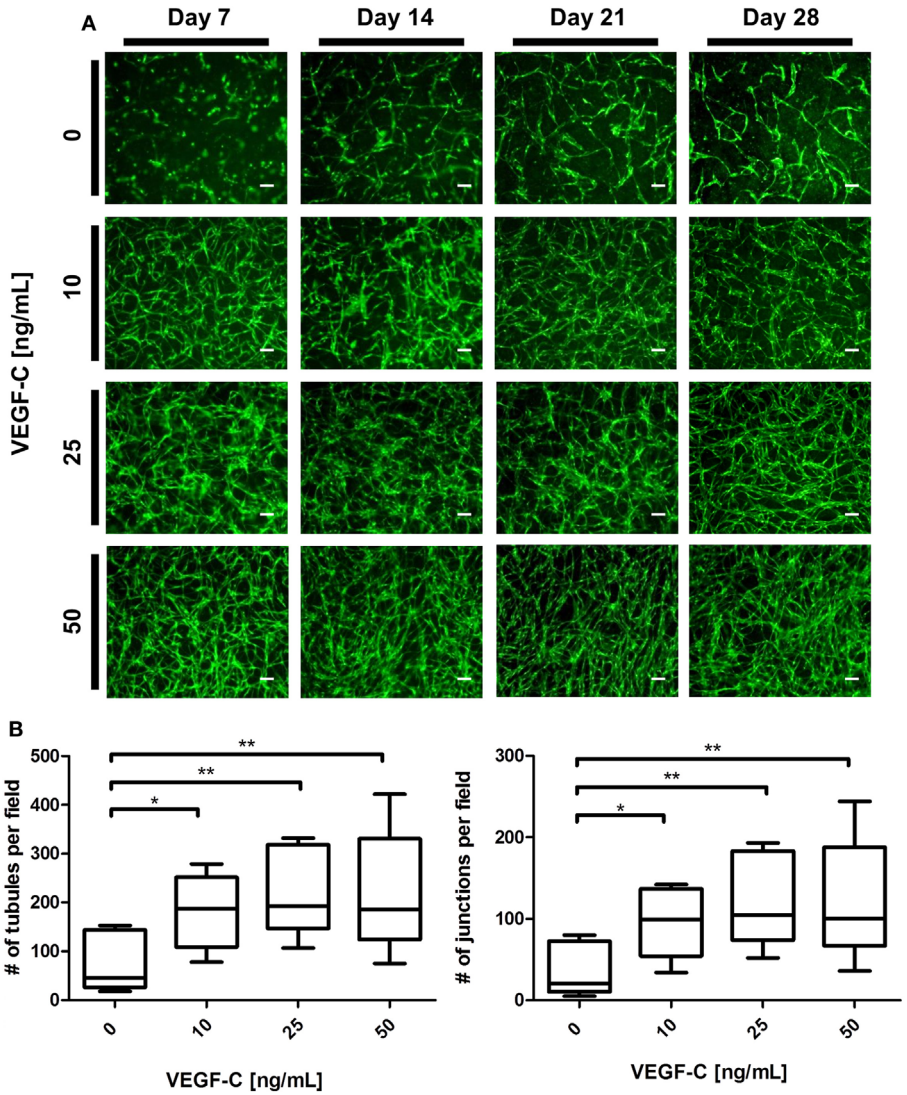

FIGURE 3 | Effect of increasing vascular endothelial growth factor (VEGF)-C concentration on lymphatic endothelial cells (LEC) (green) network formation in fibrin matrix, when cocultured with adipose-derived stromal cells (ASC) for 4 weeks. Scale bar represents 100 μm. **(A)** Fluorescent images of LEC coculture with ASC over a period of 4 weeks, showing that LEC form more extensive networks with the increasing VEGF-C concentration. Images are representative of the results of three separate experiments (with three different LEC donors). LEC were transduced with YFP. **(B)** Quantification of networks originating from three different LEC donors, with images of two clots per donor (**$p < 0.02$, *$p < 0.05$). Statistical analysis was performed using one-way ANOVA and Dunnett's *post hoc* test on logarithmically transformed data. All conditions per LEC donor were prepared in duplicate, and one field image was taken from each clot and corresponding duplicate.

the mean number of tubules of BEC was 452 (±46.46) and 260 (±33.35), respectively, and of junctions was 483 (±52.40) and 241 (±29.34), respectively (**Figure 4B**). LEC and BEC networks could also be distinguished by their morphology: BEC formed thinner, more uniform structures in comparison to the wider and more variable LEC structures (**Figures 4A** and **5A,B**). This observation was also confirmed by confocal microscopy, where BEC and LEC networks could be clearly distinguished in the presence of VEGF-C, while the LEC network was close to absent when grown in medium lacking VEGF-C (**Figures 5C,D**).

Direct Contact between Endothelial Cells and ASC Is Necessary for the Formation of both Lymphatic and Blood Vascular Network-Like Structures

Adipose-derived stromal cells have been shown previously to support vessel formation by endothelial cells *in vitro* and *in vivo* (Verseijden et al., 2010b; Rohringer et al., 2014; Holnthoner et al., 2015). Additionally, ASC-CM was shown to have a beneficial effect on the migration, proliferation, and network formation of endothelial cells (Merfeld-Clauss et al., 2010; Verseijden et al.,

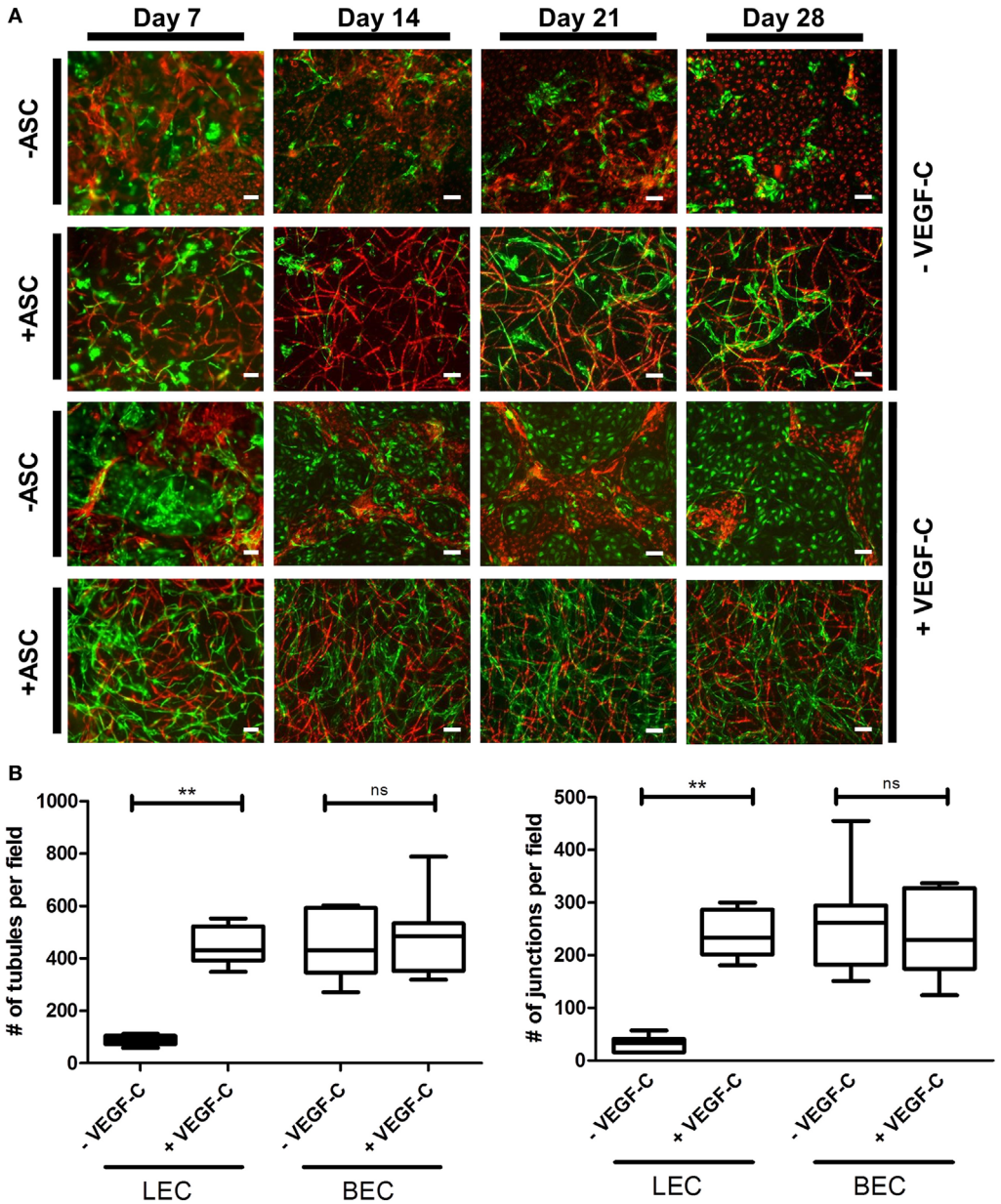

FIGURE 4 | Network formation and quantification of coculture of lymphatic endothelial cells (LEC) (green) and blood vascular endothelial cells (BEC) (red) in fibrin matrices when cultured in the presence or absence of adipose-derived stromal cells (ASC), and exogenous vascular endothelial growth factor (VEGF)-C (25 ng/mL), during the period of 4 weeks. Scale bar represents 100 μm. **(A)** Overlays of fluorescent images of cocultures show the network formation of LEC and BEC in the presence of ASC. The addition of exogenous VEGF-C results in a denser LEC, but not BEC networks. There is no network formation of LEC or BEC without ASC. Images are representative of data from two experiments with two separate human dermal microvascular endothelial cells (HDMEC) and ASC donors. The LEC were transduced with GFP and BEC with mCherry. **(B)** Network quantification data show that there is a significant increase in the number of tubules and junctions of LEC cultured with ASC when the medium was supplemented with VEGF-C (25 ng/mL), compared to when cultured in EGM-2 medium without VEGF-C. BEC do not show a significant difference in the number of junctions or tubules between the two conditions. $^{**}p < 0.02$, LEC cultured in EGM-2 vs. in EGM-2 + 25 ng/mL VEGF-C; BEC cultured in EGM-2 vs. in EGM-2 + 25 ng/mL VEGF-C. Data originate from two experiments with two HDMEC and two ASC donors.

2010b; Rohringer et al., 2014). However, direct cell–cell contact was shown to be essential for full network and tube formation (Rohringer et al., 2014). To examine whether ASC-CM had a similar effect on LEC and BEC network formation as co-culturing, these cells with ASC, LEC, and BEC were embedded in fibrin hydrogels and incubated in ASC-CM. The medium was generated by culturing ASC in EGM-2 for 48 h prior to applying the medium onto LEC and BEC. The cells were also cultured in the

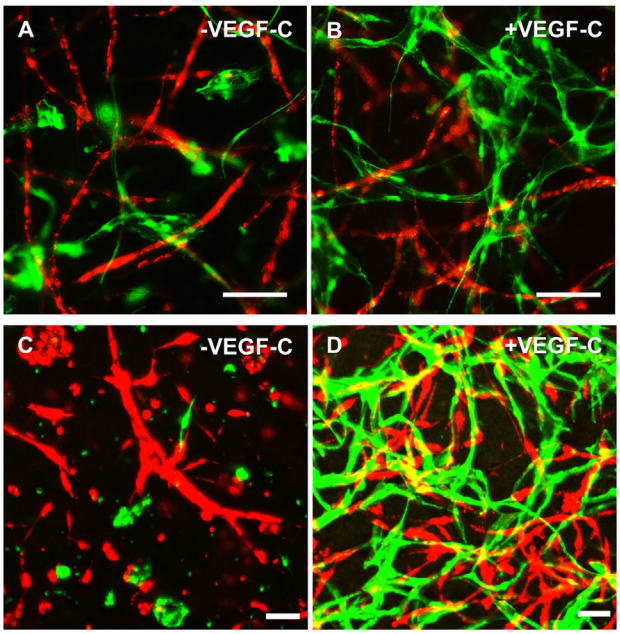

FIGURE 5 | Lymphatic endothelial cells (LEC) (green) and blood vascular endothelial cells (BEC) (red) form two separate networks in cocultures with adipose-derived stromal cells. Scale bar represents 100 µm. **(A,B)** Overlays of fluorescent images showing that BEC and LEC form two separate networks and that upon addition of exogenous vascular endothelial growth factor (VEGF)-C, LEC network becomes increasingly dense. **(C,D)** Merged Z-stacks taken with confocal microscope showing that without exogenous VEGF-C, there is limited proliferation and network formation of LEC, while in the presence of VEGF-C (25 ng/mL), LEC develop an extensive network that is separate from the BEC network. LEC were transduced with GFP and BEC with mCherry.

presence of ASC to control for the network-forming capacity of BEC and LEC. LEC were grown with the addition of VEGF-C (25 ng/mL), as this was shown to lead to network formation in coculture with ASC. When cultured with ASC, both LEC and BEC showed network formation by day 14 of culture (**Figure 6**). LEC showed more extensive network formation upon the addition of VEGF-C. There was, again, no effect of VEGF-C on the network formation of BEC. When cultured without ASC in EGM-2 medium, neither LEC nor BEC displayed network formation. With the addition of VEGF-C, LEC proliferated and formed a monolayer. BEC started forming some elongated structures, but no network formation could be observed. When the cells were cultured in ASC-CM, there was again no network formation, and the cells grew similarly to their respective counterparts in unconditioned EGM-2 medium. While BEC formed some elongated structures, they were not able to form a network by day 14. LEC again proliferated in the presence of VEGF-C and grew in a monolayer, while without VEGF-C, the cells started to elongate but could not form a network. Since we did not observe full network formation in the conditions without ASC, these networks could not be quantified and further subjected to statistical analysis.

DISCUSSION

Integration of both blood and lymphatic vasculature into tissue-engineered constructs can be crucial for the long-term viability and survival of such constructs *in vivo*. In this study, separate blood and lymphatic microvascular structures were successfully created in a 3D *in vitro* model using BEC and LEC derived from human dermis. We could follow the network development over time by fluorescently labeling the two cell populations, which represents a novel approach in studying lymphangiogenesis and vasculogenesis *in vitro*.

Since the human dermal microvascular fraction consists of both BEC and LEC, the two cell populations were firstly isolated separately, before being used in further cocultures. LEC can be distinguished from BEC by the presence of LEC-specific markers such as podoplanin, LYVE-1, prospero homeobox (Prox)-1, and VEGFR3 (Kaipainen et al., 1995; Banerji et al., 1999; Breiteneder-Geleff et al., 1999; Wigle et al., 2002; Cueni and Detmar, 2006). Podoplanin was chosen as a suitable lymphatic marker, as it has been used previously to isolate LEC from a mixed population containing LEC and BEC (Kriehuber et al., 2001; Makinen et al., 2001) due to its almost exclusive expression on lymphatic endothelium (Carreira et al., 2001; Florez-Vargas et al., 2008) and preferential staining of the smaller diameter LEC vessels (Galambos and Nodit, 2005). Immunomagnetic separation of HDMEC based on this marker resulted in a >96% pure podoplanin-negative and -positive populations (**Figures 1B,C**), where the positive population was expressed LYVE-1, which was not present in the podoplanin-negative BEC population (**Figures 1B,C**). Although VEGFR3 is a lymphatic endothelium-specific marker, our observations of a VEGFR3-positive BEC population is in accordance with previous data by Kriehuber et al. (2001) who also showed the presence of VEGFR3 on some BEC, albeit to a lesser extent than shown here. The purity of the populations is of great importance for showing the separate network formations of BEC and LEC.

Lymphatic endothelial cells and BEC populations were transduced with fluorescent proteins and cultured together with ASC for a period of 4 weeks to follow the progress of network formation over time. ASC have been shown previously to support vasculogenesis by secretion of pro-vasculogenic factors and direct cell–cell contact (Verseijden et al., 2010b; Rohringer et al., 2014; Holnthoner et al., 2015; Merfeld-Clauss et al., 2015). In addition, ASC support the migration, proliferation, and tube formation of LEC, again through direct contact and the secretion of growth factors, such as VEGF-A, VEGF-D, fibroblast growth factor-2, hepatocyte growth factor, and angiopoietin-1 (Hsiao et al., 2012; Takeda et al., 2015; Strassburg et al., 2016). Since there is controversy in literature regarding the secretion of VEGF-C by ASC in cocultures with endothelial cells (Rohringer et al., 2014; Takeda et al., 2015; Strassburg et al., 2016), the cocultures of LEC, BEC, and ASC were supplemented with 25 ng/mL VEGF-C, which had been shown previously to support LEC proliferation and network formation (Podgrabinska et al., 2002; Boardman and Swartz, 2003; Marino et al., 2014; Gibot et al., 2016). Our results support these observations. Here, we show that LEC and BEC form elongated structures in the presence of ASC and VEGF-C even in the 2D coculture, and these structures were observed to

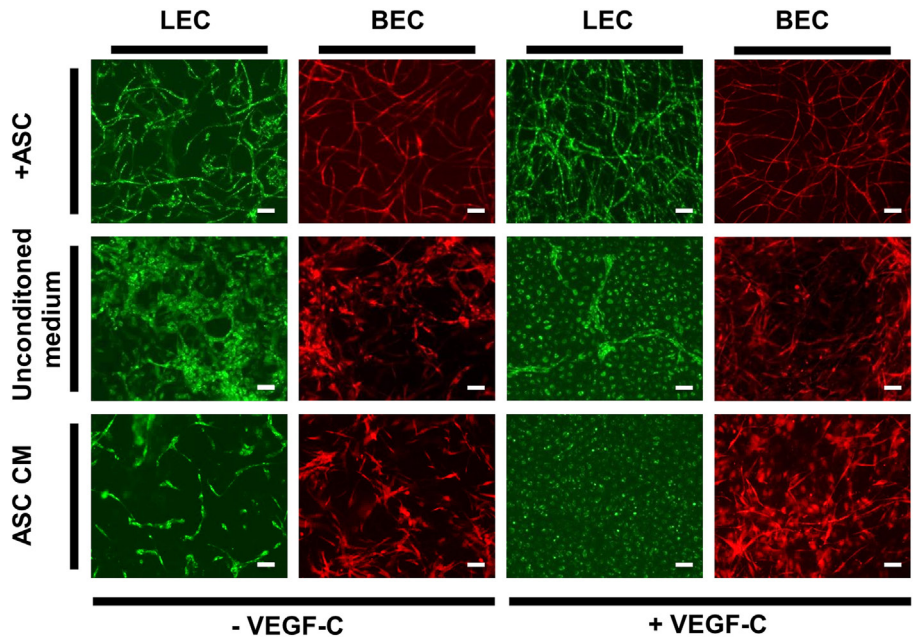

FIGURE 6 | The effect of ASC-conditioned medium (ASC-CM) on the network formation of lymphatic endothelial cells (LEC) (green) and blood vascular endothelial cells (BEC) (red). Scale bar indicates 100 μm. The first row shows successful network formation of both LEC and BEC when cultured with adipose-derived stromal cells (ASC) in EGM-2 medium. The LEC network formation is enhanced upon the addition of vascular endothelial growth factor (VEGF)-C. In the middle row, LEC and BEC were cultured in monocultures in EGM-2 medium, with or without added VEGF-C, which resulted in no network formation of either cell types. In the bottom row, the cells were cultured in the ASC-CM, which, similarly to unconditioned EGM-2, resulted in no network formation of LEC or BEC. Images were taken at day 14 of culture. LEC were transduced with mCherry and BEC with GFP. Images are representative of two experiments with two HDMEC donors.

be separate from each other. In addition, the distinction between LEC and BEC structures could be found in their morphology, as LEC formed structures of variable width, while BEC joined into thin, more uniform projections (**Figure 2**). Based on these observations, we proceeded to integrate LEC, BEC, and ASC into fibrin matrices to observe the network formation in 3D. Fibrin was chosen as a natural product of the blood coagulation cascade (Davie et al., 1991) and as suitable scaffold material as it has been described previously to facilitate successful vasculogenesis (Rohringer et al., 2014; Holnthoner et al., 2015). Without ASC, both LEC and BEC formed a monolayer and did not arrange even into primitive tube-like structures. Coculturing of both LEC and BEC with ASC had a positive effect on the network formation, while this effect was more apparent for BEC than for LEC when grown in EGM-2 medium without exogenous VEGF-C. VEGF-C significantly enhanced the network formation of LEC in cocultures with ASC, but not of BEC, indicating that VEGF-C is essential for the network formation of LEC and that, even if secreted by ASC, the amounts are not sufficient to promote network formation of LEC. Kazenwadel et al. (2012) showed that VEGF-C promotes lymphatic vessel elongation in studies of embryonic mouse LEC, but that, in cooperation with FGF-2, the vessels also grow in diameter. Although we did not measure the vessel diameter, the fluorescent images of LEC grown in different VEGF-C concentrations suggest there are some structural differences between low and high VEGF-C concentrations. The seemingly widest structures, resembling the ones shown by Kazenwadel et al. (2012), are present mostly under the conditions lacking VEGF-C, or at 10 ng/mL. Such differences are not observable in BEC networks, which form similarly dense networks at all concentrations of VEGF-C (data not shown). Most importantly, the two separate endothelial cell populations clearly form two separate networks, lacking a "mosaic" phenotype between LEC and BEC. These observations, together with our flow cytometry data, which support the purity of fluorescent BEC and LEC populations, demonstrates that two separate networks can be formed from the same dermal endothelial cell source. Kriehuber et al. (2001) also showed separate capillary tube formation by LEC and BEC when cultured together on Matrigel. Marino et al. (2014) reported the formation of two separate networks when HDMEC were cultured in fibrin hydrogels by staining the networks against CD31 and the lymphatic marker Prox-1. Their model has also shown successful anastomosis of engineered vasculature with the rat host vasculature *in vivo* (Marino et al., 2014). Helm et al. cocultured BEC and LEC in a 3D matrix consisting of collagen and fibrin with covalently bound VEGF. They, furthermore, applied interstitial flow in order to enhance capillary formation (Helm et al., 2007). The positive effect of interstitial fluid flow on LEC migration was also investigated on an *in vivo* mouse tail model (Boardman and Swartz, 2003) and *in vitro* by using a multichamber fluidic device (Ng et al., 2004). Strassburg et al. cocultured ASC and LEC *in vitro* in Matrigel to achieve tube formation. However, no fully connected lymphatic network was observed (Strassburg et al., 2016). Matrigel is a not well-defined

matrix derived from Engelbreth-Holm-Swarm tumors in mice (Hughes et al., 2010). Therefore, non-tumor-derived autologous scaffolds, such as fibrin, are a more feasible and adequate matrix for pre-vascularization strategies. Considering the recent developments in engineering lymphatic microcapillaries, the data presented here build upon the current knowledge of blood and lymphatic microvasculature formation and offer a valuable 3D model that can be followed during a period of 4 weeks.

Finally, we aimed to investigate whether direct contact between ASC and LEC or BEC was necessary for the development of vascular networks, since ASC have been shown previously to support the vessel formation of endothelial cells (Verseijden et al., 2010b; Rohringer et al., 2014; Holnthoner et al., 2015). Additionally, ASC-CM was shown to have a beneficial effect on endothelial cell migration, proliferation, and network formation (Merfeld-Clauss et al., 2010; Verseijden et al., 2010b; Rohringer et al., 2014). Since lymphatic capillaries are not surrounded by mural cells (Swartz and Skobe, 2001), we investigated whether LEC could develop into a fully established lymphatic capillary network in the presence of ASC-CM. In line with previous findings (Verseijden et al., 2010b; Rohringer et al., 2014), we did not observe network formation when LEC or BEC were cultured in ASC-CM, suggesting that cell–cell interaction or even direct contact is necessary for the development of both lymphatic and blood microcapillaries. It is, therefore, possible that while the development of lymphatic capillaries depends on direct contact with supporting cells, LEC, once developed, do not require support from pericytes for maintenance of the vessels.

Pre-vascularization of tissue-engineered constructs requires autologous sources of endothelial cells. Outgrowth endothelial cells can be isolated from peripheral blood (Fuchs et al., 2009) and have shown network-forming capacities in cocultures with ASC (Fuchs et al., 2009; Medina et al., 2010; Holnthoner et al., 2015). LEC were also suggested to be present in peripheral blood (Szöke et al., 2015) and have also been obtained previously from induced pluripotent stem cells (Lee et al., 2015). Interestingly, preliminary data from our group showed that combinations of LEC derived from human lymph nodes in triculture with ASC and HUVEC formed separate vascular networks, too (data not shown). One limitation of our study is the use of HDMEC as a source for both LEC and BEC, which is not a clinically applicable source of these cells. The use of potentially autologous cells in our model would represent an important step toward pre-vascularization of tissue-engineered constructs. Moreover, the endothelium is a highly heterogeneous organ. In this study, we used ECs from human foreskin, which represent a "golden standard" for microvascular ECs. However, ECs from other tissues possibly lead to different results, thereby limiting the conclusions of our data. Furthermore, it is difficult to assess the presence of the vascular lumen in the networks in our experimental setting. However, we have shown previously the presence of perfusable, lumen-containing structures in networks of outgrowth endothelial cells cocultured with ASC in fibrin hydrogels *in vivo* (Pill et al., 2015). While recent studies report the culture of the networks for a period of 24 h up to 10 days (Podgrabinska et al., 2002; Ng et al., 2004; Helm et al., 2007; Kazenwadel et al., 2012), we show here that the two separate networks are sustainable over the period of 4 weeks. Furthermore, our data show that network density of endothelial cells in co- and tricultures increases over time. Implantation of lymphatic and blood vascular networks in fibrin hydrogels, e.g., in a nude mouse model will shed more light on the functionality of our model *in vivo*.

Our 3D model contributes to the reemerging field of lymphatic tissue engineering, and it also represents a useful model for studying the pathogenesis of this system. In addition, the scaffold containing both the lymphatic and blood vascular networks could be used to study the influences of various angiogenic and lymphangiogenic drugs on the development and interactions of the two systems *in vitro*. Furthermore, engineering lymphatic microvasculature would be a valuable addition to microphysiological systems used for drug development and diagnostics (Muehleder et al., 2014; Tien, 2014; Hasenberg et al., 2015). Attempts to generate an artificial lymphatic drainage system on a chip have been made; however, the incorporation of LEC in such a system is currently unprecedented (Wong et al., 2013). Importantly, the integration of blood and lymphatic microcapillaries could enhance the survival of the tissues incorporated in the chips and, furthermore, contribute to a better recapitulation of physiological conditions (Muehleder et al., 2014; Tien, 2014). Considering the *in vivo* validation and acquisition of BEC and LEC from a potentially autologous source, our model could serve as a pre-vascularization strategy of both blood and lymphatic systems leading to improved survival and functionality of engineered tissues.

AUTHOR CONTRIBUTIONS

LK, MS, and SM performed experiments. KS and EP isolated and characterized cells for this study. TH, HR, UM, and WH contributed to the concept and outline of this study. LK, MS, and WH wrote the manuscript.

ACKNOWLEDGMENTS

The authors thank Dr. Marcin Osukowski for help with the statistical analyses and Philip Saunders for critical reading of the manuscript. This project has been funded by the Eurotransbio grant "VASC-MOC" (FFG #845290).

REFERENCES

Baldwin, J., Antille, M., Bonda, U., De-Juan-Pardo, E. M., Khosrotehrani, K., Ivanovski, S., et al. (2014). In vitro pre-vascularisation of tissue-engineered constructs A co-culture perspective. *Vasc. Cell* 6, 1–16. doi:10.1186/2045-824X-6-13

Banerji, S., Ni, J., Wang, S. X., Clasper, S., Su, J., Tammi, R., et al. (1999). LYVE-1, a new homologue of the CD44 glycoprotein, is a lymph-specific receptor for hyaluronan. *J. Cell Biol.* 144, 789–801. doi:10.1083/jcb.144.4.789

Beesley, V., Janda, M., Eakin, E., Obermair, A., and Battistutta, D. (2007). Lymphedema after gynecological cancer treatment: prevalence, correlates, and supportive care needs. *Cancer* 109, 2607–2614. doi:10.1002/cncr.22684

Boardman, K. C., and Swartz, M. A. (2003). Interstitial flow as a guide for lymphangiogenesis. *Circ. Res.* 92, 801–808. doi:10.1161/01.RES.0000065621.69843.49

Breiteneder-Geleff, S., Soleiman, A., Kowalski, H., Horvat, R., Amann, G., Kriehuber, E., et al. (1999). Angiosarcomas express mixed endothelial phenotypes of blood and lymphatic capillaries: podoplanin as a specific marker for lymphatic endothelium. *Am. J. Pathol.* 154, 385–394. doi:10.1016/S0002-9440(10)65285-6

Carmeliet, P., and Jain, R. K. (2000). Angiogenesis in cancer and other diseases. *Nature* 407, 249–257. doi:10.1038/35025220

Carreira, C. M., Nasser, S. M., Di Tomaso, E., Padera, T. P., Boucher, Y., Tomarev, S. I., et al. (2001). LYVE-1 is not restricted to the lymph vessels: expression in normal liver blood sinusoids and down-regulation in human liver cancer and cirrhosis. *Cancer Res.* 61, 8079–8084.

Charwat, V., Schütze, K., Holnthoner, W., Lavrentieva, A., Gangnus, R., Hofbauer, P., et al. (2015). Potential and limitations of microscopy and Raman spectroscopy for live-cell analysis of 3D cell cultures. *J. Biotechnol.* 205, 70–81. doi:10.1016/j.jbiotec.2015.02.007

Cornelius, L. A., Nehring, L. C., Roby, J. D., Parks, W. C., and Welgus, H. G. (1995). Human dermal microvascular endothelial cells produce matrix metalloproteinases in response to angiogenic factors and migration. *J. Invest. Dermatol.* 105, 170–176. doi:10.1111/1523-1747.ep12317080

Costa-Almeida, R., Granja, P. L., Soares, R., and Guerreiro, S. G. (2014). Cellular strategies to promote vascularisation in tissue engineering applications. *Eur. Cell. Mater.* 28, 51–67. doi:10.22203/eCM.v028a05

Cueni, L. N., and Detmar, M. (2006). New insights into the molecular control of the lymphatic vascular system and its role in disease. *J. Invest. Dermatol.* 126, 2167–2177. doi:10.1038/sj.jid.5700464

Davie, E. W., Fujikawa, K., and Kisiel, W. (1991). The coagulation cascade: initiation, maintenance, and regulation. *Biochemistry* 30, 10363–10370. doi:10.1021/bi00107a001

DiMaio, T. A., Wentz, B. L., and Lagunoff, M. (2016). Isolation and characterization of circulating lymphatic endothelial colony forming cells. *Exp. Cell Res.* 340, 159–169. doi:10.1016/j.yexcr.2015.11.015

Duttenhoefer, F., Lara De Freitas, R., Meury, T., Loibl, M., Benneker, L. M., Richards, R. G., et al. (2013). 3D scaffolds co-seeded with human endothelial progenitor and mesenchymal stem cells: evidence of prevascularisation within 7 days. *Eur. Cell. Mater.* 26, 49–65. doi:10.22203/eCM.v026a04

Elbjeirami, W. M., and West, J. L. (2006). Angiogenesis-like activity of endothelial cells co-cultured with VEGF-producing smooth muscle cells. *Tissue Eng.* 12, 381–390. doi:10.1089/ten.2006.12.381

Florez-Vargas, A., Vargas, S. O., Debelenko, L. V., Perez-Atayde, A. R., Archibald, T., Kozakewich, H. P., et al. (2008). Comparative analysis of D2-40 and LYVE-1 immunostaining in lymphatic malformations. *Lymphology* 41, 103–110.

Frerich, B., Lindemann, N., Kurtz-Hoffmann, J., and Oertel, K. (2001). In vitro model of a vascular stroma for the engineering of vascularized tissues. *Int. J. Oral Maxillofac. Surg.* 30, 414–420. doi:10.1054/ijom.2001.0130

Fuchs, S., Ghanaati, S., Orth, C., Barbeck, M., Kolbe, M., Hofmann, A., et al. (2009). Contribution of outgrowth endothelial cells from human peripheral blood on in vivo vascularization of bone tissue engineered constructs based on starch polycaprolactone scaffolds. *Biomaterials* 30, 526–534. doi:10.1016/j.biomaterials.2008.09.058

Galambos, C., and Nodit, L. (2005). Identification of lymphatic endothelium in pediatric vascular tumors and malformations. *Pediatr. Dev. Pathol.* 8, 181–189. doi:10.1007/s10024-004-8104-9

Gibot, L., Galbraith, T., Kloos, B., Das, S., Lacroix, D. A., Auger, F. A., et al. (2016). Cell-based approach for 3D reconstruction of lymphatic capillaries in vitro reveals distinct functions of HGF and VEGF-C in lymphangiogenesis. *Biomaterials* 78, 129–139. doi:10.1016/j.biomaterials.2015.11.027

Grainger, S. J., and Putnam, A. J. (2011). Assessing the permeability of engineered capillary networks in a 3D culture. *PLoS ONE* 6:e22086. doi:10.1371/journal.pone.0022086

Hasenberg, T., Mühleder, S., Dotzler, A., Bauer, S., Labuda, K., Holnthoner, W., et al. (2015). Emulating human microcapillaries in a multi-organ-chip platform. *J. Biotechnol.* 216, 1–10. doi:10.1016/j.jbiotec.2015.09.038

Hayes, S. C., Janda, M., Cornish, B., Battistutta, D., and Newman, B. (2008). Lymphedema after breast cancer: incidence, risk factors, and effect on upper body function. *J. Clin. Oncol.* 26, 3536–3542. doi:10.1200/JCO.2007.14.4899

Helm, C. L. E., Zisch, A., and Swartz, M. A. (2007). Engineered blood and lymphatic capillaries in 3-D VEGF-fibrin-collagen matrices with interstitial flow. *Biotechnol. Bioeng.* 96, 167–176. doi:10.1002/bit.21185

Hewett, P. W., and Murray, J. C. (1993). Human microvessel endothelial cells: isolation, culture and characterization. *In Vitro Cell Dev. Biol. Anim.* 29A, 823–830. doi:10.1007/BF02631356

Holnthoner, W., Hohenegger, K., Husa, A. M., Muehleder, S., Meinl, A., Peterbauer-Scherb, A., et al. (2015). Adipose-derived stem cells induce vascular tube formation of outgrowth endothelial cells in a fibrin matrix. *J. Tissue Eng. Regen. Med.* 9, 127–136. doi:10.1002/term.1620

Hsiao, S. T., Asgari, A., Lokmic, Z., Sinclair, R., Dusting, G. J., Lim, S. Y., et al. (2012). Comparative analysis of paracrine factor expression in human adult mesenchymal stem cells derived from bone marrow, adipose, and dermal tissue. *Stem Cells Dev.* 21, 2189–2203. doi:10.1089/scd.2011.0674

Hughes, C. S., Postovit, L. M., and Lajoie, G. A. (2010). Matrigel: a complex protein mixture required for optimal growth of cell culture. *Proteomics* 10, 1886–1890. doi:10.1002/pmic.200900758

Kaipainen, A., Korhonen, J., Mustonen, T., van Hinsbergh, V. W., Fang, G. H., Dumont, D., et al. (1995). Expression of the fms-like tyrosine kinase 4 gene becomes restricted to lymphatic endothelium during development. *Proc. Natl. Acad. Sci. U.S.A* 92, 3566–3570. doi:10.1073/pnas.92.8.3566

Kazenwadel, J., Secker, G. A., Betterman, K. L., and Harvey, N. L. (2012). In vitro assays using primary embryonic mouse lymphatic endothelial cells uncover key roles for fgfr1 signalling in lymphangiogenesis. *PLoS ONE* 7:e40497. doi:10.1371/journal.pone.0040497

Kriehuber, E., Breiteneder-Geleff, S., Groeger, M., Soleiman, A., Schoppmann, S. F., Stingl, G., et al. (2001). Isolation and characterization of dermal lymphatic and blood endothelial cells reveal stable and functionally specialized cell lineages. *J. Exp. Med.* 194, 797–808. doi:10.1084/jem.194.6.797

Kunz-Schughart, L. A., Schroeder, J. A., Wondrak, M., van Rey, F., Lehle, K., Hofstaedter, F., et al. (2006). Potential of fibroblasts to regulate the formation of three-dimensional vessel-like structures from endothelial cells in vitro. *Am. J. Physiol. Cell Physiol.* 290, C1385–C1398. doi:10.1152/ajpcell.00248.2005

Lee, S.-J., Park, C., Lee, J. Y., Kim, S., Kwon, P. J., Kim, W., et al. (2015). Generation of pure lymphatic endothelial cells from human pluripotent stem cells and their therapeutic effects on wound repair. *Sci. Rep.* 5, 11019. doi:10.1038/srep11019

Makinen, T., Veikkola, T., Mustjoki, S., Karpanen, T., Catimel, B., Nice, E. C. E., et al. (2001). Isolated lymphatic endothelial cells transduce growth, survival and migratory signals via the VEGF-C/D receptor VEGFR-3. *EMBO J.* 20, 4762–4773. doi:10.1093/emboj/20.17.4762

Marino, D., Luginbühl, J., Scola, S., Meuli, M., and Reichmann, E. (2014). Bioengineering dermo-epidermal skin grafts with blood and lymphatic capillaries. *Sci. Transl. Med.* 6, 221ra14. doi:10.1126/scitranslmed.3006894

Medina, R., O'Neill, C. L., Humphreys, M. W., Gardiner, T. A., and Stitt, A. W. (2010). Outgrowth endothelial cells: characterisation and their potential for reversing ischaemic retinopathy. *Invest. Ophthalmol. Vis. Sci.* 51, 1–35. doi:10.1167/iovs.09-4951

Merfeld-Clauss, S., Gollahalli, N., March, K. L., and Traktuev, D. O. (2010). Adipose tissue progenitor cells directly interact with endothelial cells to induce vascular network formation. *Tissue Eng. Part A* 16, 2953–2966. doi:10.1089/ten.TEA.2009.0635

Merfeld-Clauss, S., Lupov, I. P., Lu, H., March, K. L., and Traktuev, D. O. (2015). Adipose stromal cell contact with endothelial cells results in loss of complementary vasculogenic activity mediated by induction of activin A. *Stem Cells* 33, 3039–3051. doi:10.1002/stem.2074

Muehleder, S., Ovsianikov, A., Zipperle, J., Redl, H., and Holnthoner, W. (2014). Connections matter: channeled hydrogels to improve vascularization. *Front. Bioeng. Biotechnol.* 2:52. doi:10.3389/fbioe.2014.00052

Ng, C. P., Helm, C. L. E., and Swartz, M. A. (2004). Interstitial flow differentially stimulates blood and lymphatic endothelial cell morphogenesis in vitro. *Microvasc. Res.* 68, 258–264. doi:10.1016/j.mvr.2004.08.002

Petrek, J. A., Senie, R. T., Peters, M., and Peterrosen, P. (2001). Lymphedema in a cohort of breast carcinoma survivors 20 years after diagnosis. *Cancer* 92, 1368–1377. doi:10.1002/1097-0142(20010915)92:6<1368::AID-CNCR1459>3.0.CO;2-9

Pill, K., Hofmann, S., Redl, H., and Holnthoner, W. (2015). Vascularization mediated by mesenchymal stem cells from bone marrow and adipose tissue: a comparison. *Cell Regen. (Lond.)* 4, 8. doi:10.1186/s13619-015-0025-8

Podgrabinska, S., Braun, P., Velasco, P., Kloos, B., Pepper, M. S., and Skobe, M. (2002). Molecular characterization of lymphatic endothelial cells. *Proc. Natl. Acad. Sci. U.S.A.* 99, 16069–16074. doi:10.1073/pnas.242401399

Rivron, N. C., Liu, J. J., Rouwkema, J., de Boer, J., and van Blitterswijk, C. A. (2008). Engineering vascularised tissues in vitro. *Eur. Cell. Mater.* 15, 27–40. doi:10.22203/eCM.v015a03

Rohringer, S., Hofbauer, P., Schneider, K. H., Husa, A. M., Feichtinger, G., Peterbauer-Scherb, A., et al. (2014). Mechanisms of vasculogenesis in 3D fibrin matrices mediated by the interaction of adipose-derived stem cells and endothelial cells. *Angiogenesis* 17, 921–933. doi:10.1007/s10456-014-9439-0

Rouwkema, J., Rivron, N. C., and van Blitterswijk, C. A. (2008). Vascularization in tissue engineering. *Trends Biotechnol.* 26, 434–441. doi:10.1016/j.tibtech.2008.04.009

Schaupper, M., Jeltsch, M., Rohringer, S., Redl, H., and Holnthoner, W. (2016). Lymphatic vessels in regenerative medicine and tissue engineering. *Tissue Eng. Part B Rev.* 22, 395–407. doi:10.1089/ten.TEB.2016.0034

Schimek, K., Busek, M., Brincker, S., Groth, B., Hoffmann, S., Lauster, R., et al. (2013). Integrating biological vasculature into a multi-organ-chip microsystem. *Lab. Chip* 13, 3588–3598. doi:10.1039/c3lc50217a

Siow, R. C. M. (2012). Culture of human endothelial cells from umbilical veins. *Methods Mol. Biol.* 806, 265–274. doi:10.1007/978-1-61779-367-7_18

Sorrell, J. M., Baber, M. A., and Caplan, A. I. (2007). A self-assembled fibroblast-endothelial cell co-culture system that supports in vitro vasculogenesis by both human umbilical vein endothelial cells and human dermal microvascular endothelial cells. *Cells Tissues Organs* 186, 157–168. doi:10.1159/000106670

Strassburg, S., Torio-Padron, N., Finkenzeller, G., Frankenschmidt, A., and Stark, G. B. (2016). Adipose-derived stem cells support lymphangiogenic parameters in vitro. *J. Cell. Biochem.* 117, 2620–2629. doi:10.1002/jcb.25557

Swartz, M. A., and Skobe, M. (2001). Lymphatic function, lymphangiogenesis, and cancer metastasis. *Microsc. Res. Tech.* 55, 92–99. doi:10.1002/jemt.1160

Swerlick, R. A., Garcia-Gonzalez, E., Kubota, Y., Xu, Y. L., and Lawley, T. J. (1991). Studies of the modulation of MHC antigen and cell adhesion molecule expression on human dermal microvascular endothelial cells. *J. Invest. Dermatol.* 97, 190–196. doi:10.1111/1523-1747.ep12479643

Szöke, K., Reinisch, A., Østrup, E., Reinholt, F. P., and Brinchmann, J. E. (2015). Autologous cell sources in therapeutic vasculogenesis: in vitro and in vivo comparison of endothelial colony-forming cells from peripheral blood and endothelial cells isolated from adipose tissue. *Cytotherapy* 18, 242–252. doi:10.1016/j.jcyt.2015.10.009

Takeda, K., Sowa, Y., Nishino, K., Itoh, K., and Fushiki, S. (2015). Adipose-derived stem cells promote proliferation, migration, and tube formation of lymphatic endothelial cells in vitro by secreting lymphangiogenic factors. *Ann. Plast. Surg.* 74, 728–736. doi:10.1097/SAP.0000000000000084

Tammela, T., and Alitalo, K. (2010). Lymphangiogenesis: molecular mechanisms and future promise. *Cell* 140, 460–476. doi:10.1016/j.cell.2010.01.045

Tien, J. (2014). Microfluidic approaches for engineering vasculature. *Curr. Opin. Chem. Eng.* 3, 36–41. doi:10.1016/j.coche.2013.10.006

Unger, R. E., Ghanaati, S., Orth, C., Sartoris, A., Barbeck, M., Halstenberg, S., et al. (2010). The rapid anastomosis between prevascularized networks on silk fibroin scaffolds generated in vitro with cocultures of human microvascular endothelial and osteoblast cells and the host vasculature. *Biomaterials* 31, 6959–6967. doi:10.1016/j.biomaterials.2010.05.057

Verseijden, F., Posthumus-van Sluijs, S. J., Farrell, E., Van Neck, J. W., Hovius, S. E. R., Hofer, S. O. P., et al. (2010a). Prevascular structures promote vascularization in engineered human adipose tissue constructs upon implantation. *Cell Transplant.* 19, 1007–1020. doi:10.3727/096368910X492571

Verseijden, F., Posthumus-van Sluijs, S. J., Pavljasevic, P., Hofer, S. O. P., van Osch, G. J. V. M., and Farrell, E. (2010b). Adult human bone marrow- and adipose tissue-derived stromal cells support the formation of prevascular-like structures from endothelial cells in vitro. *Tissue Eng. Part A* 16, 101–114. doi:10.1089/ten.TEA.2009.0106

Weitman, E., Cuzzone, D., and Mehrara, B. J. (2013). Tissue engineering and regeneration of lymphatic structures. *Future Oncol.* 9, 1365–1374. doi:10.2217/fon.13.110

Wigle, J. T., Harvey, N., Detmar, M., Lagutina, I., Grosveld, G., Gunn, M. D., et al. (2002). An essential role for Prox1 in the induction of the lymphatic endothelial cell phenotype. *EMBO J.* 21, 1505–1513. doi:10.1093/emboj/21.7.1505

Wolbank, S., Peterbauer, A., Fahrner, M., Hennerbichler, S., van Griensven, M., Stadler, G., et al. (2007). Dose-dependent immunomodulatory effect of human stem cells from amniotic membrane: a comparison with human mesenchymal stem cells from adipose tissue. *Tissue Eng.* 13, 1173–1183. doi:10.1089/ten.2006.0313

Wong, K. H. K., Truslow, J. G., Khankhel, A. H., Chan, K. L. S., and Tien, J. (2013). Artificial lymphatic drainage systems for vascularized microfluidic scaffolds. *J. Biomed. Mater. Res. A.* 101, 2181–2190. doi:10.1002/jbm.a.34524

Conflict of Interest Statement: KS, TH, and UM are employees of TissUse GmbH that produces and markets microphysiological systems. The other authors declare no conflict of interest.

Advantages of publishing in Frontiers

OPEN ACCESS
Articles are free to read for greatest visibility and readership

FAST PUBLICATION
Around 90 days from submission to decision

HIGH QUALITY PEER-REVIEW
Rigorous, collaborative, and constructive peer-review

TRANSPARENT PEER-REVIEW
Editors and reviewers acknowledged by name on published articles

Frontiers
Avenue du Tribunal-Fédéral 34
1005 Lausanne | Switzerland

Visit us: www.frontiersin.org
Contact us: info@frontiersin.org | +41 21 510 17 00

REPRODUCIBILITY OF RESEARCH
Support open data and methods to enhance research reproducibility

DIGITAL PUBLISHING
Articles designed for optimal readership across devices

FOLLOW US
@frontiersin

IMPACT METRICS
Advanced article metrics track visibility across digital media

EXTENSIVE PROMOTION
Marketing and promotion of impactful research

LOOP RESEARCH NETWORK
Our network increases your article's readership